IAEA TECDOC SERIES

IAEA-TECDOC-2009

IAEA-TECDOC-2009

Near Term and Promising Long Term Options for the Deployment of Thorium Based Nuclear Energy

Final Report of a Coordinated Research Project

IAEA
International Atomic Energy Agency

NEAR TERM AND PROMISING LONG TERM OPTIONS FOR THE DEPLOYMENT OF THORIUM BASED NUCLEAR ENERGY

The following States are Members of the International Atomic Energy Agency:

AFGHANISTAN
ALBANIA
ALGERIA
ANGOLA
ANTIGUA AND BARBUDA
ARGENTINA
ARMENIA
AUSTRALIA
AUSTRIA
AZERBAIJAN
BAHAMAS
BAHRAIN
BANGLADESH
BARBADOS
BELARUS
BELGIUM
BELIZE
BENIN
BOLIVIA, PLURINATIONAL STATE OF
BOSNIA AND HERZEGOVINA
BOTSWANA
BRAZIL
BRUNEI DARUSSALAM
BULGARIA
BURKINA FASO
BURUNDI
CAMBODIA
CAMEROON
CANADA
CENTRAL AFRICAN REPUBLIC
CHAD
CHILE
CHINA
COLOMBIA
COMOROS
CONGO
COSTA RICA
CÔTE D'IVOIRE
CROATIA
CUBA
CYPRUS
CZECH REPUBLIC
DEMOCRATIC REPUBLIC OF THE CONGO
DENMARK
DJIBOUTI
DOMINICA
DOMINICAN REPUBLIC
ECUADOR
EGYPT
EL SALVADOR
ERITREA
ESTONIA
ESWATINI
ETHIOPIA
FIJI
FINLAND
FRANCE
GABON
GEORGIA
GERMANY
GHANA
GREECE
GRENADA
GUATEMALA
GUYANA
HAITI
HOLY SEE
HONDURAS
HUNGARY
ICELAND
INDIA
INDONESIA
IRAN, ISLAMIC REPUBLIC OF
IRAQ
IRELAND
ISRAEL
ITALY
JAMAICA
JAPAN
JORDAN
KAZAKHSTAN
KENYA
KOREA, REPUBLIC OF
KUWAIT
KYRGYZSTAN
LAO PEOPLE'S DEMOCRATIC REPUBLIC
LATVIA
LEBANON
LESOTHO
LIBERIA
LIBYA
LIECHTENSTEIN
LITHUANIA
LUXEMBOURG
MADAGASCAR
MALAWI
MALAYSIA
MALI
MALTA
MARSHALL ISLANDS
MAURITANIA
MAURITIUS
MEXICO
MONACO
MONGOLIA
MONTENEGRO
MOROCCO
MOZAMBIQUE
MYANMAR
NAMIBIA
NEPAL
NETHERLANDS
NEW ZEALAND
NICARAGUA
NIGER
NIGERIA
NORTH MACEDONIA
NORWAY
OMAN
PAKISTAN
PALAU
PANAMA
PAPUA NEW GUINEA
PARAGUAY
PERU
PHILIPPINES
POLAND
PORTUGAL
QATAR
REPUBLIC OF MOLDOVA
ROMANIA
RUSSIAN FEDERATION
RWANDA
SAINT KITTS AND NEVIS
SAINT LUCIA
SAINT VINCENT AND THE GRENADINES
SAMOA
SAN MARINO
SAUDI ARABIA
SENEGAL
SERBIA
SEYCHELLES
SIERRA LEONE
SINGAPORE
SLOVAKIA
SLOVENIA
SOUTH AFRICA
SPAIN
SRI LANKA
SUDAN
SWEDEN
SWITZERLAND
SYRIAN ARAB REPUBLIC
TAJIKISTAN
THAILAND
TOGO
TONGA
TRINIDAD AND TOBAGO
TUNISIA
TÜRKİYE
TURKMENISTAN
UGANDA
UKRAINE
UNITED ARAB EMIRATES
UNITED KINGDOM OF GREAT BRITAIN AND NORTHERN IRELAND
UNITED REPUBLIC OF TANZANIA
UNITED STATES OF AMERICA
URUGUAY
UZBEKISTAN
VANUATU
VENEZUELA, BOLIVARIAN REPUBLIC OF
VIET NAM
YEMEN
ZAMBIA
ZIMBABWE

The Agency's Statute was approved on 23 October 1956 by the Conference on the Statute of the IAEA held at United Nations Headquarters, New York; it entered into force on 29 July 1957. The Headquarters of the Agency are situated in Vienna. Its principal objective is "to accelerate and enlarge the contribution of atomic energy to peace, health and prosperity throughout the world''.

IAEA-TECDOC-2009

NEAR TERM AND PROMISING LONG TERM OPTIONS FOR THE DEPLOYMENT OF THORIUM BASED NUCLEAR ENERGY

FINAL REPORT OF A COORDINATED RESEARCH PROJECT

INTERNATIONAL ATOMIC ENERGY AGENCY
VIENNA, 2022

COPYRIGHT NOTICE

For further information on this publication, please contact:

Nuclear Fuel Cycle and Materials Section
International Atomic Energy Agency
Vienna International Centre
PO Box 100
1400 Vienna, Austria
Email: Official.Mail@iaea.org

Printed by the IAEA in Austria
September 2022

IAEA Library Cataloguing in Publication Data

Names: International Atomic Energy Agency.
Title: Near term and promising long term options for the deployment of thorium based nuclear energy / International Atomic Energy Agency.
Description: Vienna : International Atomic Energy Agency, 2022. | Series: IAEA TECDOC series, ISSN 1011–4289 ; no. 2009 | Includes bibliographical references.
Identifiers: IAEAL 22-01535 | ISBN 978–92–0–139722–5 (paperback : alk. paper) | ISBN 978–92–0–139622–8 (pdf)
Subjects: LCSH: Thorium. | Thorium — Utilization. | Nuclear reactors. | Nuclear energy.

FOREWORD

There has been an interest among Member States in the use of the thorium fuel cycle to address the sustainable growth of nuclear energy. Thorium based fuels have been studied for their potential applications in almost all types of reactor, including water cooled reactors, high temperature reactors, fast reactors and molten salt reactors, albeit on a smaller scale than uranium and uranium–plutonium fuels.

Thorium has several inherent physical and neutronic characteristics that may be exploited in current and next generation nuclear energy systems to achieve, for example, enhanced capabilities for high conversion, further augmented inherent safety characteristics and reduced minor actinides production.

Some Member States view near to medium term deployment of thorium fuels in proven reactor types as not only feasible, but also attractive in meeting expanding energy needs. Several options are also currently under consideration or active development for deployment in the longer term.

On the suggestion of the Technical Working Group on Fuel Performance and Technology, in 2011 the IAEA launched a coordinated research project entitled Near Term and Promising Long Term Options for the Deployment of Thorium Based Nuclear Energy. This research project provided a platform for sharing research results and previous experiences among national laboratories and research institutes of participating Member States. The need for coordinated examination of how thorium fuel types may be deployed and what hinders progress towards such goals was addressed by the project to develop strategies for the timely deployment of thorium based nuclear energy systems that can serve as a component of the global energy supply. Canada, China, Czech Republic, Germany, India, Italy, Switzerland, the United Kingdom and the United States of America all participated in the coordinated research project; this publication is an outcome of the project.

The IAEA would like to thank the organisations and individuals which contributed to the coordinated research project. The IAEA expresses its appreciation to the Chief Scientific Investigators for the preparation of this publication. The IAEA officers responsible for this publication were U. Basak and K. Agarwal of the Division of Nuclear Fuel Cycle and Waste Technology.

EDITORIAL NOTE

This publication has been prepared from the original material as submitted by the contributors and has not been edited by the editorial staff of the IAEA. The views expressed remain the responsibility of the contributors and do not necessarily represent the views of the IAEA or its Member States.

Neither the IAEA nor its Member States assume any responsibility for consequences which may arise from the use of this publication. This publication does not address questions of responsibility, legal or otherwise, for acts or omissions on the part of any person.

The use of particular designations of countries or territories does not imply any judgement by the publisher, the IAEA, as to the legal status of such countries or territories, of their authorities and institutions or of the delimitation of their boundaries.

The mention of names of specific companies or products (whether or not indicated as registered) does not imply any intention to infringe proprietary rights, nor should it be construed as an endorsement or recommendation on the part of the IAEA.

The authors are responsible for having obtained the necessary permission for the IAEA to reproduce, translate or use material from sources already protected by copyrights.

The IAEA has no responsibility for the persistence or accuracy of URLs for external or third party Internet web sites referred to in this publication and does not guarantee that any content on such web sites is, or will remain, accurate or appropriate.

CONTENTS

1. INTRODUCTION

1.1. BACKGROUND

Thorium is widely distributed with an average concentration of 10 ppm in earth's crust and is almost 3 times more abundant in nature than uranium. Thorium is a fertile material but produces fissile ^{233}U during reactor irradiation:

$$^{232}_{90}Th + n \rightarrow {}^{233}_{90}Th \xrightarrow{\beta^-} {}^{233}_{91}Pa \xrightarrow{\beta^-} {}^{233}_{92}U$$

For the deployment of thorium fuel cycle in nuclear reactors, the fertile thorium is required to be used along with some fissile materials. These could be either ^{233}U or ^{235}U or ^{239}Pu. ^{233}U is the best fissile material in terms of the ratio of neutron yield per fission to neutrons absorbed. Its fission products have less poisoning neutronic effects. In case of application of a pure ^{233}U/ ^{232} Th mix in fuel composition, i.e., absence of ^{238}U in 'fresh' fuel in thorium-uranium fuel cycle, the amount of minor actinides in spent fuel drops significantly. Thus, thorium fuel cycle using ^{233}U as fissile material generate at least one order of magnitude less long-lived minor actinides than U/U-Pu fuel cycles. Moreover, multiple recycling of ^{233}U is possible due to lower non fissile absorption of neutrons in ^{233}U than in ^{235}U and ^{239}Pu for thorium fuel cycle. However, ^{233}U is always accompanied by ^{232}U produced by (n, 2n) reaction from ^{232}Th in the reactor and the decay products of ^{232}U contain 2.2–2.6 MeV hard gamma emitters ^{212}Bi and ^{208}Tl (see Fig.1). Due to the presence of ^{232}U, ^{233}U bearing thorium fuels are required to be handled remotely in a well shielded facility.

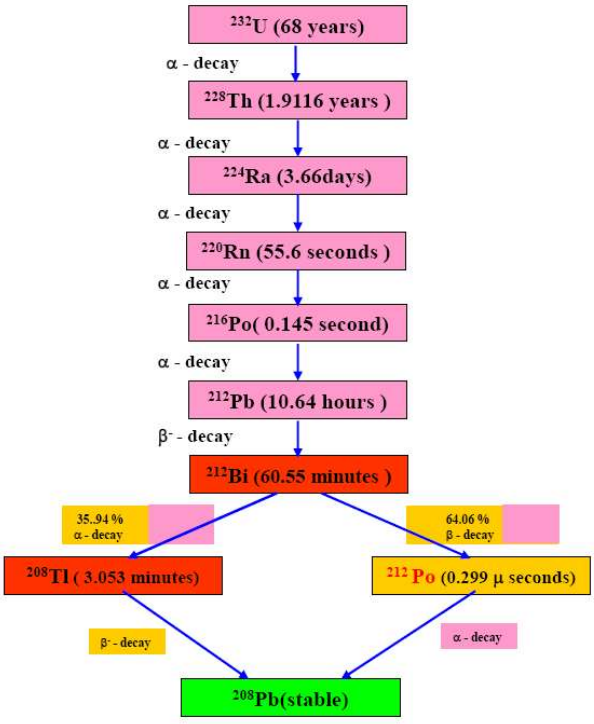

FIG.1. Decay series of ^{232}U.

The incentives for use of thorium based fuels are:

— Natural abundance of thorium resources;
— Inert nature of thoria (ThO_2);

— Better thermo- physical properties compared to urania (UO_2);
— High burnup capability;
— Suitability of high conversion ratio fuel cycles;
— Inherent proliferation resistance characteristics.

The back end of thorium fuel cycle is very challenging as ThO_2 is one of the refractories having the highest melting point and is very stable thermodynamically. It melts at 3390^0C (3663^0K) compared to UO_2 which melts at 2865°C (3138^0K). ThO_2 does not undergo any phase changes till its melting point. This high temperature stability as well as chemical inertness of ThO_2 based fuels complicates the solution treatment for the separation of thorium compounds and their dissolution for reprocessing.

The IAEA has covered the prospective use of thorium as an energy source in several publications in the past [1–3].

A coordinated research programme (CRP) on "Near Term and Promising Long-Term Options for the Deployment of Thorium Based Nuclear Energy" was launched in 2011 and completed in 2015. Participating countries were Canada, China, Czech Republic, Germany, India, Italy, Switzerland, United Kingdom and the United States of America through 10 research agreements and 3 research contracts. There were 3 research coordination meetings held in 2012, 2014 and 2015 in Vienna, Milan and UK respectively. There were 13 participating organisations from Canada, China, Czech Republic, Germany, India, Italy, Russian Federation, UK, USA. Some of the outputs of this CRP have been published by contributors in various journals and conference proceedings after completion of CRP and have been referred in this publication.

1.2. OBJECTIVE

The objective of this publication is to provide a comprehensive summary of the research work carried out under the CRP entitled Near Term and Promising Long Term Options for the Deployment of Thorium Based Nuclear Energy and to provide an overview of participating Member States' approaches for the utilization of thorium resources in both thermal and fast reactors.

1.3. SCOPE

This CRP was intended to encourage the development and sharing of research results on enhanced capabilities of thorium based fuels for high conversion ratio fuel cycle, improved inherent safety characteristics, reduced minor actinide productions etc. Based on the research results carried out under the IAEA coordinated research project, this report highlights reactor systems for thorium deployment, thorium fuel cycle implementation scenarios, thermo-physical properties and irradiation performances of thorium based oxide fuels.

1.4. STRUCTURE

This report is organized in nine main sections.

Section 1 provides a brief introduction indicating several advantages of the thorium fuel cycle.

Section 2 describes use of thorium fuel in heavey water reactors. Specifically, the following subjects are dealt with:

(a) Reactor design aspects of Advanced Heavy Water Reactor;
(b) Powder metallurgical technique for the manufacturing of thorium based oxide fuels;
(c) Irradiation performance of thorium based fuels for heavy water reactor;
(d) Innovative dry reprocessing of thorium oxide fuels;
(e) Data base generated for some important thermophysical properties of thorium based oxide fuels.

This section is contributed by BARC, India and CNL, Canada.

Section 3 deals with implementation scenario of Th-Pu oxide fuels in a light water reactor and mainly the following subjects are considered:

(a) Full reactor core design for use of thoria- plutonia fuels;
(b) Full core 3D analysis;
(c) Design options for high conversion light water reactor.

This section is contributed by HZDR, Germany and University of Cambridge, UK.

In Section 4, analysis of two types of thorium-based fuelling strategies, namely thorium & high enriched uranium mixed oxide fuel and thorium & low enriched uranium (separate) schemes for in situ utilization in High Temperature Reactors are described.
This section is contributed by INNET, Tsinghua University, China.

Section 5 describes the deployment of thorium in molten salt reactors (MSR) and specifically deals with the following:

(a) Fuel cycle technology for MSRs based on one fluid and two fluid design sheme for reprocessing;
(b) Impact of fission products on neutronics;
(c) Reactor performance in closed thorium — uranium fuel cycle;
(d) Actinide recycling based on some fuel cycle senarios.

This section is contributed by NRI, Czech Republic and PSI, Switzerland.

Section 6 deals with use of thorium fuels in Fast Reactors namely European Lead System (ELSY), Advanced Recycle Reactor (ARR) and Molten Salt Fast Reactor (MSFR).
This section is contributed by Politecnico di Milano, Italy.

In Section 7, some of the challenges of actinide recycle and transmutation by analyzing a multi-stage transmutation scenario, starting with or without an interim Pu burning in current LWRs and implementing full actinide recycle in advanced reactors are described.
This section is contributed by Wetinghouse Electric Company, USA

Section 8 deals with the effectiveness of full actinide recycle as a nuclear waste management strategy when implemented over a limited timeframe.
This section is contributed by Wetinghouse Electric Company, USA

In Section 9, a summary of the CRP is presented.

2. UTILIZATION OF THORIUM IN HEAVY WATER REACTORS

2.1. INTRODUCTION

India has over the years developed a high level of expertise in heavy water reactor technology. The country has the requisite infrastructure for construction and deployment of a large fleet of these pressure tube based small and medium sized reactors. At present, 17 units of natural UO_2 based pressurized heavy water reactors (PHWRs) are under operation, five units are under construction and several more are planned to be constructed in the next few decades.

As a part of technology demonstration for large-scale utilization of thorium, Bhabha Atomic Research Centre (BARC) has designed a 300 MWe Advanced Heavy Water Reactor (AHWR) with advanced safety features. AHWR is a vertical pressure tube type reactor with heavy water as moderator and boiling light water coolant which transfers heat from reactor core by natural circulation. The reactor has a slightly negative void-coefficient of reactivity and has several passive safety systems for decay heat removal, emergency core cooling, confinement of radioactivity, etc., which are based on natural phenomena for their operation like gravity/natural convection without requiring operator intervention [4].

The reactor core has 444 vertical coolant channels with each having a single long fuel assembly. The fuel assembly is similar in many respects to the conventional Boiling Water Reactor (BWR) fuel, but in a configuration to suit the circular cross-section of the pressure tube (unlike square channel of BWR). The fuel cluster is a cylindrical assembly of about 4300 mm in length and 118mm nominal diameter. It has 54 fuel pins which are arranged in three concentric rings — 12 pins in the inner ring, 18 pins in the middle ring and 24 pins in the outer ring. The fuel pins are assembled into a cluster by the top and bottom tie-plates, spacers and central rod acting as the tie-rod.

2.2. FUEL CYCLE STRATEGIES

The absence of fissile material in natural thorium requires that fertile thorium is converted to fissile ^{233}U for its use. A different fuel management/cycle strategy from that adopted for uranium is therefore required for launching thorium based reactor programme. In the first instance, thorium can be used along with either enriched uranium or plutonium for producing energy in a nuclear reactor. Fuel cycle strategies have been worked out for AHWR with both Pu and low enriched uranium (LEU) as external fissile feed.

2.2.1. AHWR with LEU as external fissile feed

The reactor AHWR-LEU will use (Thorium-LEU) mixed oxide (MOX) as fuel with LEU having ^{235}U enrichment of 19.75%. From optimum fuel utilization considerations, the average fuel discharge burnup has to be kept as high as possible, especially for an open fuel cycle. The initial fuel cluster configuration of AHWR-LEU reactor is shown in Fig. 2, considering high fuel discharge burn up of ~ 60 GW. d/t to generate maximum energy from thorium. In 80 of the initial core fuel clusters, two of the twelve inner ring fuel pins will also contain burnable absorber gadolinia. The initial core fuel clusters will be gradually replaced by reload fuel clusters of a configuration shown in Fig. 3, when they attain burnups in the range of 20–40 GW.d/t.

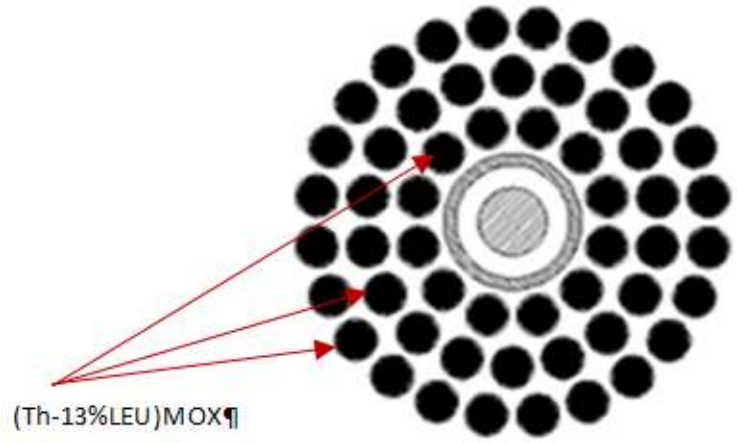

FIG. 2. General arrangement of AHWR-LEU initial core fuel cluster (courtesy of V. Shivkumar, BARC).

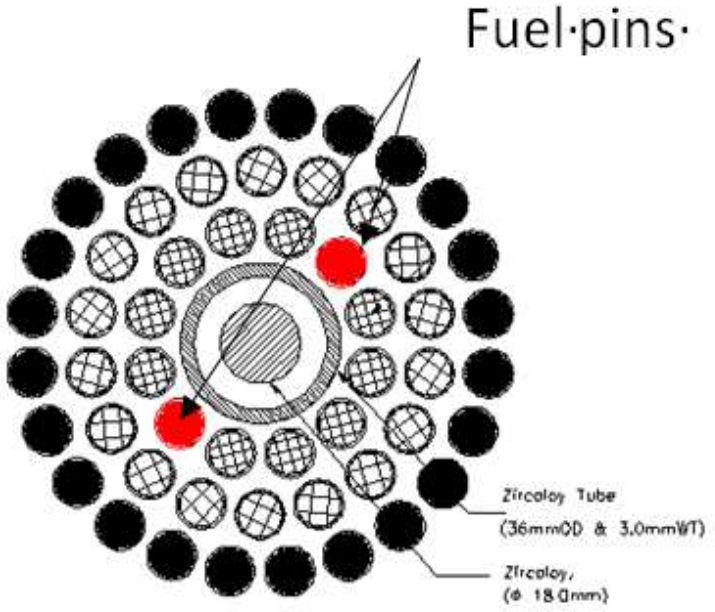

FIG. 3. General arrangement of AHWR-LEU reloads fuel cluster (courtesy of V. Shivkumar, BARC).

When the reactor is in operation with initial fuel cluster, the equilibrium core condition will be achieved at an average burn up of 30 GW. d/t in almost ten years. The reactor will be operated in this configuration for the rest of its life. The pressure tube type design of the reactor facilitates operation continuously in this equilibrium core mode which is achieved by employing on-power refuelling or by small-size batch refuelling under off-power at frequent intervals. The fuel requirements for this reactor are brought out in Table 1.

TABLE 1. FUEL MATERIAL REQUIREMENTS FOR AHWR-LEU

		Initial core	Equilibrium core
Fuel feed material (powder)	Nat. ThO_2	52t	4.7t
	Enriched UO_2 (19.75% ^{235}U)	8t	1.3t
Fabricated products	(Th-LEU) MOX Pellets	60t	6t/year
	Fuel Pins	24 000 nos.	2400 nos./year

The reactor can also be designed for closed fuel cycle during its lifetime. A scheme for recycling of fissile and fertile materials is schematically brought out in Fig. 4.

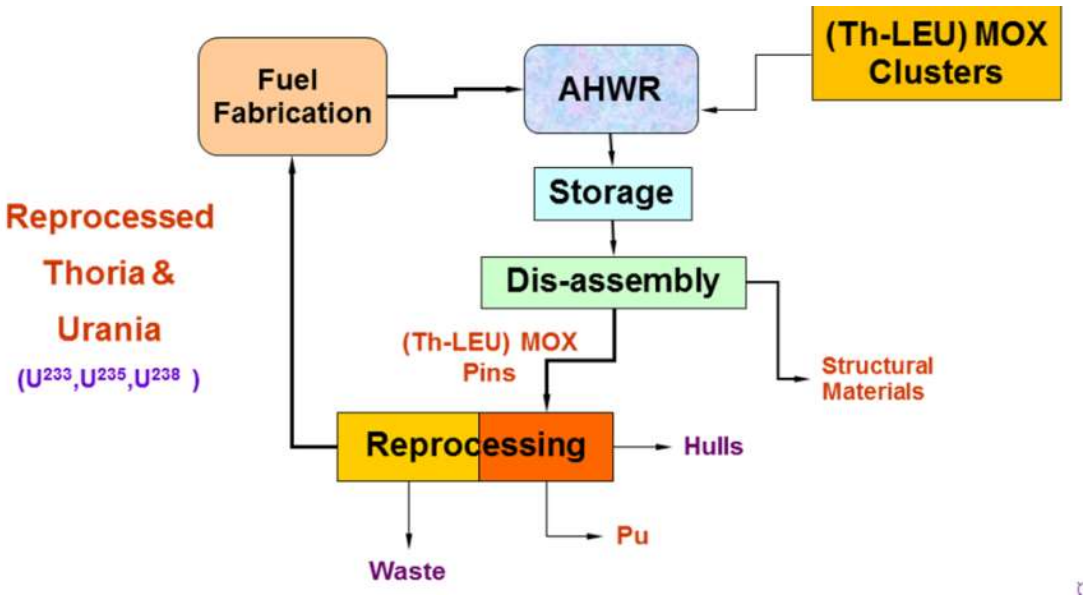

FIG. 4. AHWR-LEU fuel cycle with recycling of fissile and fertile materials (courtesy of V. Shivkumar, BARC).

The recycling of uranium in this case which contains fissile components (^{233}U and ^{235}U) will improve fuel utilisation. It is however observed that as the number of recycle increases, the isotopic composition of uranium (^{232}U, ^{233}U, ^{234}U, ^{235}U, ^{236}U, ^{237}U and ^{238}U) in discharged fuel varies widely. This aspect needs to be factored in fuel fabrication and reactor operation. The equivalent fissile content for each batch is to be evaluated and the MOX composition for each batch has to be suitably adjusted during fuel fabrication. This variation in isotopic composition and MOX composition is to be further followed up during fuel management in reactor. From practical considerations, it therefore appears that the number of recycling would have to be limited to two or three. This recycling of uranium would typically improve the fuel utilisation by about 3040%, when compared to the open cycle.

2.2.2. AHWR with Pu as external fissile fuel

In this case, AHWR will use the external fissile feed plutonium in the form of Thorium plutonium mixed oxide (TOX) type fuel. The equilibrium core condition will be achieved when the reactor is operating at an average burn up of ~ 20GWd/t with composite fuel configuration as shown in Fig. 5.

The adoption of closed fuel cycle helps in generating a large fraction of energy from thorium. For closed fuel cycle, AHWR will use Th based Pu and Th based ^{233}U MOX fuels. ^{233}U and Pu are to be obtained from reprocessing its spent fuel and PHWR fuels respectively. Further Pu will be obtained by reprocessing its spent fuel (Fig. 6). Multiple recycling of ^{233}U is easier to implement in this case as there is no significant degradation of fissile isotopic content. As the reactor is not provided by ^{233}U from any external source, the fuel management strategy is to load the entire core initially with plutonium based MOX fuel only.

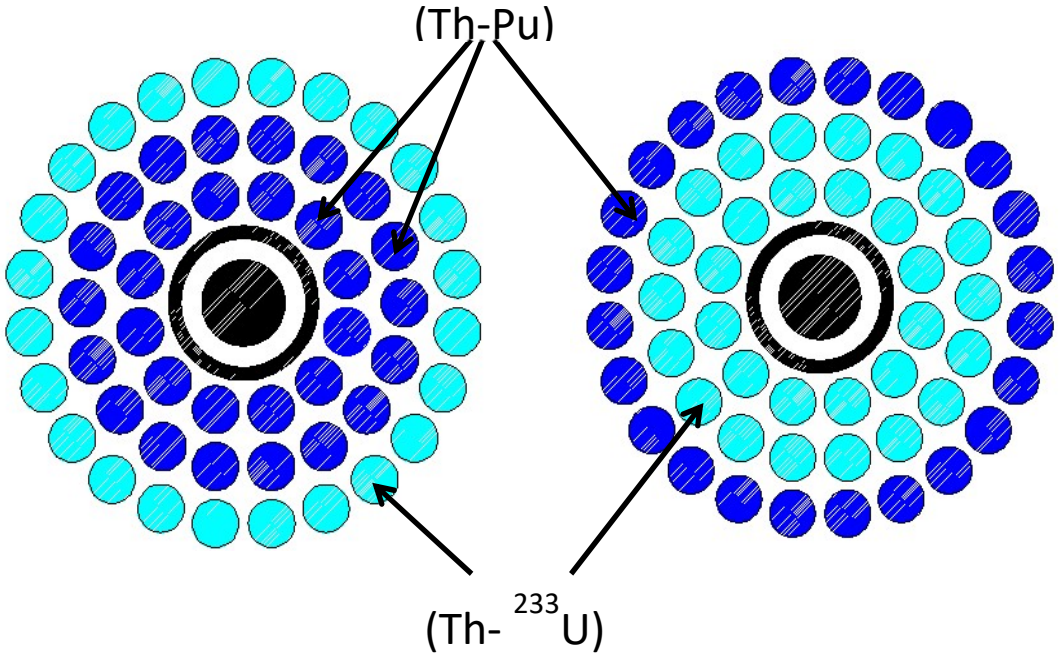

FIG. 5. General arrangement of pins in the two alternatives of Composite Fuel cluster (courtesy of V. Shivkumar, BARC).

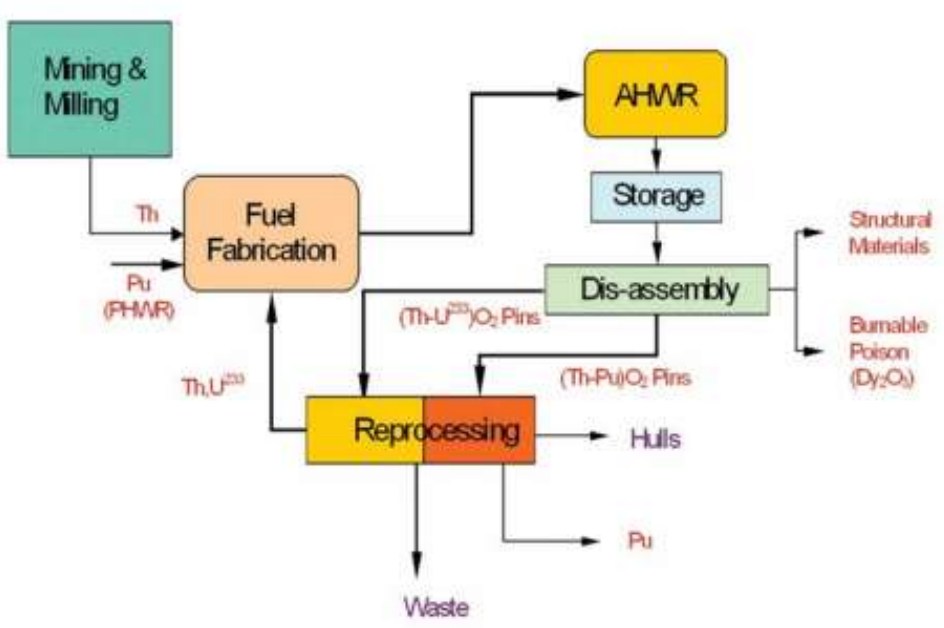

FIG. 6. Materials flow of AHWR (with Pu as external fissile feed) in equilibrium core condition (courtesy of V. Shivkumar, BARC).

2.3. REACTOR DESIGN ASPECTS

2.3.1. Reactor physics

The nuclear database for Th–U and Th–Pu reactor systems is significantly less compared to that of the U-Pu reactor systems. The accurate modelling of the effect on neutronics due to changes in moderator temperature, channel temperature, fuel temperature, coolant void and burnup is an important aspect in reactor design. The reactor physics evaluations for the thoria based AHWRs are being carried out with the available nuclear data. Some of the conservativeness in the predictions will be further refined with increasing experience and data-base generation. A Critical Facility to carry out reactor physics experiments for AHWR has been constructed at BARC. Experiments are planned to use the different thoria based fuels to simulate AHWR lattice. The reactor design for AHWR has been worked out with the following objectives:

1) High fraction of energy from thorium;
2) Negative coolant void reactivity coefficient (core average);
3) Negative fuel temperature coefficient;
4) Negative power coefficient;
5) Two independent and functionally diverse fast acting shutdown systems.

One of the important objectives for AHWR is to achieve a negative void coefficient of reactivity. In the conventional pressure tube type reactor systems, the voiding of coolant would make the void reactivity positive. In AHWR design, an increased resonance absorption under harder neutron spectrum helps in achieving negative void reactivity. This has been made possible by engineering the reactor core with a very small lattice pitch configuration with a high pressure tube diameter (a 225 mm lattice pitch with 120 mm pressure tube diameter). The other reactivity coefficients which have operational and safety connotations like fuel temperature coefficient, channel temperature coefficient and moderator temperature coefficient are also negative. Another important reactor physics consideration in AHWR has been to work out a favorable flux

distribution for a thermal-hydraulic design with natural circulation of coolant. In the pressure tube system, the axial flux distribution is a cosine distribution predominantly dictated by the moderator unlike in a BWR where there is bulk boiling, and the axial power profile is bottom-peaked. To enhance the thermal margins in the top regions of the fuel, a differential fissile content is being used along the length of the fuel assembly. A flat power distribution in the cluster has been achieved by radially grading the fissile contents in the three concentric rings of the cluster. In the case of AHWR- low enriched uranium (LEU) fuel cluster, the LEU fraction in the mixed oxide (MOX) is 30wt% in the inner ring pins, 24wt% in the middle ring pins, 18wt% in the lower half of the outer ring pins and 14wt% in the upper half of the outer ring pins. The variation of fuel power variation in the fuel pins of different rings of the fuel cluster is shown in Table 2.

The reactor physics design is optimised to meet the thermal-hydraulics requirements of reactor core design. The maximum channel power of the reactor core is restricted to 2.85 MW and two strategies of refuelling based on single reshuffle and 1st reshuffle have been worked out to achieve this which is shown in Fig. 7.

TABLE 2. VARIATION IN POWER WITH BURNUP IN AHWR-LEU FUEL CLUSTER

Burnup (GW. d/t)	Ring power factors of various rings of cluster			U-235 (wt%)
	Inner	Middle	Outer	
0	0.87	1.04	1.04	4.12% (top half)
10	0.98	1.02	0.99	
30	1.05	0.99	0.98	
70	0.92	0.91	1.11	
0	0.80	0.93	1.15	4.47% (bottom half)
10	0.90	0.94	1.09	
30	1.01	0.96	1.03	
70	0.94	0.91	1.10	

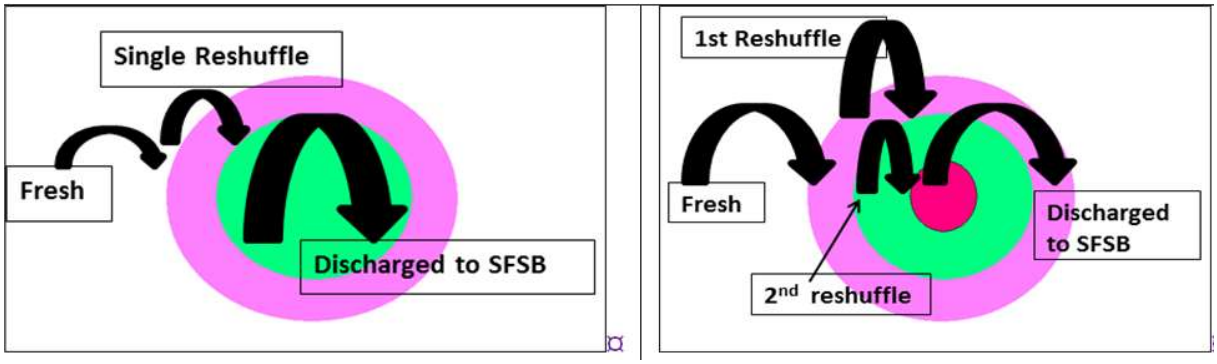

FIG. 7. Refuelling strategies worked out for AHWR-LEU (courtesy of V. Shivkumar, BARC).

2.4. FUEL FABRICATION

The use of thorium in water cooled power reactors requires fabrication of MOX/TOX type fuels. The thoria based MOX/TOX fuels for the AHWRs can be broadly categorized into the following:

1) (Th-LEU) MOX, where the UO_2 fraction will be high, in the range of about 10-30wt%;
2) (Th-Pu) TOX, where the PuO_2 fraction will be low, in the range of about 2-8wt%;
3) (Th-^{233}U) MOX, where the UO_2 fraction will be low, in the range of about 2-5wt%.

The proportion and the type of fissile material in the MOX have an influence on not only the fuel fabrication process aspects but more importantly on the type of facilities required for fuel fabrication. The (Th-LEU) MOX fuel can be fabricated in contained environment similar to that used for the conventional UO_2 fuel of LWRs and HWRs. The fabrication of the plutonium bearing (Th-Pu) TOX fuel is carried out in glove box facilities. The fabrication of the (Th-^{233}U) MOX fuel is to be carried out remotely inside shielded hot-cells. This is because the ^{233}U generated in reactors from thorium is accompanied by ^{232}U, whose daughter products are hard gamma emitters. The radiation levels in the uranium separated after reprocessing of the thoria based fuel increases considerably within a short span of time. Fuel fabrication developmental works have been carried out on these fuel types for use in AHWRs. These were done for optimizing process parameters, evolving fuel fabrication specifications, development of equipment and quality control techniques. Fuel fabrication involves the mixing of UO_2 and PuO_2 powders to obtain the desired MOX/TOX fuel composition followed by pre-compaction, granulation, and final compaction in cylindrical pellets. These pellets were sintered at high temperatures to get the desired density.

2.4.1. (Th-LEU) MOX fuel fabrication

AHWR type (Th-LEU) MOX fuel pins were fabricated for experimental fuel irradiation with the LEU having 9% ^{235}U enrichment and UO_2 fraction in the MOX of 11 wt%. The characteristics of the starting UO_2 and ThO_2 powders and that of the fabricated pellets are given in the below Table 3. The thoria powder obtained by calcination of thorium oxalate has a 'platelet' morphology whereas, the UO_2 powder, derived from ammonium di urinate route has a ‘spherical’ morphology. The pre-milling of the as received thorium oxide powder to break the platelet morphology helps in improving its compressibility and sinterability. A comparison of the morphologies of the powders is shown in Fig. 8.

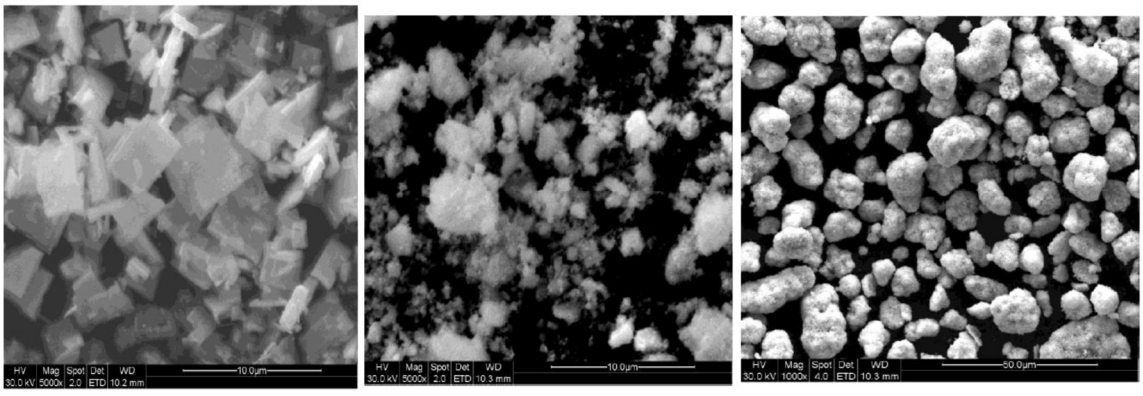

As received ThO_2 powder | ThO_2 powder after milling in attritor for 3hrs | As received UO_2 powder

FIG. 8. A comparison of the morphologies of the powders (courtesy of P. Mishra, BARC).

Dopants like MgO are also added in thoria powder during precipitation stage to enhance its sinterability. Pellets were fabricated by conventional powder pellet route involving the co-milling of UO_2 powder with pre-milled ThO_2 powders for about 30 minutes to ensure homogeneity of UO_2 in the thoria matrix. The powder mixtures were pre-compacted at 150 MPa and granulated. The granules (size: ~1mm) were admixed with 0.25 wt% binder/lubricant. These granules were compacted into cylindrical pellets at a compaction pressure of 350 MPa. The green pellets were sintered at high temperature of $1650^{O}C$ in reducing atmosphere to obtain high density pellets of 94%TD (theoretical density) (Fig. 9).

TABLE 3. CHARACTERISTICS OF STARTING POWDERS AND FABRICATED PELLETS

Starting powders			Finished pellets	
Characteristics	ThO_2	UO_2	Characteristics	(Th-LEU) MOX
Apparent density (g/cc)	0.7	1.2	Diameter	9.75
Specific surface area (m^2/g)	1.53	2.15	L/D ratio	1.0
Theoretical density (g/cc)	10.0	10.96	Density	94% TD

A good homogeneity of UO_2 in the thoria matrix is an important consideration in fabrication of MOX fuels. This was achieved by having suitable milling operation as can be seen from alpha-autoradiography measurements of as fabricated fuel pellets shown in Fig. 9 (b), which indicates uniform distribution of uranium in thorium matrix.

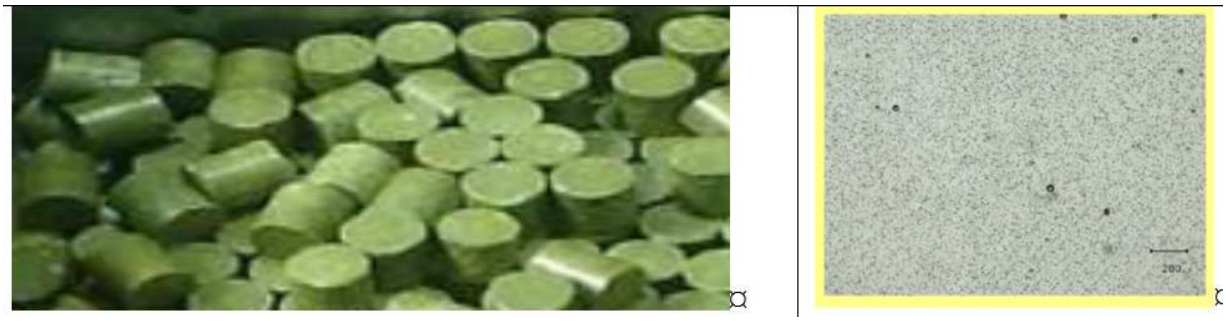

(a)Fabricated fuel pellets. *(b)Alpha-autoradiography of fuel pellet.*

FIG. 9. (Th-LEU) MOX fuel pellet by powder-pellet route (courtesy of P. Mishra, BARC).

2.4.2. (Th-Pu) MOX fuel fabrication

AHWR type (Th-Pu) MOX fuel pins were fabricated for experimental irradiations with PuO_2 fraction in the MOX of 1wt% and 8wt% in glove box facilities. The characteristics of the starting ThO_2 and PuO_2 powder and that of the finished pellets are given in the below Table 4.

TABLE 4. CHARACTERISTICS OF STARTING POWDERS AND FABRICATED PELLETS

Starting powders			Finished pellets	
Characteristics	ThO_2	PuO_2	Characteristics	(Th-Pu) MOX
Apparent density (g/cc)	0.70	1.2	Diameter, mm	9.75
Specific surface area (m^2/g)	1.53	13.6	L/D ratio	1.0
Theoretical density (g/cc)	10.0	11.46	Density	94% TD

The pellets were fabricated by powder metallurgical route involving mixing & milling of powders followed by precompaction and granulation. The granules were compacted into cylindrical pellets and sintered at high temperature in reducing atmosphere to obtain sintered density of 94% theoretical density (TD). A good homogeneity of PuO_2 in the thoria matrix achieved by having suitable milling operation was confirmed by alpha-autoradiography measurements.

2.4.3. (Th-^{233}U) MOX fuel fabrication

Advanced fabrication methods more amenable for the fabrication of (Th-^{233}U) MOX fuel remotely inside shielded hot-cells are being developed. Experimental studies have been carried out on Coated Agglomerate Pelletisation (CAP) and Impregnated Agglomerate pelletisation (IAP) processes were carried out using natural UO_2. These processes help in reducing the operations involving dusty UO_2 powder and also in reducing the number of steps to be carried out in hot cells. The details of the two processes are schematically shown in Figs. 10 and 11.

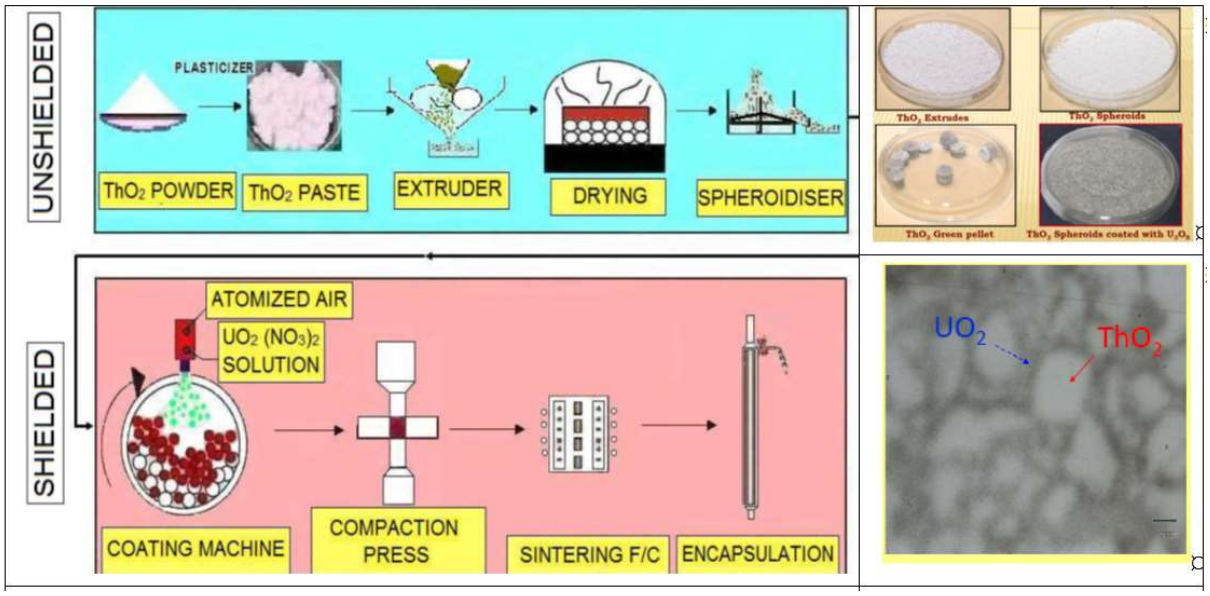

Process Flowsheet

Alpha auto-radiography of fuel pellet cross-section

FIG. 10. Coated agglomerate pelletisation (courtesy of P. Mishra, BARC).

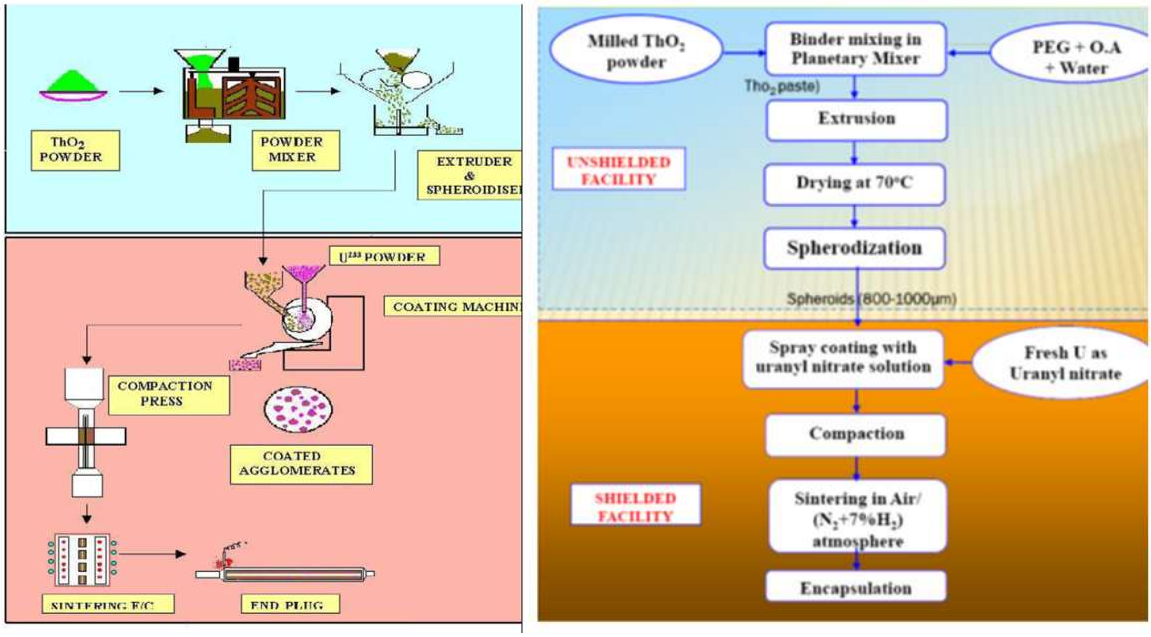

FIG. 11. Impregnate agglomerate pelletisation process flow sheet (courtesy of P. Mishra, BARC).

2.4.4. Fuel fabrication specifications

The fabrication developments carried out for the different types of thoria based MOX fuel of were used to formulate fabrication specifications for AHWR and are as follows:

Thoria powder:

- Median particle size: 1-2 microns;
- Bulk Density: 1.00 ± 0.20 g/cc;
- The thorium content after ignition: minimum of 99.9 weight %;
- Loss on ignition not to exceed 0.5% by weight of thorium.

Thoria based MOX pellets:

- Pellet density: 92-94% TD;
- Pellet diameter: 9.75 ± 0.05mm;
- L/D ratio of the pellet: 1.1–1.4.

The cylindrical surface of pellets requires to have a surface roughness not exceeding 1.6 microns r.m.s. surface texture by visible comparison with standards. Variation in UO_2 content in the MOX is to be within ± 3% of the specified content. O/M ratio (ratio of oxygen to (Th+LEU) atoms) are to be 2-2.01. E.B.C (Equilivalent boron content) of impurities is less than 2.5ppm. Total hydrogen equivalent in the pellet is not to exceed 1ppm.The maximum size of the PuO_2/UO_2 clusters allowed in the pellet is to be 400 µm as seen in alpha-auto radiography.

Microstructure: The grain size is required to be in the range of 5–50 microns on sample pellets longitudinally sectioned, polished and etched.

2.5. IRRADIATED FUEL PERFORMANCE STUDIES

2.5.1. AHWR fuels

As part of the fuel development programme for AHWR, experimental irradiations were carried out with thoria based MOX/TOX fuel in research reactor Dhruva. This was helpful in studying thoria based fuel behaviour in terms of fission gas releases, fuel temperatures, fuel pellet swelling, irradiation effects etc. and the effect of variation in fabrication parameters. This study also provided information on fission product activity and minor actinide generation to carry out fuel cycle studies. A detailed performance analysis on these fuel pins was carried out during the post irradiation examination in BARC.

A six (Th-Pu) TOX fuel pin cluster has completed its irradiation and another with six (Th-LEU) MOX fuel pins is under irradiation testing. The reactor physics analytical predictions in terms of fuel cluster power with burnup have been found to be consistent with actual measurements. The fuel cluster power measurements (variation of cluster power with burnup) were found to be matching well with the reactor physics analysis predictions. The peak fuel cluster peak linear rating during the irradiation was evaluated to be about 35 kW/m.

The experimental cluster consists of six fuel pins around a central spacer capture rod assembled together by structural components and the salient parameters of the fuel pins are given in Table 5.

TABLE 5. SALIENT PARAMETERS OF EXPERIMENTAL AHWR TYPE FUEL PIN

Parameter	Value
Pellet outer radius (mm)	4.85
Pellet end geometry	Flat
Fuel density (%TD)	93
Clad inner diameter (mm)	10.0
Clad outer diameter (mm)	11.2
Active fuel stack length (mm)	3000
Plenum volume (cc)	13.23
Fuel surface roughness (microns)	0.8
Clad surface roughness (microns)	0.8
Fill gas and Pressure (bar)	He, 3.0
UO_2 fraction in (Th-U) MOX pins	0.11
PuO_2 fraction in (Th-Pu) MOX pins	0.01

The fuel performance analysis that is required for these experimental thoria based MOX/TOX fuel pins are similar to that carried out for UO_2 fuels. The fuel pin performance behaviour was analysed by using modified GAPCON-Thermal computer code. The code has the thermo-physical properties of the thoria-based fuel like thermal conductivity, heat capacity, thermal expansion, etc. The burnup degradation factors and density correction factors available for urania fuels have been used for analysing the thoria based fuels. The various fuel performance phenomena viz. fuel densification, fuel relocation, thermal expansion, swelling, fission gas

release etc. are modelled. The fuel pin power envelope and the fuel pin power axial distribution used in the analysis are shown in Figs. 12(a) and 12 (b) respectively. The salient results of the fuel performance analysis are given in Table 6.

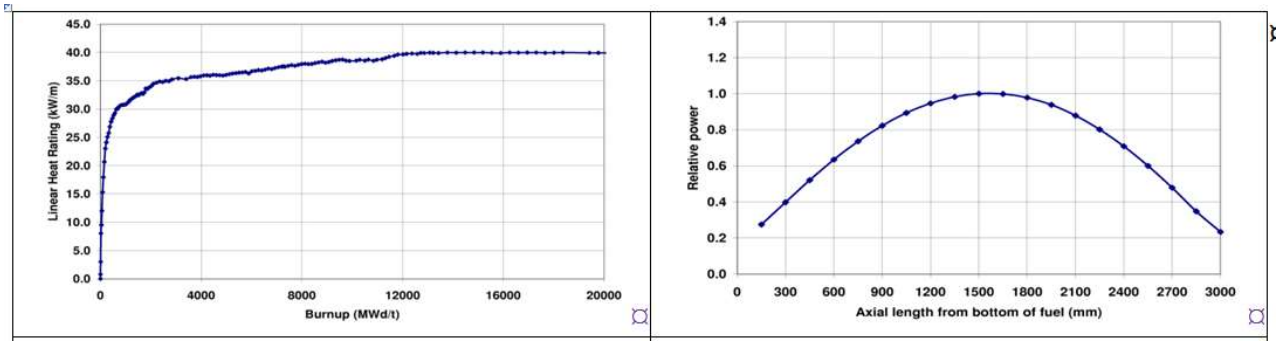

(a) Power history for the analysis (b) Axial power distribution in fuel pin

FIG. 12. Power profile for analysis of experimental AHWR type fuel pins (courtesy of P. Mishra, BARC).

TABLE 6. PERFORMANCE ANALYSIS FOR EXPERIMENTAL AHWR FUEL PINS

S. No.	Parameter	Units	Linear power rating (kW/m)			
			35	40	35	40
			(Th-Pu) TOX pins		(Th-LEU) MOX pins	
1	Peak fuel centre temperature	(°C)	1016	1114	1031	1207
2	Fission gas release at STP	(mm^3)	233	577	243	911

2.5.2. PHWR fuels

Two types of fuel clusters consisting of short fuel pins designated as AC-6 and BC-8 were irradiated in the pressurized water loop (PWL) of a research reactor in BARC. Five fuel pins were arranged in one cluster (AC-6). These fuel pins contained sintered pellets of (Th-4%Pu) O_2. Free standing Zircaloy-2 cladding tubes were used for this cluster (AC-6). For other cluster (BC-8), collapsible graphite coated Zircaloy-2 cladding tubes were used and the fuel pins contained UO_2, ThO_2, (Th-6.75%Pu) O_2 and (U-3%Pu) O_2 sintered pellets [5].

The thermal neutron flux, the temperature and pressure of the coolant in the loop was $5x10^{13}$ n/cm2/sec, 240° C (513^0K) and 105 kg/cm^2 respectively. The linear heat rating of the fuel pins was in the range 35–42 kW/m. The one fuel cluster (AC-6) was irradiated up to a calculated fuel burnup of 18.5 GW. d/tHM. The BC-8 fuel cluster was irradiated up to a calculated average fuel burnup of 4.5 GW. d/tHM. The burnup of the peak rated fuel pin was calculated to be 10.8 GW. d/t (HM).
Post irradiation examination (PIE) of the fuel pins from the two fuel clusters was carried out in the hot cell facility of BARC. Irradiated fuel clusters (AC-6 and BC-8) are shown in Fig. 13 and Fig. 14. Non-destructive examination of the fuel pins namely visual examination, fuel pin

diameter measurement, leak testing, gamma spectrometry, gamma scanning, ultrasonic testing and eddy current testing were carried out. Destructive examination included fission gas analysis and microstructural examination. Microstructural characterization on the fuel samples taken from the fuel pins was carried out using optical microscopy, scanning electron microscopy, β-γ autoradiography and α-autoradiography techniques.

The visual examination was carried out on fuel clusters as well as individual pins of the cluster using a wall mounted periscope. No abnormality or defects of any type was visible on the surface of the cladding of the fuel pins. Visual examination of the fuel pins did not show any evidence of corrosion or discoloration of cladding surface.

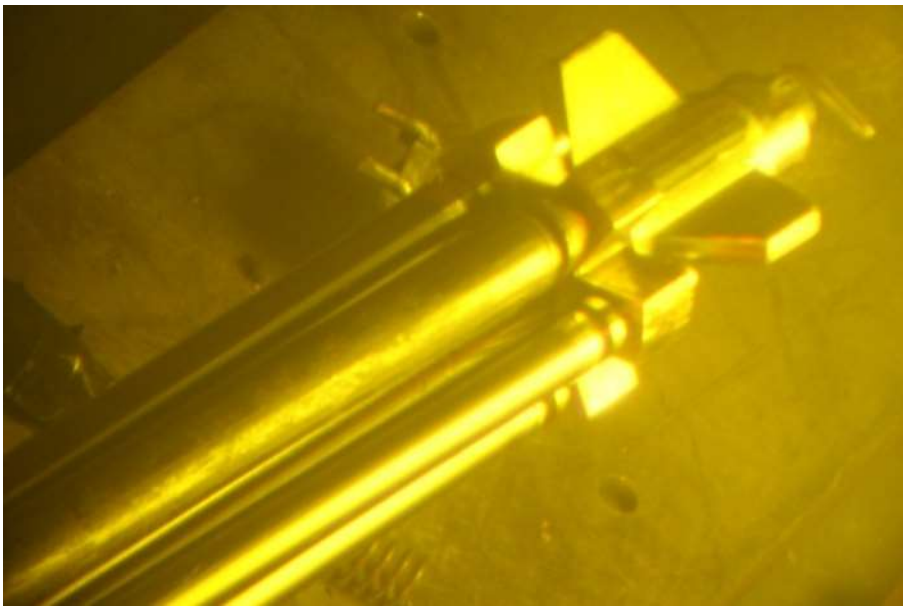

FIG. 13. Periscopic view of AC-6 fuel cluster (courtesy of P. Mishra, BARC).

FIG. 14. Periscopic view BC-8 fuel cluster from one end (courtesy of P. Mishra, BARC).

Conventional fuel etching techniques to reveal the grain structure could not be applied to thoria based fuel because of its chemical inertness. Hence, fractured pieces of fuel were used to

prepare replica samples. Examination of the replica foil with impressions of the fuel grains was carried out under a scanning electron microscope (SEM). SEM micrograph showing the impressions of the fuel grains from TH-5 fuel pin of AC-6 cluster on the replica foils is shown in Fig. 15 (a). Study of the morphology and size of the fuel grains was done using the replica micrographs. As shown in the figure, bimodal grain size distribution was observed in few regions; larger grains up to 30 μm and small grains of 2-5 μm size. The average grain size was measured to be 14 μm. The average grain size and distribution in the fuel was similar to that of the as-fabricated fuel. Observations indicated absence of grain growth in fuel during irradiation. Examination of grains sticking on the replica foil showed submicron size fission gas bubbles on the surfaces of smaller grains as shown in Fig. 15 (b).

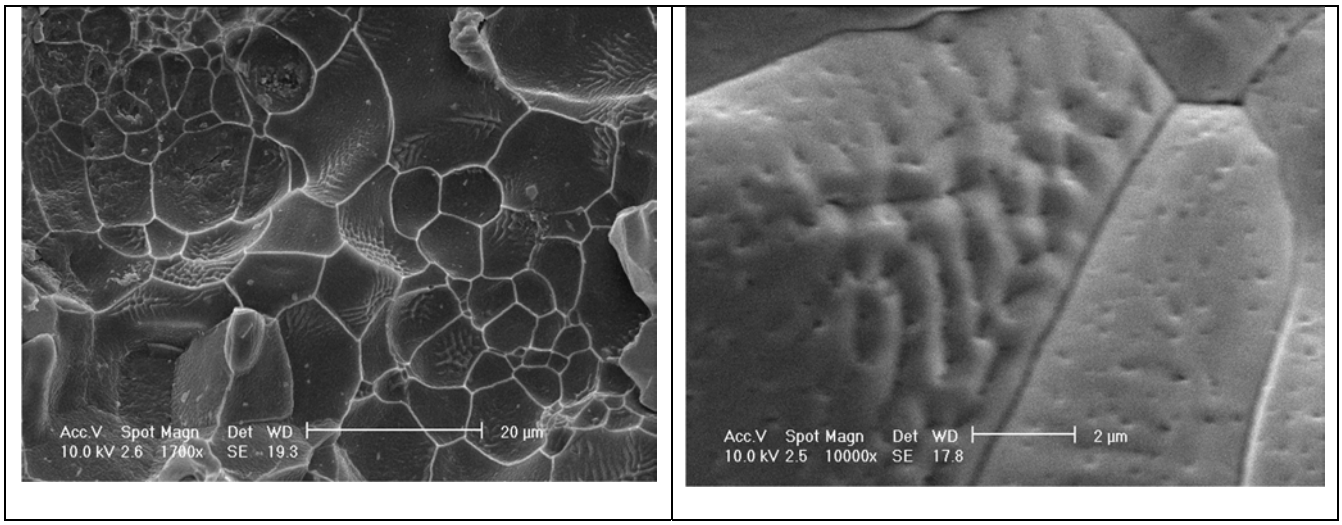

(a) (b)

FIG. 15. (a) Impressions of fractured grains on replicating foil (b) Grain faces of fuel showing fine fission gas bubbles (courtesy of P. Mishra, BARC).

Examination of metallographic samples taken from the fuel pin; TH-2 revealed presence of a massive hydride blister in the cladding. The cladding defect in the photomacrograph appeared as cracks on the inner surface of the cladding. A higher β-γ activity was noticed in the fuel close to region of defect in the cladding, indicating a cooler area in the fuel, probably due to ingress of water from the defected clad at that location. However, no wash out of fuel was observed. Massive hydride blister formed on the inner surface of the cladding along with cracks was observed during the examination.

Examination of the replica (see Fig. 16 (a)) prepared from the fractured pieces of the (Th-Pu) O_2 (TOX)fuel from pin P-02 of BC-8 cluster was carried out to measure fuel grain size. The average grain size in the fuel was observed to be 30 μm, which was similar to the grain size in the as-fabricated fuel. Grain growth was absent in the fuel.

Fractured pieces of fuel grains sticking on the replicating foil are shown in Fig. 16(b). Surface of most of the grains did not show any feature except for a few locations which revealed fission gas bubbles on the grain face. Presence of fission gas bubbles on a face of the grain of (Th-Pu) O_2 fuel and most faces devoid of the bubbles shows the presence of a Pu-rich region at that face.

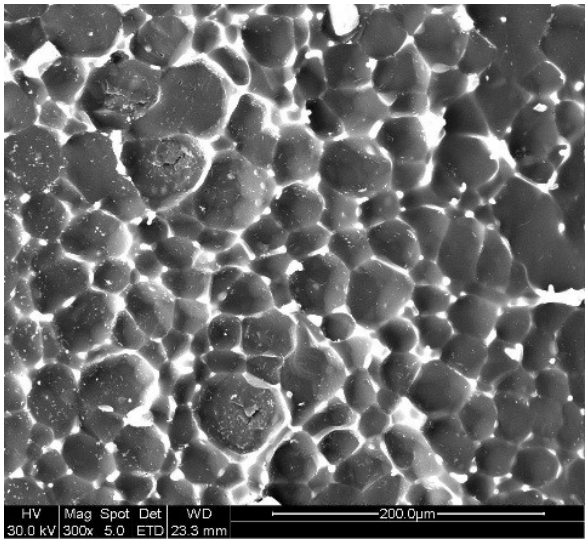

FIG. 16. (a) Replica of fractured piece of (Th-Pu)O_2 fuel from P-02 fuel pin (courtesy of P. Mishra, BARC).

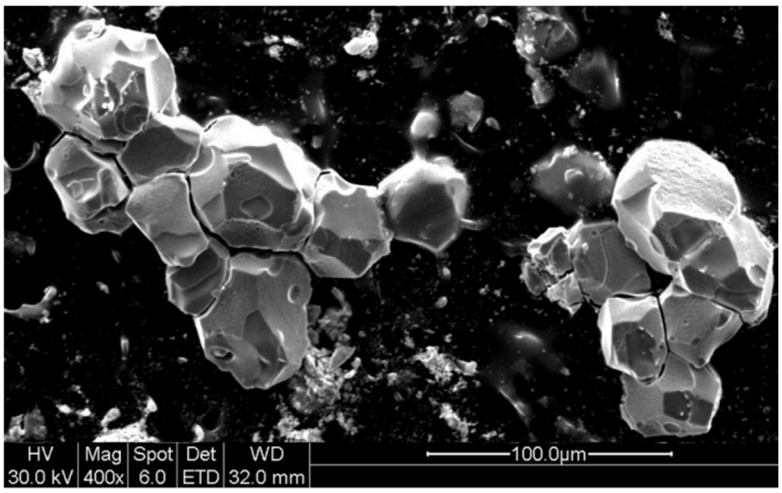

FIG. 16. (b) Grains of the Th-Pu TOX fuel (courtesy of P. Mishra, BARC).

From the above observations, it may be concluded that four fuel pins out of five pins of AC-6 cluster remained intact during irradiation. One fuel pin showed an internal hydride defect. Absence of fuel wash out in the failed fuel pin indicates better performance of thoria based fuels under defected conditions. All the pins of BC-8 cluster were found to be intact after irradiation. Other observations include:

- Negligible fission gas release (<1%);
- Very less craking in fuel;
- No fuel restructuring;
- No swelling and dimensional changes;
- Absence of any fuel clad interaction;
- No fission product migration.

These observations indicated that good performance of thoria based fuels during irradiation and may be attributed to lower fuel central temperature of 1100^{O} C (estimated) and high thermal conductivity of fuel.

2.6. DRY REPROCESSING OF THORIA AND THORIA BASED FUEL FOR HEAVY WATER REACTOR

2.6.1. Fluoride volatility process

Reprocessing of used thoria-based fuel is one of the eleven key science and technology areas that are being studied as part of the Thoria Roadmap Project at Canadian Nuclear Laboratories (CNL, formerly Atomic Energy of Canada Ltd). The most widespread method for reprocessing used thoria fuel is the aqueous thorium extraction process (THOREX) which is based on the well established plutonium-uranium extraction (PUREX) process for reprocessing used UO_2 fuel. CNL studied the THOREX process extensively in the 1970s and 1980s under the Thorium Fuel Reprocessing Project at the Whiteshell Nuclear Research Establishment. More recently, CNL has studied alternative methods to reprocess thoria-based fuel.

Fluoride volatility is a non-aqueous reprocessing method that has been well studied for uranium-based fuel [6–8]. It employs the high chemical reactivity of fluorine gas or other fluorinating agents to convert the species in irradiated fuel to fluoride compounds. The relative volatilities of the fluorinated compounds are exploited to separate the fuel constituents by distillation or other methods. Table 7 provides a listing of the melting points and boiling points of the fluorides of actinide and fission product elements.

Fluoride volatility has also been studied as a method of reprocessing used thoria-based fuel [9–11]. As shown in Table 7, the boiling points of uranium hexafluoride and thorium tetrafluoride differ significantly. It is therefore possible to separate fissile ^{233}U from irradiated thoria fuel by fluorination. Reports from Oak Ridge Nuclear Laboratory describe fluoride volatility experiments on $(ThU)O_2$ sol-gel microspheres containing 3.9% uranium [9]. Microspheres with size ranges between 149–210 microns were fluorinated with pure fluorine at temperatures between 753 and 930˚K for up to 3.5h. A maximum of 15% of the uranium was removed from the microspheres due to their low porosity and large thorium content, both of which impeded diffusion of fluorine into the microspheres.

A study from Kali-Chemie AG in Hannover, Germany investigated fluoride volatility reprocessing of thorium containing fuels in a fixed bed and in a fluidized bed [10]. Materials tested were unirradiated sintered particles of U/Th oxides or oxidized U/Th carbides as well as mixtures of uranium and thorium oxides with non-active fission product elements (Zr, Cs, Mo, Ru, Sr, Ba, Rb, Te, Pd). Particles were 0.3-0.8 mm and the ratio of U:Th was 1:5 or 1:20. Five grams of material was used per experiment and the fluorinating gas mixture was 1:1 F_2 to N_2 at a flow rate of 8 L/min. The various combinations of fluorination, hydrofluorination, and pyrohydrolysis cycles at varying temperatures were studied. Volatilization of as much as 99.5% of the uranium from the samples was reported.

A group from the Department of Nuclear Engineering at Kyoto University studied the fluoride volatility process on $(ThU)O_2$ samples in a small boat and in a fluidized bed [11]. The unirradiated fuel material with a Th:U ratio of 3 to 1 was crushed to a particle size below 88 microns and fluorinated at temperatures between 450^0C (723^0K) and 580^0C (853^0K). It was discovered that particle agglomerates formed due to the exothermic fluorination reaction using 100% F_2 at temperatures above 500^0C (773^0K). The agglomerates inhibited the gas solid

reaction and to mitigate the problem of agglomeration, the researchers varied the concentration of fluorine parabolically with time at the early stages of fluorination over durations of 10 minutes and 60 minutes. Using the longer duration, over 99% of the uranium was volatilized from the sample within 4 to 5h at a temperature of 580^{0}C (853˚K). Reaction temperature and particle size were also investigated as variables in the study. Higher temperatures and smaller particle sizes resulted in greater uranium volatilization.

TABLE 7. MELTING AND BOILING POINTS OF FLUORIDES OF ELEMENTS FOUND IN IRRADIATED THORIA FUELS

Compound	Melting point (K)	Boiling point (K)	Compound	Melting point (K)	Boiling point (K)
UF_3	~1775	decomposes	TeF_6	---	238 (sub)
UF_4	1233	1693	FeF_2	1375	~2075
UF_5	<675	---	FeF_3	~1275	~1375
UF_6	338	329 (sub)	NiF_2	~1275	~1875
PaF_5	---	<725	CoF_3	~1475	~1575
PuF_3	1698	2550	CrF_3	~1375	~1675
PuF_4	1310	---	RuF_5	374	586
PuF_6	324	335	RhF_4	---	1025
ThF_4	1383	1953	RhF_5	---	>575
ZrF_4	1191	1176 (sub)	PdF_3	---	~875
NbF_5	290	308	SnF_2	>875	>1475
MoF_6	290	308	SnF_4	---	927 (sub)
SbF_3	565	592	BaF_2	1558	2490
IF_5	282	373	SrF_2	1623	2733
TeF_4	403	557	CeF_3	1597	2573

At CNL, a fluoride volatility experimental apparatus was developed to perform experiments on unirradiated (ThU)O_2 fuel and simulated irradiated thoria fuel. The apparatus allowed for small, fixed powder bed fuel samples in alumina sample boats to be exposed to a fluorine gas mixture at elevated temperatures. Experimental variables that were studied were temperature and particle size.

Unirradiated (Th, U) O_2 fuel samples with particle sizes less than 45 microns were exposed to a fluorine gas mixture for a total of 6 hours at a gas flow rate of 30 mL/min, with intermediate crushing steps after 2 and 4 hours or exposure, at temperatures between 400^{0}C (673°K) and 700^{0}C (973°K). The amount of uranium volatilized was greatest at 700^{0}C (973°K) and decreased with lower temperatures. Less than 3% of the original uranium content in the sample remained after 6 hours of total exposure at 700^{0}C (973°K). The amount of uranium volatilized as a function of the fluorine exposure time indicated that after two hours of exposure, approximately 11.5% of the original uranium content remained in the sample. After four hours

of exposure with an intermediate crushing step after 2h, approximately 4.2% of the original uranium content remained in the sample. After six hours of exposure with intermediate crushing steps after 2h and 4h of exposure, less than 2% of the original uranium content remained in the sample. The intermediate crushing steps described above were found to be important to expose uranium in the samples to fluorine gas.

A simulated irradiated thoria fuel sample representing low burnup pure thoria and containing non-active fission product and minor actinide simulants was exposed to the fluorine gas mixture for a total of 6 hours at a gas flow rate of 30 mL/min, with intermediate crushing steps after 2 and 4 hours of exposure, at 700^0C (973°K). Uranium removal of approximately 99.7% was achieved in this experiment.

Experiments on unirradiated thoria material were followed up with fluoride volatility experiments on irradiated thoria fuel. The experiments were performed in the hot cells at Canadian Nuclear Laboratories. Small samples of irradiated material were exposed to a fluorine gas mixture at 700^0C (973˚K) for various exposure times.

2.7. THERMO PHYSICAL PROPERTIES OF THORIA BASED AHWR FUELS

(Th-^{233}U) O_2 (TOX) and (Th-Pu) O_2 (MOX) have been considered as the proposed fuels for AHWR. The thermo-physical data of these fuels plays an important input to the fuel designers to predict fuel irradiation performances till the designed discharge burnup is achieved leading to better fuel economics of nuclear power plants. The data also acts as an effective tool for the evaluation of reactor performances in normal and accidental conditions. The data base generated for some important properties like thermal conductivity, thermal expansion, high temperature hardness, fracture toughness etc. of these fuel systems have been presented and analysed.

2.7.1. Material

Sintered pellet samples of ThO_2, ($Th_{1-y}U_yO_2$ containing 2, 4, 6, 10, 20 % UO_2, and ($Th_{1y}Pu_y$) O_2 containing 2, 4, 6 and 10% PuO_2 were fabricated by powder pellet route, involving mechanical mixing, cold compaction and high temperature sintering. Progressive milling technique was used for obtaining good homogeneity in the fuel mix. ThO_2 powder was doped with 500 ppm MgO which act as sintering aid. The details of the fabrication procedure along with the fabrication flow sheet are given in Ref. [12]. Sintered samples of different size and shape were made which are suitable for different measurements.

2.7.2. Physical properties

2.7.2.1. Thermal conductivity/Thermal diffusivity

Thermal conductivity of the samples was determined from the experimentally measured thermal diffusivity data by transient Laser flash method [13]. Measurements were carried out in vacuum (6.65×10^{-3} Pa) in the temperature range 600^0C to 1600^0C (873^0K to 1873^0K). Clark and Taylor [14] method of radiation heat loss correction was used for the calculation of thermal diffusivity. Thermal conductivity was calculated by multiplying thermal diffusivity by heat capacity and density of the samples.

Thermal conductivity (k) has been calculated from the experimentally measured thermal diffusivity (α, cm^2/s), temperature corrected density (ρ, g/cc) and literature values of specific heat (C_p, (J/K)/kg) and using the following relation:

$$k = C_p \alpha \rho \text{ (W/m. K)} \quad (1)$$

The specific heat of mixed ($Th_{1-y}U_y$) O_2 and (Th_{1-y} Pu_y) O_2 solid solutions at any temperature were calculated from the literature values of specific heats for pure ThO_2 [15]and UO_2 [16] and PuO_2 using Neumann Kopp's law. For the normalization of thermal conductivity data corresponding to a density of 95% T.D. the following relation [17] was used:

$$f = (1 - p)^{1.5} \quad (2)$$

'f' is the fractional thermal conductivity and 'p' the porosity.

This equation gives the influence of randomly oriented, spherical porosity on the thermal conductivity. The thermal conductivity could be expressed in the following standard form applicable for insulators and dielectric solids:

$$k = 1 / (A+B \cdot T) \quad (3)$$

where 'A' and 'B' are constants representing influence of photon scattering by lattice imperfections and influence of phonon-phonon scattering respectively [18].

(Th1-yUy) O2

Thermal conductivity data as a function of temperature and UO_2 content could be expressed by the following relation:

$$k\,[ThO2] = 1/(-0.032 + 2.36 \times 10^{-4}\,T) \quad (4)$$

$$k[Th0.96U.04]O_2 = 1/(-0.045 + 2.62 \times 10^{-4}T \quad (5)$$

$$k[Th0.94U.06]O_2 = 1/(-0.029 + 2.60 \times 10^{-4}T) \quad (6)$$

$$k[Th0.90U.10]O_2 = 1/(-0.18 + 2.58 \times 10^{-4}\,T) \quad (7)$$

$$k[Th0.80U.20]O_2 = 1/(0.028 + 2.47 \times 10^{-4}\,T) \quad (8)$$

Subsequently thermal conductivity of ($Th_{1-y}U_y$) O_2 [95%TD] as a function of composition (y) and temperature (T (K)) in the temperature range 600 to 1600^0C (873 to 1873^0K) are given by:

$$k(y,T) = 1/[-0.046 + 0.003y + (2.52 \times 10^{-4} + 1.073 \times 10^{-7}\,y)T] \quad (9)$$

The data for ThO_2 and ThO_2-4% UO_2 are shown in Fig. 17 along with the experimental data of this study and those of others.

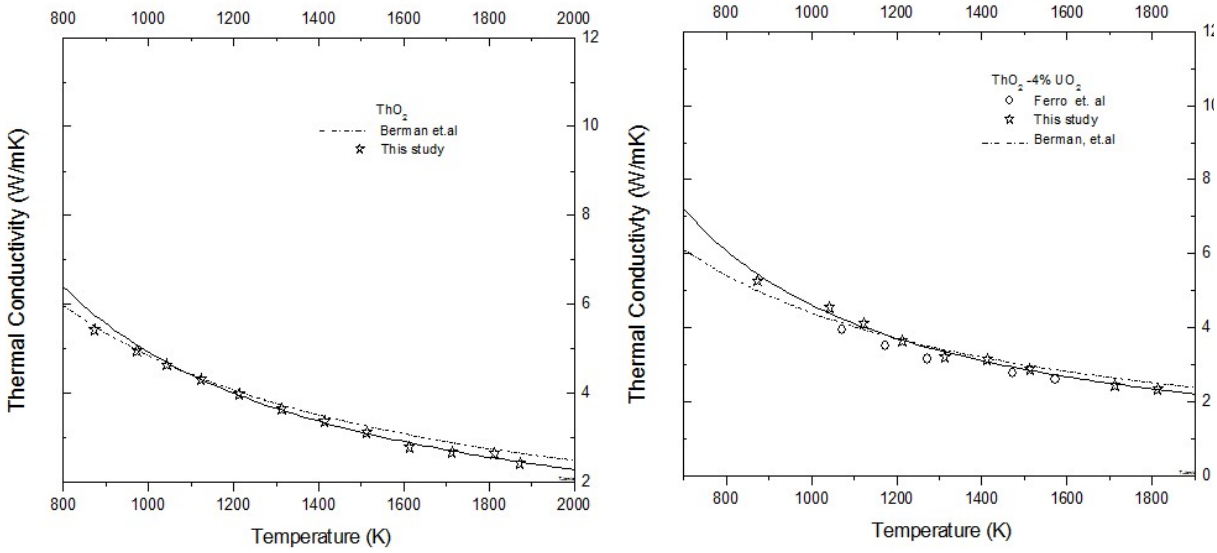

FIG. 17. Thermal conductivity of ThO_2 and $(Th_{0.96}U_{0.04})$ O_2 (95% T D) as a function of temperature (reproduced from Ref. [22]).

(Th1-y Puy) O2

Figure 18 shows the thermal conductivity (k) of $(Th_{1-y}Pu_y)$ O_2 as a function of temperature and PuO_2 content after correcting to 95% theoretical density. The thermal conductivity of $(Th_{1-y}Pu_y)$ O_2 as a function of composition, y [wt%], and temperature, T [K] can be expressed by:

$$k(y,T) = 1/[-0.084 + 1.74y + (2.63 \times 10^{-4} + 1.74 \times 10^{-4}\, y)\, T\,] \qquad (10)$$

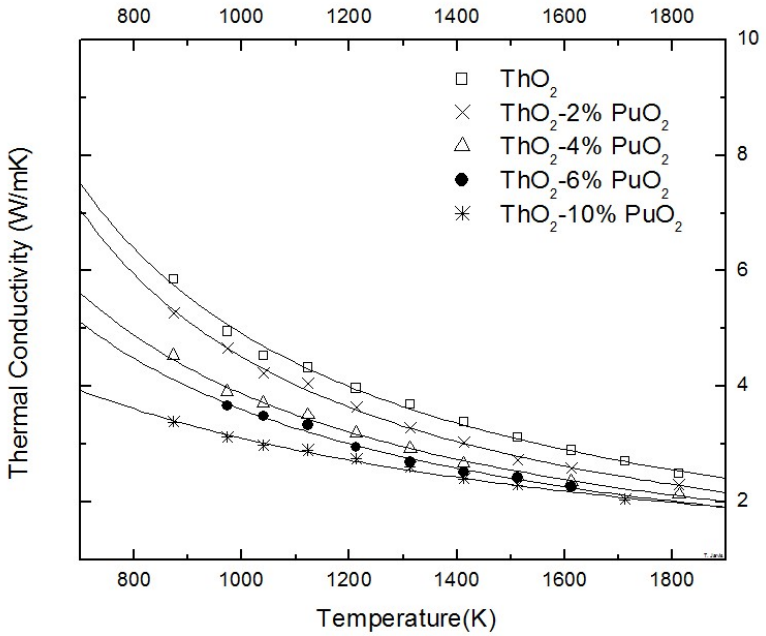

FIG. 18. Thermal conductivity of $(Th_{1-y}$ $Pu_y)$ O_2 as a function of temperature (reproduced from Ref. [22]).

2.7.2.2. Thermal expansion of ThO_2-UO_2 and ThO_2-PuO_2

Thermal expansion was measured by a high temperature horizontal dilatometer in the temperature range 27^0C-1500^0C (300^0K –1773^0K). During the measurement, samples were heated continuously from room temperature to 1773K at a heating rate of 6K/min in argon atmosphere. The length change of the sample was measured continuously by a LVDT maintained at constant temperature. The dilatometer is capable of measuring a length change of ±0.1μm. The uncertainty (maximum) of measurement was found to be ± 5 %, in this temperature range from 300^0C-1500^0C (573^0K –1773^0K) for both ThO_2-UO_2 and ThO_2-PuO_2 solid solutions.

$(Th_{1-y}U_y)\ O_2$

Bakker et al [15] estimated the percentage linear thermal expansion data of $(Th_{1-y}U_y)\ O_2$ ($0<y<1$) by obtaining the linear interpolation of the values of Touloukian [19] and Martin [20]. He obtained two different relations in two different set of temperature ranges:

$$\left(\frac{\Delta L}{L_0}\right) \times 100 = -0.18 - y0.087 + (5.10 \times 10^{-4} + y4.70 \times 10^{-4})T + (3.73 \times 10^{-7} - y4.002 \times 10^{-7})T^2 - (7.59 \times 10^{-11} - y11.98 \times 10^{-11})T^3$$

$$(for\ 273\ K < T < 923\ K) \quad (11)$$

$$\left(\frac{\Delta L}{L_0}\right) \times 100 = -0.18 - y0.15 + (5.097 \times 10^{-4} + y6.69 \times 10^{-4})T + (3.73 \times 10^{-7} - y6.16 \times 10^{-7})T^2 - (7.59 \times 10^{-11} - y19.784 \times 10^{-11})T^3$$

$$(for\ 923\ K < T < 2000\ K) \quad (12)$$

Percentage linear thermal expansion obtained in this study for ThO2 containing 4% and 10% UO2 (300≤T≤1473K) are given by:

$$\left(\frac{\Delta L}{L_0}\right) \times 100 = -0.27 + 8.15 \times 10^{-4}T + 2.22 \times 10^{-7}T^2 - 8.73 \times 10^{-11}T^3 \quad (13)$$

$$\left(\frac{\Delta L}{L_0}\right) \times 100 = -0.24 + 6.8341 \times 10^{-4}T + 4.44 \times 10^{-7}\ T^2 - 16.54 \times 734 \times 10^{-11}T^3 \quad (14)$$

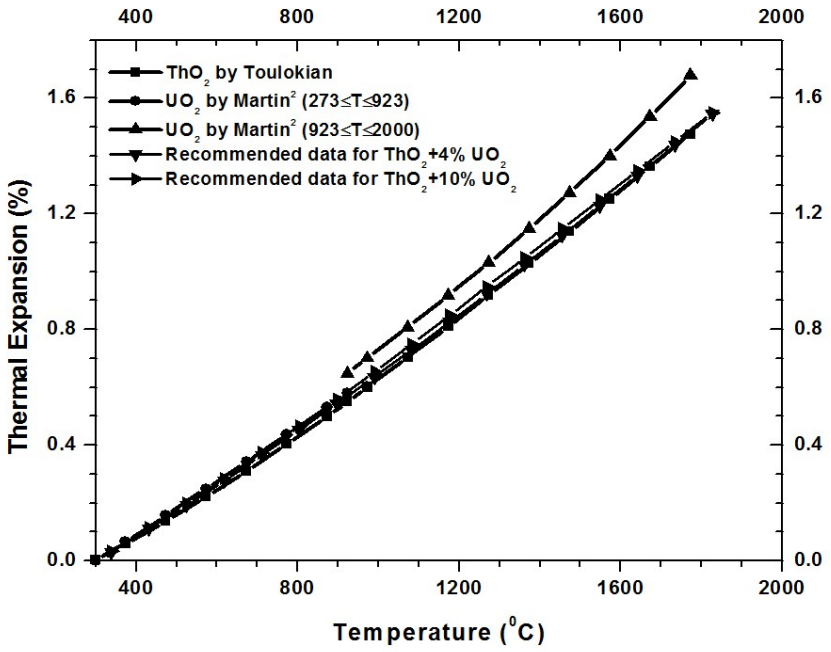

FIG. 19. Thermal expansion data for ThO2 containing 4 and 10 % UO2 as a function of temperature along with literature data for ThO2(reproduced from Ref. [22]).

The data obtained by taking average between the experimental data and the data indicated by Bakker [15] for above compositions are given below and shown in Fig. 19 along with the data for ThO_2 and for UO_2 by Martin [20].

Thus, the percentage linear thermal expansion for ThO_2 containing 4% and 10% UO_2 (300≤T≤1773K) are given by:

$$\left(\frac{\Delta L}{L_0}\right) \times 100 = -0.25 + 7.76 \times 10^{-4}T + 1.21 \times 10^{-7}T^3 - 4.74 \times 10^{-12}T^3 \quad (15)$$

$$\left(\frac{\Delta L}{L_0}\right) \times 100 = -0.23 + 7.01 \times 10^{-4}T + 2.43 \times 10 - 7T^3 - 5.17 \times 10^{-1}\ T^3 \quad (16)$$

ThO_2 and UO_2 form an ideal solid solution and the lattice parameter changes linearly at room temperature in the whole composition range hence, thermal expansion of the solid solutions $(Th_{1-y}U_y)\ O_2$ could be reasonably approximated at various temperatures by taking linear interpolated expansion data of ThO_2 and UO_2 as per their weight fraction [21–22].

(Th1-yPuy) O2

The percentage linear thermal expansion for ThO_2 containing 2, 4, 6 and 10% PuO_2 are given below:

$$[PuO_2: 2\%]: \left(\frac{\Delta L}{L_0}\right) \times 100 = -0.35 + 9.31 \times 10^{-4}T + 2.92 \times 10^{-7}T^2 - 8.46 \times 10^{-1}\ T^3 \quad (17)$$

$$[PuO_2: 4\%]: \left(\frac{\Delta L}{L_0}\right) \times 100 = -0.38 + 11.4 \times 10^{-4}T + 1.87 \times 10^{-8}T^2 + 5.16 \times 10^{-12}T^3 \quad (18)$$

$$[PuO_2: 6\%]: \left(\frac{\Delta L}{L_0}\right) \times 100 \ = -0.372 \ + \ 10.5 \times 10^{-4}T \ + 2.37 \times 10^{-7}T^2 - 9.10 \times 10^{-1} \ T^3 \quad (19)$$

$$[PuO_2: 10\%]: \left(\frac{\Delta L}{L_0}\right) \times 100 \ = -0.44 \ + \ 13.5 \times 10^{-4}T \ - \ 1.56 \ \times 10^{-7}T^2 \ 5.67 \times 10^{-1} \ T^3 \quad (20)$$

Like thoria-urania system, ThO_2 and PuO_2 also form an ideal solid solution and thus thermal expansion of the solid solutions $(Th_{1-y}Pu_y)\ O_2$ (where 0<y<1) could be reasonably approximated at various temperatures by taking linear interpolated expansion data of ThO_2 and PuO_2 as per their weight fraction (Fig. 20).

$$\left(\frac{\Delta L}{L_0}\right) \times 100 \ = -0.18 - 0.049y + (5.08 \times 10^{-4} + 2.25 \times 10^{-4}y)T + (3.73 \times 10^{-7} - 2.51 \times 10^{-7}y)T^2 + (-7.59 \times 10^{-11} + 12.45 \times 10^{-11}y)T^3 \quad (21)$$

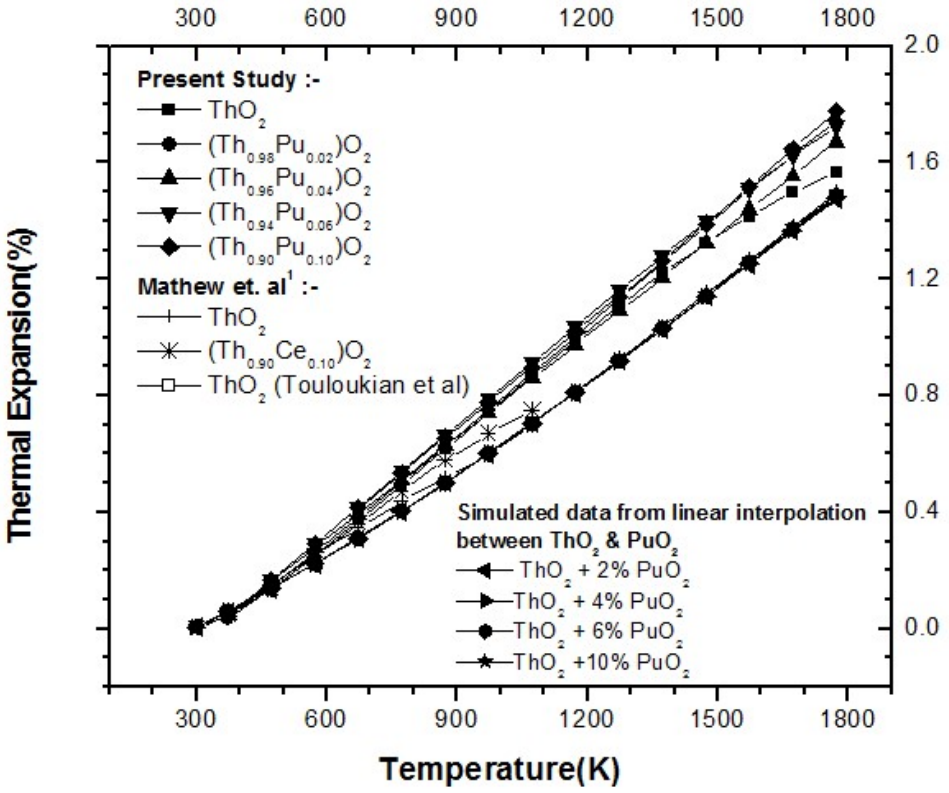

FIG. 20. Thermal expansion for $(Th_{1-y}Pu_y)O_2$ as a function of temperature showing both experimental and simulated data by linear interpolation method (reproduced from Ref. [22]).

2.7.2.3. Hot hardness

Hardness was measured using the relation: $H_V = 1.854 \cdot P_H / d^2$, where d is average diagonal length in micron and P_H is Indenter load in Kg. High temperature hardness was measured using a NIKON hot hardness tester. Hardness measurements were performed at room temperature and high temperatures on metallographically polished surface of the pellet. Vicker′s diamond pyramid indenter was used with an indentation load of 200g and dwelling time 5 seconds. At each temperature at least two to three indentions were made to arrive at a particular data.

High temperature hardness was measured at various temperatures from 227^0C -1327^0C (500^0K to 1600^0K) for ThO_2 and ThO_2 containing 4, 10 and 20% UO_2. It was observed that hardness decreased with increase in temperature and UO_2 content. For ThO_2-4% UO_2, the change in slope was observed at 1100K indicating the onset of creep processes. The predominant deformation mechanism expected from this temperature onwards would be the diffusion controlled climb, glide and grain boundary sliding.

2.7.2.4. Elastic constant

Elastic constants like Young's Modulus, Shear Modulus, Bulk Modulus, Poissons ratio etc. were calculated by pulse echo method by measurement of time of flight for Longitudinal and Shear wave velocities at ambient temperature. From the 'time of flight' data and 'thicknesses of the samples these constants were calculated using standard relations. A centre frequency of 5 MHz was used for both long wave and short wave transducer.

For isotropic media shear modulus 'G', Young's modulus 'E', bulk modulus 'K' and Poison's ratio 'ν' can be estimated from the longitudinal (V_L) and shear velocities (V_S) [23]. V_L and V_S are obtained from the experimentally measured time of flight and thickness of the sample at room temperature:

$$G = \rho V s^2 \tag{22}$$

$$E = G\left[\frac{3V_L^2 - 4V_S^2}{(V_L^2 - V_S^2)}\right] \tag{23}$$

$$K = \rho\left(\frac{3V_L^2 - 4V_S^2}{3}\right) \tag{24}$$

where ρ is density

$$\gamma = \frac{V_L^2 - 2V_S^2}{2(V_L^2 - V_S^2)} \tag{25}$$

2.7.2.5. Fracture toughness and compressibility

Fracture toughness was measured by indentation technique using Vickers diamond pyramid indenter. Indentations were made on metallographically polished surface of samples with a load of 1 Kg. when cracks generate from the corners of the indentations beyond a critical load, the crack lengths and the lengths of the diagonals were measured from which fracture toughness, fracture surface energy and fracture modulus were calculated using the following relation [24]:

$$K_{1C} = 0.016\sqrt{\frac{E}{H_V}} \times \frac{P_H}{c^{\frac{3}{2}}} \tag{26}$$

where 'c' is the half diagonal of the radial crack giving the surface trace (m), 'a' is half diagonal of the indent trace (m). Fracture surface energy, 'γ' and fracture modulus 'E_f' were calculated using following relations:

$$\gamma = \frac{(1-\gamma^2)(K_{1C}^2)}{2E} \tag{27}$$

$$E_f = \frac{K_{1C}^2}{J_{IC}} = \frac{2E}{1-\gamma^2} \tag{28}$$

Compressibility is one of the input parameters in calculating dilatational contribution to specific heat of the material and Gruneisen parameter. Compressibility 'β' can be expressed in terms of:

$$\beta = \left[\frac{\rho\left(3V_L^2 - 4V_S^2\right)}{3}\right]^{-1} = \frac{1}{K} \tag{29}$$

The results of the elastic properties measured by ultrasonic time of flight measurement method and the fracture toughness and fracture surface energy for ThO_2+2%UO_2 are given in Table 8.

TABLE 8. CALCULATED DATA FOR THO_2+2%UO_2 (95.72%T.D.) AT 298 K

Sr. No.	Property	Numerical value at 298 K
1	Lattice parameter, nm	0.559
2	Molar volume, m^3	2.636×10^{-5}
3	Coefficient of linear expansion, 1/K, (298-1600 K)	9.662×10^{-6}
4	Coefficient of volumetric expansion, 1/K, (298-1600 K)	2.899×10^{-5}
5	Theoritical density, Kg/m^3	10.019×10^{3}
6	Shear modulus, G GPa	97.899
7	Elastic modulus, E GPa	246.375
8	Bulk modulus, K GPa	169.9
9	Poison′s ratio, γ	0.2583134
10	Compressibility, β GPa^{-1}	5.886×10^{-3}
11	Micro-hardness (VHN)	787.11
	(GPa)	7.72
12	Yield stress (GPa)	2.147
13	Yield strain	0.00871
	(%)	0.871
14	Fracture Toughness, K_{1C} ($MPa*m^{0.5}$)	1.204
15	Fracture surface energy, J_{IC} (J/M^2)	2.744
16	Fracture Modulus, E_f ($\times10^{12}$) (Nm^{-2})	0.528

2.7.2.6. Yield stress(Y) and yield strain (e)

Yield stress of ceramics with ionic bond is calculated using relation [25]:

$$\frac{P_H}{Y} = \frac{H_V}{Y_{\sin\phi}} = 1 + 1.2\,ln\left[\left(\frac{E}{Y}\right) \times \pi^{0.5} \times \frac{\cot\phi}{8(1-\gamma^2)}\right. \tag{30}$$

where 'ϕ' is half of the indenter apex angle. Yield strain 'ε' is obtained from $\varepsilon = Y / E$.

2.8. CONCLUSIONS

The wide range of activities being carried out for the thoria fuel based AHWR has provided considerable insight into various aspects associated with large-scale utilization of thorium. The developmental studies which have focused on fuel fabrication and reactor design aspects have generated a large database for utilising thorium fuel. This experience has provided key elements for working out a road map to deploy thoria based fuels in water cooled reactors, especially in heavy water reactors.

An innovative dry reprocessing method for thoria based oxide fuels for PHWRs based on fluoride volatility process has been described. However, this is done in laboratory scale.

Some of the important thermo physical and mechanical properties data of $(Th_{1-y}U_y)O_2$ and $(Th_{1-y}Pu_y)O_2$ fuels system have been assessed/generated with precision. This includes generation of a data base on thermal conductivity, thermal expansion, hot hardness and bulk modulus, Young's modulus, Shear modulus, Poison′s ratio etc. These data will be of immense help as an input data for developing a computer code or to predict in-reactor fuel performance under normal and accidental condition.

3. THORIUM BASED MIXED OXIDE FUEL FOR LIGHT WATER REACTORS

3.1. THORIUM MOX FUEL FOR PLUTONIUM RECYCLING IN PWR

Today, the plutonium is recycled to some extent along with uranium, in the present operating LWRs in the form of U-Pu mixed oxide (MOX) to waste minimization, U-resourse saving, SNF stocks management and, to some extend, to dispose of excess plutonium. However, this is not an efficient process for Pu disposition as Pu is also produced from uranium. The more attractive process for excess Pu disposition is by the use of Th-Pu mixed oxide fuel (TOX). This not only eliminates production of new Pu, but also increases Pu destruction rate significantly. Studies have been performed on steady-state and accident analysis of 100% TOX PWR in comparison with 100% MOX PWR core.

In this report, 2D fuel assembly level analysis has been done. The analysis is dedicated

- To determine amount of Pu required in TOX and MOX for achieving standard fuel cycle length;
- To determine and also to compare control materials worth;
- To estimate and compare Pu destruction efficiency of TOX and MOX fuels.

In this work, the commercial lattice code HELIOS 1.9 [26] was used for neutronic analysis. The study involves the use of HELIOS library with 190 neutrons and 48 gamma energy groups.

3.1.1. Reference UOX PWR core

In order to compare the conventional uranium oxide (UOX) fuel with MOX and TOX, a typical four-loop Westinghouse PWR was used as a reference core. The fuel loading pattern, the burnable poison (BP) designs, and the beginning of cycle (BOC) exposure distribution were adopted of UOX PWR core were adopted from literature [27]. The fuel assembly, core parameters and the reactor core operating conditions are summarized in Table 9. The initial fuel

enrichment and loading pattern are shown in Fig. 21 [28]. In this work, the MOX and TOX fuel assembly geometry are considered to be fully compatible with that of the reference UOX core.

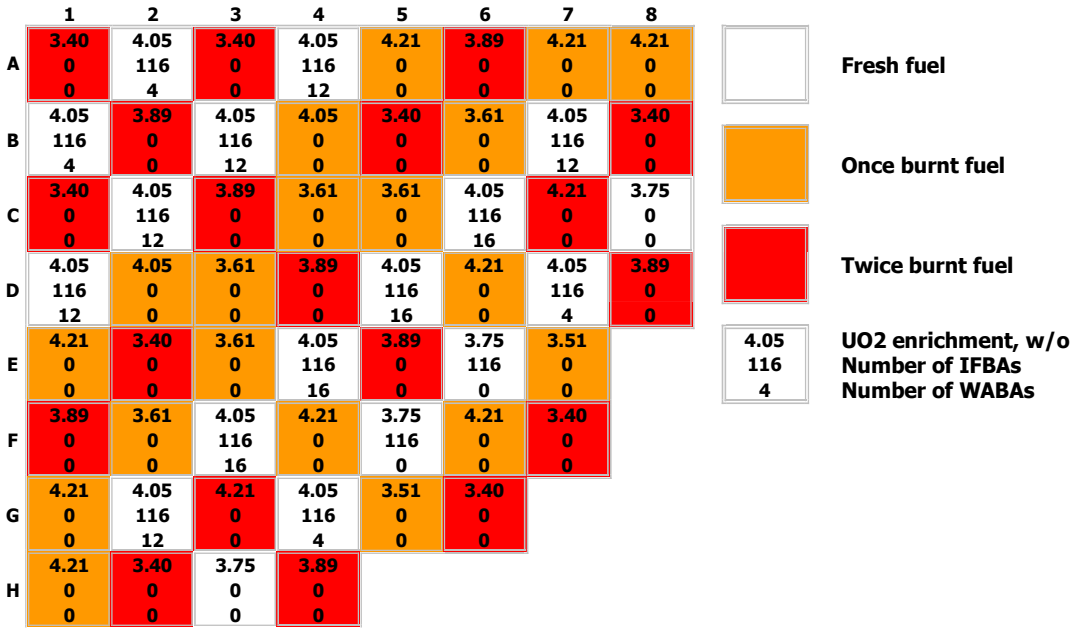

FIG. 21. Reference UOX core: loading pattern and initial enrichment (¼ core) (reproduced from Ref. [28] with permission courtesy of Elsevier).

TABLE 9. PARAMETERS OF REFERENCE UOX (reproduced courtesy of Elsevier [28])

Operating parameter	Value
Total thermal output, MW_{th}	3358
Number of fuel assemblies in the core	193
System pressure, bar	155
Total core flow rate, kg/s	22000
Core inlet temperature, ºC	265.5
Active fuel height, cm	366
Assembly array	17 × 17 pins
Total number of fuel rods per assembly	264
Assembly pitch, cm	21.5
Fuel rod pitch, cm	1.26
Number of guide tubes	25
Guide tube inner/outer radius, cm	0.5715/0.6120
Cladding outer radius, cm	0.4750
Cladding thickness, cm	0.0570
Cladding material	Zircaloy
Fuel enrichment, w/o of U-235	3.61 to 4.21
Fuel pellet radius, cm	0.4095

3.1.2. Determination of Pu loadings

The Pu loadings in the MOX and the TOX fuel were adjusted to achieve industry standard fuel cycle length of 18 calendar months assuming a three-batch fuel management scheme. This corresponds approximately to 490 effective full power days assuming a 90% capacity factor. The fuel cycle length was obtained by applying the Linear Reactivity Model (LRM) [29] to the results of 2D fuel assembly burnup calculations. Pu-containing fuels are known to have harder neutron spectrum than typical UO_2 fuel, increasing the leakage from the core. Therefore, the discharge burnup was estimated assuming the leakage reactivity of 0.35% which is somewhat higher than that of the typical UO_2 fuel. The actual leakage reactivity depends on several factors (i.e., fuel loading pattern) and can be accurately estimated only via 3D full core calculations. The considered fuel assembly geometry was identical to that of the reference UOX PWR core (Table 9). The initial Pu isotopic vector (Table 10) corresponds to that of a typical spent PWR fuel (4.2 w/o ^{235}U initial enrichment, 50 GW. d/t discharge burnup and 10 years of cooling). Accumulation of ^{241}Am from decay of ^{241}Pu was neglected so that ^{241}Am does not appear in the Pu vector. The assumed density of ThO_2 was 9.50 g/cm^3 while that of PuO_2 was 10.89 g/cm^3, which constitute 95% of their theoretical densities.

After several iterations the required Pu content was found to be equal to 7.85v/o and 8.60v/o for MOX and TOX fuels respectively.

Figure 22 shows the multiplication factor k-inf of the MOX and the TOX fuel assemblies as function of burnup. The k-inf of the UOX fuel with a ^{235}U enrichment required to achieve 18 months fuel cycle length was plotted for comparison purposes. The k-inf of the MOX and the TOX fuels exhibits a quite similar behavior during the burnup. Nevertheless, the reactivity swing of the Pu fuels is significantly lower than that of the UOX fuel. For this reason, the TOX and the MOX fuels will have a lower power level mismatch between fuel assemblies at different burnup levels as compared to the UOX fuel. Therefore, the radial core power peak is expected to be less pronounced in the mixed oxide cores than in the UOX core.

It is to be noted that within the MOX and the TOX fuel assemblies all fuel pins had an identical material composition. In other words, no inter-assembly enrichment zoning, typical for a pressurized water cooled reactor (PWR) core with partial MOX loading [30–31] was required to manage the fuel assembly power peaking.

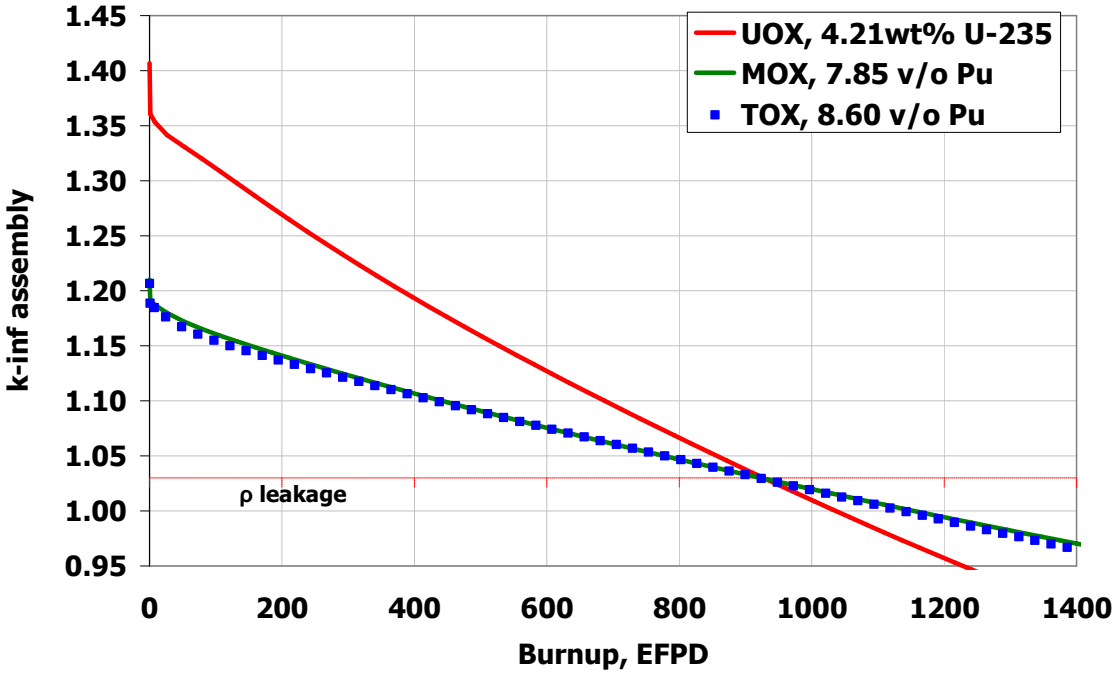

FIG. 22. Fuel assembly k-inf vs. burnup (reproduced from Ref. [28] with permission courtesy of Elsevier).

TABLE 10. INITIAL Pu ISOTOPIC VECTOR (reproduced courtesy of Elsevier [28])

Isotope	w/o
^{238}Pu	2.5
^{239}Pu	54.1
^{240}Pu	23.9
^{241}Pu	12.7
^{242}Pu	6.9

3.1.3. Reactivity control

Table 11 compares the boron worth (BW) of UOX, MOX and TOX fuels calculated on the fuel assembly level. The BW coefficient is defined as the change in reactivity per one ppm change in the soluble boron concentration and was calculated using the following equation:

$$BW = \frac{k_1 - k_2}{k_1 \times k_2 \times (B_1 - B_2)} \times 10^5 \left[\frac{pcm}{ppm}\right] \quad (31)$$

Where B_1 and B_2 are the two boron concentrations, while k_1 and k_2 are the corresponding criticality values. Table 11 reveals that the BW of the MOX and the TOX fuels is about one half of that of a typical UOX fuel. In PWRs, soluble boron (SB) is typically used in combination

with burnable poison for suppressing the excess reactivity. Slow reactivity changes due to fuel depletion, fission products buildup, variation in Xe concentration, etc. are compensated by adjusting the SB concentration. Although the concentration of SB is relatively easy to adjust, its maximum concentration is limited to about 2000 ppm, primarily by coolant chemistry considerations and the coolant temperature reactivity coefficient [32]. As a result, a much smaller amount of excess reactivity can be controlled by SB in Pu containing lattices than in conventional UOX ones.

TABLE 11. NATURAL BORON WORTH ESTIMATED ON FUEL ASSEMBLY LEVEL (PCM/PPM) (reproduced courtesy of Elsevier [28])

	UOX	MOX	TOX
BOL	-5.8	-2.5	-2.5
EOL	-9.5	-3.4	-3.7

BOL: beginning of life EOL: end of life

In this study, we proposed the use of SB enriched in ^{10}B to deal with reduced BW. The enrichment of boron from the natural level of about 20% to 40% brings BW of the Pu containing fuels close to the value of the UOX fuel. It is to be noted that enriched SB boron is commercially available and routinely used by several utilities [33].

To reduce further the SB requirements and to flatten the core radial power distribution, some of the fresh fuel assemblies in the MOX and the TOX cores contained 16 or 24 wet annular burnable absorber (WABA) rods with natural boron acting as neutron absorber. The utilized WABA rod design was identical to that of the reference UOX core.

The rod cluster control assembly (RCCA) considered in this work is a typical PWR spider type assembly with 24 identical rods. The rods are made of stainless steel and filled with a neutron absorbing material. Ag-In-Cd (AIC) alloy and B_4C are commonly used as control rod neutron absorbers. AIC is typically utilized in Western PWRs. Full B_4C control rods are routinely used in Russian VVERs [34]. In some of the Westinghouse PWRs, B_4C is utilized in hybrid Ag-In-Cd/B_4C control rods [35]. In order to select the control rod neutron absorbing material to be used, we compared the worth of the AIC and B_4C control rods in the UOX, MOX, and TOX lattices. The control rod worth was calculated at BOL as the difference in reactivity between rodded and unrodded fuel assemblies. Table 12 demonstrates that the worth of the AIC control rod in the MOX and TOX lattices is significantly reduced and constitutes only about 60% of that of the UOX fuel. On the other hand, the B_4C control rod worth of Pu-bearing fuels is comparable to those of AIC and B_4C control rods in UOX lattice. Therefore, in order to increase the individual control rod worth, we considered B_4C as a control rod absorbing material to be used in the MOX and the TOX cores.

TABLE 12. BOL CONTROL ROD WORTH RELATIVE TO THAT OF AIC UOX (reproduced courtesy of Elsevier [28])

	AIC	B4C
UOX	100%	115%
MOX	61%	92%
TOX	64%	103%

3.1.4. Plutonium destruction efficiency

Table 13 compares the Pu and the TRU incineration efficiency of the MOX and TOX cores. The Pu and the TRU generation rates in the UOX fuel are given as a reference. In the TOX core a somewhat higher initial Pu loading is required to achieve the target fuel cycle length as compared to the MOX core. Nevertheless, as it was expected, the Pu burning efficiency of the TOX fuel is significantly higher than that of the MOX fuel and is almost doubled. Moreover, the Pu destruction rates of the TOX are very close to those reported for 100% U-free PWR cores [36–37]. However, the overall TRU destruction rates in the TOX core are higher only by a factor of 1.5 due to the considerable amount of ^{233}U generated in the TOX core.

TABLE 13. Pu AND TRU INCINERATION PERFORMANCE (reproduced courtesy of Elsevier [28])

	UOX	MOX	TOX
Initial Pu, kg/assembly	0.0	38.4	42.0
Discharged Pu, kg/assembly	5.3	26.1	18.2
Discharged TRU kg/assembly	5.8	28.2	20.3
Discharged U-233 + Pa-233, kg/assembly	-	-	6.9
% Pu burnt	-	32%	57%
% TRU burnt	-	26%	35%*
Pu generation rate, kg/GWe-Year	+238.0	-530.7	-1031.5
TRU generation rates, kg/GWe-Year	+261.6	-438.4	-638.9*

* Including U-233 and Pa-233, not including other actinides from the Th-232 chain

3.2. DESIGN OF MOX AND TOX FULL CORES

3.2.1. Reference PWR core

A typical four-loop Westinghouse PWR was selected as a reference core for the comparison of the conventional UOX fuel with the MOX and TOX fuels. The real UOX PWR core operational parameters including fuel loading pattern, burnable poison (BP) designs, and beginning of cycle (BOC) exposure distribution were adopted from Galperin et al [27]. The reference UOX core included nine fuel types with different initial enrichments and BP designs. Both Wet Annular Burnable Absorber (WABA) rods and Integral Fuel Burnable Absorber (IFBA) rods were used. The major fuel assembly and core parameters as well as the reactor core operating conditions

of the UOX core are summarized in Table 9. The initial fuel enrichment and loading pattern are shown in Fig. 23a. The MOX and TOX fuel assembly geometry considered in this work is fully compatible with that of the reference UOX core.

3.2.2. Determination of Pu loadings

As previously reported, the required Pu content was found to be equal to 7.85v/o and 8.60 v/o for MOX and TOX fuels respectively. The assumed initial Pu isotopic vector (Table 13) corresponds to that of a typical spent PWR fuel (4.2 w/o ^{235}U initial enrichment, 50 GW. d/t discharge burnup and 10 years of cooling).

3.2.2.1. Operational parameters: TOX and MOX cores

Major operational parameters of the MOX and TOX cores (Fig. 23(b)) are similar to those of the reference UOX core (Fig. 23(a)). Nevertheless, some modifications were introduced in order to cope with some specific challenges associated with the use of Pu-bearing fuels. The RCCA (¼ core) locations are given in Fig. 24. The fuel assembly and core parameters and the reactor core operating conditions of the UOX, MOX, and TOX cores are compared in Table 14. The summary of modifications is given in the following sub-sections.

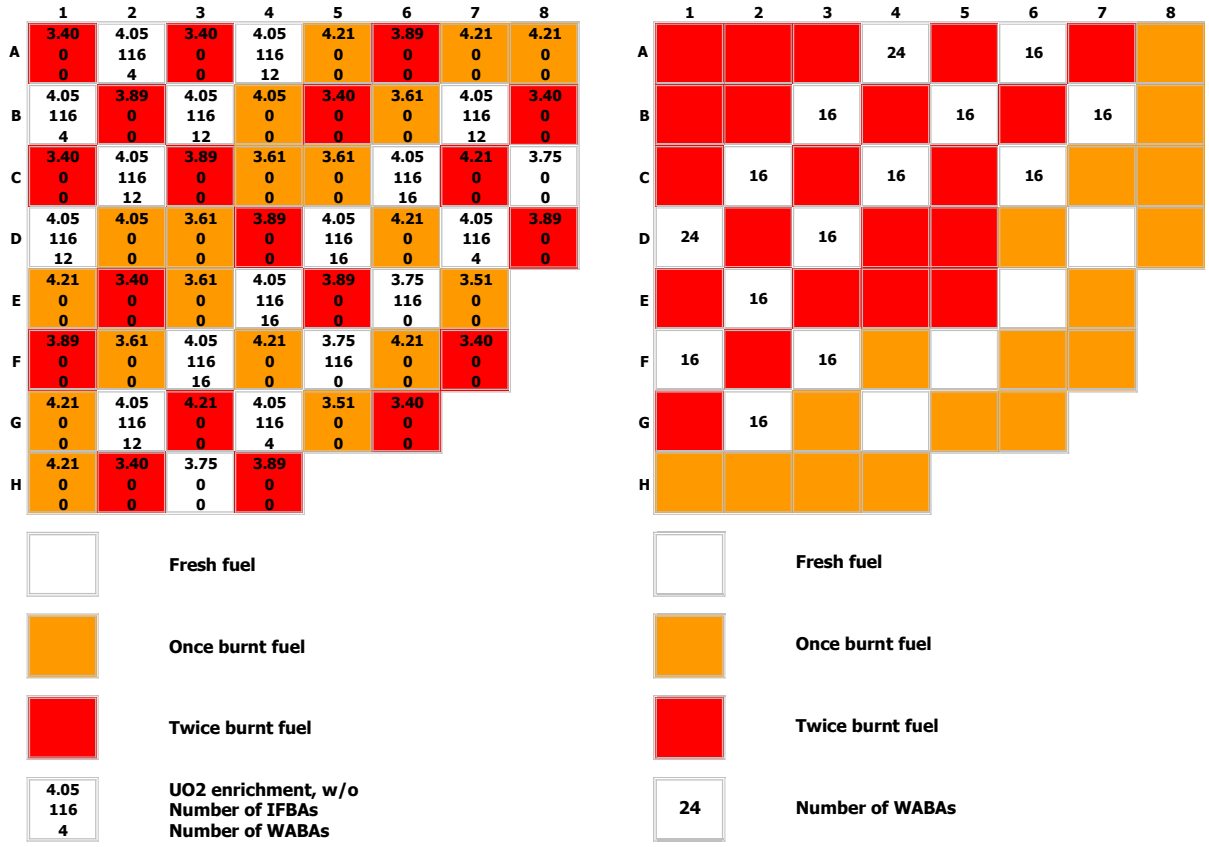

(a) UOX core (b) MOX and TOX cores

FIG. 23. UOX, MOX and TOX cores loading patterns (¼ core) (reproduced from Ref. [28] with permission courtesy of Elsevier).

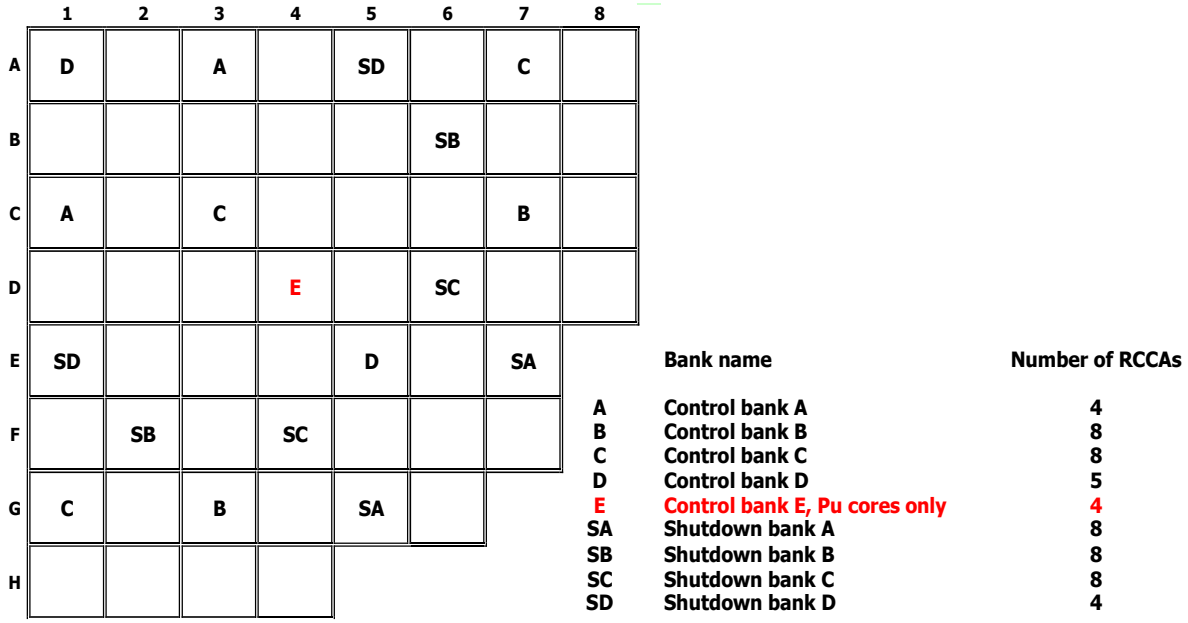

FIG. 24. RCCA locations (¼ core) (reproduced from Ref. [28] with permission courtesy of Elsevier).

TABLE 14. OPERATIONAL PARAMETERS OF THE CONSIDERED CORES (reproduced courtesy of Elsevier [28])

Operating parameter	UOX	MOX	TOX
Core			
Total thermal output, MW_{th}	3358	3358	3358
Number of fuel assemblies in the core	193	193	193
Average core power density, W/cm^3	104	104	104
System pressure, bar	155	155	155
Total core flow rate, kg/s	22000	22000	22000
Core inlet temperature, ºC	265.5	265.5	265.5
Soluble boron B-10 content	natural	40%	40%
Fuel assembly			
Active fuel height, cm	366	366	366
Assembly array	17 × 17	17 × 17	17 × 17
Total number of fuel rods per assembly	264	264	264
Number of IFBA rods per assembly	116	-	-
Number of WABA rods per assembly	4 to 16	16 to 24	16 to 24
Assembly pitch, cm	21.5	21.5	21.5
Fuel rod pitch, cm	1.26	1.26	1.26
Number of guide tubes	25	25	25
Guide tube inner radius, cm	0.5715	0.5715	0.5715
Guide tube outer radius, cm	0.6120	0.6120	0.6120
Fuel Rod			
Cladding outer radius, cm	0.475	0.475	0.475
Cladding thickness, cm	0.057	0.057	0.057
Cladding material	Zircaloy	Zircaloy	Zircaloy
Fuel pellet			
Fuel material	UO_2	$(U\text{-}Pu)O_2$	$(Th\text{-}Pu)O_2$
Fissile content	3.61 to 4.21 w/o of U-235	7.85 v/o of Pu	8.60 v/o of Pu
Fuel pellet radius, cm	0.4095	0.4095	0.4095
IFBA burnable poison			
IFBA coating thickness, mm	0.0105	-	-
BP material	ZrB_2	-	-
BP loading, mg/cm of B-10	0.62	-	-
WABA burnable poison			
BP material	Al_2O_3-B_4C	Al_2O_3-B_4C	Al_2O_3-B_4C
BP loading, g/cm of B-10	0.006	0.006	0.006

3.2.2.2. Reactivity control

For the Pu bearing lattices having reduced control rod worth due to neutron spectrum hardening, the following modifications to reactivity control systems were introduced:

- Boron enriched up to 40% of ^{10}B is used as a solution to the issue of reduced soluble boron worth;
- Strong absorbing B_4C along with an extra control rod bank in place of AIC alloy;
- WABA BP with variable number of rods was used to flatten the core power distribution;
- In the UOX core, there are 4 control and 4 shutdown banks. In the MOX and TOX cores one additional control bank (E) was introduced to mitigate further the reduced control rod worth. The locations of the RCCAs for the UOX, MOX, and TOX cores are shown in Fig. 24.

3.2.2.3. Fuel loading pattern

A 3-batch in-core fuel management scheme was used for the full core 3D simulation of both 100% MOX and 100% TOX cores. Following several transition cycles, equilibrium loading patterns with a typical low-leakage configuration was established for both cores (Fig. 23(b)).

3.3. FULL CORE 3D ANALYSIS

3.3.1. Critical boron concentration, radial power peaking

The critical boron concentration during the burnup for all three cores is shown in Fig. 25. Both MOX and TOX cores achieve a similar fuel cycle length of about 490 effective full power days. For these cores, the maximum boron concentration is clearly below 2000ppm, as mandated by operational requirements, and is even lower than that of the UOX core. This is mainly due to the use of 40% enriched boron which reduces the soluble boron requirements approximately by half as well as due to the utilization of WABA BP.

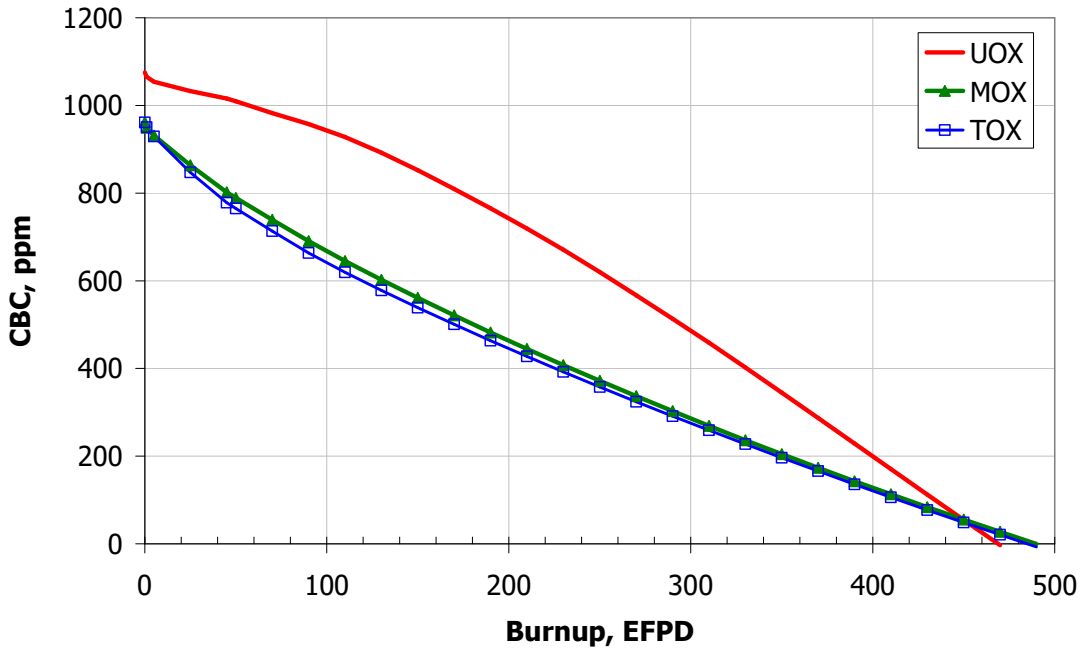

FIG. 25. Critical boron letdown curve (reproduced from Ref. [28] with permission courtesy of Elsevier).

The effect of the WABA BP on the BOC radial power distribution in the TOX core is demonstrated in Fig. 26. In the WABA-free core (Fig. 26(a)) a power peak of more than 1.6 can be observed. After the introduction of the WABA BP the core radial power was considerably flattened while the power peak was reduced to a value of 1.29 (Fig. 26(b)).

Figure 27 compares the evaluation of the radial power peaking factor during the burnup for the UOX, MOX, and TOX cores. The power peaking factor in the MOX and TOX cores with WABA BP is lower than that of UOX core during the entire depletion period. In Pu bearing cores without BP loadings the BOC power peak is significantly higher than that of UOX core. In contrast to the poisoned MOX and TOX cores, the power peak decreases with burnup and becomes comparable to that of the UOX core only after about 300 effective full power days.

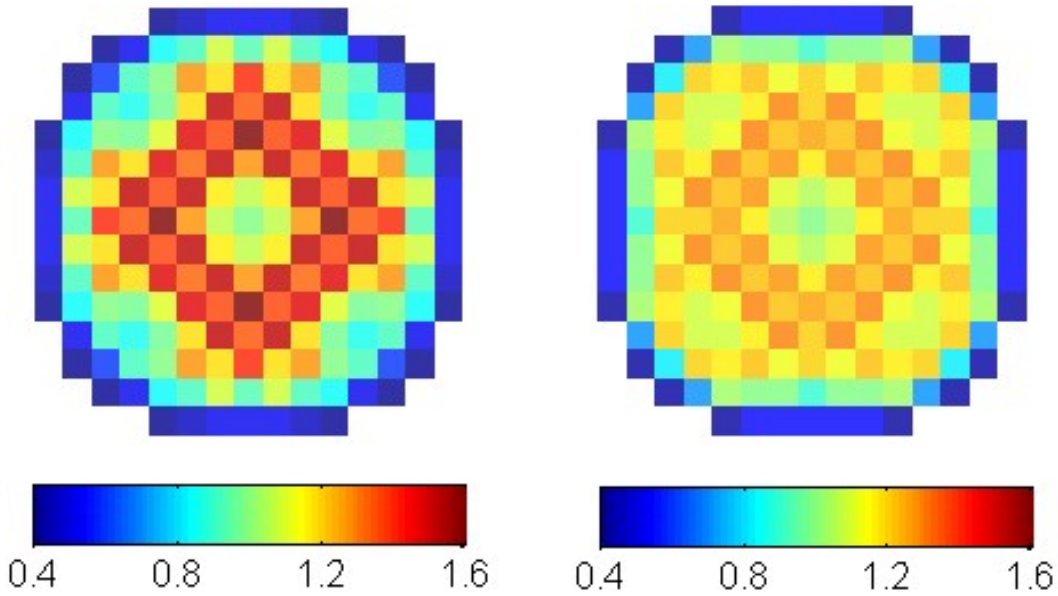

(a) no WABA
Power peak = 1.61

(b) with WABA
Power peak = 1.29

FIG. 26. Radial power distribution at BOC in the TOX core (*reproduced from Ref. [28] with permission courtesy of Elsevier).*

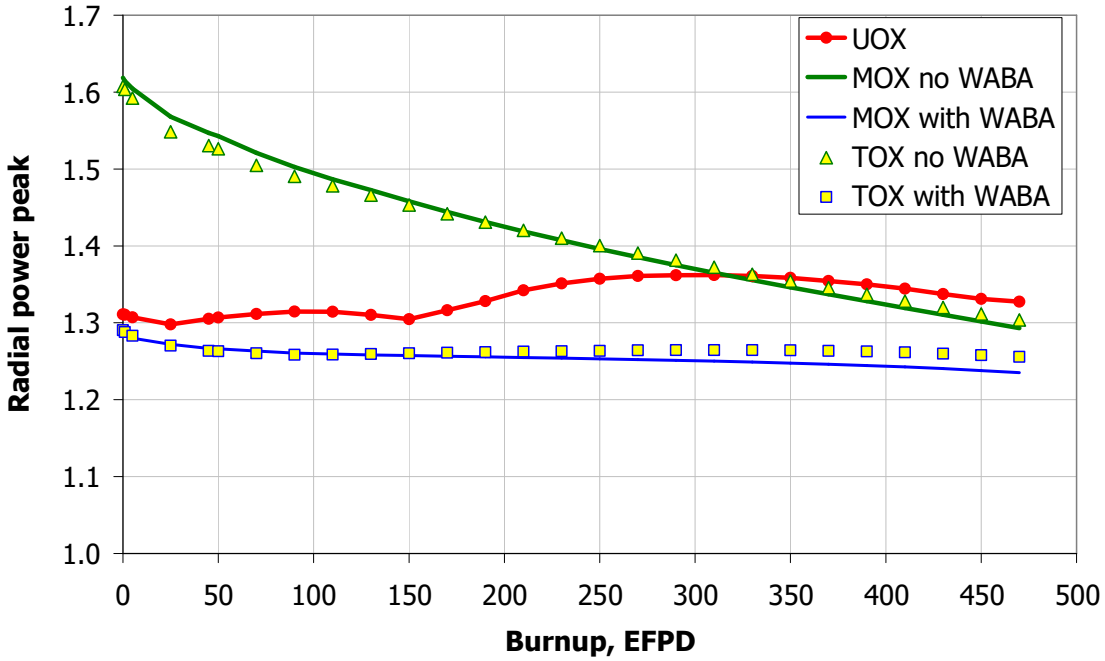

FIG. 27. Radial power peaking factor vs. burnup (reproduced from Ref. [28] with permission courtesy of Elsevier).

3.3.2. Reactivity coefficients, kinetic parameters

The core average reactivity coefficients, including Doppler fuel temperature coefficient (DC), moderator temperature coefficient (MTC), and SB reactivity worth, were evaluated at BOC and EOC for two operating states, namely:

— Hot Full Power (HFP), equilibrium Xe, all rods out, critical SB;
— Hot Zero Power (HZP), no Xe, all rods out, critical SB.

The summary of the reactivity coefficients for all considered cases is presented in Table 15. The reactivity coefficients are always negative for all calculated cores. In the MOX case, the DC is somewhat more negative than in the UOX case, while the TOX core has the most negative Doppler coefficient. The reason for the more negative Doppler coefficient in Pu bearing cores is found in the fact that ^{240}Pu owns a very strong neutron absorption resonance at 1 eV, thus increasing the Doppler feedback in comparison to ^{235}U [38]. The more negative DC in TOX core is also due to the fact that ^{232}Th has stronger Doppler Effect than ^{238}U. In general, at HZP conditions the DC is more negative than at HFP due to the lower core fuel temperature. The MTC values are rather close for all three cores while the MOX core provides the strongest moderator temperature feedback. The MTC magnitude at EOC is noticeably higher than at BOC. 'Very' negative DC and MTC are beneficial during accidents leading to fuel and moderator temperature increase while disadvantageous during overcooling transients. The Pu bearing cores exhibit approximately the same negative BW. For these cores, the magnitude of the BW is still somewhat lower than that of the reference UOX core despite of the use of enriched SB. The magnitude of the BW increases with the depletion of fissile material and the corresponding 'softening' of the spectrum.

TABLE 15. SUMMARY OF CORE REACTIVITY FEEDBACK PARAMETERS (reproduced courtesy of Elsevier [28])

		DC, pcm/K			MTC, pcm/K			BW, pcm/ppm		
		UOX	MOX	TOX	UOX	MOX	TOX	UOX	MOX	TOX
HFP	BOC	-2.6	-3.0	-3.6	-25.8	-33.1	-28.4	-7.2	-5.6	-5.7
	EOC	-2.9	-3.2	-3.8	-57.8	-59.4	-50.0	-8.8	-7.3	-7.8
HZP	BOC	-3.0	-3.5	-4.3	-16.8	-23.5	-19.0	-7.5	-5.9	-6.0
	EOC	-3.3	-3.6	-4.4	-43.5	-45.4	-37.8	-9.2	-7.6	-7.9

Table 16 compares kinetic parameters calculated at HFP conditions. Due to the harder neutron spectrum, the prompt neutron lifetime in the Pu fueled cores is significantly reduced and constitutes only about one-third of that of the UOX core. The effective delayed neutrons fraction (β_{eff}) of the MOX core is smaller than that of the UOX core while the TOX fuel has the smallest β_{eff} values among the considered cores. In Pu bearing fuels, β_{eff} is reduced because ^{233}U and fissile Pu actinides have lower delayed neutron yields (β) as compared to ^{235}U (Table 17). The reason for differences between MOX and TOX fuels is as follows. ^{238}U has a much larger β than that of ^{235}U and Pu nuclides (Table 17). In the MOX fuel, ^{238}U is responsible for about 8% of the total number of fission events and, consequently, contributes to the increase in the total β. The delayed neutron yield of ^{232}Th is even higher than that of ^{238}U. Nevertheless, in the TOX fuel ^{232}Th is accountable for less than 2% of the total number of fissions. Therefore, despite having a higher β, the ^{232}Th contribution to the delayed neutron source is lower than that of ^{238}U.

TABLE 16. CORE KINETIC PARAMETERS (reproduced courtesy of Elsevier [28])

Case	β_{eff}, pcm		Λ, μsec	
	BOC	EOC	BOC	EOC
UOX	637	547	16.0	19.2
MOX	420	435	5.8	6.9
TOX	360	382	6.0	7.3

TABLE 17. DELAYED NEUTRON FRACTION OF IMPORTANT FISSILE AND FERTILE ACTINIDES (reproduced courtesy of Elsevier [28])

Nuclide	Average delayed neutron fraction ($\overline{\beta}$), pcm
^{233}U	271
^{235}U	665
^{239}Pu	226
^{241}Pu	546
^{232}Th	2386
^{238}U	1892

3.3.3. Shutdown margins

The SDM is an important criterion for the reactor core controllability. According to the US Nuclear Regulatory Commission (USNRC) definition, the shutdown margin (SDM) is "the instantaneous amount of reactivity by which the reactor is subcritical or would be subcritical from its present condition, assuming all rod cluster control assemblies (RCCAs) are fully inserted except for the single RCCA of highest reactivity worth, which is assumed to be fully withdrawn" [39]. Typically, the minimum required SDM is 1.0 to 1.3%Δρ (1000 to 1300 pcm).

In this study, we calculated the SDM as a difference in reactivity between HFP critical state with completely withdrawn RCCAs and HZP state with all tripped RCCAs except that with the highest reactivity worth (hot shutdown). The boron and xenon concentrations are assumed to be unchanged. Generally, slow variations in the reactivity caused by the change in the Xe concentration are compensated by adjusting the SB content. SB is also used as a means of assuring the required SDM under cold shutdown conditions. It is worth mentioning that the control rod banks can be used to compensate for small reactivity changes and power adjustments.

The results of the SDM calculations show that all three cores exhibit sufficient SDM at both BOC and EOC (Table 18). For all considered cores, the SDM at the EOC is somewhat degraded as a result of an increased magnitude of the temperature reactivity coefficients. The UOX core has the highest SDM due to the higher RCCA reactivity worth. Among the Pu bearing cores, the MOX core has the lowest SDM at both BOC and EOC due to the more negative MTC values.

TABLE 18. HFP TO HZP SHUTDOWN MARGIN (Reproduced courtesy of Elsevier [28])

Item	Reactivity components, pcm	BOC			EOC		
		UOX	MOX	TOX	UOX	MOX	TOX
a	ρ_{HFP}, all RCCA out	0	0	0	0	0	0
b	ρ_{HZP}, all RCCA out	1620	1900	1911	2595	2583	2471
c	ρ_{HZP}, all RCCA in	-5576	-3970	-4154	-4692	-3695	-4081
d	ρ_{HZP}, all RCCA in but one	-4183	-3332	-3512	-3686	-3006	-3376
e	Highest RCCA worth[1]	1393	637	642	1006	689	704
f	SDM available[2]	3765	2999	3161	3317	2706	3039

[1] Item c / Item d
[2] Item d reduced by 10% to accommodate modeling uncertainties

3.3.4. Conclusions

This section summarizes a 100% Th-Pu Mixed Oxide (TOX) PWR core design for Pu recycling. Steady state neutronic behavior and fuel cycle performance of the TOX core were compared with those of the 100% U-Pu Mixed Oxide (MOX) and operating all-U (UOX) cores. The major differences in the safety parameters between the considered cores can be summarized as follows:

The worth of the control materials is significantly reduced in the Pu bearing cores. This issue was successfully addressed by the use of enriched soluble boron and by the utilization of B_4C as a control rod absorbing material instead of a typical Ag-In-Cd (AIC) alloy. The TOX fuel has about 50% more negative Doppler coefficient.

In the TOX core, the effective delayed neutron fraction, β_{eff}, is smaller by about a factor of two as compared to the typical UOX fuel and even lower than that of the MOX. A significantly reduced β_{eff} may compromise the core response during reactivity initiated accidents (RIA) although more negative DC may potentially compensate this inferior effect.

In general, the results of the 3D full core analysis demonstrate the potential feasibility of the full TOX PWR core design with respect to the reactivity control requirements under steady state conditions.

However, further investigation is required to answer the question whether the 100% TOX core is capable to meet required safety criteria under RIA conditions.

3.4. THORIUM –PLUTONIUM MOX FUEL FOR PLUTONIUM DISPOSITION

3.4.1. Thorium-plutonium MOX options

This part of the work studied optimal approaches for Pu-Th MOX fuel utilization in existing and advanced PWR designs. The objective of this work was to identify ways in which to maximise plutonium incineration in a thorium dioxide matrix, while keeping the design within operational and safety constraints.

Without extensive operating experience, optimisation techniques were used as a tool to explore the design space to understand the limits of operating Pu-Th MOX fuel in a full core. This is done by iterating between many different core configurations and eliminating infeasible ones. The advantage of such a method is that we place no preconceived biases for core design which might be completely different or very similar to those of uranium-fuelled cores. The result of this process is a list of possible designs that map out the boundaries of the operating design space that serves as a guide for designing Th-Pu MOX cores.

Having understood the relationships and trade-offs between different design objectives of homogeneously mixed Th-Pu fuel, we examine whether a heterogeneous assembly configuration will allow achieving higher plutonium incineration and/or operational and safety advantages.

To form a baseline of our investigations, we first looked at homogeneously mixed Th-Pu fuel without any form of burnable poisons (BP's). This gave us an unhindered view of the core parameters and allowed mapping out the operating space for this fuel. As we progressively increased the amount of plutonium loaded into the fuel, we found that there was a cut-off point at which the plutonium content was too high, causing a Moderator Temperature Coefficient (MTC) to become positive which rendered the core infeasible. To a lesser degree of importance, the maximum radial power form factor was also beyond allowable limits.

It was then postulated that using BP's would help alleviate both high radial form factors (RFF) and positive MTC. However, at high levels of plutonium concentration, the positive MTC contribution from epithermal-fast fissions was too high for BP's to make a notable impact. This meant that the threshold for the maximum amount of plutonium in the fuel remained.

The final analysis then looked at how a heterogeneous assembly might help increase Pu incineration. Heterogeneous configurations have been looked at before, but prior investigations were almost exclusively focused on U-Pu-Th fuels. Therefore, the performance of a Th-Pu heterogeneous configuration has yet to be documented. The main idea of spatial separation of Th and Pu is to allow better breeding of ^{233}U, which would help extend burnup of the fuel, thus allowing a deeper burn of plutonium.

However, it was found that the homogeneous fuel with and without BP's was able to achieve much higher plutonium incineration than any configuration of heterogeneous fuel, while still attaining a decent discharge burnup. This is because the heterogeneous cases efficiently bred ^{233}U but also burned it at the same time, in contrast to the homogeneous case that rapidly burned Pu while slowly breeding ^{233}U which only started contributing appreciable power towards the end of fuel life, thus allowing more Pu to burn.

Table 19 shows the assembly design variables and objectives which have been examined in this work.

TABLE 19. SUMMARY OF CASES EXAMINED

Assembly design	Homogeneous		Heterogeneous
	Burnable poisons		
Variables	Pu composition, Core loading pattern		
Objectives	Cycle length, Discharge burnup, Critical boron, MTC and Max RFF		

3.4.1.1. Results

Traditionally, a core is operated within certain operational and safety bounding limits. For example, the plant operator has a certain cycle length target, but has to remain within certain parameter limits, e.g., fuel discharge burnup, radial power form factors (RFF), critical boron concentration (CBC), and will always maintain negative reactivity coefficients. However, as the aim of this work is to explore the design space, we ignore these bounding limits and treat these constraints as objectives instead. This forces the optimisation algorithm to find the achievable limit of each parameter. For example, instead of simply setting a constraint of 'negative MTC', we instead 'minimise MTC' to see how negative an MTC we are able to achieve with the given fuel inventory. Nevertheless, a large negative MTC is a disadvantage in bringing the reactor from HFP to HZP, as it is in accidental overcooling events. But for the purpose of this scoping study, these constraints are not implemented to avoid limiting the search procedure and the explored solution space. This approach allowed us to view the extent of the operating parameters and filter the archive, post-optimisation.

The optimisation was performed for the following five operating parameters:

- Minimising the maximum RFF over the cycle;
- Maximising discharge burnup;
- Maximising cycle length;
- Minimising the maximum CBC (usually happens at Start of Cycle - SOC);
- Minimising the maximum value of the MTC (usually happens at SOC).

Discharge burnup here refers to the End of Cycle (EOC) burnup of the thrice burnt fuel due for discharge at the end of the cycle in this 3-batch reloading scheme.

The MTC values calculated for all the compositions during the equilibrium cycle monotonically decreased over the cycle. Therefore, it was enough to minimise the SOC MTC which served as the biggest constraint. The MTC was calculated with a moderator temperature perturbation of 5K.

For each objective, the optimisation tool based on Genetic Algorithm (GA) is run for 200 generations with a population size of 500, which produced 50 archived LP's for each fuel composition. While an exhaustive search was not feasible, it was found that the optimisation converged after 100 000 evaluations (200 generations × 500 evaluations (population members)). Multiple runs with different random number seeds were used to confirm that the results for each run were consistent.

The obtained optimal loading patterns (LP's) were run sequentially until equilibrium was reached. The performance of 3 cores for each objective namely the un-optimised core, the optimised core and the equilibrium core using the optimised LP was studied. The results are similar for each fuel composition studied ranging from 10% to 20% of Pu in the fuel.

Using the optimised LP's, the core behaviour barely changes for optimal CBC and MTC. For Optimal discharge burnup and RFF, there is a bigger change in the RFF between the optimised and un-optimised equilibrium using these LP's, because there are fresh fuel assemblies dispersed throughout the core, and RFF is very sensitive to slight changes in fresh fuel placement. But besides that, for Optimal Discharge BU and RFF, there are negligible differences between the optimised and equilibrium cores.

The biggest difference, however, between the optimised LP and its equilibrium counterpart comes from using Optimal Cycle, i.e., maximising cycle length. The Optimal Cycle LP improves cycle length when used on the un-optimised core, with deteriorations in MTC and CBC performance, while used to equilibrium; it loses cycle length but gains a high discharge burnup. It was found that in equilibrium these two very different LP's eventually achieve the same discharge burnup. Let us first examine how we can increase discharge burnup from our un-optimised case using optimal discharge burnup.

In summary, we have found that the optimal cycle and optimal discharge burnup LP's are very different, yet they both achieve similarly high discharge burnups in equilibrium. For plant operators that require an increase in cycle length, the use of optimal cycle can be of benefit, while being assured that the discharge burnup lost in that particular cycle can be recovered and maintained after the transient cycle.

3.4.2. Burnable poison options

Choices of burnable poisons were examined next, primarily with an aim to identify the most effective options for assuring negative MTC for fuels with high Pu content. The overall objective of this work was to maximise Pu incineration. Thus, we aim to load the reactor with the highest possible amount of Pu. However, this amount is constrained by two important factors: RFF and, more importantly, MTC. The large form factors in higher Pu composition fuels stems from the large differences in burnup between fresh and burnt fuel. The positive MTC can potentially be the result of the large soluble boron concentrations needed to maintain criticality for such reactive fuel. The conventional solution to these problems is the use of burnable poisons. Here, we first analyse the real contributions to MTC in our Th-Pu fuel. We

then analyse if BP's that satisfy operational constraints (e.g. minimal burnup penalty) are then able to satisfy the safety constraints e.g. RFF and MTC.

Figure 28 plots the normalised neutron flux spectrum at nominal and perturbed conditions for a homogeneous Th80%Pu20% fuel assembly and the difference (perturbed — nominal) between these two spectra. It is clear that there is a decrease of thermal neutrons and an increase of epithermal neutrons above 100 eV. From Fig. 29, we see that the key nuclides that play a large role are ^{239}Pu, ^{241}Pu and ^{233}U. To understand this better, we break this down further to MTC contribution over energy range for each isotope (Fig. 30). We see that for both fresh and depleted fuel, the main contribution to positive MTC is an increased fission in the epithermal range of ~100 to 10 000 eV. This positive contribution is partially offset by the negative contribution in the thermal range below 1 eV, especially for ^{239}Pu which gives an overall small positive contribution at 0.1 GW. d/t or a total negative contribution at 85 GW. d/t. In contrast, ^{241}Pu has a large positive contribution, but very small negative contribution — hence an overall positive contribution to MTC (Fig. 30).

These changes in MTC can be clearly attributed to the changes in the parameter η — the number of neutrons emitted in fission per neutron absorbed in the fuel, plotted for ^{239}Pu in Fig. 30 for 0.1 GW. d/t (Fig. 30(a)) and 85 GW. d/t (Fig. 30(b)). An interesting point to note is that while ^{233}U is believed to be a thermal absorber, thus contributing to negative MTC with a shift of the spectrum to higher energies, it still contributes quite significantly to the positive MTC of the fuel at high burnup. As mentioned, it is an increase in fission as shown by an increase in the parameter η in the epithermal range that causes this.

The results indicate that the MTC of our fuel is predominantly affected by fissions in the epithermal energy range. This is to be taken into consideration when choosing a suitable burnable poison that will help improve the MTC of the fuel.

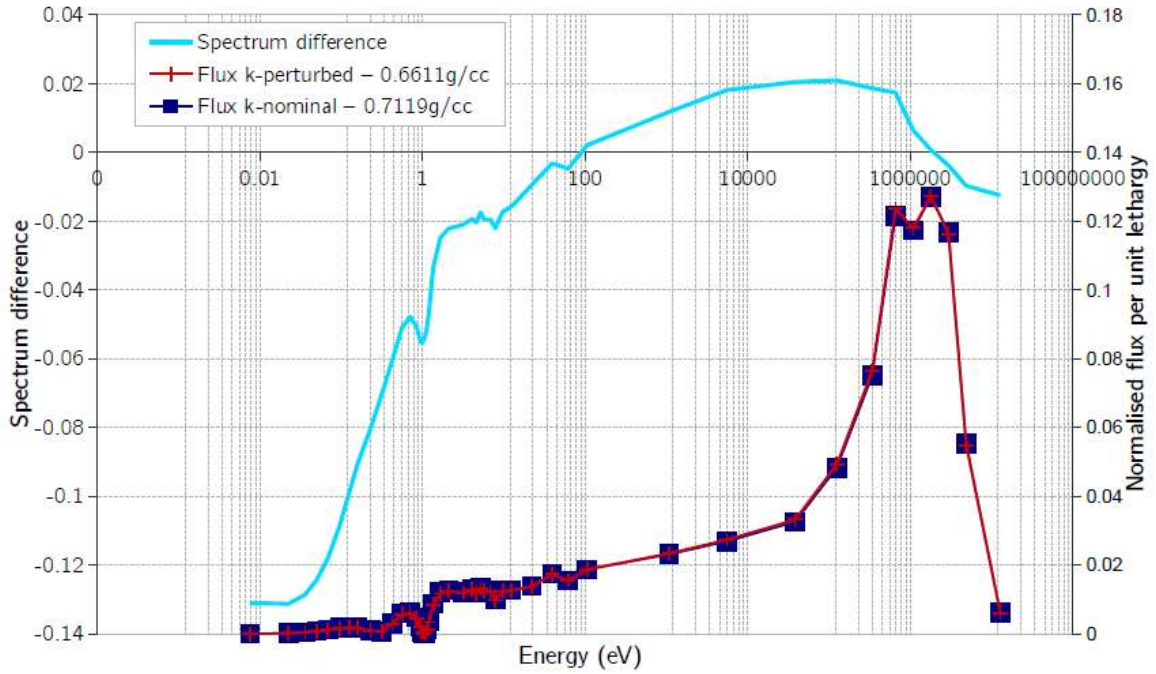

FIG. 28. Spectrum difference of the flux change between nominal moderator density of 0.7119 g/cc to an increase in temperature with a density of 0.611 g/cc (reproduced from Ref. [40] with permission courtesy of Elsevier).

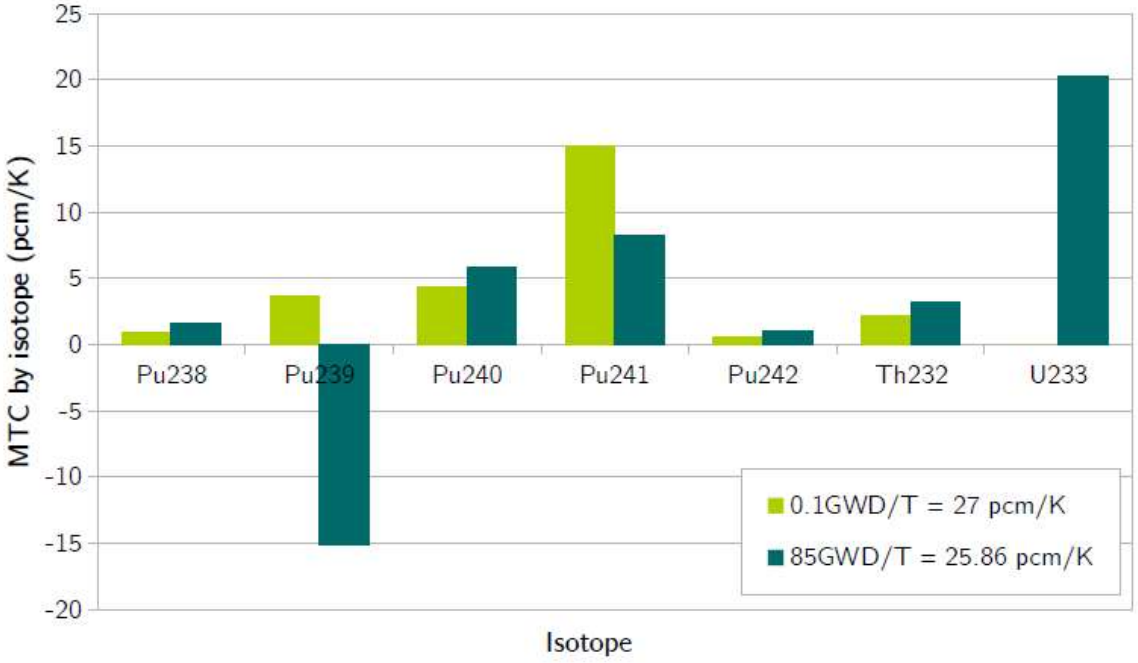

FIG. 29. Th80%Pu20% — MTC contribution by isotope for fresh and twice burnt fuel at core average boron (1600 ppm), MTC at 0.1 GWD/T = 26.59 pcm/K and 85 GW.d/t = 25.86 pcm/K (*reproduced from Ref. [40] with permission courtesy of Elsevier).*

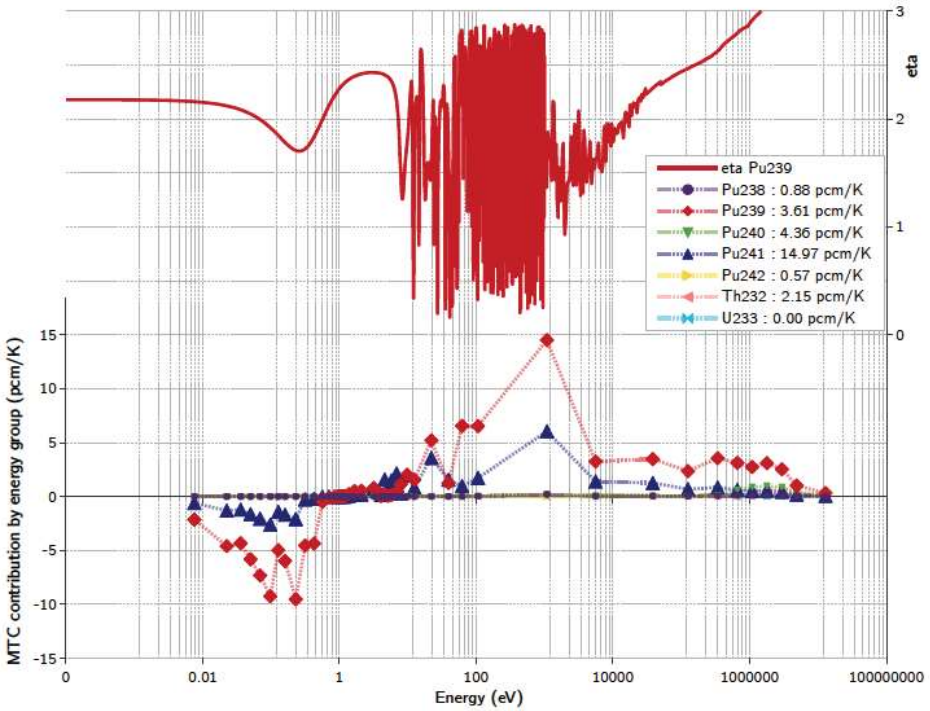

(a) 0.1 GWD/T. MTC = 26.587 pcm/K

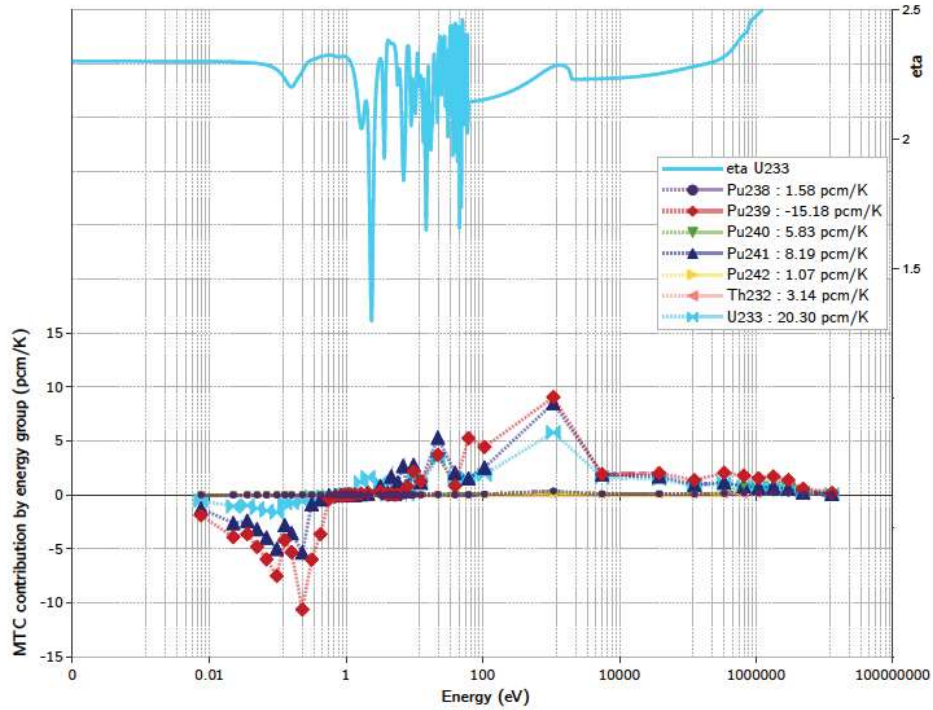

(b) 85 GWD/T. MTC = 25.857 pcm/K

FIG. 30. (a) Th80%Pu20% — Breakdown of MTC by energy group for each isotope for fresh and twice burnt fuel at core average boron (1600 ppm), using the LRM; and (b) plot of the parameter η for key nuclides — ^{239}Pu and ^{233}U (reproduced from Ref. [40] with permission courtesy of Elsevier).

A wide range of burnable poison materials and their arrangement within a fuel assembly were examined in the context of high Pu loading Th-MOX. The selection was affected by the capability of initial reactivity hold down, residual reactivity penalty and favourable effect on MTC. The selection was narrowed down to the following options:

1) IFBA of 0.004 cm thickness on all pins containing 50 wt% ^{10}B;
2) Homogeneously mixed 0.2 wt% ^{155}Gd;
3) Homogeneously mixed 0.2 wt% ^{177}Hf.

The first two were chosen due to their reasonable reactivity hold-down in the first cycle. In contrast, ^{177}Hf was chosen to test the hypothesis that MTC is affected by epithermal-fast fission, since it offers more resonance absorption in the relevant energy range compared to the other options.

Figure 31 shows the CBC, MTC and RFF of 3 un-optimised equilibrium LP's for a core with no BP's, and for the 3 BP configurations discussed above. It was determined that ^{177}Hf, ^{155}Gd and IFBA in increasing order give reasonable reactivity hold-downs. This is reflected in an improvement in RFF (Fig. 31(a)) but, more importantly, a reduction in required CBC from Fig. 31(b) for all LP's in that same order, with IFBA giving the most hold-down, and ^{177}Hf, the least. On the other hand, this behaviour is not necessarily reflected in the MTC.

First, we note from Fig. 31(c) that BP's do indeed reduce MTC for LP2 and LP3 (low leakage) compared to fuel with no BP but provide no reduction in MTC when LP1 (high leakage) was used. This indicates that leakage has a much bigger effect on MTC than BP's. Thus, the inclusion of BP's in fuel assemblies that are loaded using LP1 is unnecessary. However, it can still help if LP2 or LP3 is adopted, where fresh fuel assemblies are loaded in the interior of the core.

The second behaviour to note is that ^{177}Hf, which provided the least reactivity hold-down, and consequently the least reduction in CBC, is able to give a lower MTC, -2.9483 pcm/K compared to IFBA, -0.2786 pcm/K. This reaffirms our earlier conclusion that epithermal-fast fission above 100 eV has more effect on MTC than CBC, where ^{177}Hf offers more resonance absorption in this particular region than the other nuclides.

Conversely, ^{155}Gd deteriorates MTC, 5.9131 pcm/K, compared to the case with no BP's, -0.0875 pcm/K, despite causing a reduction in CBC. This is due to its steep decrease in absorption cross section in the thermal region, whereby the shift in spectrum to higher energies results in an insertion of positive reactivity. This reverse in behaviour is only seen when using LP1. As leakage reduces the positive contribution from epithermal-fast fission, the influence of the reduction in ^{155}Gd absorption in the thermal range becomes larger.

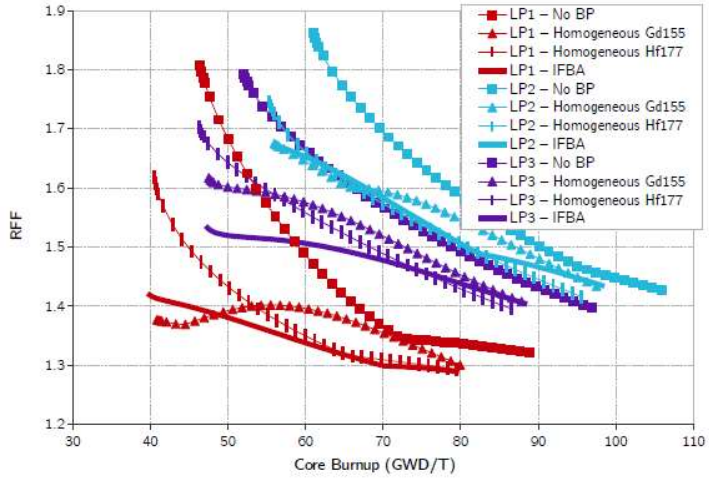

(a) RFF

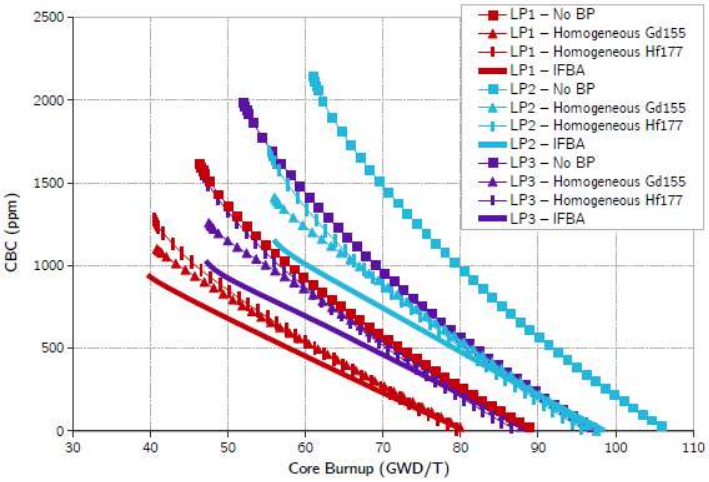

(b) CBC

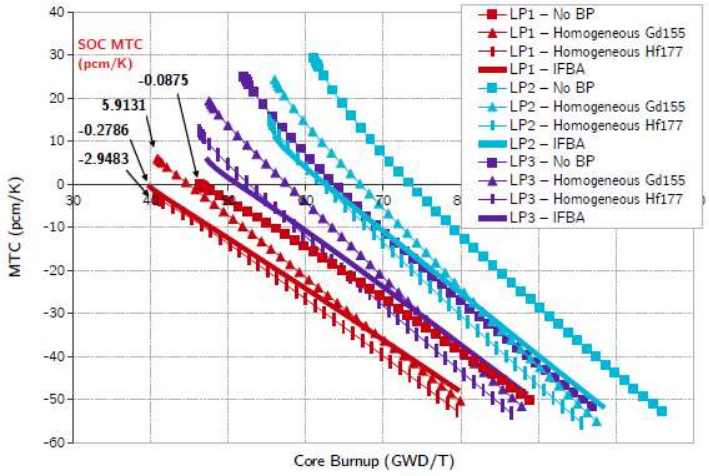

(c) MTC

FIG. 31. BP effect on core performance: Full-core results (*reproduced from Ref. [40] with permission courtesy of Elsevier).*

3.4.3. Heterogeneous fuel options

Finally, heterogeneous fuel configurations were examined with an aim to extend the achievable fuel discharge burnup through efficient breeding on ^{233}U. Higher fuel burnup was expected to allow deeper burn of initial Pu.

The studied fuel assembly geometries had seed-blanket configurations as shown in Fig. 32. The blanket was assumed to reside in the core for 3 subsequent seed cycles. The fuel composition that we limit our analysis to is Th80%Pu20% since it contains the maximum amount of plutonium that can achieve a core wide negative MTC (although this depends heavily on the core loading pattern). To allow for a fair comparison between our analysis of the different types of heterogeneous configurations and the homogeneous assemblies analysed in previous sections, we will use exactly the same mass of plutonium but distributed differently in each assembly region to create heterogeneity.

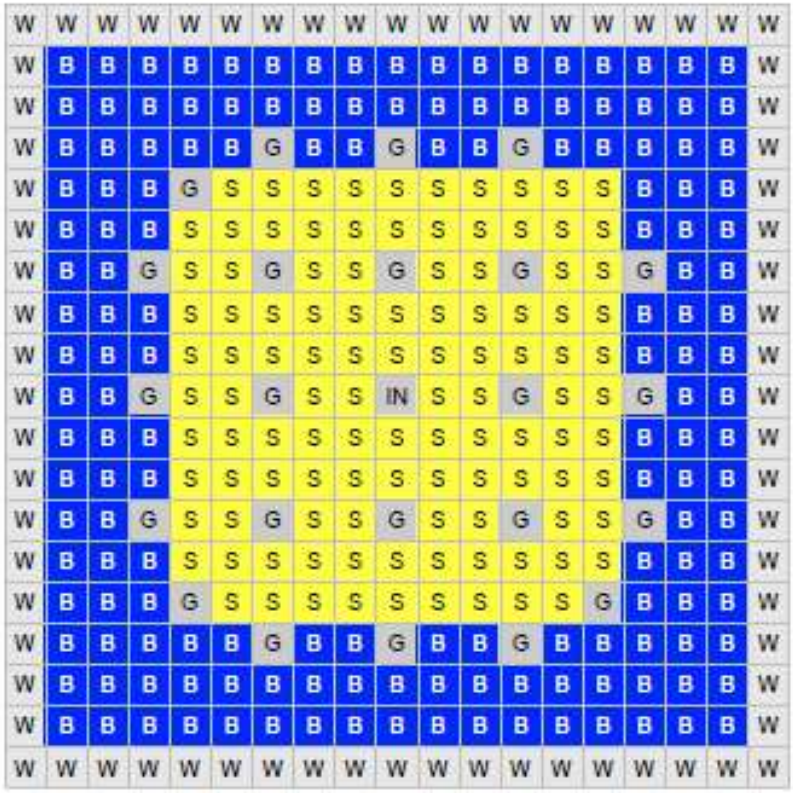

FIG. 32. Geometry of assembly with 3 blanket rows; S = seed region pin; B = blanket region pin; IN = instrumentation tube; G = guide tube; and W = water gap (not to scale) (*reproduced from Ref. [41] with permission courtesy of Elsevier).*

In order to limit the number of free design parameters, the study was limited to:

- Setting the central region of the assembly as the seed;
- Limiting the number of blanket pin rows to 3, i.e. a seed to blanket ratio of 108/156 pins ≈ 40/60.

The parameters that were varied and their effects are:

— Fraction of total plutonium mass in the seed (inner) region. This changes the degree of heterogeneity of the assembly. Hence for a fixed amount of Pu, we vary the fraction of total Pu in the seed region, with the remaining Pu placed in the blanket region. The respective Pu content is then homogeneously mixed with pure Th. Note that a Pu fraction in the seed of 1.0 means that all the Pu in the assembly is placed in the seed region and the blanket consists entirely of Th. Traditionally, we define the region with higher fissile content as the 'seed' region and the region with higher fertile content as the 'blanket'. As we have designated the central region of the assembly as the seed, for a 3 blanket row configuration, plutonium fractions in the seed below 0.4 are not analysed as this causes an inversion of the seed and blanket regions;
— Radius of blanket (outer region) pins. As the amount of Pu is fixed, an increase in blanket pin size increases the amount of Th needed to accommodate the volume increase. This means that the total amount of thorium in the assembly will increase compared to the homogeneous cases depending on the size of the pins in the blanket region. The seed pin size is kept constant at 0.4095 cm. Increasing the blanket pin size also affects the H/HM ratio of this region.

The different configurations of the heterogeneous assembly are shown in Table 20. The heterogeneous assembly configurations will be benchmarked against homogeneous Th80Pu20 fuel simply referred to as 'Homogeneous' and 'Homogeneous + IFBA'.

TABLE 20. SUMMARY OF ANALYSED CASES (reproduced courtesy of Elsevier [41])

Blanket pin radius (cm)	Fraction of Pu in seed region							
	0.4		0.6		0.8		1	
	wt% Pu in region							
	S	B	S	B	S	B	S	B
0.4095	19.57	20.30	28.98	13.65	38.16	6.89	47.11	0.00
0.45		16.89		11.34		5.71		0.00
0.5		13.74		9.21		4.63		0.00

(S = seed region and B = blanket region)

The results show that for Pu fractions in the seed of 0.8 and below (which we will refer to as cases 0.8Pu down to 0.4Pu), the criticality curves behave similarly to the homogeneous fuel. However, for a Pu fraction in the seed of 1.0 (case 1Pu), we found that there is a reactivity hold-down at the beginning of life which indicates increased breeding of ^{233}U from neutron capture in Th. The reactivity is then higher than for the homogeneous case from a burnup of 40 GW. d/t onwards which indicates fissioning of this bred fuel thus achieving a higher discharge burnup. This behaviour is seen for the two other cases with blanket fuel pin sizes of 0.45 and 0.5 cm. However, there is a slight decrease in criticality.

To understand this, we look at the evolution of Pu and ^{233}U in the assembly. While blanket pin size marginally affects the amount of ^{239}Pu burnt, increasing the pin size increases the amount of ^{233}U that is created. The reasons for this are:

— Increasing blanket pin size increases Th content in the assembly which increases the capture rate in Th and breeding of ^{233}U;
— A bigger pin size decreases moderation (i.e. harder spectrum). ^{232}Th is an epithermal absorber thus a harder spectrum results in a higher capture rate in Th and subsequent ^{233}U breeding. Nevertheless, ^{233}U is a thermal absorber, which means the harder spectrum reduces ^{233}U fission. Hence the ^{233}U in the blanket is less effective while the large amount of Th in fatter blanket pins acts as a constant neutron sink.

Examination of MTC behaviour revealed the following trends (Fig. 33).

— There appears to be an inverse relationship between MTC and boron concentration;
— The MTC for cases which have a Pu fraction in the seed of 1.0 have almost twice the MTC as the other Pu fraction cases;
— For cases with a blanket pin radius of 0.4095 cm (i.e. all pins in the assembly are the same size), the MTC and CBC for cases with a Pu fraction between 0.4 and 0.8 are almost identical to the homogeneous case.

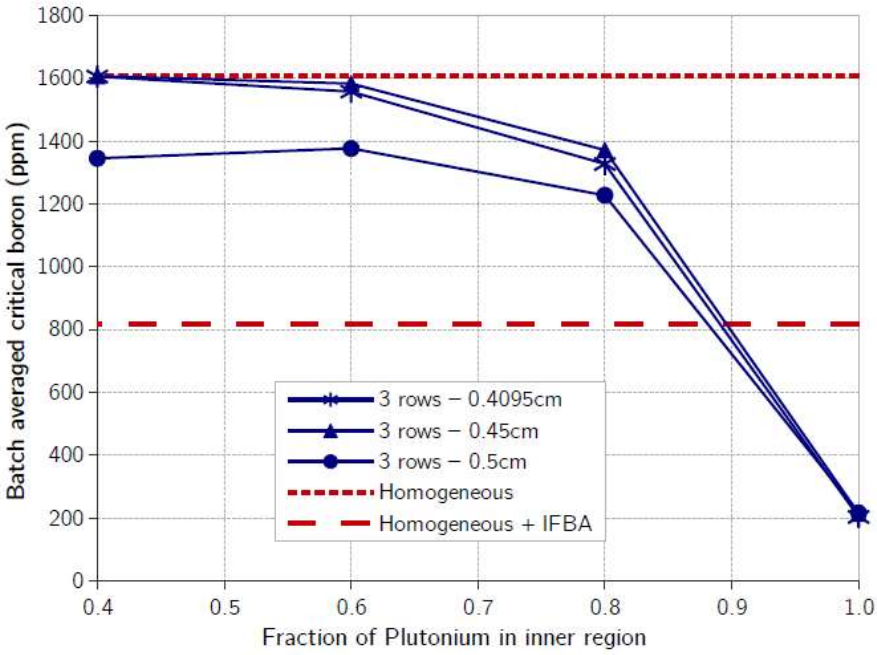

(a) Batch average critical boron.

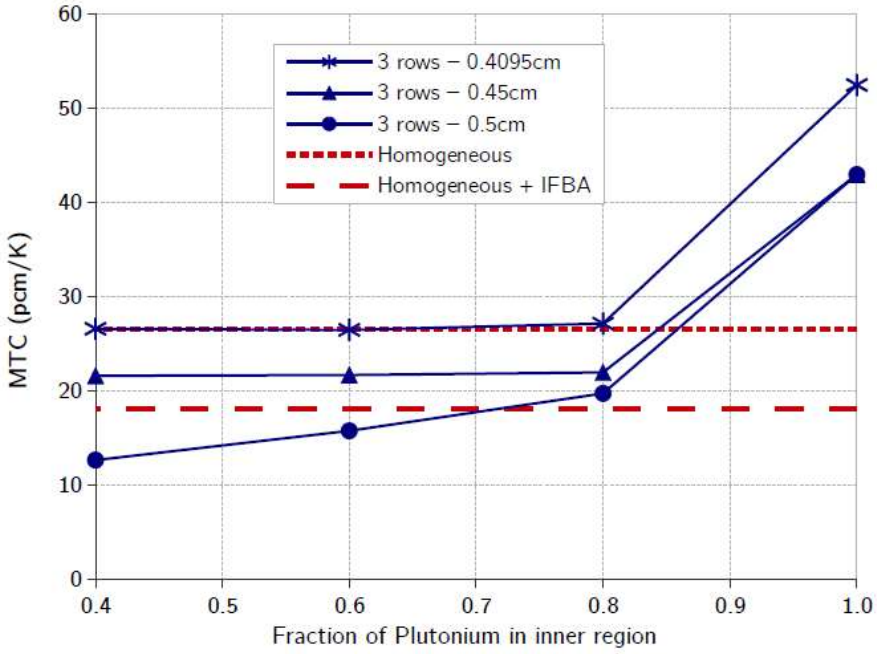

(b) MTC of fresh fuel.

FIG. 33. MTC of fresh fuel at batch average critical boron for a varying fraction of Pu in the seed region and different blanket pin sizes (reproduced from Ref. [41] with permission courtesy of Elsevier).

The observation that the MTC and critical boron for cases 0.4–0.8Pu are similar to the homogeneous case is expected, since the k-inf curves are almost identical to the homogeneous case. The assembly with a blanket pin radius of 0.5 cm has a slightly lower value of MTC which decreases with decreasing Pu fraction in the seed. However, this reduction is due to the increase of the Th to Pu ratio in the pins, which will necessarily reduce MTC, i.e., it is equivalent to a reduction in Pu content.

In contrast, for case 1Pu, a smaller CBC is required due to the reactivity hold-down at the start of life. Despite this, the MTC does not reduce accordingly, but is twice the value of the other cases.

In order to understand the observed behaviour of MTC, we compare two cases:

— Case 1Pu: 100% total plutonium in seed — MTC = 52.5 pcm/K;
— Case 0.8Pu: 80% total plutonium in seed — MTC = 27.2 pcm/K.

The MTC contribution by isotope is shown in Fig. 34. Note that the sum of each component by isotope equals the total MTC. We find that the main difference between the two cases is in the contribution of ^{239}Pu.

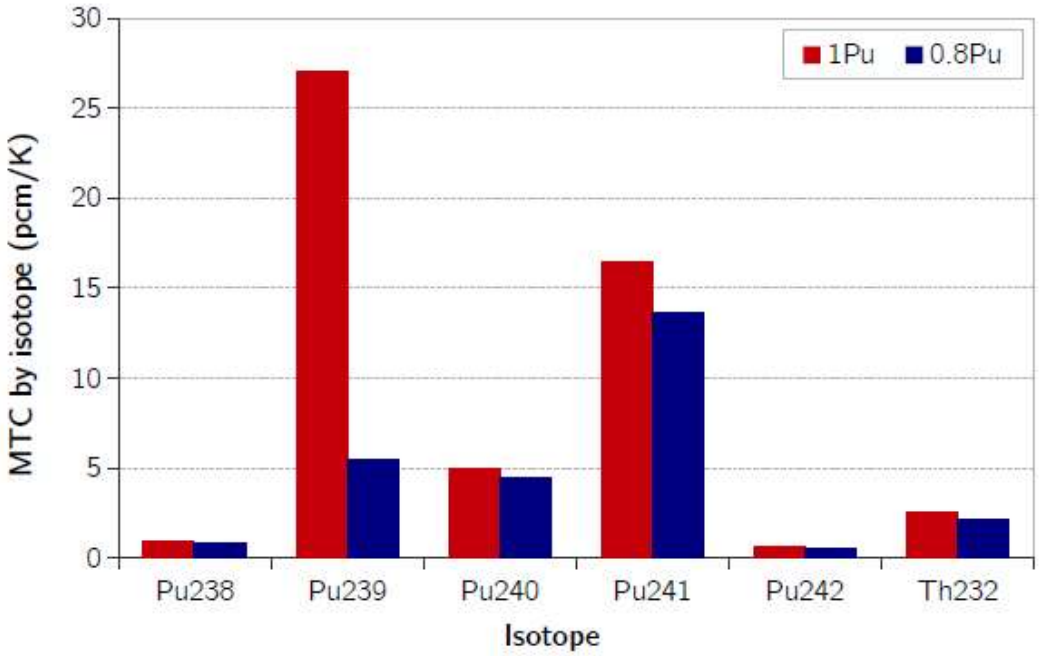

FIG. 34. MTC contribution by isotope, MTC for case 1Pu = 52.5 pcm/K and case 0.8Pu = 27.2 pcm/K (reproduced from Ref. [41] with permission courtesy of Elsevier).

The main contribution to positive MTC of high Pu content fuel comes from increased fission in the epithermal region of the spectrum. However, the main difference between cases 1Pu and 0.8Pu is at energy levels of 1 eV and below. We found that in case 0.8Pu, there is more negative contribution to the MTC compared to case 1Pu, which has a positive contribution at 0.3 eV.

Examining the flux spectrum for the seed and blanket for both cases, we see that the blanket for case 1Pu has a large thermal peak. As the blanket consists purely of thorium, the neutrons that are slowed down by the moderator have a better chance of thermalizing, unlike case 0.8Pu where the plutonium present in its blanket (20% of the total Pu mass) absorbs many of the thermal neutrons present.

Having settled on a Pu fraction which will give reasonable MTC and discharge burnup for 3 cycles, we now analyse if a heterogeneous assembly is able to breed more ^{233}U and hence incinerate more ^{239}Pu than a homogeneous assembly. As mentioned, we replace the seed pins

every blanket cycle, for 3 cycles. Thus, we sum the ^{239}Pu mass incinerated and ^{233}U mass created in 3 seed batches and 1 blanket batch over the 3 cycles mentioned. Table 21 shows that the heterogeneous assemblies do poorly compared to the simple homogeneous case, with and without BP's. Note that increasing the blanket pin size increases the ^{233}U created and left at the end of cycle. As mentioned earlier, a bigger pin size decreases moderation. Therefore, the harder spectrum is more conducive for capture in ^{232}Th and subsequent breeding of ^{233}U but not the fissioning of ^{233}U.

TABLE 21. MASS AND PERCENTAGE OF TOTAL Pu INCINERATED OVER THREE BLANKET CYCLES (reproduced courtesy of Elsevier [41])

Cases	Pu239(kg)	Pu(kg)	%Pu
Homogeneous	152.04	179.43	60.39
Homogeneous+IFBA	151.43	178.76	60.17
3rows–1Pu–0.4095cm	119.72	136.72	46.00
3rows–1Pu–0.45cm	122.47	140.58	47.30
3rows–1Pu–0.5cm	120.43	138.16	46.48
3rows–0.9Pu–0.4095cm	110.02	127.47	45.84
3rows–0.9Pu–0.45cm	110.93	128.96	46.34
3rows–0.9Pu–0.5cm	110.24	128.37	46.15

(3 seed reloadings)

To create a fair comparison between the heterogeneous and homogeneous assembly, we divide the homogeneous assembly into inner and outer regions, having the same number of pins as the heterogeneous case 1Pu. Setting aside the issue of MTC, the 1Pu case was chosen for this comparison rather than case 0.9Pu, because case 1Pu reloads the exact same amount of Pu as the homogeneous case, at every refuelling stage. Setting aside the issue of MTC, the 1Pu case was chosen for this comparison rather than case 0.9Pu, because case 1Pu reloads the exact same amount of Pu as the homogeneous case, at every refuelling stage.

Comparison of the fission reaction rates between these inner and outer regions and their sum is presented in Fig. 35. Figure 35(a) presents the incineration or fissioning of ^{239}Pu. The outer region of case 1Pu consists of pure thorium, so there are no reactions in ^{239}Pu. However, in the seed, which contains all of the plutonium mass, the reaction rate is higher than in either region of the homogeneous case. Conversely ^{233}U is able to breed more efficiently in the outer region (blanket) of case 1Pu due to the absence of competition with plutonium for neutrons. This, and having a more thermal spectrum than the seed, allows ^{233}U to readily fission. In the homogeneous case, however, while the ^{239}Pu fission reaction rates are lower than the 1Pu case, this process is happening in both inner and outer regions, as opposed to just the inner region for case 1Pu. Nevertheless, ^{233}U is slowly being bred and fissioned, but at a slower rate than case 1Pu (Fig. 35(b)). The summation of these effects is shown in Fig. 35(c). For the homogeneous case, ^{239}Pu dominates power share for most of the fuel's life, thus incinerating more plutonium, as distinct from case 1Pu where the power shifts to ^{233}U quite early on.

Thus, to conclude, it was originally assumed that the breeding of ^{233}U in the heterogeneous assembly would extend the discharge burnup of the fuel, resulting in a deeper burn of Pu. It was

found that indeed the discharge burnup is higher compared to the homogeneous case. However, for the heterogeneous case, the power share of ^{233}U is dramatically higher as well. Therefore, there still remains more Pu that has not been burnt, but not enough to sustain criticality. In contrast, for the homogeneous case, Pu has a much larger power share for most of the cycle, while slowly building ^{233}U. The^{233}U then fissions towards the end of the cycle incinerating any remaining Pu that cannot otherwise sustain criticality on its own. This behaviour is the deeper burn of Pu that we initially were expecting to achieve more effectively with the heterogeneous case than the homogeneous case. It is in fact was found to be the opposite.

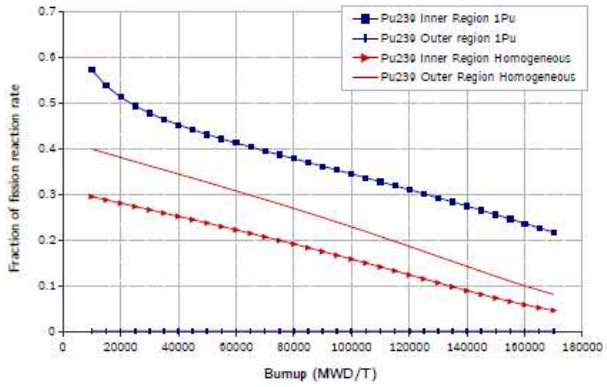

(a) Pu239

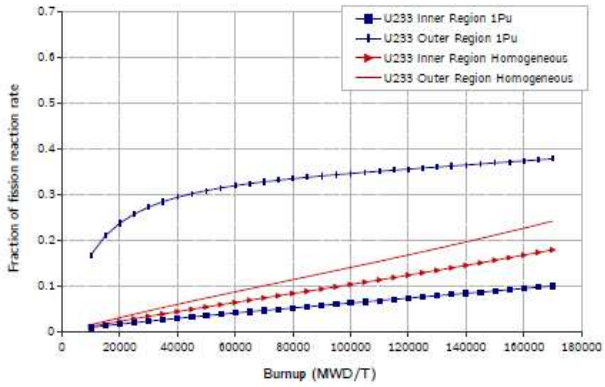

(b) U233

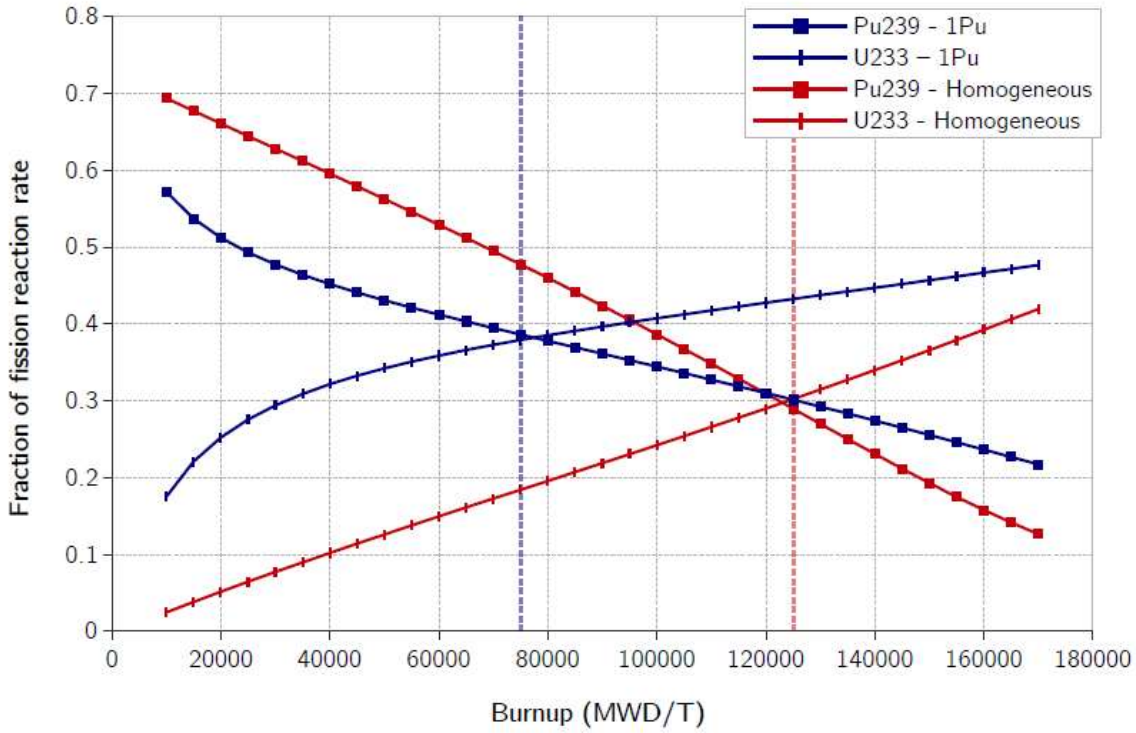

(c) Summation of reaction rates for the whole assembly. The dotted lines show the point at which power share in the assembly shifts from Pu239 to U233.

FIG. 35. Fraction of fission reaction rate by isotope for inner and outer region of assembly (reproduced from Ref. [41] with permission courtesy of Elsevier).

3.5. HIGH CONVERSION LIGHT WATER REACTOR DESIGN OPTIONS

This part of the work focused on further investigations into design options of Thorium fuelled LWRs with high conversion ratio.

In this part, we proposed and analysed a conceptual design of Pressurized Water Reactor with boiling channels. The aim of this concept is to address two main issues associated with high conversion (HR) PWR designs studied earlier, namely, reduced core average power density due to the concentration of fissile material in the seed region and related compromise that have to be made on the conversion ratio in order to assure reasonable power output. An initial attempt was made to optimize a high conversion ratio PWR without reducing the core power density below nominal 104 W/cc. The starting point for the new concept is the same heterogeneous seed-blanket fuel assembly arrangement but with a number of modifications. The main idea behind the concept is to create an intermediate neutron spectrum by allowing partial two phase coolant flow regime inside the seed zones. Although in conventional PWRs limited sub-cooled boiling is allowed, it is an undesired phenomenon because it leads to preferential deposition of crud, precipitation of soluble boron and resulting axial power shape distortion. In high conversion PWRs [42] however, the excess core reactivity is very small and may allow operation entirely without soluble boron using only mechanical (control rods) shim. In such case, boiling may no longer be an issue as long as the operating and safety envelope of the core is preserved. Allowing boiling in some locations would reduce moderation and improve the breeding performance. In addition, large latent heat of coolant phase transition allows removing much higher power from the same volume. Boiling heat transfer is also more efficient as long as bubbly flow regime (nucleate boiling) is maintained.

The following design objectives and constraints have to be met for the high conversion partially boiling PWR core:

- Core design with conversion ratio greater than unity to assure sustainable fuel cycle;
- Continuous operation for long fuel cycle length of at least one year;
- No compromise for core safety margin at steady state (similar to the conventional LWR designs).

Despite the boiling in the seed channels, the outlet core average coolant enthalpy will be the same as in a typical PWR. This is in order to assure that the coolant remains in a liquid phase in all primary loop components and thermal efficiency of the plant is not affected. In other words, the coolant will still have to be sub-cooled at the core outlet after two-phase flow from the high power seed channels is mixed with a single phase coolant from the lower power blanket channels.

Finally, the coolant flow pressure losses will not require replacement of the existing main recirculation pumps.

The design procedure was divided into two stages, 2-dimentioanl (2D) and 3-dimentioanl (3D) single assembly analysis. The 2D neutronic optimization was carried out using BOXER [43] and SERPENT codes [44]. It was performed in order to gain understanding of the main design parameters trade-offs necessary to achieve maximum fissile inventory ratio (FIR) at the fuel end of life. The optimization process examined design parameters such as seed fuel dimensions, seed region size, and blanket region size and fuel type in that region. The 2D calculations were based on the assumption of uniform axial void distribution, which would clearly not be the case.

Therefore, 3D fuel assembly analysis coupled with thermal hydraulic feedback would be required to confirm feasibility of this concept.

Following the above considerations, it is clear that 3D thermal hydraulic design issues may still need to be addressed and require further modifications of the 2D optimized model. The fuel central line temperature (T_{CL}) is required to remain below the limiting value of melt incipient under anticipated transient conditions. A possible solution to reduce T_{CL}, is to increase the number of seed fuel pins by reducing their lattice pitch without changing the original seed region volume fraction. Larger number of seed pins would reduce the linear heat generation rate and the heat flux. This modification, however, implies that seed and blanket pin lattices would no longer have the same pitch. In order to ensure correct thermal-hydraulic feedback, a number of modifications were required to the THERMO module, which is a part of the BGCore system [45–46].

It is also to be noted that two phase flow pressure losses are higher than for a single phase flow, which would result in a lateral flow from the boiling (seed) channels towards the blanket channels. Therefore, BWR fuel assemblies are canned in order to prevent such flow redistribution between the high and low void assemblies. In the designs studied here, the use of cans encasing the boiling seed regions is also possible. It may also prove unnecessary due to the very tight pitch of the blanket fuel lattice and thus high resistance to the lateral flow. Detailed sub-channel analysis is required to investigate this phenomenon. Therefore, this issue was ignored in the current analysis.

In order to improve the breeding performance, several modifications were required to the original seed-blanket model so it could operate under boiling regime in the seed region.

The selected reference model has operating power density of 70 W/cc to achieve FIR above unity without allowing boiling in the core as suggested in previous studies. In order to quantify the effect of boiling on FIR, the operating conditions of the reference model were artificially changed. (It was assumed that boiling in the seed channels can be maintained through variation of flow resistance coefficients at the assembly inlet leading to appropriate redistribution of the flow between seed and blanket channels). Figure 36 demonstrates the effect of different power densities and void fraction values on FIR.

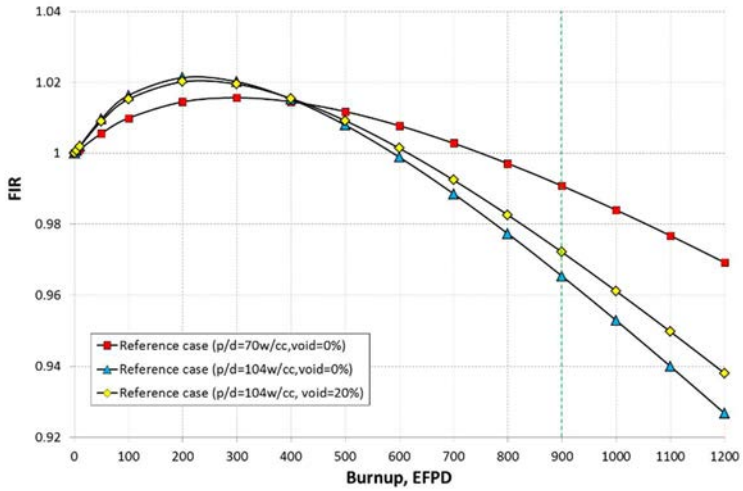

FIG. 36. FIR at $T_{discharge}$ for reference case at different operation conditions (reproduced from Ref. [46] with permission courtesy of Elsevier).

All the curves exhibit similar behaviour with initial increase in FIR due to efficient neutron capture in the blanket followed by a decrease due to rapid depletion of fissile material in the seed, more uniform power distribution between the seed and blanket and, thus, less captures in Th because of accumulation of ^{233}U in the blanket. The high power density case FIR is substantially lower at EOL because such monotonic decrease in FIR continues until higher burnup.

Previous studies found that reduced moderation resulted in better breeding performance, which was also observed here. For example, introducing boiling in the seed region (20% void fraction) improves the breeding performance (i.e., higher FIR at EOL) compared to zero void value. This is because higher void fraction increases the leakage rate into the blanket and somewhat hardens the spectrum also increasing the resonance absorption in Thorium.

The blanket region size in the reference model was selected to maximize the capture of neutrons leaking from the seed region. Due to the fact that the operating conditions in the seed region were changed, the blanket region had to undergo a modification in order to improve neutron captures. Moreover, it was also decided to investigate the use of two possible fuel forms for the blanket region — ThH_2 and ThO_2. Each fuel form presents potential advantages. On one hand, admixing moderator material to the fuel in the ThH_2 case improves the resonance captures in Th because of the lower self-shielding, ultimately resulting in better breeding performance. In addition, thermal conductivity of hydrides is much higher than in the oxide fuel. On the other hand, ThO_2 has a much higher melting point and its performance as a nuclear fuel is much better understood.

A model of seed assembly surrounded by a large blanket zone was created in SERPENT. The cumulative neutron captures in the blanket were examined as a function of distance from the seed, with changes in the seed coolant void fraction. The blanket region size was selected at the point where the cumulative captures reached 95% of total for ThO_2 and ThH_2 blanket materials. The use of ThO_2 fuel would result in a thicker blanket (25.2 cm) than the one obtained for ThH_2 fuel case (17.64 cm). These results are not surprising due to the less efficient neutron moderation in ThO_2 in comparison to ThH_2. Table 22 summarizes the obtained blanket sizes for both ThO_2 and ThH_2. The less expected result is that the void fraction in the seed has remarkably small effect of the capture rate distribution in the blanket.

TABLE 22. BLANKET SIZE FOR DIFFERENT FUELS (Reproduced courtesy of Elsevier [46])

Fuel	Pitch size [cm]	Blanket size [cm]	No. of pin rows
ThH_2	1.26	17.64	14
ThO_2	1.26	25.2	20

We then examined different seed assembly arrays of N × N pins, which were placed in the centre and surrounded by the blanket. The core power density was fixed at 104 W/cc with void fractions in the seed, varying from 10% to 30%. The fissile material content was adjusted to achieve the same cycle length of 300 days (or 900 days total in core residence time) as described in the methodology section.
Furthermore, the effect of the seed pin geometry modifications on FIR was also examined. The reference seed pin radius selected to be that of a typical PWR, 0.4095 cm. Then, the pin radius

was increased by 10% and 20%, while the cell pitch remained fixed at 1.26 cm (although it may earlier) need to be reduced to reduce the linear heat generation rate as discussed

A setup example is shown in Fig. 37. Select results for the 2D simulations obtained from BOXER are shown in Figs. 38 and 39 for ThH_2 and ThO_2 respectively.

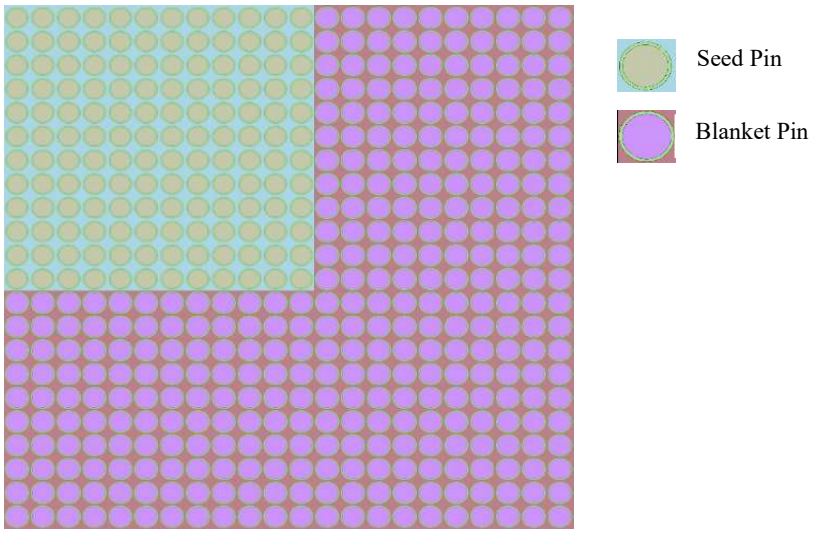

FIG. 37. Quarter of a high-conversion Th-^{233}U fuel assembly (reproduced from Ref. [46] with permission courtesy of Elsevier).

.

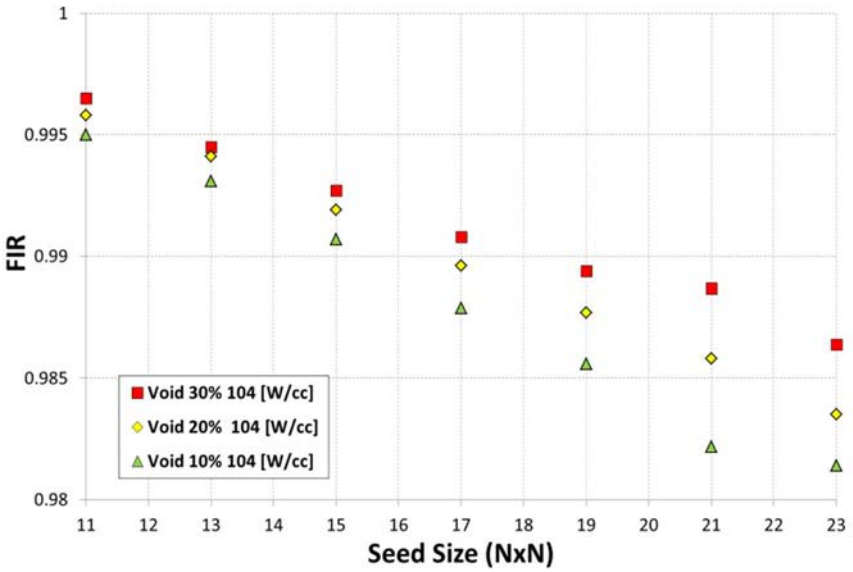

FIG. 38. FIR at EOL as a function seed size, ThH_2 fuel, Rs=0.4914 [cm] (reproduced from Ref. [46] with permission courtesy of Elsevier).

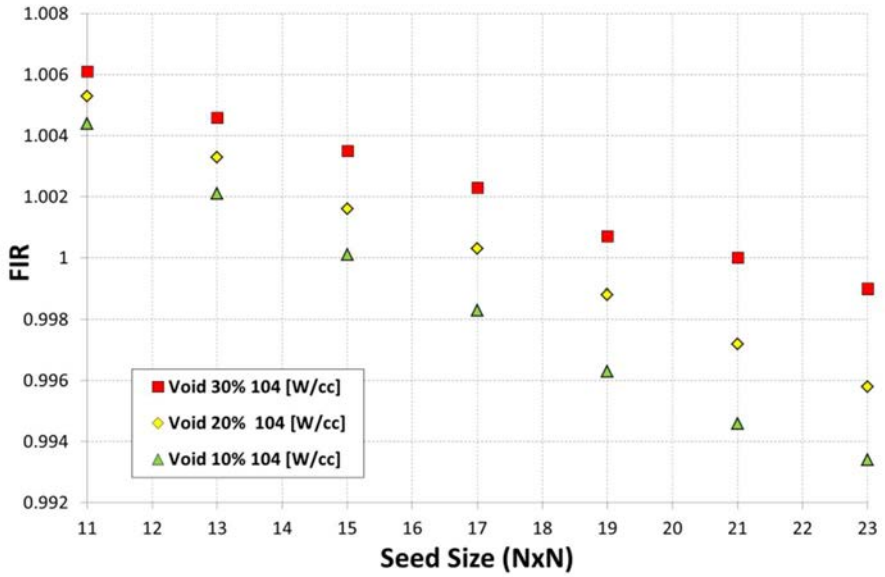

FIG. 39. FIR at EOL as a function seed size, ThO_2 fuel, Rs=0.4914 [cm] (*reproduced from Ref. [46] with permission courtesy of Elsevier).*

.

From the results it is observed that FIR is highly sensitive to the seed pin dimensions and coolant void fraction and reduced moderation (higher void fraction and larger pin diameter) improves the breeding significantly. The seed region size (total number of seed pins) also has significant effect on the breeding. Reducing the seed region size improves FIR but it also requires higher initial fissile content for the void fraction of 20% and different fuel types. Smaller seed region also implies smaller relative volume fraction of the seed and thus higher power peaking, which will most definitely challenge the core thermal design. Seed fuel pin radius of 0.4914, average void fraction of about 20% and 15 × 15 to 17 × 17 seed array size seem to provide reasonable combination of parameters to achieve FIR~1 at the reference core power density. This is of course remaining to be properly evaluated and confirmed by thermal hydraulic analysis.

The results also suggest that the use of ThO_2 fuel in the blanket would be preferred over ThH_2 fuel to achieve FIR above unity at EOL. However, the use of hydride fuel form improves the moderation and creates a much more thermalized neutron spectrum in the blanket region. This, in turn, will increase the neutron absorption in thorium and reduce the relative blanket volume fraction, consequently allowing higher core average power density. It was found that the blanket thickness has to be only 17.64 cm as opposed to 25.2 cm in ThH_2 and ThO_2 cases respectively. Although, high thermal flux increases the probability of neutron capture in the thorium, it is also increasing the burnup rate of ^{233}U once it is accumulated in substantial quantities resulting in less efficient breeding performance on the overall balance. Furthermore, absorption in hydrogen contained in the fuel is also non-negligible which also negatively affects breeding. Therefore, it can be concluded that ThO_2 is a preferable choice of blanket fuel form the breeding performance point of view. This assertion however will have to be confirmed by thermal hydraulic analysis in which power density distribution considerations may prove otherwise.

In the next stage, we examined the behaviour of the models presented above in 3D single assembly configuration. The optimal 3D fuel assembly configuration has to meet the following constraints:

1) For a reasonable margin before melting, the center line temperature of fuel need to be below 1800 C;
2) Minimum Departure from Nucleate Boiling (MDNBR) need to be above 1.3 at steady state.

The average coolant temperature at the upper plenum will be as in a typical PWR ~ 326°C.

Moreover, any geometry modifications (e.g. pin dimensions) require adjustment of the core pumping power. Therefore, in order to maintain the attractiveness of the suggested design, the core pumping power will be similar to that of a typical PWR (~ 4.5 MW).

Three-dimensional models of the geometries were modelled in BGCore code in order to study if they can operate under the mentioned above constraints. The fuel assemblies were modelled as two channels with common lower and upper plena.

The goal of this work is to find a design that can allow maintaining the core average power density equal to a standard PWR. Therefore, different seed sizes were examined with respect to complying with the mentioned constrains. The examined seed sizes were 17 × 17, 19 × 19, 21 × 21 and 23 × 23, where 23 × 23 is the largest seed size that would still ensure FIR above unity according to the 2D analysis. The examination started with the 23 × 23 seed region.

The fuel assembly performance was examined with BGCore code in order to determine the temperature and the thermo-hydraulic properties distribution of the fuel and the coolant to ensure feasibility of the design [41]. The heterogeneity of the model causes a high power peaking in the seed region. Therefore, it was expected that the center line fuel temperature at the Beginning of Life (BOL) would be higher than in a standard PWR. As a result, in order to reduce the power peaking in an efficient way and in order to increase the effective heat transfer surface, the seed dimensions were changed. The original seed pins were replaced by pins with smaller diameter in such a way that the moderator volume (Vm) to fuel volume (Vf) ratio remained constant. That resulted in a larger number of seed pins in the same seed area. The modified dimensions are summarized in Table 23.

TABLE 23. SUMMARY OF MODIFIED ASSEMBLY PARAMETERS (reproduced courtesy of Elsevier [46])

Pin pitch, cm	1.26
Seed fuel pellet radius, cm	0.4914
Seed cladding outer radius, cm	0.5569
Blanket fuel pellet radius, cm	0.5300
Blanket cladding outer radius, cm	0.6155
Effective core height, cm	366
Moderator Vol. to Fuel Vol. in Seed	0.629
Seed/Blanket fuel material	^{233}U O_2-ThO_2
Number of seed pins	529
Number of blanket pins	1320

The initial model of 23 × 23 seed pins with uniform axial enrichment distribution resulted in a very high T_{CL}. However, even when the modified (30 × 30 seed size model) was examined, the T_{CL} remained above the limiting value of 1800°C. Additional reduction in seed pin diameters was unrealistic due to geometrical constrains of the material (the pins have to be sufficiently mechanically rigid to withstand vibrations and other mechanical and thermal stresses that can developed due to coolant flow, temperature gradients and radiation damage). Therefore, in order to overcome the high T_{CL} a non-uniform axial distribution of the fissile material in the seed region was examined. In this work, we divided the seed region into two enrichment zones. As can be seen in Fig. 40, the split enrichment reduces the T_{CL} to about 1800 ^{0}C at the hottest point. Moreover, the split enrichment also allows to increase the value of minimum departure from nucleate boiling above the limiting value of 1.3.

The results demonstrate that it is possible to meet the TH constrains with seed size of 23 × 23. Therefore, as it was mentioned earlier, we examined different seed sizes. Figure 41 shows T_{CL} for different seed sizes with split enrichments.

The ʿdouble-humpʾ shape of the fuel temperature curve corresponding to split enrichment case is a result of superposition of regions with drastically different void fraction and fuel enrichment.

As it is clearly seen in Fig. 41, the only model to comply with T_{CL} under 1800°C is the 23 × 23 model. However, the 21 × 21 model also ensure a compliance with the hard limit of the melting point (T_{CL}<2800 ^{0}C). But in our case, we would select the 23 × 23 model, which was modified to 30 × 30 seed pins in the same region with smaller pins as it was presented earlier.

Under these operating conditions, we obtained the void fraction and coolant density distributions at the beginning of life (BOL) which on average roughly corresponded to the desirable values obtained in preliminarily analyses.

We have determined the average void fraction in the seed region for the split-enrichment assembly, which, in this case, is about 20% on average and 42.5% at the core outlet. Typical PWR systems operate with average coolant density of 650–700 kg/m^3, while in this model, the seed region has an average coolant density of 530 kg/m^3 due to relatively high void fraction. As mentioned earlier, this increases the neutron leakage from the seed to the blanket, and by that increases FIR.

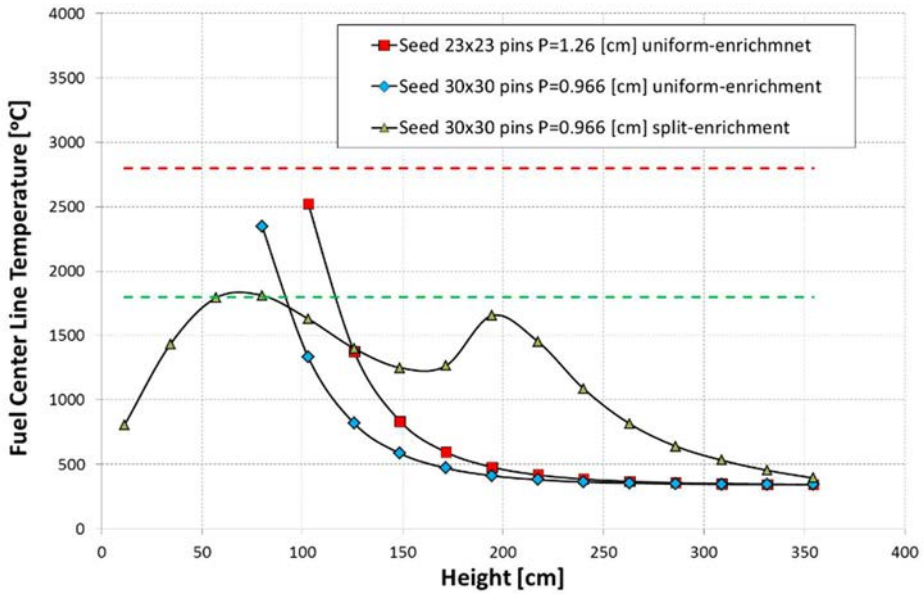

FIG. 40. Number of seed pins effect on centre line temperature (*reproduced from Ref. [46] with permission courtesy of Elsevier).*

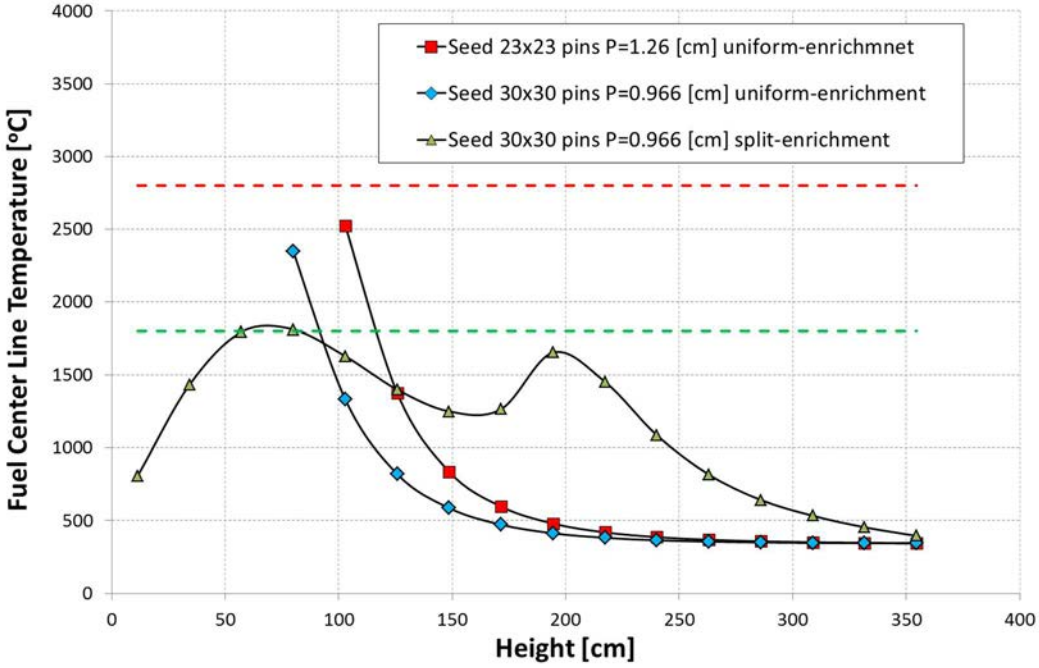

FIG. 41. TCL as function of seed size and height (*reproduced from Ref. [46] with permission courtesy of Elsevier).*

The presented above conditions roughly correspond to those examined in the 2D simulations. However, due to buildup of fissile material in the blanket and its correspondingly increasing power share, the boiling in the seed channel gradually diminishes and disappears completely after about one hundred days of irradiation.

Preliminary studies on the reference model showed that there is a strong dependence of the void fraction profile on time. The split enrichment was used in this case too in order to ensure that the TH margins would comply.

With burnup however, the buildup of new fissile material causes a rapid power shift from the seed to the blanket region. As a result of this rapid power reduction in the seed region, the boiling in this channel decreases significantly in a relatively short time until it diminishes completely. The presence of void fraction in the model poses another design challenge. The profile of the void fraction influences strongly the power/temperature distribution in the seed region. As mentioned earlier in order to reduce the initial temperature peak the enrichment split will over-compensate the void fraction effect at the beginning of irradiation. However, the presence of boiling disappears in about 100 days, and this in turn causes a strong shift of power to the top part of the seed region, which results in a rapid temperature rise (Fig. 42). As mentioned, the moderator density in the seed is changing quickly with time and significantly affects the axial power profile.

In order to overcome this challenge and maintain boiling conditions in the seed, it would be desirable to control the mass flow rate into the seed region in such way that the void profile shape would remain relatively constant. Such a possibility was considered during initial stages of this work this work, but practicality of such flow rate control is questionable and requires further investigation. It was therefore left out of scope of this part.

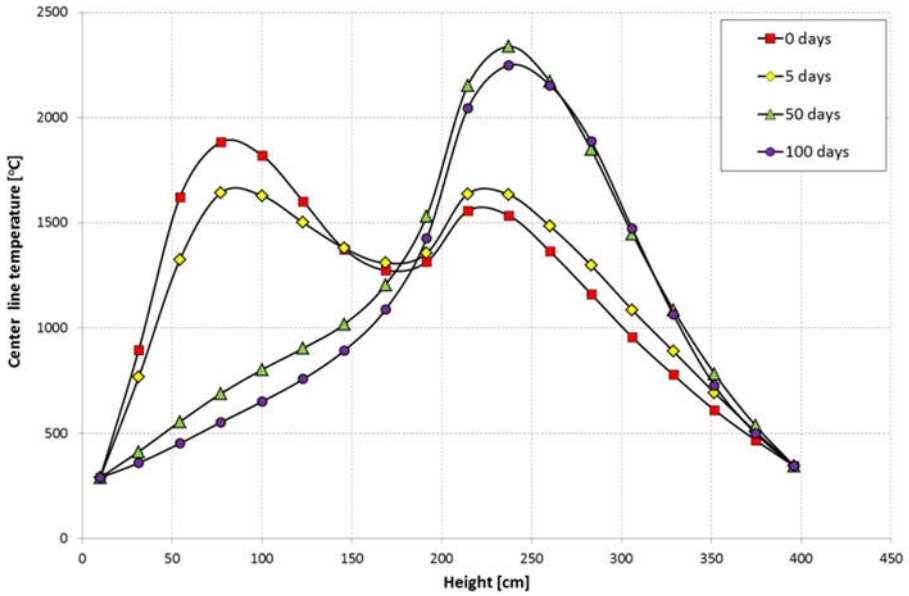

FIG. 42. Central line temperature axial distribution at different time steps (*reproduced from Ref. [46] with permission courtesy of Elsevier).*

Instead, it was assumed that there is a mechanical means of mass flow control in the seeds regions of the core at discrete time intervals (e.g during refuelling outages). For example, the core support plate may have flow orifices with different dimensions so that an assembly placed in different locations would have different flow resistance between the seed and the blanket. As the assembly is irradiated, the blanket power share rises while the seed power share is reduced. During refuelling outage, reshuffling of the fuel assemblies would allow relocation to a position with higher loss coefficient for the seed channel which would reduce the seed flow rate and reinstate boiling conditions.

Furthermore, the proposed concept is assumed to operate without soluble boron, with only control rods used to compensate the excess reactivity during the cycle. The presence of the control rods in the core may offer additional flexibility in maintaining the axial power profile such that the peak fuel temperature is within the allowable limits.

Here, for simplicity, we assumed that the coolant density profile is constant during the entire fuel irradiation time.

In addition to the geometry selections discussed in previous sections, we examined two types of axial reflectors for the seed region, one made out of stainless steel and the other made with pure thorium (ThO_2). Thorium reflectors would capture most of the leaking neutrons and lead to an increase in FIR but reduce conversion ratio in the seed region because of its poor reflecting properties. Stainless Steel, on the other hand, is a good reflector which would increase the conversion ratio in the seed. The effect would be notable especially at the top of the assembly where the void fraction is high and the moderation low, which results in substantial leakage of neutrons.

The design selected in the previous sections was modelled using BGCore system. FIR as a function of burnup is presented in Fig. 43 for the two different reflectors. The simulation was performed with constant coolant density profile, as mentioned earlier.

As can be seen from Fig. 43, the FIR at EOL is above unity for the two types of reflectors. However, as expected, the use of thorium axial blankets is slightly more beneficial and results in higher FIR value at EOL. Therefore, by assuming that it is possible to control the mass flow rate in the seed regions, it would be in principle possible to achieve FIR above unity as suggested by the presented analysis.

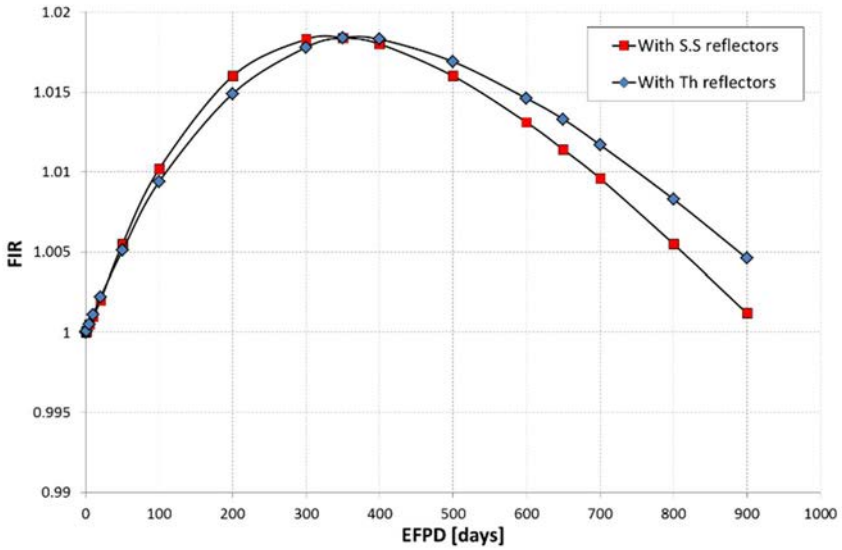

FIG. 43. FIR as a function of effective full power days for two different assemblies (*reproduced from Ref. [46] with permission courtesy of Elsevier).*

3.5.1. Conclusions

This part of the research explored the possibility of creating a PWR system with boiling channels to achieve high conversion ratio (FIR value above unity), while keeping the power density of a typical PWR system at 104 W/cc. In order to simulate such a heterogeneous system, both in terms of material composition (highly enriched seed and a fertile blanket) and TH conditions, it was required to update the capabilities of the TH module THERMO in the BGCore package.

The main part of this work dealt with the neutronic optimization of high conversion PWR with boiling channels. We investigated the influence of different parameters such as: blanket dimensions, seed pin radius and blanket fuel materials, on the FIR value at EOL. The results reported here suggest that it is possible to achieve FIR above unity for several examined cases. However, these results were obtained under the assumption that the void profile is uniform. Therefore, a full 3D fuel assembly study was required.

The last stage dealt with the 3D fuel assembly analysis. A coupled neutronic with thermal hydraulic feedback analysis was performed in order to obtain more realistic results. However, as the power shifts from the seed to the blanket with the fuel irradiation, the assembly average void fraction was constantly decreasing. Therefore, mechanical control of the mass flow rate through the seed channels would be required to sustain boiling regime throughout the irradiation campaign. Practical way of implementing such flow rate control requires further investigation. One option could be to use fixed but different orificing in different position on the core support plate. This will allow each fuel assembly to be reshuffled during refuelling outage to positions with progressively higher flow resistance in the seed region.

In the remaining part of the study, we assumed that hypothetical possibility of varying coolant flow in the seed during burnup to maintain relatively constant void profile is available. A range of possible 3D designs was examined to make sure that an assembly could operate under all the imposed design constraints. BOL was found to be the most restrictive point in time, since it is the point where the seed is fresh and produces most of the power in the assembly. The selected assembly design that meets all the thermal hydraulic constraints was then simulated in BGCore system assuming constant coolant density profile. The results reported in the last section indicate that it is possible to achieve FIR above unity in a PWR with boiling channels without reducing the core power density below 104 W/cc.

4. THORIUM–URANIUM FUEL CYCLE IN HIGH TEMPERATURE GAS REACTOR

4.1. INTRODUCTION

High temperature gas-cooled reactors (HTGRs) have excellent performance in utilization of thorium-based fuel, due to their high degree of neutron economy. Some breeding or near-breeding fuelling schemes for HTGRs have been proposed since 1970s [47–48]. There are two ways to utilize thorium in thermal reactors, namely breeding and in situ utilization. For HTGRs, the in situ utilization can avoid the challenges of reprocessing of the tri- structural isotropic fuel particles (TRISO), compared with breeding. Moreover, the pebble-bed HTGRs are more suitable for in situ utilization of thorium fuel due to the superior flexibility of fuelling. Two types of thorium-based fuelling strategies of in situ utilization in HTR-PM (China), namely the

Th+HEU MOX fuel schemes and the Th+LEU SEP (separate) schemes, respectively, are shown below (Fig. 44) [49].

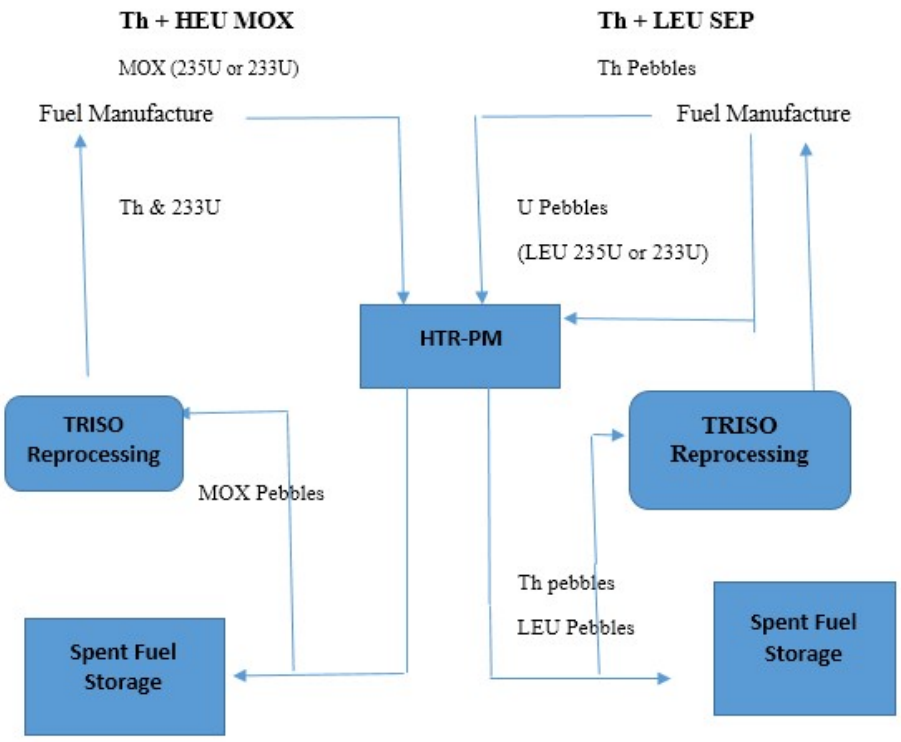

FIG. 44. Schematic figure of ThU-MOX and SEP fuelling schemes.

Breeding and in situ utilization of thorium in thermal reactors have different requirements for the fuelling strategy. For the breeding purpose, the burning of converted ^{233}U has to be avoided as much as possible, and the neutron loss in fission products has to be lowered, indicating the requirement of thorium discharge burn-up as low as possible. On the other hand, the on-line successive refuelling, one of the main features of the pebble bed HTGRs, is also required by the thorium-based breeding in thermal spectrum. However, the reprocessing of the rigid tri-structural isotropic fuel particles featured by the combination of crushing and burning of the C-SiC coating and aqueous solvent extraction process, is more difficult than those of the traditional reactor fuels and needs to be developed. Moreover, the relatively high neutron leakage of pebble bed HTGRs (typically more than 10%) suppresses the possibility of thermal breeding of ^{233}U. Hence breeding is somehow unsuitable for the thorium utilization in pebble bed HTGRs.

The in-situ utilization of thorium based fuels demands high discharge burn-up. The more thorium fuels are depleted, the more ^{233}U is produced and burned to support the chain reaction. The enhancement of burn-up in tri- structural isotropic fuel particles is limited due to the accumulation of the fission products, mainly the gaseous ones. The fission product release rate of ThO_2 fuels is much less than that of UO_2 fuels. Hence the discharge burn-up of the thorium-based fuels can be higher than typical uranium fuels. The technology of fuel fabrication provides the possibility of combining oxides of uranium and thorium in one fuel particle and in different particles, corresponding to the MOX and separate (SEP) cases. The irradiation history of uranium and thorium fuels cannot be separated completely. Therefore, it is difficult to

increase the thorium burn-up further in the MOX schemes. On the other hand, there is a flexibility of refueling in pebble bed HTGR. This makes the irradiation time of thorium pebbles in the SEP schemes can be increased several times than that of uranium pebbles, indicating significant improvement in the utilization of thorium could. Moreover, it is attractive that the in situ utilization of thorium in HTGRs needs no reprocessing, which avoids the complexity and challenges of technology.

High enriched uranium (HEU), with typical enrichment of 93%, is the ideal option for the feed material in the Th-U cycles of HTGRs, as performed in AVR and THTR 300 in Germany [50]. However, the concerns on the proliferation of weapon-grade nuclear materials confine the direct application of HEU fuels in civil nuclear facilities. Fortunately, the risk of HEU proliferation of Th-U cycles in pebble bed HTGR (PB-HTGRs) could be minimized. Firstly, since the concentration of heavy metal nuclides in HTGR fuels is more than an order of magnitude more dilute than in other types of fuels [51], the required amount of HTGR fuels corresponding to a significant quantity of uranium or plutonium is very large, compared with other nuclear fuels. Secondly, the reprocessing of HTGR's fuels is more complicated than other reactor fuels. Furthermore, once the fuel pebbles with HEU-Th MOX particles enter the pebble bed core, a series of technical measures ensure them recycled through the core for some passages and discharged only when achieving very high burn-up, e.g. 90 GW. d/tHM. The residual amount of ^{235}U and plutonium isotopes in spent pebbles is very small. To say the least, if some burned fuel pebbles are taken away for extracting the residual uranium, ^{232}U, the Th-U fuel cycle by-product which has decay daughters with large amount of energetic gamma radiation, could hardly be separated from the desired ^{235}U by using chemical approaches. HEU in Th based MOX type HTGR fuels are much more proliferation resistant than other non-Th based MOX fuels.

For the so-called 'separate loading scheme', i.e. uranium and thorium fuels are loaded into different pebbles, only LEU is selected as feed material. Since the uranium particles contain much more fissile nuclei than the thorium ones, the former will afford much more nuclear power than the latter, implying more rigorous challenges to the integrality of the uranium coated particles, especially for HEU loading. Hence, only LEU is considered in the SEP schemes.

The ultimate aim of the in situ utilization of thorium is to reduce the loading requirement of fissile uranium, namely ^{235}U. This is often represented by the quantity of uranium ore requirement, i.e., the required amount of U_3O_8 per energy production. Generally, the requirement of heavy metal loading per energy production is inversely proportional to the discharge burn-up of fuel elements. Furthermore, the required amount of fissile material is proportional to the enrichment of loaded fuel.

The major purpose of this study is to investigate the possibility of minimizing the on-site refueling effort within the realistic framework of the HTR-PM. The HTR-PM is a demonstration power plant with two PB-HTGR modules of 250 MW (th) and one steam turbine with output of 200 MW(e), which started construction in December 2012. The term of 'realistic framework' means that the supposed Th-U-loaded HTR-PM will obey all the design limits of the real LEU-loaded one. The requirement of uranium ore per energy production is taken to represent the effect of minimizing on-site refueling effort. On the other hand, the requirement of loaded thorium per energy production is also an important parameter in the fuel economy consideration. Although the reprocessing is not considered in this work, the residual ^{233}U in the spent fuels is still investigated to argue the necessity of possible reprocessing in the future.

4.1.1. Thorium-Uranium MOX schemes

Parametric analysis is performed on two parameters: the atomic fraction of uranium in heavy metal and the C/HM ratio, in which the former represents the fissile enrichment in heavy metal and the latter is inversely proportional to the heavy metal loading. For given combination of those two parameters, the discharge burn-up is adjusted to keep the reactor core critical. For comparison, the real fueling scheme of HTR-PM fueled by 8.5% enriched uranium is called the LEU scheme.

The discharge burn-up increases as the uranium fraction increases and the C/HM ratio decreases. The trend of discharge burn-up along with the uranium fraction is reasonable, since increasing the uranium fraction is equivalent to increasing the fissile enrichment in heavy metal. On the other hand, the decrease of C/HM ratio means improving heavy metal loading in the fuel pebbles, reducing the neutron leakage of the reactor core and enhancing the neutron economy.

The major features of the ThU-MOX core, including fueling-related features and safety-related features, are much sensitive to the C/HM ratio, equivalent to the heavy metal loading per fuel pebble. As the heavy metal loading increases, it seems to hold generally that the fueling related features get better and the safety related features get worse. For the optimized parameter combination with C/HM ratio of 300 and uranium fraction of 8.5%, the uranium ore saving compared with the LEU scheme is about 8%, corresponding to about 20 kg/GWd of U_3O_8, while the relative increase of separative work is about 15%. At the same time, the requirement of thorium loading is about 10 kg/GWd of ^{232}Th. Although some improvement in reducing on-site refueling effort is obtained, it is clear that the in situ utilization of thorium is not sufficient for the ThU-MOX schemes.

4.2. SEP SCHEMES AND RESULTS

Since the thorium depletion cannot be improved further when mixed and experiencing the identical irradiation history with HEU in the ThU-MOX schemes, the SEP schemes are considered as the reasonable solution for enhancing the thorium utilization. For the SEP schemes, one may take different recycling strategies for uranium pebbles and thorium pebbles, which can be easily distinguished by using the burn-up measurement system of gamma-spectroscopy. The residence time of thorium pebbles can be lengthened simply by setting sufficiently high discharge threshold for burn-up of thorium pebbles. The LEU is chosen as the feed material because the proliferation risk would increase after using individual uranium pebbles with HEU. The presence of considerable ^{238}U in LEU leads to more risks of reactivity introduction in water ingress accidents. Hence, the mass of heavy metal in one fuel pebble is set as 7 grams, as set in the real LEU scheme of the HTR-PM. The ratio of uranium to thorium is adjustable from 8:7 to 12:3. For the sake of comparison with the LEU scheme, the discharge burn-up of uranium pebbles are fixed at the level of 90 GWd/tHM, while the discharge burn-up of thorium pebbles is adjustable. Correspondingly, the enrichment of uranium is adjusted to keep the reactor core critical.

Firstly, the most important parameter analyzed is the uranium ore requirement per energy production. the uranium ore requirement decreases significantly as the discharge burn-up of thorium increases. However, trends like ‘saturation’ appear when thorium discharge burn-up goes beyond 100 GW. d/tHM. This saturation of uranium ore saving is attributed to the fact that the bonus from converted fissile nuclides will be offset by the increase of fission products in

thorium fuels at high burn-up levels. Therefore, the discharge burn-up of thorium pebbles more than 100 GW. d/tHM is sufficient for maximizing the thorium utilization in the SEP schemes.

On the other hand, another trend emerges that the uranium ore requirement decreases as the uranium to thorium ratio increases, Although the presence of thorium in the reactor core promotes the production of fissile material, it also introduces extra neutron absorption. Hence, if thorium fraction is as high as about half, the neutron absorption of thorium provides more negative contribution to neutron balance than the positive contribution from converted ^{233}U, which demands more ^{235}U, and of course, more uranium ore to keep the core critical. When the thorium fraction goes down, the weakening trend of thorium absorption effect is more rapid than the reduction of fissile production from thorium, leading to the results of uranium ore requirement about 4% lower than the LEU case for the U to Th ratio of 12:3. It is reasonable that the uranium ore requirement will return to the level of LEU case if the thorium fraction approaches zero. Thus, the U: Th of 12:3 case will be near the optimized scheme for the SEP fueling strategy.

As the thorium discharge burn-up increases, the thorium loading requirement decreases drastically, especially in the case of U to Th ratio of 12:3. The lowest result, i.e. less than 0.5 kg/GW. d, is more than one degree of magnitude lower than the corresponding values in MOX schemes. That means quite low thorium supply corresponding to considerable uranium ore saving, the very aim of in situ utilization of thorium. The essential differences of thorium loading requirement between both types of schemes are the utilization fraction of thorium during the fuel cycles. For the deepest discharge burn-up about 200 GW. d/tHM, the thorium fuel will be depleted for more than 20%, far greater than 6% in the MOX schemes. That also indicates that although more discharge burn-up can hardly give more uranium ore saving, it can further save the thorium loading effort.

In summary, the residence time of thorium pebbles can be lengthened up to more than 10 years to obtain optimized utilization of thorium within the HTR-PM. The uranium ore saving is enlarged as thorium burn-up increases and thorium fraction decreases, up to ~4% (10 kg/GW. d of U_3O_8), compared with real LEU loading. As the thorium burn-up increases, thorium loading requirement decreases dramatically to less than 0.5 kg/GW. d, one degree of magnitude lower than the MOX schemes (about 10 kg/GW. d). That means that one saves 10 kg of U_3O_8 while loading only 0.5 kg of thorium. For the optimized cases, the enrichment of LEU in the SEP schemes is close to the LEU-only scheme, which indicates nearly equal separation works. The thorium utilization in the SEP schemes is more sufficient than the MOX schemes, up to more than 20%. On the other hand, similar to the thorium loading requirement, the ^{233}U production rate also decreases dramatically as burn-up increases. This value as low as 0.01 kg/GW. d indicates that the reprocessing of spent fuel is not worthy for SEP case, compared with the MOX schemes.

4.3. FURTHER OPTIMIZATION OF SEP SCHEMES

Since one of the disadvantages of SEP schemes is the relatively low uranium ore saving compared with the MOX schemes, further optimizations for the SEP schemes are performed. There exist other parameters influencing the neutronic features of the reactor. The self-shielding effect of fuel kernels is mainly determined by the diameter of fuel kernel. When the kernel diameter increases, the self-shielding effect of kernel gets stronger, and the neutron absorption fraction of heavy metals decreases. Consequently, the neutron spectrum and the neutronic characteristics in the reactor core will be slightly adjusted by varying the fuel kernel diameter. All the schemes correspond to the U/Th ratio of 12:3 and 72-pass refueling of thorium pebbles,

and the uranium discharge burn-up remains unchanged (90 000 MW. d/tHM). Obviously, the uranium enrichment decreases as the fuel kernel diameter increases, hence the uranium ore requirement also decreases. This can be attributed to the softer neutron spectrum corresponding to the larger fuel kernel which benefits the fissions and harms the resonance absorptions. Softening of neutron spectrum can also be demonstrated by the fact that the maximum water ingress reactivity decreases remarkably as the fuel kernel diameter increases. Consequently, enlarging the size of fuel kernel can further optimize the uranium ore saving and further lower the uranium separation work since the required uranium enrichment is very close to the uranium-only loading scheme, i.e. 8.5%. The optimized uranium ore saving by increasing kernel size is about 6.2%, corresponding to kernel diameter of 80 μm.

Since enhancing the heavy metal loading improves the uranium saving and thorium utilization in the MOX schemes, heavy metal mass per pebble is also important for the optimization of SEP schemes. The results of varying heavy metal mass per pebble, corresponding to the U/Th ratio of 12:3, 72-pass thorium fuel recycling and kernel diameter of 800 μm. As the heavy metal loading increases, the uranium ore requirement decreases firstly, reaches the minimum around the heavy metal mass per pebble of 8 grams, and increases after that. This can be explained by the hardening of in-core neutron spectrum as the heavy metal loading increases, which harms the neutron economy. However, from the point of view of neutron balance, when the heavy metal loading increases slightly, the negative impact of spectrum hardening is still weaker than the positive impact of the decrease of neutron leakage, hence the required uranium enrichment can be suppressed slightly; as the heavy metal loading increases further, the negative impact of spectrum hardening dominates, leading to the increase of uranium ore requirement. Hardening of neutron spectrum can also be demonstrated by the fact that the maximum water ingress reactivity increases remarkably as the heavy metal loading increases. On the other hand, for the cases with heavy metal mass per pebble greater than 8 grams, the maximum water ingress reactivity is remarkably greater than that in the LEU loading case. Consequently, the further optimization for 800μm diameter fuel kernel case is to enhance the heavy metal mass per pebble to 8 grams, and the optimized uranium ore requirement is 217.6 kg/GW.d, corresponding to uranium saving of about 7.3%, which is much close to the optimized MOX scheme.

Further optimization of SEP schemes is focused on two options: enlarging the fuel kernel and enhancing the heavy metal loading. On the other hand, extra cost in other engineering issues restricts the optimization of those two options, providing the optimized scheme so far: the scheme with U/Th ratio of 12:3, 72-pass thorium fuel recycling, kernel diameter of 800μm and heavy metal mass per pebble of 8 grams. The corresponding uranium enrichment is about 8.9% and the uranium saving is about 7.3%. This result reveals that the SEP schemes can provide the uranium ore saving similar to the MOX schemes, with more than one order of magnitude lower thorium loading requirement and much less separative works for uranium. Hence, it is further demonstrated that the SEP schemes is better choice than the MOX schemes in the in situ utilization of thorium in PB-HTRs.

4.4. CONCLUSIONS

The feasible options of thorium-based fuelling aimed at in situ utilization of thorium in HTR-PM are investigated, with emphasis on the neutronics and thermal-hydraulics. It describes not only the features concerning thorium utilization and uranium saving, but also the safety-related features. The heavy metal loading per fuel pebble will have to be larger than the real LEU scheme of the HTR-PM and have to be confined less than 13 g/pebble to avoid the maximum fuel temperature higher than 1620 ºC, the design limit of the HTR-PM's fuel elements. The optimized result of MOX schemes gives about 8% (20 kg/GW. d) saving of uranium ore

compared with the LEU scheme of the HTR-PM. On the other hand, the uranium pebble fraction about 80% in the mixed fuel pebbles gives rise to about 4% (10 kg/GW. d) saving of uranium ore compared with the LEU scheme of the HTR-PM. It seems that the MOX schemes have better performance on the thorium in situ utilization.

However, the SEP schemes are more attractive than the MOX schemes since the former have more benefits than the latter. The SEP schemes utilize the LEU fuels (<20%), which gives not only less separation works, but also good non-proliferation features. The SEP schemes provide convenient fuel manufacture, discrimination during operation, and separate reprocessing of U and Th fuels if possible. The SEP schemes needs much lower thorium loading requirement than MOX, mainly due to the long recycle time and relatively sufficient burning of thorium fuels. Also, the SEP schemes have quite sufficient consumption of the converted ^{233}U, making the further processing unneeded. All these factors make the SEP schemes more superior than the MOX schemes.

Furthermore, although the normal configurations of SEP schemes can only provide about half uranium saving compared with the MOX schemes, the further optimization of the former gives similar uranium saving (~7.3%) to the latter. Two kinds of parameter optimization are utilized: enlarging the fuel kernel and enhancing the heavy metal loading. Within the parameter range of the optimization, the safety-related parameters, including the fuel temperature, the maximum power density, the maximum power per pebble and the maximum water ingress reactivity, are all in the acceptable range. This result indicates that the SEP schemes can provide the uranium ore saving similar to the MOX schemes, with more than one order of magnitude lower thorium loading requirement and much less separative works for uranium. Hence, it is further demonstrated that the SEP schemes is a better choice than the MOX schemes in the in situ utilization of thorium in PB-HTGRs.

In summary, the flexibility of fuelling of PB- HTGRs provides good performance of the in situ utilization of thorium, especially for the SEP schemes. One of the key challenges of optimization of SEP schemes is high burn-up of thorium fuel pebbles with relatively large fuel kernel. Fortunately, the fission product release rate of ThO_2 is much lower than UO_2, indicating higher resistance for high burn-up of ThO_2 than UO_2. Furthermore, more rigid fuel particle coating can be studied to improve the containment for the fission products.

5. DEPLOYMENT OF THORIUM IN MOLTEN SALT REACTOR SYSTEMS

5.1. INTRODUCTION

Molten Salt Reactor (MSR) has advantages of high resources utilization, reduced waste generation, and lower risk with an exclusion of severe accidents due to liquid fuel. This reactor type may become more economical than current nuclear reactors since it not only operates at low pressures but also has negative reactivity coefficients and thereby requiring a simplified safety approach. It may very well fit the ’low waste, low risk‘ criteria for the public towards a better acceptance of nuclear energy generation in the future.

The MSR fuel consists of a molten carrier salt mixed with the salts of actinides and fission products (FPs). MSR can be, in general, designed with fluoride or chloride carrier salts, in thermal or fast neutron spectrum, and in Th-U or U-Pu fuel cycle. Only few combinations of these options allow for sustainable operation in the breeding or iso-breeding closed fuel cycle.

The fluorides have generally lower parasitic capture probability than chlorides. At the same time, fluorides, even in fast MSR, provide softer neutron spectrum than chlorides due to the higher scattering cross-section of ^{19}F and its lower atomic number. Also, the solubility of PuF_3 in the fluoride carrier salts may be limited. Hence, there are three main options for the sustainable MSR iso-breeder design with Th fuel:

— Thermal spectrum fluoride salts MSR in Th-U cycle;
— Fast spectrum fluoride salts MSR in Th-U cycle;
— Fast spectrum chloride salts MSR in Th-U or U-Pu cycle.

This study will focus predominantly on the thermal and fast spectrum MSR with fluoride salts and on the Th-U iso-breeding fuel cycle. It is divided into four parts. The first part focusses on the fuel cycle technology for the fluoride salts, the second part addresses the interconnection between the fuel cycle technology and neutronics impact of FPs, the third part analyses the iso-breeding Th-U closed cycle performance at equilibrium, and finally in the fourth part several fuel cycle scenarios are compared.

5.2. MSR FUEL CYCLE TECHNOLOGY

MSR is classified to be a non-conventional nuclear reactor type, which exhibits some very specific features based on the liquid state of the fuel. It can circulate through the primary circuit and act simultaneously as the coolant. Furthermore, the liquid state enables a continuous refill or removal of the fuel from the core. It is often referred as on-line reprocessing and especially in thermal MSR it is necessary for keeping the Th-U breeder reactor in operation for a long time. The continuous reprocessing allows not only for the typical neutron poisons removal (FPs like xenon, krypton, lanthanides), but also for a very effective extraction of bred fissile material (^{233}U). The fuel salt clean-up technology is strongly linked with the MSR fuel cycle and with the continuous refill of the new fuel (thorium) into the reactor system. It is related to another MSR advantage; it has no need of solid fuel fabrication. A typical molten salt fuel consists of thorium and uranium fluorides dissolved in carrier molten salt. As a reference carrier salt for thermal spectrum MSR is considered ^{7}LiF-BeF_2 and ^{7}LiF for fast spectrum MSR.

5.2.1. MSR fuel reprocessing

The separation processes proposed for the MSR fuel reprocessing are generally based on the established pyrochemical techniques. Unlike the solid Th based fuel reprocessing, the MSR on-line reprocessing takes advantage of the possibility to separate protactinium ^{233}Pa from the MSR system to eliminate its parasitic neutron capture ^{233}Pa (n, γ) $\rightarrow$ ^{234}Pa, which leads to the undesirable ^{234}U production. This separation can significantly increase the breeding gain.

The on-line reprocessing refers here to the continual removal and refill of the salt. The reprocessing itself will be probably based on batches and will take certain time. There are only few techniques for direct and continuous separation of FPs from the fuel salt. One of them is the helium sparging technique for the gaseous and noble metal FPs removal through the off-gas system.

The thermal MSR design and operation were already verified during the molten salt reactor experiment (MSRE) project. It was, however, not operated with Th and the on-line reprocessing was never fully realized. Hence, it may represent a killing point for the breeding and for the MSR deployment in a closed Th-U cycle [52]. While the thorium fuel for MSR breeder can be prepared ex-situ, the on-line reprocessing and recycling of ^{233}U will have be done in-situ and

tightly connected with the MSR system. Furthermore, the choice of separation technology will strongly influence the fuel salt chemistry.

The primary processing of the fresh thorium fuel salt is relatively easy. The suitable method of the oxide-free thorium tetrafluoride, ThF_4, processing is based on the reaction of thorium dioxide ThO_2 with anhydrous hydrogen fluoride HF. The process is well known and mastered. It can be performed by gradual hydrofluorination of thorium dioxide ThO_2 at the temperature range from 250°C to 550°C. The final product ThF_4 is of the MSR fuel quality and can be easily dissolved in MSR carrier salt based on the $^{7}LiF–BeF_2$ mixture [53].

However, the on-line reprocessing of the irradiated MSR fuel is considered as extremely difficult and complicated radiochemical technology. It has a great number of limitations caused by chemical character of the liquid MSR fuel, its high radioactivity and heat generation, and finally by the direct link to the reactor chemistry itself. Even though the on-line reprocessing technology was never fully tested, there was a significant chemical and technological background achieved in ORNL in 1960s and 1970s [52]. Simplified scheme of fuel cycle of MSR Th-breeder is shown in Fig. 45 [54].

The general aim of the MSR fuel on-line reprocessing is to keep the FPs concentration in the reactor low and simultaneously maintain the required fissile material load. On-line reprocessing means, that part of the salt is continuously redirected from the primary circuit to the reprocessing unit, where the FPs are extracted and uranium (^{233}U) or other potential actinides are dissolved again in the carrier salt and returned back into the primary circuit. The efficiency of FPs removal from the salt does not need to be high; however, it is important to keep the actinides losses very low during this process. The main mission of the on-line reprocessing of the fertile salt in the blanket circuit is to separate protactinium ^{233}Pa and reduce so its parasitic neutron capture. The protactinium is thereafter stored outside the reactor till it decays to ^{233}U.

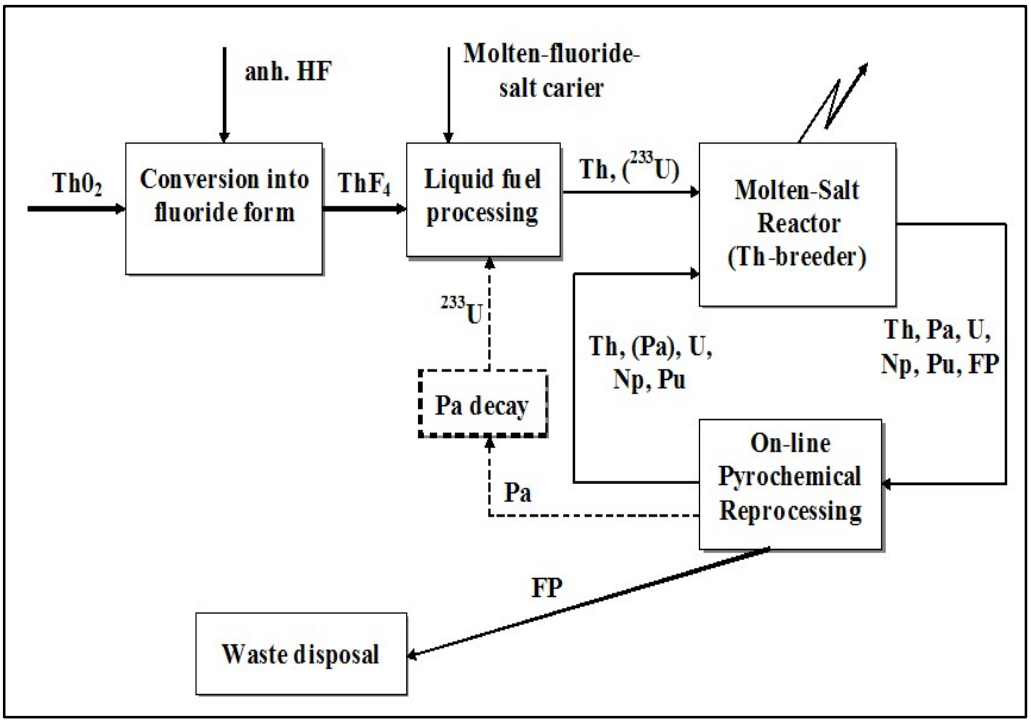

FIG.45. Scheme of fuel cycle of MSR Th-breeder (*reproduced from Ref. [54] with permission courtesy of Elsevier).*

The general spirit of MSR on-line reprocessing of the MSR fissile fluid circuit is to keep the reactor in steady-state conditions by continuous cleaning-up of the fissile-fluid circuit salt. It means, that some part of the salt circulating in the primary circuit is piped to the reprocessing unit, where the fission products are extracted and then moved to waste, whereas the separated uranium (^{233}U) or other potential actinides are dissolved again in the carrier salt and returned back into the fissile-fluid circuit. As there is all the time the same concentration of fission products in the primary circuit, the removal of these elements in reprocessing unit need not be absolute, however no actinides may be moved into the waste stream. The main mission of the on-line reprocessing of the fertile-fluid circuit is to separate freshly originated protactinium ^{233}Pa to remove it from the neutron flux. The protactinium is thereafter stored outside the reactor till it is converted by beta decay to ^{233}U. The original partitioning techniques proposed by ORNL for MSR fuel on-line reprocessing were fused salt fluoride volatilization and molten salt / liquid metal extraction [52]. The current effort is focused mainly on the electrochemical separation techniques from fluoride molten salt media which do not introduce any other chemicals into the process.

The choice of fluoride salts suitable for electrochemical separations is made on the basis of low melting points, high electrochemical stability, high solubility of selected compounds and favourable physical properties such as viscosity, electrical conductivity etc. The candidate salt solutions are:

1) Eutectic mixture of LiF-NaF-KF (FLINAK);
2) Mixture of LiF-BeF_2 (FLIBE);
3) Eutectic mixture of LiF-CaF_2.

In eutectic mixture of LiF-NaF-KF and/or in LiF-CaF2 melts, both uranium and thorium and most of fission products (lanthanides) can be electrochemically separated.

5.2.2. Single-fluid MSR reprocessing design

Fast or thermal spectrum MSR Th-U breeder can be designed either as single-fluid system, where the fissile (^{233}U) and fertile (^{232}Th) materials are mixed together in the fuel salt or as a two-fluid system with separated fissile and fertile salts [55]. Both designs bring some advantages and drawbacks and, naturally, they significantly affect the fuel cycle technology including the on-line reprocessing. The engineering design of a reactor core with single-fluid can be simpler. However, the respective on-line reprocessing technology may be more challenging, and it may have lower utilization of neutron leakage and thus potentially lower breeding gain. The design of two-fluid MSR may be challenging and complicated. At the same time, the breeding gain can be higher and the on-line reprocessing technology simpler, especially in case of the fertile-fluid circuit [53, 56]. These two designs can be also combined into a one-and-half-fluid system, where the fissile and fertile salts are mixed in the core; nonetheless, the fertile salt blanket is still used to utilize the leaking neutrons.

The main principles of the on-line reprocessing technology devoted to single-fluid thermal spectrum MSR design were already described and discussed [53]. Here the reprocessing technology has two main missions:

- To extract FPs which represent neutron poisons;
- To separate fissile material ^{233}U or its precursor ^{233}Pa which is freshly bred.

The main separation methods proposed for chemical partitioning within the MSR fuel cycle are:

- Fluoride volatilization processes;
- Molten salt / liquid metal (ms/lm) extraction processes;
- Electrochemical separation processes;
- Gas extraction method by he sparging [52].

The basic complication for the reprocessing design resides in the fact that the MSR carrier salt FLIBE is neither enough stable for direct electro-separation of all spent fuel components nor suitable for individual extraction of lanthanides and thorium by liquid metal extraction technique. For all that a promising technology for single-fluid MSR system was proposed based on recent development in electrochemical partitioning of uranium, thorium and fission products from fluoride molten salt media. The flow-sheet diagram taking into account the possibility of electrochemistry is shown in Fig. 46 [54].

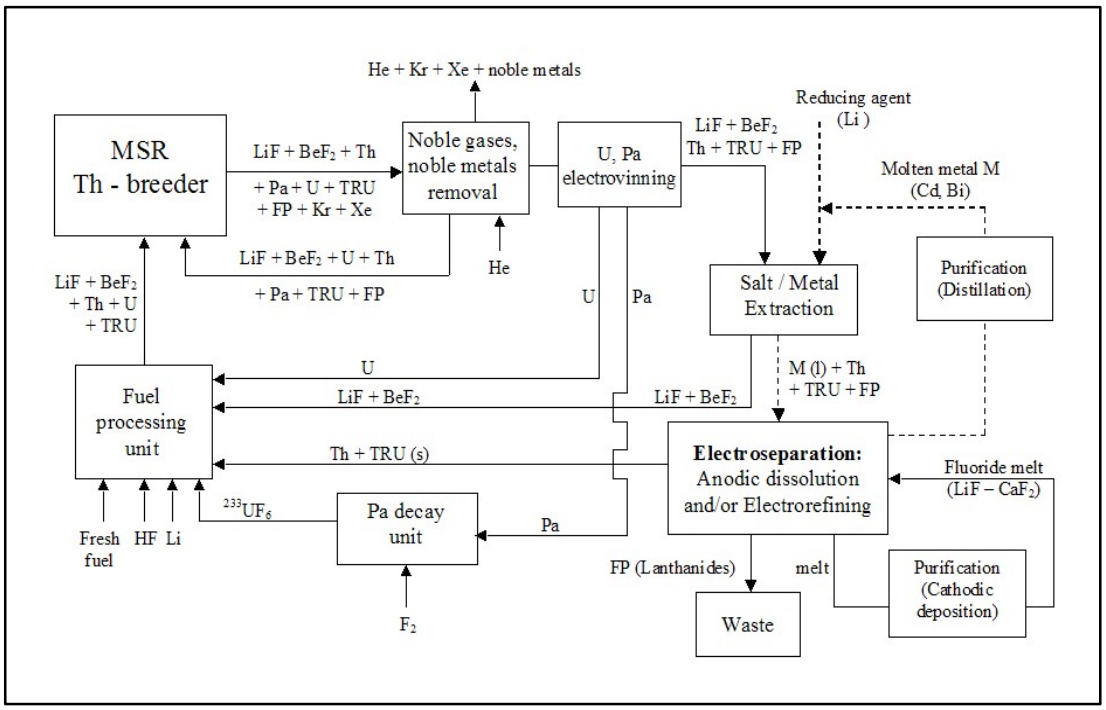

FIG. 46. Conceptual flowsheet of single-fluid MSR Th-breeder on-line reprocessing technology (reproduced from Ref. [54] with permission courtesy of Elsevier).

The principle of proposed on-line reprocessing technology is based on a combination of non-selective molten salt/liquid metal reductive extraction and subsequent selective electro separation processes.

5.2.3. Two-fluid MSR reprocessing design

The requirements for reprocessing of two- fluid system, fissile-fluid and fertile-fluid circuits are quite different. The rate of fissile-fluid reprocessing is determined mainly by the requirement to extract ^{233}Pa from the fertile-fluid circuit as fast as possible and keep the concentration of fission products at the acceptable level in order to eliminate (n, γ) reaction leading undesirable ^{234}U.

Based on the thermodynamic data of FLIBE melt and the thermodynamic properties of PaF_4, there is a presumption that protactinium could be separated directly from this melt. The conceptual on-line reprocessing flowsheets of fissile-fluid and fertile-fluid MSR circuits are shown in Figs. 47 and 48 [54][55].

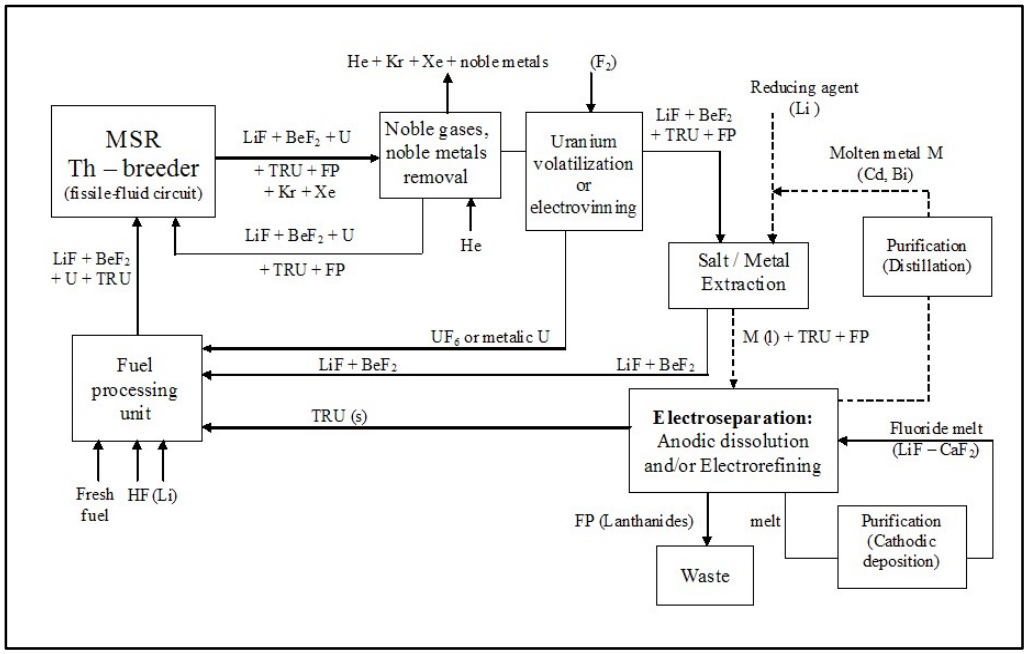

FIG. 47. Conceptual flowsheet of MSR fissile-fluid circuit on-line reprocessing technology (*reproduced from Ref. [54] with permission courtesy of Elsevier).*

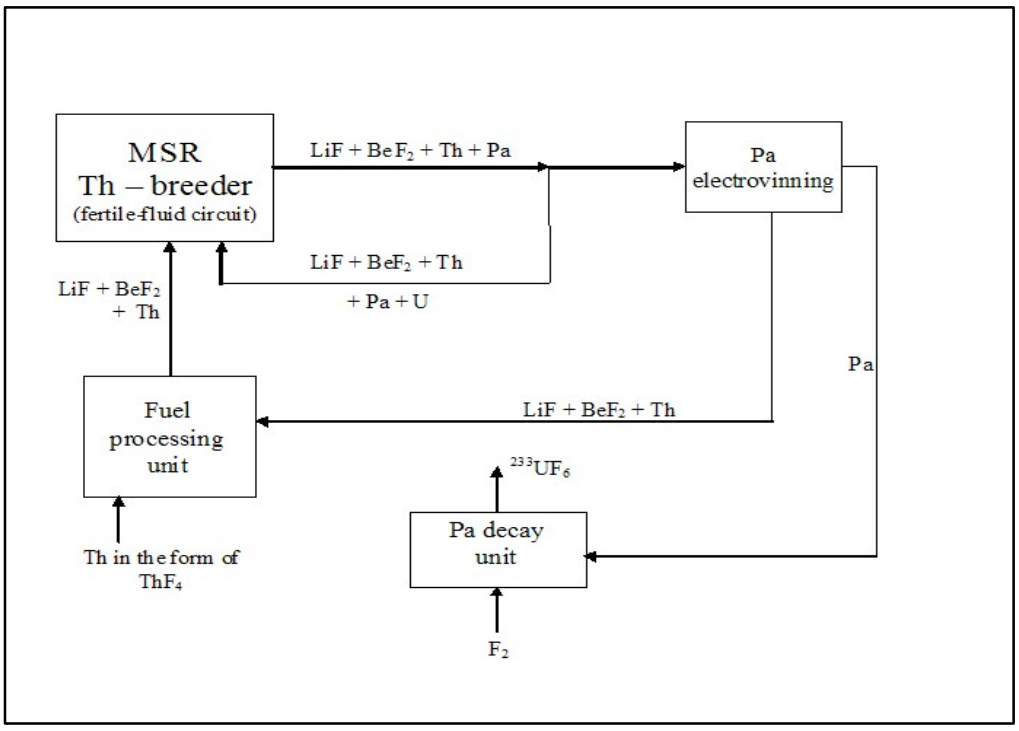

FIG. 48. Conceptual flowsheet of MSR fertile-fluid circuit on-line reprocessing technology (*reproduced from Ref. [54] with permission courtesy of Elsevier).*

The reprocessing technology for two-fluid MSR design could be simplified. At the same time the breeding performance of the system may be increased. Nonetheless, special approach to the non-proliferation issues will be necessary. To ensure the highest breeding ratio of the reactor system, the protactinium removal time has to be as short as possible. The reason for it is to

prevent undesirable nuclear n, γ reaction of $^{233}Pa \rightarrow {}^{234}Pa$ in the reactor core and to allow its decay (with half-life of 27 days) into ^{233}U outside of the neutron flux. Then the isolated protactinium is practically pure ^{233}Pa isotope, nonetheless, it contents small amount of ^{232}Pa and ^{234}Pa. Especially the ^{232}Pa may help to contaminate the ^{233}U with small amount of ^{232}U.

The appropriate way, how to increase proliferation resistance of the MSR Th-U fuel cycle is via increasing of the physical protection of the system — by denaturing of the bred fissile ^{233}U by other uranium isotopes present in MSR fuel circuit. It can be realized by mixing of the separated protactinium with uranium from the MSR fuel circuit before the protactinium decay. In the U vector of the fissile salt there is always small amount of ^{232}U. This isotope can significantly decrease the proliferation risk by increasing the radiation barrier caused by its decay daughter products (mainly ^{208}Tl, which emits 2.6 MeV gamma photons).

Generally, the on-line reprocessing of liquid molten salt fuel is technically difficult, and the chemical partitioning process has to be based on differences in chemical stability of individual fluorides of actinides and FPs in the melt. Thorium tetrafluoride and majority of the FPs fluorides are more stable in the carrier melt than the uranium and protactinium tetrafluorides. Hence, the uranium and protactinium have to be separated as first. Accordingly, majority of on-line reprocessing flowsheet includes the separation of uranium. Later, it will be shown in the fuel cycle scenario part that this disadvantage may represent to certain extend an advantage. It will be assumed that only uranium and protactinium are recycled rapidly and in-situ and that the rest of the salt can be processed much later and ex-situ.

5.3. FISSION PRODUCTS IMPACT ON THE NEUTRONICS

The mutual link between the MSR fuel cycle neutronics and the on-line reprocessing chemistry is extremely strong. Intensity of the salt irradiation and related power production affect the required capacity of the on-line reprocessing unit; at the same time, the reprocessing rate has influence on the composition of the fuel salt. The neutron economy in the thermal MSR breeder is tight; hence a fast removal of the most poisoning FPs from the salt is necessary. The on-line reprocessing approaches were discussed, as one of the MSR advantages, in the previous part. Here the analysis of the FPs composition and the respective neutron capture distribution is presented, with accent on the mutual link between neutronics and chemistry. The study is based on a thermal spectrum MSR initially fuelled by pure ^{233}U.

5.3.1. Assumptions

The thermal MSR system used in this study was adopted and optimized for high breeding gain at the beginning of life with ^{233}U fissile load [56]. The task of the referred study was to identify the main neutron poisons among the FPs on the basis of their production rates and neutron capture cross sections in the thermal spectrum MSR. The knowledge of these data can determine the technology of chemical partitioning and the details of the conceptual reprocessing flowsheet. The study focused on fuel composition at the initial phase of the burn-up and assumed that the fuel consists of the ^{232}Th and ^{233}U isotopes dissolved in the carrier salt. Primarily, the individual FP formation rates and their influences on neutron economy were monitored. A comparison was made between single, and a two-fluid core configuration as shown in Fig. 49. The main assumptions for the simulation were:

— Salt composition for single-fluid reactor: $LiF\text{-}BeF_2\text{-}ThF_4\text{-}UF_4$ - 71.7–16–12–0.3 mole % with density 3.313 g/cm^3;
— Fuel salt composition for two-fluid reactor: $LiF\text{-}BeF_2\text{-}{}^{233}UF_4$ - 68.434–31.3–0.266 mole % with density 1.842 g/cm^3;

— Monte Carlo code MCNPX v2.7 in burnup mode;
— ENDF/B-VII.0 library and data for 900 K temperature;
— Power — 12.5 W/gHM.

Very higher thermal power output of the fuel salt (497 kW/l equivalent to 12.5 W/gHM) was assumed in [56]. Such a power would be still acceptable for the thermal hydraulics. However, it may jeopardize the breeding performance of the single-fluid design, because both the ^{233}Pa amount in the core and its parasitic capture rate are directly proportional to the reactor power. The same power was adopted in the study, which focuses on FPs influence on the breeding gain.

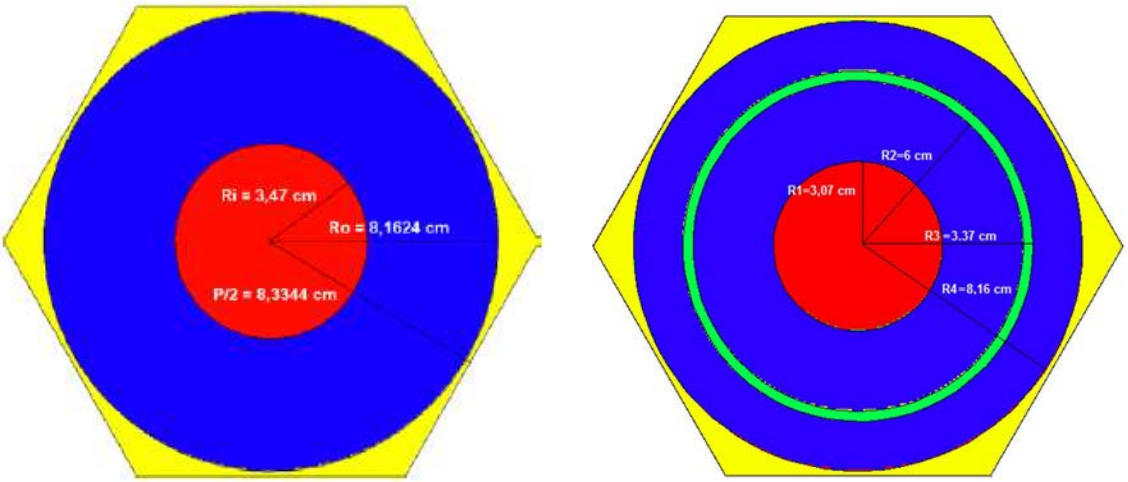

FIG. 49. Comparison of the fuel channels used in the study for single-fluid (left) and two-fluid (right). Graphite block (blue), fuel salt (red), fertile salt (green), and helium (yellow) (courtesy of Jan Uhlir, Research Centre Řež).

5.3.2. Results

The first major result of this study is that the FPs composition virtually does not differ between the single-fluid and two-fluid MSR designs. As it is shown in Fig. 50, the FPs composition originated from fresh fuel after one-day of irradiation is dominated by Ce, Xe, and Zr. Nonetheless, the Ce capture cross-section is low, and it does not represent a major neutron poison. The distribution of FPs capture rate in the irradiated fuel is shown in Fig. 51. Before the removal of noble gases, it is dominated by Xe. Once the Xe is removed by the off-gas system, the major poisons became Sm, Pm, and Nd. Their capture rates distribution in the salt entering the salt/metal extraction and electroseparation, according to scheme in Fig. 49, is presented in Fig. 52. The noble gas removal (helium sparging) at 100 % efficiency helps to prevent more than 98 % of overall parasitic absorption on fission products in the core. The Sm, Pm, and Nd are responsible for three quarters of the remaining 2 % of FPs capture rate.

Based on these calculations, it is evident that the reprocessing technology focuses predominantly on the lanthanide's removal, especially on Sm, Pm, and Nd. These elements affect the neutron economy at most and thus also the breeding performance.

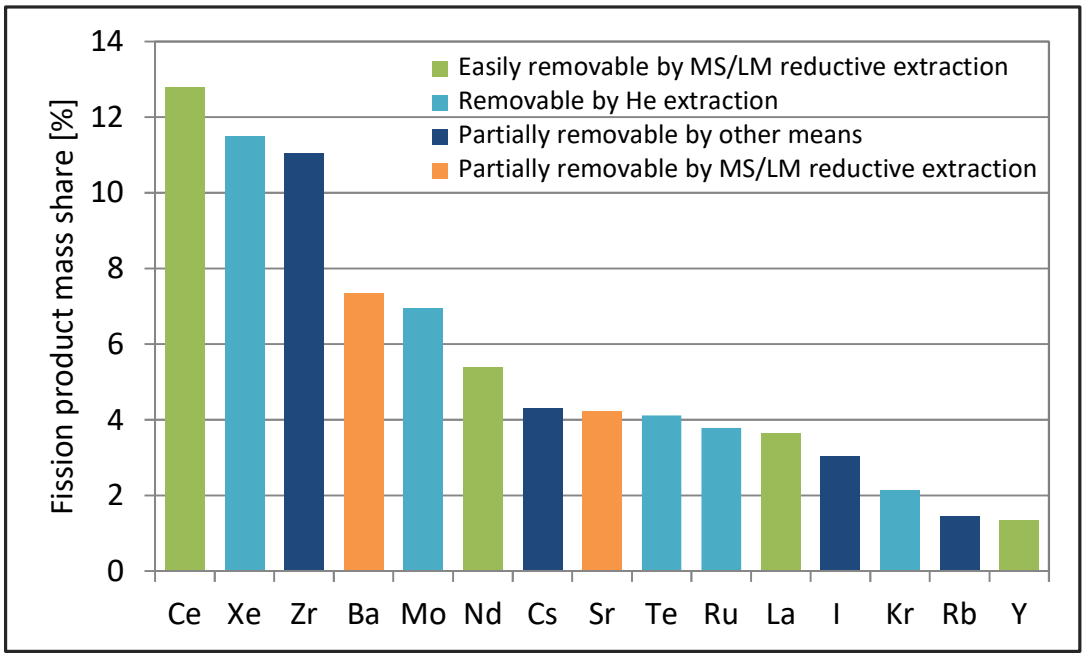

FIG. 50. Mass production of main fission products originated from fresh fuel after one-day reactor operation (reproduced from Ref. [55] with permission).

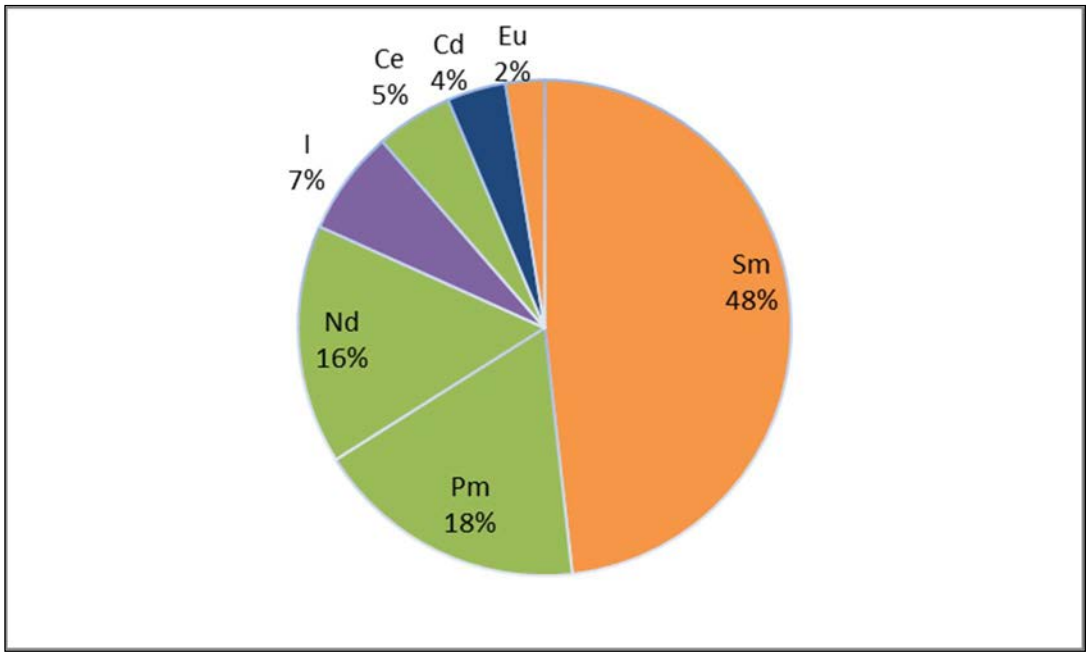

FIG. 51. Distribution of fission products capture rate leaving the MSR core (before noble gases removal) (reproduced from Ref. [55] with permission).

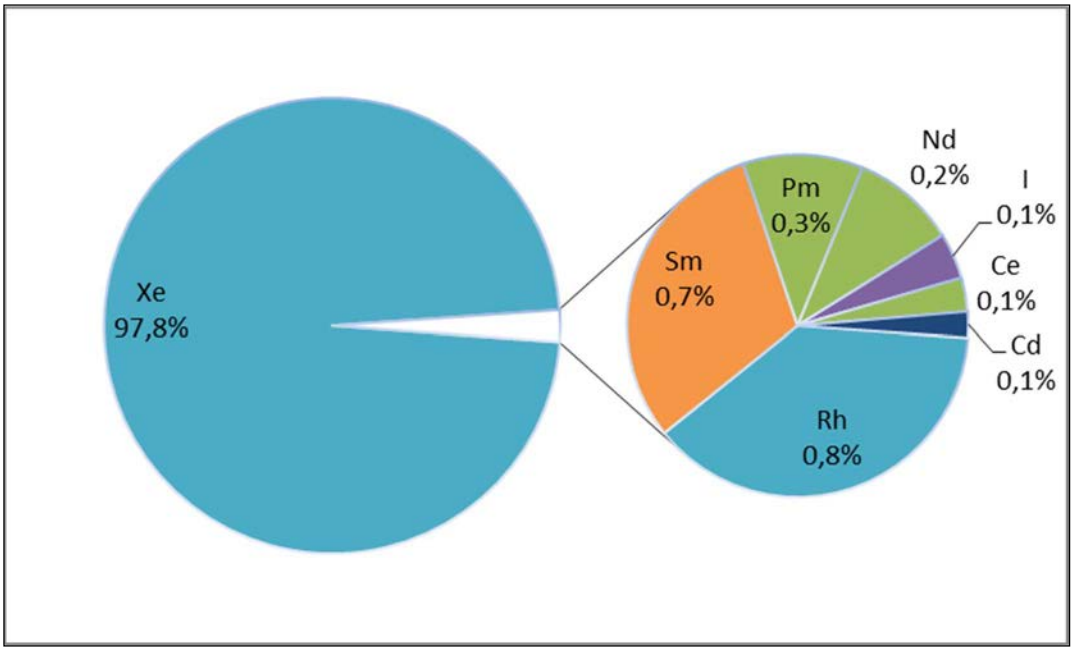

FIG. 52. Distribution of fission products capture rate entering the reprocessing unit (before salt/metal extraction and electroseparation) (reproduced from Ref. [55] with permission).

To achieve good neutron economy, satisfactory breeding performance and acceptable operational economy the reprocessing technology is required to be optimized. The way, how to do it, is in different reprocessing rates and separation efficiencies for various groups of fission products. Whereas Sm, Pm, and Nd requires the fastest and robust removal, the rest can be treated slower or with lower separation efficiency. The current investigation confirms that electrochemical separation of main actinides and fission products from the fuel circuit is possible, but the further technological development is necessary.

It may be noted that the presented results are relevant for the beginning of the reactor life. With increasing burnup, the fuel composition will change, and the build-up of higher actinides will have negative influence on the neutron economy. It is therefore necessary to study the neutronics performance at the equilibrium state, when the concentrations of all higher actinides are already stabilised.

5.4. MSR PERFORMANCE IN EQUILIBRIUM CLOSED THORIUM-URANIUM CYCLE

Closed Th-U fuel cycle is generally tight from the neutron economy point of view; because ^{233}U produces, practically independently of the neutron spectrum, in average only 2.5 neutrons per fission. Accordingly, iso-breeding conditions can be achieved only if low absorption materials are used. The fluoride salts ^{7}LiF and BeF_2 as well as the graphite, which is chemically compatible with the salts, belongs to the materials with the lowest neutron absorption. Hence, they are used as a carrier salt or as a moderator in many proposed MSR reactors. Flexibility in MSR lattice allows for designing reactors with different neutron spectrum, from thermal through epithermal to fast. The molten salt reactor with simplified fuel recycling and salt cleaning and the analysis of fuel cycles are given in Ref.[57-59] The most representative design for the graphite moderated thermal MSR is the Molten Salt Breeder Reactor (MSBR) [60] developed in Oak Ridge National Laboratory. The non-moderated fast MSR can be represented by Molten Salt Fast Reactor (MSFR) [61] proposed in the frame of EU project EVOL. The compositions of these two cores differ. In the MSBR case, the core consists of two zones with different graphite shares and thus with different moderation. The same salt is flowing through

both of these zones. Its respective molar composition is: 71.7% LiF, 16% BeF_2, 12% ThF_4, and 0.3% UF_4 and its density at 600°C (873°K) is 3350 kg/m^3. The MSFR core contains only fluoride fuel salts composed of 77.5 molar % of LiF and 22.5 molar % of Actinides (Ac), mainly Th ~20% and U ~2.5%. The salt density at 750°C is 4100 kg/m^3. In both cores the Li is foreseen to be enriched in ^{7}Li up to 99.999 atomic %.

These two salts have several advantages and disadvantages. The MSFR salt has higher melting point, on the other hand, the MSBR salt includes Be and may have higher tritium production. Furthermore, based on the above fuel salt molar compositions and densities, it can be seen that the Ac specific mass in the MSFR salt is by 60% higher than in the MSBR salt. Generally, compared to oxide or metallic fuel, salt is a low density fuel form with only 1500-2500 kg/m^3 partial actinide density. The actual actinide density in the MSBR core is further diluted by the graphite. Hence, if the iso-breeding conditions has to be achieved, the neutron absorption of the other non-fuel materials proposed for MSR cores will be very low.

5.5. SELECTED FUEL CYCLE SENARIOS

5.5.1. Reactivity evolution and FPs sensitivity

The MSR performance was in the previous part analysed at beginning of equilibrium cycle, where the salt is clean and without FPs. However, a 6-month irradiation period between two fuel reprocessing was simulated for each case of the parametric study. The relative burn-up of the fuel in Fission Material (FIMA) % strongly depends on the core size and the respective flux level. Accordingly, the burn-up in FIMA % during the 6 months irradiation strongly differs between the cases. Figure 53 shows that it ranges from 0.1 FIMA% for thermal MSR to 0.9 FIMA% for fast MSR. It is related to higher total Ac mass load in the thermal MSR. Even though the burn-up differs, the reactivity impact of the created FPs can be evaluated relative to FIMA%. It provides burn-up reactivity in PCM/FIMA%, which predominantly quantifies the reactivity worth of the produced FPs. Figure 53 shows that the thermal MSR is sensitive to the FPs, which introduce strong negative reactivity. On the other hand, reactivity change in fast MSR is virtually zero or positive. Also, in this core the FPs introduce negative reactivity. It is however weaker. Moreover, it is compensated by the reduction of Th capture. Accordingly, zero or even slightly positive reactivity swing can be observed for fast MSR. This phenomenon will be analysed in the next sub-section. The Th capture reduction occurs also in thermal MSR; nonetheless, the absolute Th mass is much higher and the relative change thus smaller. Furthermore, the relative FPs neutron capture rate is higher in thermal spectrum. This is also the reason why an intensive on-line reprocessing is necessary in thermal MSR to achieve the breeding. Based on Fig. 53, it can be also concluded that criticality at the beginning of equilibrium cycle can be sufficient criteria for fast MSR operation in iso-breeding cycle. On the other hand, thermal MSR will still need excess reactivity to compensate for the FPs negative reactivity even in the case of the fast FPs removal.

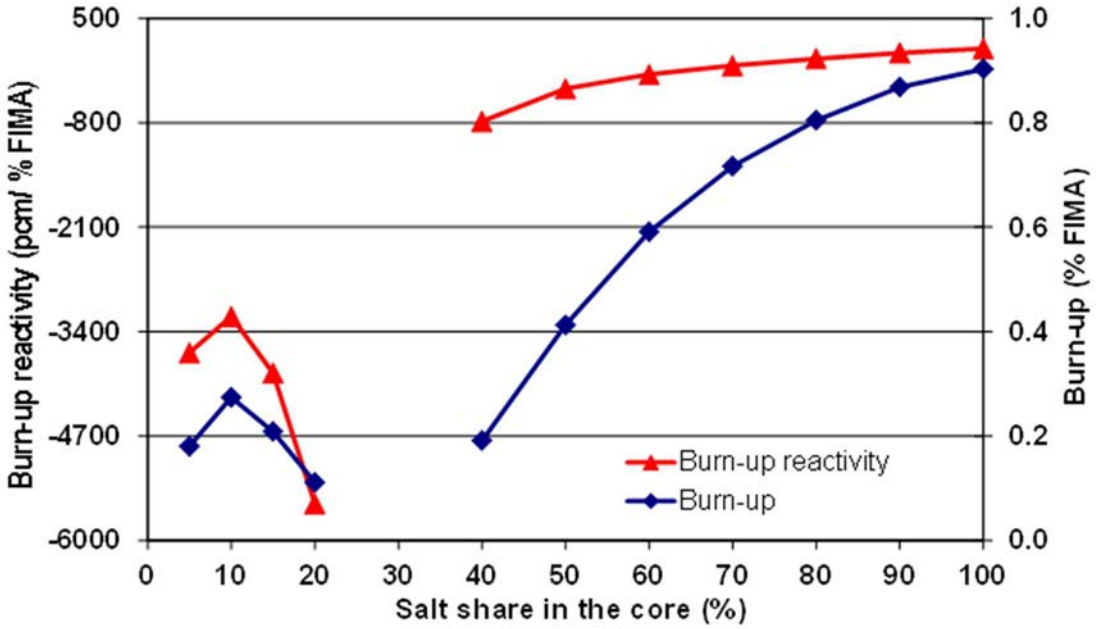

FIG. 53. The burn-up (FIMA %) and the burn-up reactivity (in pcm/% FIMA) assuming 6 months irradiation period, 1500MWth power, and classical channel geometry geometry (courtesy of Krepel Jiri, Paul Sherrer Institut).

5.5.2. Fuel cycle length and reprocessing strategy

In the above parametric study, it was assumed that the fuel salt is cleaned or reprocessed after every 6 months of irradiation at 1500 MWth power, that the actinides are recycled without reprocessing losses, and that the actinides molar share in the salt after cleaning was constant at 22.5 molar %. In other words, the FPs removal and Th refiling happened at the same time period. Furthermore, entire salt volume was processed. Such an intensive reprocessing strategy may be not economical.

The fast iso-breeding MSR reactors without graphite is critical for core radius of 107.8 cm. It corresponds to a volume of 7.3 m^3. This is slightly less than the 9 m^3 volume of the MSFR core. In the following study the core size was thus adjusted to fit the MSFR salt volume. It was assumed that salt volume in the primary circuit is 18 m^3 and that half of the salt is in the core. Since the adjusted core is bigger than the iso-breeding core, slight breeding is expected. On the other hand, recycling efficiency of 100% was used only for U. For the other Ac 1 % losses were allowed and simulated.

The imposed power of the reactor was slightly lower than for MSFR. The power of 2.6 GWth was selected so that every year of effective operation corresponds roughly to 1 ton of burnt fuel. Since only the core is simulated in this study and since it includes only half of the salt, the simulated core power was only 1.3 GWth. The presented masses thus correspond to half of the overall salt inventory in the primary circuit.

Seven salt treatment schemes are shown in Table 24 [62]. The first six schemes are based on batch-wise strategy, where the FPs removal and Th refilling has the same frequency. The last scheme relies on continuous FPs removal model by fictitious decay constant. However, Th is still refilled batch-wise on a 1-month basis.

TABLE 24. SEVEN SIMULATED SALT TREATMENT SCHEMES AND RESPECTIVE SALT VOLUME REQUIRED FOR REACTOR OPERATION (reproduced from Springer [62])

Scheme Nr.	FPs treatment	Th refilling	Minimal required salt volume
1	18000l each 24M	each 24M	36 m^3
2	9000l each 12M	each 12M	27 m^3
3	4500l each 6M	each 6M	22.5 m^3
4	2250l each 3M	each 3M	20.25 m^3
5	750l each 1M	each 1M	18.75 m^3
6	25l each 1day	each 1day	18 m^3
7	continuous	each 1M	18 m^3

These schemes were selected so that in all cases the equivalent reprocessing rate is equal to 25 l/day. It corresponds to reprocessing of whole primary circuit volume (18 m3) in 2 years. In all cases the same reprocessing unit capacity is applicable; for instance, in the first scheme, the reprocessing unit will start with two years delay and take the daily amount of spent salt from another storage volume outside of the primary circuit. Hence, the delay is the only implication for the reprocessing unit. On the other hand, for the reactor operation, different salt amounts are required for each scheme. In case of whole primary circuit reprocessing, it is assumed that the salt in the core will be replaced with another fresh salt and that the burned salt will be reprocessed independently during the next two years. Thus, a minimum of twice the volume of primary circuit is necessary to operate the core. The minimal required volume to operate the reactor in given scheme is also shown in Table 24.

The first major result shown in Fig. 54 is that the reactivity is increasing with burn-up for all selected recycling schemes. Only in the case of a 1-day batch, the time is too short to see the oscillations in the chart. There are two major evolutions during the fuel irradiation; Th mass is being reduced and mass of soluble FPs grows. Since the reactivity grows with the burn-up, the positive component introduced by reduced Th capture has to be stronger than the negative component introduced by parasitic FPs capture.

In equilibrium cycle the overall breeding gain is zero in all EQL3D simulations. In other words, the mass flows are stabilized, and only fertile material is added to the core to replace the FPs. The simulated core acts as an iso-breeder or break-even reactor. The capability for additional breeding is thus measured indirectly through the average reactivity excess. Any reactivity excess represents potential for fertile material insertion, which can be used for supplementary breeding. The 24 months case provides the highest reactivity excess.

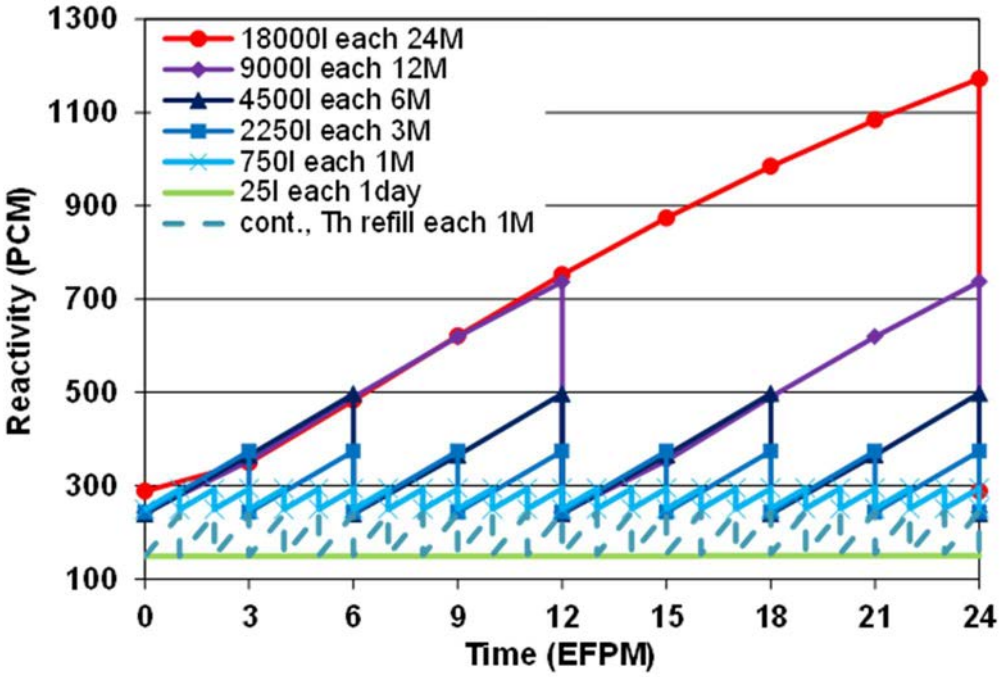

FIG. 54. Reactivity swing during 24 months of operation for 7 selected reprocessing strategies geometry (courtesy of Krepel Jiri, Paul Sherrer Institut).

The reactivity swing in Fig. 54 is proportional to the length of the batch. The longest 24 months batch shows the strongest reactivity increase. On the other hand, the initial reactivity depends on the Th and FPs amount. These amounts differ between the cases and so the curves start at different levels. The initial (in), average (av.), and final (out) masses as well as the mass differences for the Th and soluble FPs in the core during one batch are shown in Table 25 together with the relevant reactivities. It shows that the highest average reactivity excess of 730 PCM is reached by the 24 months batch, which has the lowest average FPs amount of 272 kg. All other cases have in average more FPs in the reactor. The continuous case represents a maximum with 558 kg of FPs.

One of the mass indicators relevant also for breeding performance is the $^{233}U/^{232}Th$ ratio. It is shown in Fig. 55. The ratio evolves in all cases mainly because of the Th mass oscillations (Fig. 56). The Uranium mass stays almost constant during the cycle (Fig. 56). Assuming that the spectrum of all calculated cases is similar, the $^{233}U/^{232}Th$ mass ratio will also be the same. Nevertheless, since the FPs content and so the excess reactivity differs between the cases the average $^{233}U/^{232}Th$ mass ratio differs.

The iso-breeding ratio corresponds to the values of the continuous reprocessing scheme. Accordingly, the 24 months case is acting as breeder during the first few months and as a burner in last several months of operation. The evolution of ^{233}U mass in Fig. 56 corresponds to this fact. It also shows that the amounts of ^{233}U slightly differ between the cases. It is valid also for higher U isotopes. The common share of actinides and FPs is fixed at 22.5 molar % of the salt, thus higher initial FPs mass in the salt implies lower mass of actinides.

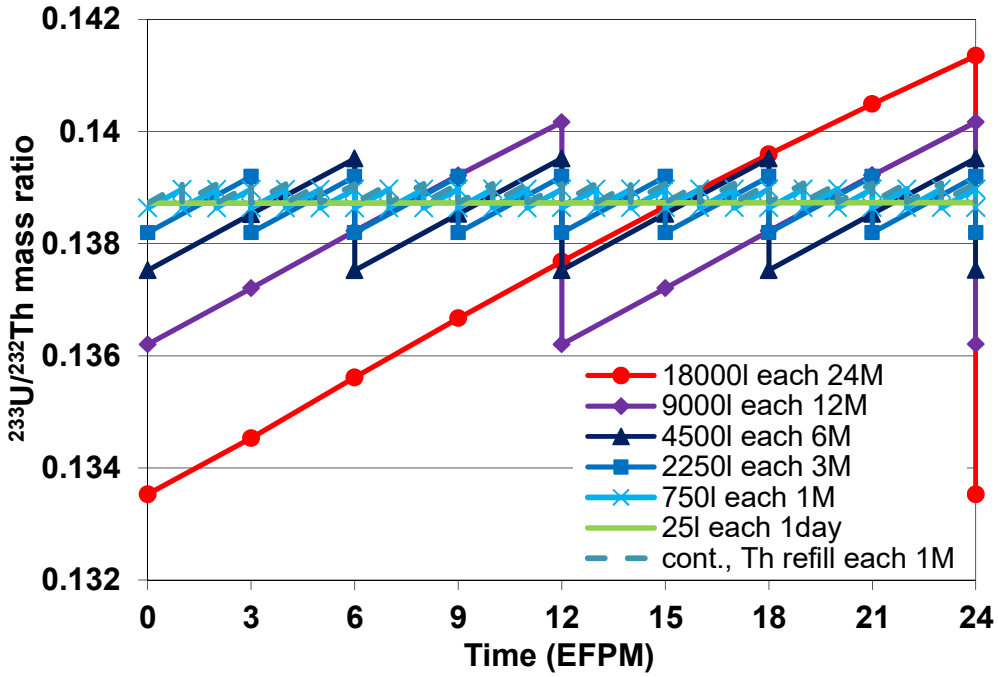

FIG. 55. Ratio of ^{233}U and ^{232}Th during 24 months of operation for 7 selected reprocessing strategies geometry (courtesy of Krepel Jiri, Paul Sherrer Institut).

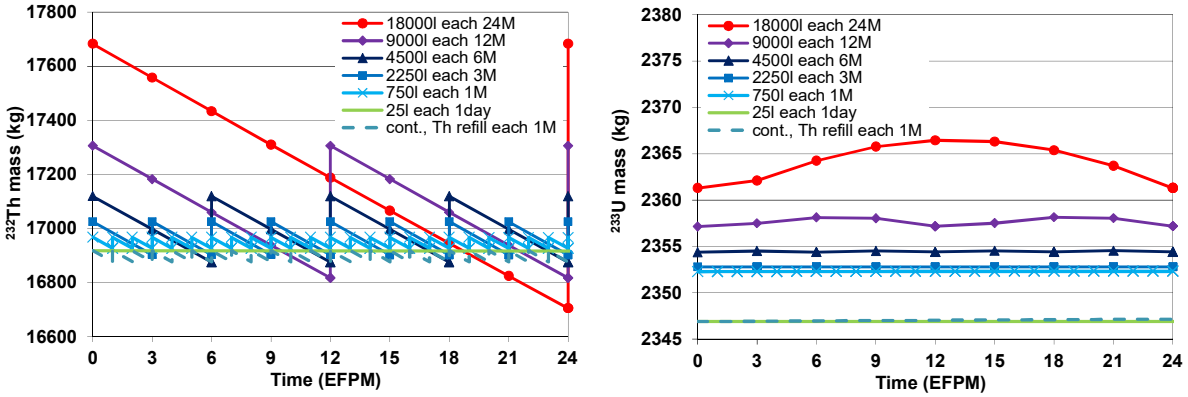

FIG. 56. ^{232}Th mass evolution during 24 months of operation for 7 selected reprocessing strategies (a) Th mass (b) U mass (courtesy of Krepel Jiri, Paul Sherrer Institut).

The continuous case provides unique results in the sense that the FPs mass is constant during the operation and only the Th mass oscillates, since it is refilled on a 1month basis. Accordingly, the ratio of reactivity and Th mass difference from Table 25 provides Th importance and corresponds to - 2.2 pcm/kg. Knowing this number, the soluble FPs importance can be calculated from case 5 where both FPs and Th are handled on 1 month basis. The outcome is importance of - 2.015 pcm/kg for the soluble FPs.

TABLE 25. INITIAL, AVERAGE AND FINAL MASSES AND REACTIVITIES DURING THE CORE OPERATION

Scheme	Th initial	Th average	Th final	Th Δm	FPs initial	FPs average	FPs final	FPs Δm	ρ_{in}	ρ_{av}	ρ_{out}	Δρ
Nr.	(kg)	(kg)	(kg)	(kg)	(kg)	(kg)	(kg)	(kg)	(PCM)	(PCM)	(PCM)	(PCM)
1	17683	17194	16705	-978	0	272	543	543	289	730	1172	884
2	17306	17061	16817	-489	271	406	541	271	243	490	737	494
3	17120	16997	16875	-245	405	473	541	135	239	368	497	258
4	17025	16964	16903	-122	473	506	540	68	243	309	374	131
5	16968	16947	16927	-41	517	528	540	22	249	271	293	44
6	16918	16917	16917	-1	558	558	558	1	149	149	150	1
7	16918	16898	16877	-41	558	558	558	0	149	193	238	90

Using the 24 months batch case and data from Table 25 as an example, 543 kg of soluble FPs are built-up during the 24 months of operation. It corresponds to -1100 pcm of negative reactivity. In the same time Th mass is reduced by 978kg and introduces 2150 pcm of positive reactivity. The overall reactivity is thus strongly increasing with the burn-up. This is rather unexpected. In solid fuel fast reactors with U-Pu iso-breeding cycle this behavior is usually much weaker or opposite. The difference is caused mainly by volatile and gaseous FPs removal and by the higher capture and lower fission cross sections of ^{232}Th, if compared to ^{238}U. The Th mass change has thus higher impact.

This Th-U cycle feature can be used in MSR for the reactivity control during operation. The high reactivity swing in the 24 months case can be thus eliminated by continuous or batch-wise Th addition to the core. The FPs can be still handled on a 24-month basis. Once the reactivity swing is eliminated, the longest batch case becomes neutronically the most interesting option for the reactor operation relying on 25 l/day reprocessing unit. It will have the highest breeding gain and the average FPs mass in the core will be only a half of the continuous case amount. The major disadvantage will be the twice higher salt volume required for the operation.

5.5.3. Impact of the reprocessing method

There are several different techniques, which can be applied to the reprocessing of the spent fuel salt:

- Fluoride volatilization techniques; fluorination of the molten salt mixture;
- Electro-separation processes;
- Molten salt / liquid metal reductive extraction;
- Gaseous and volatile FPs removal (He sparging);
- Vacuum distillation, fraction evaporation or possibly precipitation.

Irradiated MSR fuel in Th-U cycle consists of carrier salt (LiF, LiF-BeF_2, NaF-BeF_2, etc.), fertile actinide (mainly ^{232}Th), fuel (mainly U vector), by-products (Np, Pu, and MA) and fission products.

The ultimate aim of any reprocessing method, assuming a closed fuel cycle, is the FPs removal and recycling of everything else. Unfortunately, as it was stated already in the technological

part of this section, FPs are removed from the molten salts usually as the last component and it may require a combination of several above mentioned techniques. The importance of each component from the irradiated MSR fuel differs.

- From a reactor physics point of view, it is important to recycle ^{233}U as the main fissile element of the Th-U cycle; the other components are not substantive;
- From a sustainability point of view, it may be important to recycle the main fertile element Th and possibly also some rare elements (Li, Be);
- From an economical point of view, it may be interesting to recycle all components. Nevertheless, it will depend on their price and on the reprocessing costs. In some cases, their direct disposal, e.g. by vitrification, may be cheaper.

It may be required by the selected fuel cycle to recycle the main fissile nuclide ^{233}U swiftly, whereas the other fuel components may be recycled with delay. Fortunately, the fluoride salts foreseen for MSR have one important feature. Some elements like U, Np, and to a certain extent also Pu form volatile hexafluorides and can be separated by the volatilization technique, or actually fluorination. The volatilization of fluoride salts mixtures is a robust and tested reprocessing method [63], which was patented in the US as early as 1958 (patent nr. US2833617A). It enables relatively simple separation of the selected elements from the irradiated carrier salt. Since it can be remotely operated it is also suitable for recycling of salt containing ^{232}U. This isotope has in its decay chain several hard gamma emitters, e.g. ^{208}Tl and ^{212}Bi, and remote handling of the salt will be necessary.

The aim of this section is to evaluate a reprocessing strategy, which will, in situ, rely only on the volatilization technique. The need to postpone the treatment of the remaining salt may be also based on the radiological protection of the reprocessing facility workers. The activity of the FPs and of the ^{232}U decay chain left in the salt may require storage time from 10 to 20 years [64]. The isotope ^{228}Th, as a direct product of ^{232}U decay, has a half-live of 1.9 years and the other nuclides in the chain decay fast. Accordingly, after U separation by volatilization, the activity of *e.g.* ^{208}Tl or ^{212}Bi in the remaining salt will be determined by 1.9 years half-live of ^{228}Th. This half-live will thus influence also the necessary storing time before reprocessing of the other fuel salt components.

The volatilization technique has a feature that due to the different chemical potentials UF_6 tends to leave the salt mixture as the first, NpF_6 as the second, and PuF_6 as the last. In reality they are not so strictly separated. However, by adjusting of the volatilization duration, it can be roughly selected, which mixture of the three elements will be separated. Furthermore, U and Np can be removed from the salt with very high efficiency, whereas Pu only to a certain extent. Three ideal scenarios were thus simulated in this study [65], the first assuming several reprocessing methods to recycle all Ac and the second two assuming only volatilization method:

- 100% of U and 99% of other Ac recycling;
- 100% of U and 99% of Np recycling;
- 100% of U only recycling by volatilization.

In all cases, U was always recycled with 100 % efficiency. For the other actinides, 99% efficiency of the method was assumed in both removal or recycling cases. The reprocessing was applied batch-wise after every 12 months of operation. The other conditions and core description were adopted from the parametric study for two cases:

- The thermal MSR; the case with 15% salt in the core;
- The fast MSR; the case with 100% salt in the core.

At this place it is also to be mentioned that the frequency of batch-wise reprocessing or the continuous reprocessing may change the results. In this study, the fuel is reprocessed once a year and so, for instance in all Ac recycling scenario, 1% of the equilibrium mass is annually removed through the losses. In case of online-reprocessing the removal, rate will depend on the ratio of the daily processed volume and the total volume of the fuel salt in the core. For the MSFR core [66], the foreseen online reprocessing rate may be 40 l/day and the total salt volume will be 18 m^3. Accordingly, it takes 450 days to reprocess whole salt amount. Assuming equal efficiency of the reprocessing technology, it corresponds to 0.8% annual reprocessing losses, and it is thus slightly lower than the 1% rate used in this study. In the presented results 'other Ac' denotes sum of the masses of higher than ^{239}Pu nuclides. The variable used in the charts is the Effective Full Power Years (EFPY) of a reactor with 2.6GW_{th} power. This power was selected, as in the previous study, so that every year of operation corresponds roughly to 1 ton of burned fuel. Since in this study transition from fresh fuel towards equilibrium cycle is simulated, the fresh fuel composition needs to be specified. For simplicity the critical ^{233}U and ^{232}Th mixture was selected as an initial fuel.

5.5.4. Scenario 1: 100% of U and 99% of other actinides recycling

In the ideal case all actinides will be recycled on-line and in situ. The removed FPs will be replaced by the ^{232}Th. The core will tend to converge from an initial composition to an equilibrium composition. The actual evolution of selected isotopes from the fresh fuel (^{233}U and ^{232}Th mixture) towards equilibrium is shown in Fig. 57. The masses tend to stabilize on a relatively low level. The results were obtained assuming 99% efficiency of the reprocessing technology for other isotopes, only U was recycled fully. In both thermal and fast cases, the total mass of ^{239}Pu and other actinides stabilize slightly below 50 kg. The mass of ^{238}Pu is however almost twice higher in the thermal (180 kg) than in the fast (90kg) MSR. Similarly, the mass of ^{237}Np is by 50% higher in thermal MSR.

Thanks to the 99% efficiency, there is a certain mass of actinide present in the waste with separated FPs. The cumulative mass of removed actinides over the 100 EFPY of operation is shown in Fig. 58. The total mass of all removed transuranic elements is around 160–220kg after 100 years of reactor operation with 2.6 GW_{th} power.

This scenario represents an ideal case with almost minimal achievable waste production. Nonetheless, since everything else than FPs is recycled, the requirements for the reprocessing facility will be demanding. It may be questionable, if such a demanding facility will be built for every MSR unit. Accordingly, simplification of the in situ reprocessing may be required.

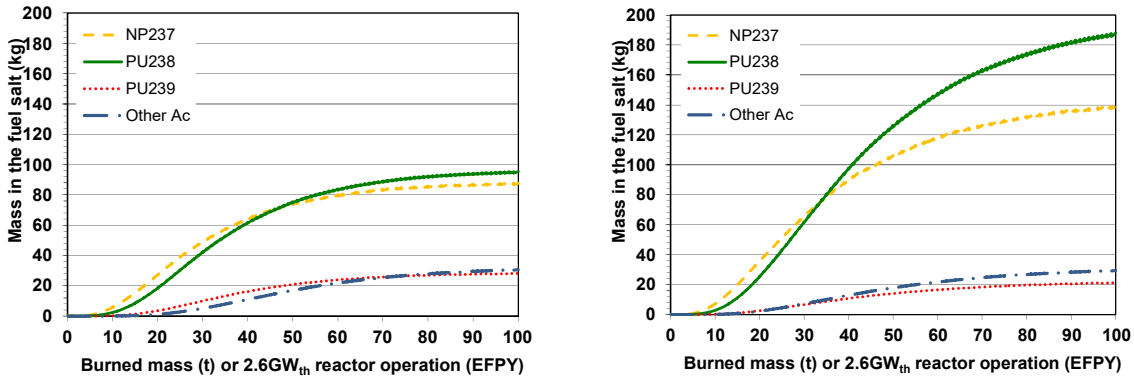

FIG. 57. Mass evolution of selected nuclides from initial fuel towards the equilibrium in fast (left) and in thermal (right) spectrum MSR for scenario 1 (reproduced from Ref. [57] with permission curtesy of ASME).

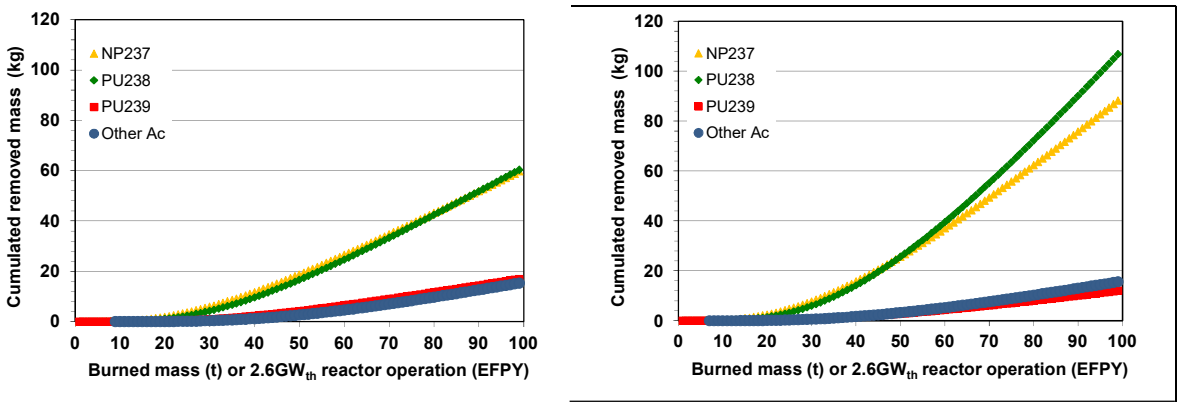

FIG. 58. Cumulated mass of Ac removed from the core in scenario 1 (only 1% reprocessing losses) in fast (left) and in thermal (right) spectrum MSR (reproduced from Ref. [57] with permission curtesy of ASME).

5.5.5. Scenario 2: 100% of U and 99% of Np recycling

In previous scenario, only the reprocessing loses are responsible for the actinide presence in the waste. In this scenario U 100% and Np 99% will be by recycled as before; however, 99% of Pu and other Ac will stay in the waste. Accordingly, the ^{237}Np mass in the core (Fig. 59) and in the cumulative waste (Fig. 60) evolves similarly as in the previous case. However, the other presented masses are strongly changed.

Thanks to the regular removal of Pu after each 12 months the corresponding ^{238}Pu mass in the core oscillates (Fig. 59). The maximum mass is reached just before the reprocessing and corresponds in both the thermal and fast cases roughly to 20 kg. Since the ^{238}Pu amount in the core is lower, also the production of consequent ^{239}Pu and other actinides is reduced. At the same time, these nuclides are not recycled and thus their mass in the waste grows. The amount of ^{239}Pu in the waste is roughly tripled, from 20 to 60 kg in the fast case. The biggest difference is the cumulative mass of removed ^{238}Pu after 100 EFPY, which according to the spectra corresponds to 1200 or 1600 kg. It represents the major actinides in the waste. It has a relatively short half-life of 88 years. Thus, its activity is very high. However, similarly like the activity of FPs, it will be strongly reduced already after 1000 years. Furthermore, it decays to proliferation-safe ^{234}U and it may have certain value as a material for nuclear batteries.

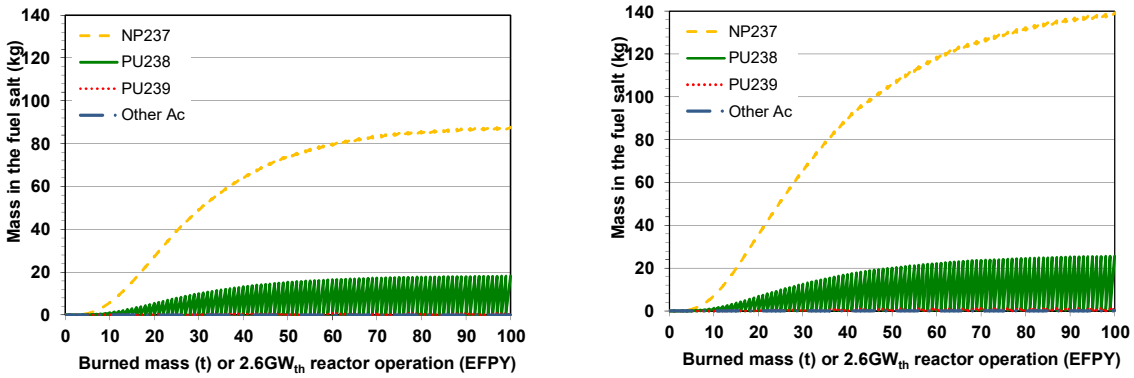

FIG. 59. Mass evolution of selected nuclides from initial fuel towards the equilibrium in fast (left) and in thermal (right) spectrum MSR for scenario 2 (reproduced from Ref. [57] with permission curtesy of ASME).

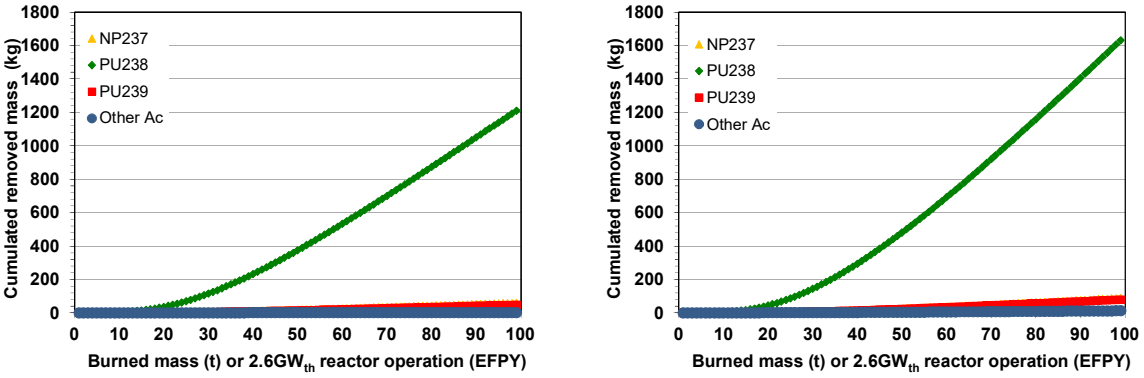

FIG. 60. Cumulated mass of actinides removed from the core in scenario 2 in fast (left) and in thermal (right) spectrum MSR (reproduced from Ref. [57] with permission curtesy of ASME).

5.5.6. Scenario 3: 100% of U only recycling

In the last scenario, only U is recycled by volatilization and other nuclides are removed from the core, with 99% efficiency. The maximal mass of ^{237}Np in the core after 100 EFPY of operation stabilizes at 18–25 kg, according to the core spectrum (Fig. 61). Thanks to its regular removal, it oscillates as the ^{238}Pu in the previous case. Since the ^{237}Np amount in the core is reduced, the production of ^{238}Pu and higher actinides are also lower. Thus, there are at maximum only 2 kg of ^{238}Pu in the core.

The cumulative mass of ^{237}Np removed from the core during 100 EFPY of operation (Fig. 62) is now dominating the waste with 1400 or 1700 kg for the fast or thermal spectra, respectively. Compared to the previous two cases with 60 or 90 kg of ^{237}Np, it is a tremendous increase. On the other hand, the mass of ^{238}Pu in the waste is just slightly increased from 60–107 kg in scenario 1 to 145–167 kg in scenario 3. Surprisingly, the masses of ^{239}Pu and of the remaining other Ac are both reduced in this scenario. The ^{239}Pu mass decrease is moderate; nevertheless, the other actinides decrease is strong; from 15–16 kg to 0.2–2 kg.

In this scenario ^{237}Np nuclide represent the major actinide in the waste. It has long half-life of 2.1 million years. Thus, its activity is very low. On the other hand, it is chemically relatively mobile. Moreover, both ^{237}Np and its decay product ^{233}U may raise some proliferation concerns. Accordingly, this may not be an optimal scenario.

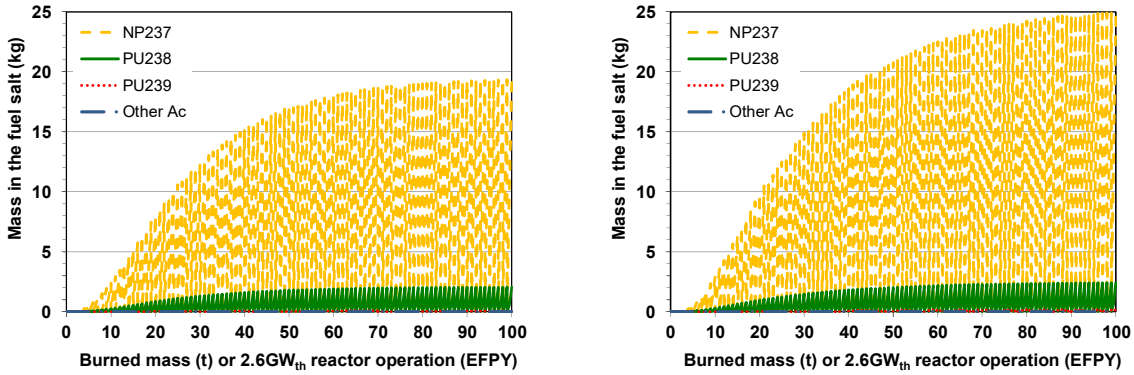

FIG. 61. Mass evolution of selected nuclides from initial fuel towards the equilibrium in fast (left) and in thermal (right) spectrum MSR for scenario 3 (reproduced from Ref. [57] with permission curtesy of ASME).

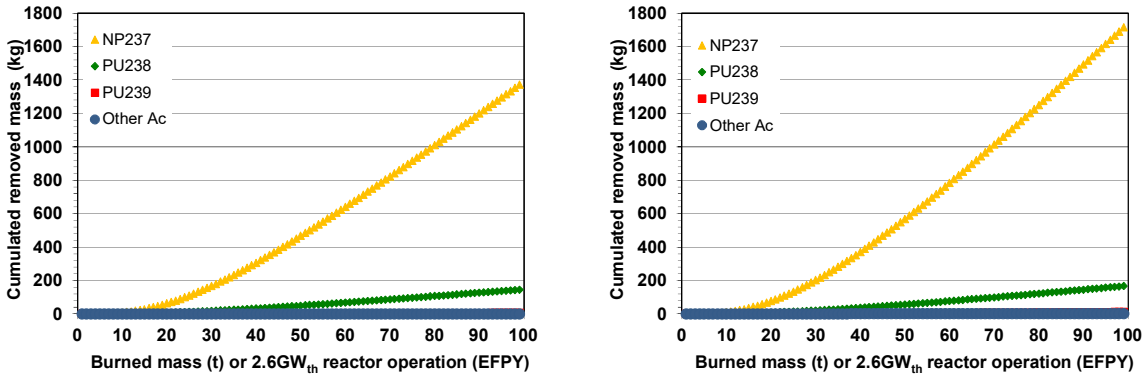

FIG. 62. Cumulated mass of actinides removed from the core in scenario 3 in fast (left) and in thermal (right) spectrum MSR (reproduced from Ref. [57] with permission curtesy of ASME).

5.5.7. Recycling scenarios comparison

The first parameter to be compared is the maximal mass of selected nuclides in the core after 100 EFPY of regular operation and just before the reprocessing. This serves as an approximate for the equilibrium state. The mass is presented in Table 24. It shows that the total mass of selected nuclides is the highest in the case of all Ac recycling. In the case of U and Np recycling, it is reduced to more than half. In the case that only U is recycled the mass drops by more than one order. Accordingly, the mass of these elements in the reprocessing facility will be the lowest for the U only recycling scenario. It is interesting that the mass of other actinides (mainly ^{240}Pu, ^{241}Pu, and ^{241}Am) especially in the fast spectrum MSR is almost negligible if only U or U and Np are recycled.

The second parameter for comparison, shown also in Table 26, is the cumulative mass of actinides removed from the core during the first 100 EFPY of reactor operation with 2.6 GW_{th} power. It can be seen that thanks to the 1% of losses, the scenario of all actinides recycling produces surprisingly the highest amount of other actinides in the waste. It corresponds to approximately 0.3 kg per year or 15 kg cumulative after 100 EFPY.

TABLE 26. MASS IN KG OF SELECTED ACTINIDES IN EQUILIBRIUM CORE AT LAST SIMULATED CYCLE(100) BEFORE REPROCESSING AND IN THE CUMULATIVE WASTE AFTER 100 EFPY OF OPERATION

Location	Salt in equilibrium core before reprocessing						Cumulative waste after 100 EFPY of operation					
Spectrum	Fast MSR			Thermal MSR			Fast MSR			Thermal MSR		
Recycling	All Ac	U+Np	Only U	All Ac	U+Np	Only U	All Ac	U+Np	Only U	All Ac	U+Np	Only U
NP237	87.6	87.6	19.4	139.1	139.1	25.0	59.7	59.7	1371.3	88.2	88.2	1713.6
Pu238	95.4	18.1	2.0	188.0	25.6	2.4	60.3	1210.0	144.6	106.7	1631.1	166.6
(U234)	—	—	—	—	—	—	(14)	(290)	(36)	(23)	(383)	(41)
Pu239	28.2	0.7	0.1	21.4	1.2	0.2	16.9	47.7	6.1	12.0	79.1	11.2
Other Ac	30.7	0.0	0.0	29.5	0.2	0.0	15.3	1.5	0.2	15.6	12.1	1.9
Sum (kg)	241.9	106.5	21.5	378.0	166.1	27.6	152.2	1318.9	1522.3	222.5	1810.6	1893.4

In all the actinides recycling scenario, the highest amount of higher actinides are produced. In the U + Np recycling scenario, ^{238}Pu is the major waste. In the U only recycling scenario, ^{237}Np is the major waste.

It is to be mentioned here that the cumulative removed mass of ^{238}Pu, presented in Table 26 and in the previous figures, represent only an ordinary sum of the annually removed mass. It is sufficient for illustration of the differences. Nonetheless, for more realistic evaluation ^{238}Pu decay has to be accounted for, because its half-life of 88 years is comparable with the time period assumed for cumulating. Accordingly, a significant part of it may already decay to ^{234}U. Thus, for instance the presented ^{238}Pu mass of 1210 kg for the U and Np recycling in the fast MSR corresponds to 920 kg of ^{238}Pu and 290 kg of ^{234}U. Hence, 25 % of the mass has already decayed. The respective mass of created ^{234}U is shown in Table 26 in parenthesis.

One of the options of the simplified reprocessing idea is the direct disposal of the spent carrier salt by vitrification. Thus, the cumulative masses of actinides waste production in the three studied reprocessing scenarios were compared also by means of long term radiotoxicity generation. For this comparison only the fast MSR case was selected. Figure 63 shows that all actinides recycling scenario 1 provides the lowest actinide radiotoxicity in both short and long term. All three scenarios show strong decrease after 1000 years and secondary peak after 100 000 years. If only U is recycled the radiotoxicity is the lowest from all three cases between 1000 and 20 000 years.

In Fig. 64, the actinides from scenario 1 case are divided into four groups according to the decay chain to which they belong. In Fig. 65, similar break-down is done for the remaining two scenarios. It can be seen that the radiotoxicity evolution is in all three cases driven by the ^{238}U decay chain. It is caused mainly by ^{238}Pu in short term and by ^{234}U in longer term, which both belongs to the ^{238}U chain. The importance of the other three decay chains, or actually decay series, varies between the cases. For better understanding of this behavior the first scenario with all actinides recycling was selected as an example and each of the four decay chains was analyzed component-wise (see Fig. 65).

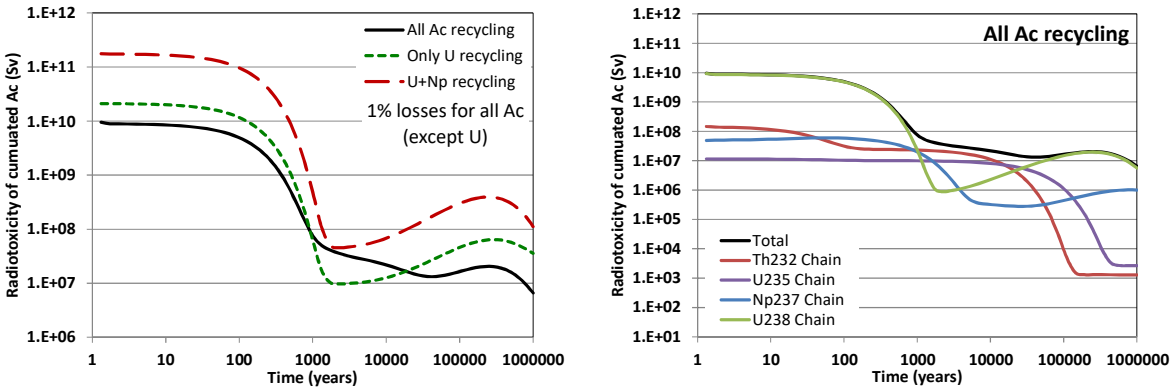

FIG. 63. Ingestion radiotoxicity generation from the cumulated actinides waste after 100EFPY of reactor operation. Comparison of all three scenarios (left), break-down of the scenario 1 curve into four decay chains (right) (reproduced from Ref. [57] with permission curtesy of ASME).

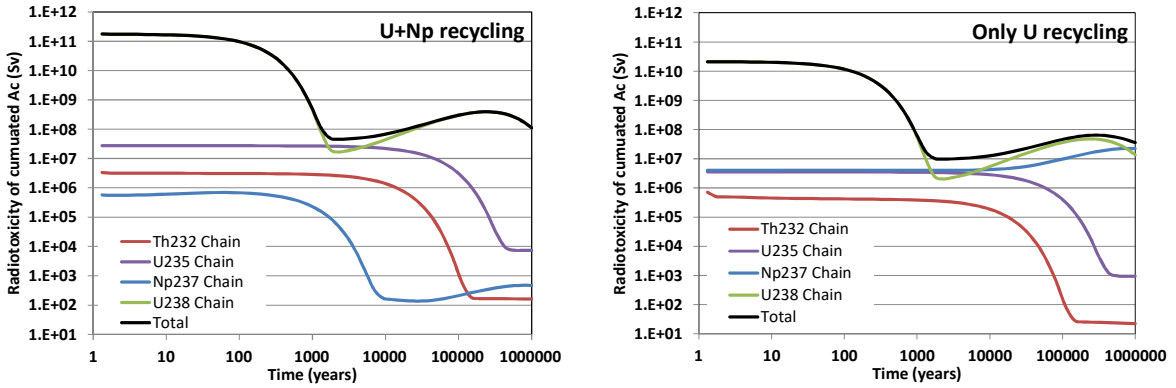

FIG. 64. Ingestion radiotoxicity generation from the cumulated actinides waste after 100 EFPY of reactor operation, break-down of the scenario 2 curve (left) and scenario 3 curve (right) into four decay chains (reproduced from Ref. [57] with permission curtesy of ASME).

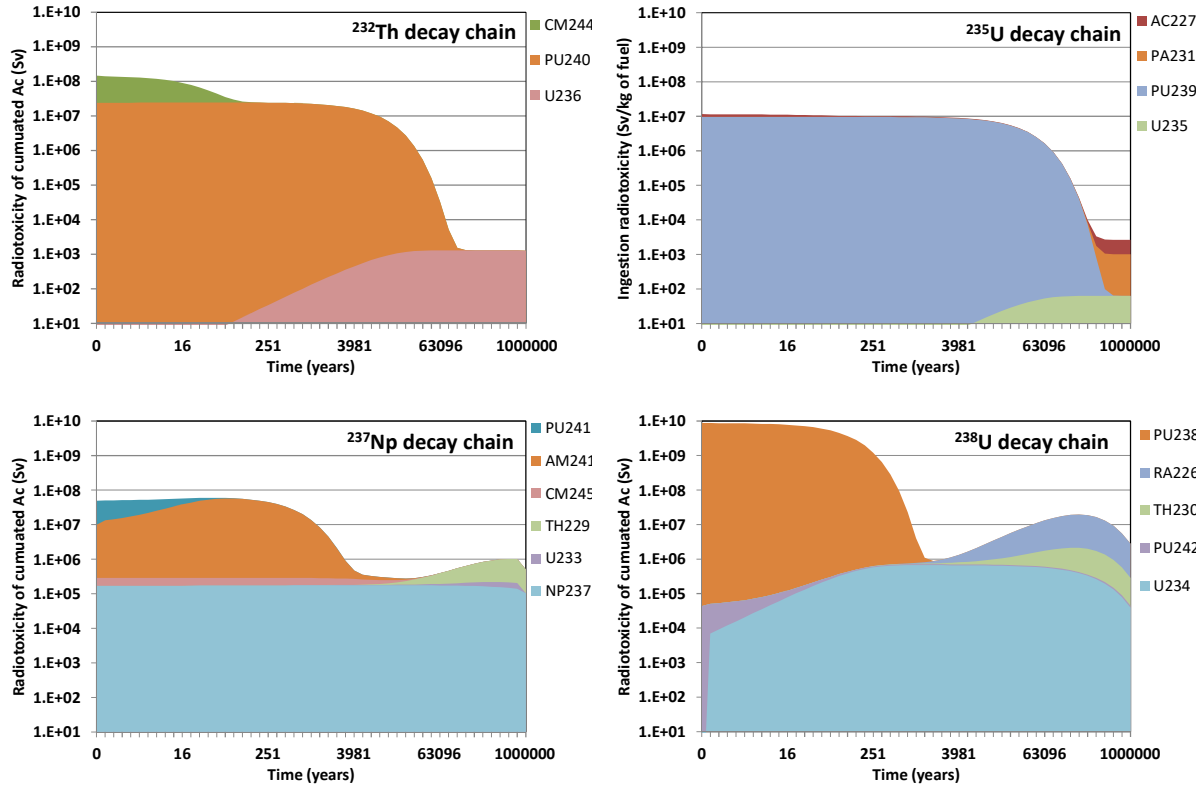

FIG. 65. Ingestion radiotoxicity generation from the cumulated waste in all actinides recycling scenario, after 100 EFPY of reactor operation for each of the four decay chains (reproduced from Ref. [57] with permission curtesy of ASME).

According to Fig. 65, the ^{238}U decay chain dominates, because of the ^{238}Pu fast decay to ^{234}U, with half-live of 88 years. It is the reason for the primarily radiotoxicity decrease after 1000 years. The secondary peak is, on the other hand, driven by the establishment of quasi-equilibrium state between ^{234}U and its daughters; only in the U recycling scenario, it is also partly supported by ^{237}Np daughters.

The radiotoxicity of the ^{237}Np decay chain is driven by three main isotopes: ^{241}Pu, ^{241}Am, and ^{237}Np. The share of ^{237}Np and the other two isotopes determines the behaviour of this chain. If ^{237}Np dominates, the induced radiotoxicity is practically constant during the first 100 000 years and then grows thanks to the ^{237}Np daughters' buildup (Fig. 64). On the other hand, if ^{241}Pu and ^{241}Am dominate then the radiotoxicity initially decreases following the relatively short ^{241}Am half-life of 432 years (Fig. 64). Firstly later, it is driven by ^{237}Np decay with its 2.1 million years half-life. The ^{235}U decay chain has in all three cases two main actors: ^{239}Pu which decays to ^{235}U. The shape of this radiotoxicity curve is the same in all three cases; just the absolute level differs according to the initial ^{239}Pu mass. The ^{232}Th decay chain is dominated by ^{244}Cm and ^{240}Pu. The ^{244}Cm is present only in all actinide recycling scenario. The absolute mass of ^{240}Pu strongly differs between the cases.

5.5.8. Reprocessing efficiency as a variable for parametric study

In the fuel cycle scenarios defined above, it was assumed that the efficiency of the reprocessing is 99%. Accordingly, only 99% of selected actinides were either recycled or removed. Thus, there was always 1% loss for all actinides except of U, which was 100% recycled. In this section, the reprocessing efficiency will be used as a variable for parametric study. It will range

from 99%, which corresponds to all actinides recycling scenario, through 75%, 50%, 30%, 15%, and 1% efficiencies. Such a low efficiency of reprocessing is unrealistic. Nonetheless, for instance, the 1% efficiency actually corresponds to the U only recycling, where other actinides are removed from the core. Accordingly, the artificial reprocessing efficiency range covers the space between the previously studied scenarios 1 and 3.

Even though some of the analysed efficiencies are unrealistic, the results illustrate the range of possible mass evolution in the core. Since in this study the reprocessing is done batch-wise and once per year, the actinide mass in the core oscillates according to the level of reprocessing efficiency. The respective maximal masses in the core before reprocessing are shown in left of Fig. 66. They increase with growing reprocessing efficiency.

The annually removed mass corresponds to the product of actinide mass in the core and the reprocessing losses. Since one of these parameters is incessantly growing with the efficiency and second is linearly decreasing (see Fig. 66), in some cases the product shows local maximum around 80% efficiency. Figure 66 also shows the cumulative actinide mass, removed from the core during the 100 years of reactor operation with 2.6 GW_{th} power, as a function of reprocessing efficiency. This result confirms that the lowest mass of ^{239}Pu and higher actinide is obtained for lowest reprocessing efficiencies; *e.g*, in the case of ^{237}Np or ^{238}Pu being removed from the core.

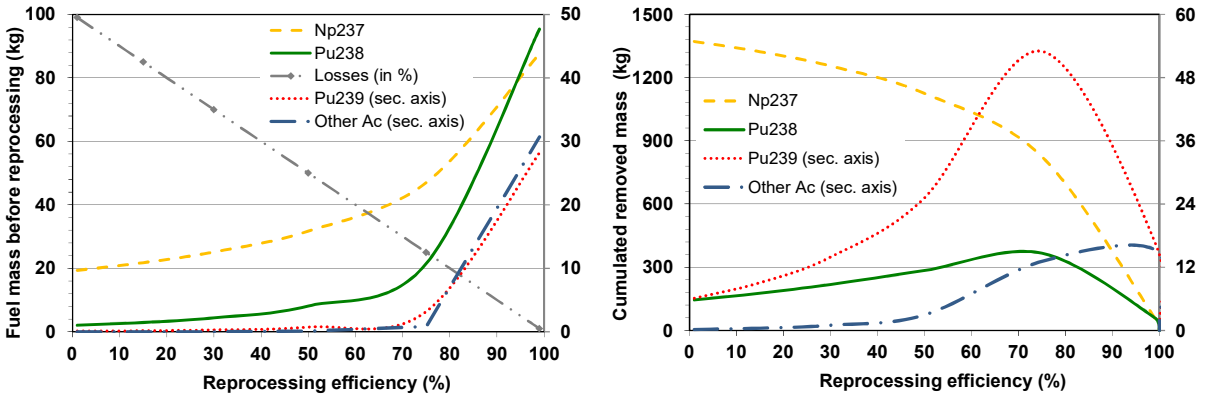

FIG. 66. Equilibrium actinide mass in the core before reprocessing (left) and cumulated actinide mass removed from the core during 100 EFPY (right) as a function of recycling efficiencies (reproduced from Ref. [57] with permission curtesy of ASME).

5.6 SUMMARY

MSR has many advantages, which are enabled by the liquid state of the fuel. One of them is the possibility to on-line reprocessing of the fuel. Liquid fuel in a form of molten salts provides several reprocessing advantages; however, it is still technically difficult, and the chemical partitioning process has to be based on differences in chemical stability of individual fluorides of actinides and FPs in the melt. Thorium tetrafluoride and majority of the FPs fluorides and are more stable in the carrier melt than the uranium and protactinium tetrafluorides. Hence, the uranium and protactinium have to be separated as first.

The MSR performance in closed Th-U cycle was accessed from several different perspectives and with several simplifying assumptions. From these mainly the frequent salt cleaning each 6 months with zero reprocessing losses and the applied JEFF 3.1 XS library may influence the

final results. Nonetheless, it gives insight to the fuel cycle features of MSR. The thermal iso-breeding MSR core will be relatively large to minimize the leakage. It is also quite sensitive to the FPs build-up and may require continuous salt cleaning. On the other hand, fast iso-breeding MSR core can be quite compact, and it is less sensitive to the to the FPs build-up. At the same time its performance may depend on the ^{233}U capture cross section, which is probably underestimated in JEFF 3.1 cross section library.

The fast MSR core in the Th-U cycle shows positive reactivity swing. In this case, simple ThF_4 addition to the core may be used for the on-line reactivity control during the operation and the FPs removal from the salt may be based on batch-wise reprocessing after longer irradiation period. Also, the simplified reprocessing scenario of fluoride salts has some promising features, and it can be used for batch-wise operation of fast MSR. Finally, the Breed-and-Burn mode seems not feasible for fluoride salts. The chloride salts can perform well on a cell level in the Breed-and-Burn mode for both Th-U and U-Pu cycle. However, leaky and reasonable core size cannot be achieved without dedicated leakage utilization (blanket, reflector, etc.).

MSR with liquid fuel may fulfil the “low waste, low risk” requirement of the broad public towards a better acceptance of nuclear energy generation in the future as it has a potential for high resources utilization, low waste production, and risk reduction with the exclusion of severe accidents.

6. THORIUM USE IN FAST REACTORS

6.1. INTRODUCTION

Fast reactors (FRs) have the potential of extending fissile material resources as the fissile material can be produced from fertile materials with conversion ratio more than one. Th-based thermal reactors and U-based FRs started to be considered in view of their capability to operate with continuous recycle of all actinides, while potentially burning legacy TRU (TRansUranic isotope) wastes, thus drastically limiting the actinide wastes to be disposed.

The specific advantages of Th-based FRs include a very low generation of TRUs leading to improved thermal performances of repositories. In addition, the low breeding capability of Th cycle may enhance the consumption of an external supply of TRUs. Following these considerations, studies about Th use in FRs have started gaining momentum [1–3].

Despite the potential advantages, the implementation at an industrial scale of the Th closed cycle needs to overcome formidable challenges, including difficulties in dissolution and reprocessing of used fuel [67], and fabrication of highly radioactive recycled fuel [68].

In 2001, the Generation IV International Forum (GIF-IV) selected the MSR as one of the six innovative nuclear reactors with the potential to meet the compelling need for an increasingly sustainable, economical, safe and proliferation resistant nuclear energy production [69, 56]. Few years after the selection of the MSR among the Generation-IV reactors, the concept evolved in the direction of fast-spectrum Th-based MSRs [70–71] identified as Molten Salt Fast Reactor (MSFR) [66] and mainly developed in the frame of the EURATOM EVOL (Evaluation and Viability of Liquid Fuel Fast Reactor System) Project [72].

6.2. INVESTIGATED REACTOR DESIGNS

Three core designs have been selected in this work to investigated Th performances in FRs: two traditional FR systems and the MSFR. Both U- and Th-based versions of the two selected solid-fuel FRs have been investigated.

6.2.1. European lead system (ELSY)

The European lead system (ELSY) [73] was designed during the EURATOM sixth framework program (2002-2006) and further developed in the LEADER (Lead-cooled European Advanced Demonstration Reactor) project of the seventh framework program (2007–2011). It is an iso-breeder lead-cooled FR for electricity production and capable of minor actinide burning. It was designed to work in a traditional U-Pu fuel cycle, with oxide fuel and a homogeneous core configuration (i.e., without blankets). The ELSY design presented by Alemberti et al [73] has been chosen as reference in this work. An additional modified version has also been designed to maintain the iso-breeder behavior in a Th cycle [74–75]. In this way, the new core can be operated with ^{232}Th as the only feed and maintain positive reactivity at equilibrium. In line with the nominal U-Pu core, Th oxides were selected as fuel form [76–78]. Same pin and assembly designs as for the U-Pu counterpart have been adopted for the Th core. Characterizing parameters of the standard U-Pu ELSY core and of the preliminary designed Th-U version are summarized in Table 27, while schematic representations of core and fuel assembly designs are reported in Fig. 67 [79].

Replacing ThO_2 feed with UO_2 feed without any core modifications leads to a strongly negative equilibrium reactivity, as a consequence of the well-known inferior breeding performance of Th vs U in a fast spectrum. In order to maintain an iso-breeding configuration, the core height has been increased from 1.2 m to 1.7 m to achieve criticality at the end of the equilibrium cycle. The choice of increasing the core height is not necessarily optimal from a design viewpoint. It minimizes leakages compared to other options, which in turn minimizes the actinide inventory necessary to achieve iso-breeding. Increasing the core height also allows to maintain the lead velocities and the lead axial temperature increase in the core, two of the main constraints in the ELSY design. Some information about the impact of different design choices on the ELSY performance parameters are already described [79–80].

TABLE 27. MAIN DESIGN PARAMETERS FOR ELSY CORE DESIGN

	U-based	Th-based
CR	~1	~1
Thermal / electric power	1500 / 600 MW	1500 / 600 MW
Coolant	Pb	Pb
Coolant inlet / outlet temperatures	673 / 753 K	673 / 753 K
Clad / duct material	T91	T91
Assembly type	Hexagonal	Hexagonal
Assembly flat-to-flat distance: wrapper in /out	20.3 / 21.1 cm	20.3 / 21.1 cm
Assembly center-to-center distance	21.6 cm	21.6 cm
Pin lattice / pitch	Triangular/15.5mm	Triangular/15.5 mm
Pins per assembly	169	169
Active core height	1.2 m	1.7 m
Pellet diameter; clad diameter (inner / outer)	9.1; 9.4/10.6 mm (1.5 mm hole)	
Number of assemblies in inner / middle / outer zone	163/102 /168	163/102 /168
Fuel form / smeared density	Oxides / 87%TD*	Oxides / 87%TD*
Fuel TD*	10.96 g/cm^3	10.96 g/cm^3
Number of control and safety rods	18	18
Number of batches	3	3
Refueling interval / time	2 years / 30 d	2.82 years / 30 d
Core HN** inventory	51 t	72 t

* Theoretical Density
** Heavy Nuclides

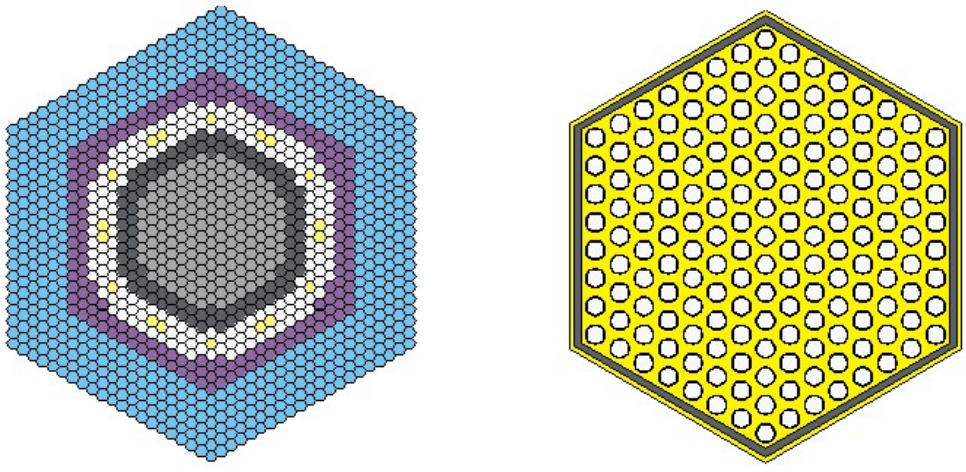

(a) (b)

FIG. 67. (a) ELSY core layout. Light grey=inner core; dark grey=middle core; white=outer core; yellow=control rods; violet=dummy assemblies; blue=lead; (b) ELSY assembly layout (reproduced from Ref. [86] with permission).

The discharge burnup in the ELSY is limited by fuel cladding damage (<100 dpa). The standard U-Pu core complies with this constraint. In order to maintain the cladding damage within acceptable limits, the average discharge burnup (64 GWth-d/t_{HM}) of the U-Pu core has been adopted for the Th-U core. This choice led to ~ 8.5-year fuel irradiation time, compared to the 6 years of the U-Pu option. Given the reduced specific power of the Th core design due to the taller core, the longer irradiation time still leads to a cladding fluence ~10 % below that of the U-Pu fuel. In view of the similar spectrum, cladding damage is also expected to remain smaller than, or comparable to, the U-Pu case.

Smeared densities are typically 80-90 %TD. For simplicity, a smeared density of 87%TD and the UO_2 TD of 10.96 g/cm^3 were assumed for all cases considered. The fuel linear expansion coefficient depends on the fuel type, but differences are generally small for the fuels considered [76]. Therefore, the same linear expansion coefficient, equal to $12 \cdot 10^{-6}$ K^{-1}, has been considered for all fuels.

6.2.2. Advanced recycle reactor (ARR)

The second FR design employed is the sodium-cooled Toshiba-Westinghouse ARR [81]. Both metallic and oxide fuel options were foreseen in the original ARR, but only U was considered as fertile material. The only blanket present was a lower axial blanket which allows to achieve a CR close to 1 for the metallic fuel option, and inferior to 1 for the oxide fuel option. Some modifications have been made to the original core design to lower the CR (burner designs) as well as to reach iso-breeder configurations [82–84]. Both U and Th options have been considered. Table 28 reports the main core parameters for the resulting 4 ARR versions while Figs. 68 and 69 show the radial core layouts and the assembly layout, respectively. Note that the core design is identical for the Th and U-based burner options, while the two iso-breeder cores have the same radial core map but different axial blankets.

TABLE 28. MAIN DESIGN PARAMETERS FOR ARR CORE DESIGN [86]

	U-based burner	Th-based burner	U-based iso-breeder	Th-based iso-breeder
CR	~0.4/0.5*	~0.3/0.4*	~1	~1
Thermal / electric power	1000 MW / 420 MW			
Coolant	Na			
Coolant inlet / outlet temperatures	668 / 823 K			
Clad / duct material	HT-9			
Assembly type	Hexagonal with duct			
Assembly flat-to-flat distance: wrapper in /out	12.4 cm / 13.0 cm			
Assembly center-to-center distance	13.3 cm			
Pin lattice / pitch	Triangular / 7.41 mm			
Pins per assembly	271			
Active core height	0.6 m			
Pellet diameter; clad diameter (inner / outer)	4.71; 5.44 / 6.50 mm			
Inner / outer fuel assemblies	192 / 132			
Fuel form / smeared density	Oxide / 85%TD		Metallic (10% Zr alloy) / 75%TD	Nitride (95% N-15 in N) / 85%TD
Fuel TD	10.51 g/cm^3	11.14 g/cm^3	16.01 g/cm^3	12.33 g/cm^3
Assemblies used as external radial blanket	-	-	90	90
Assemblies used as internal radial blanket	-	-	7	7
Number of control and safety rods	37	37	30	30
Upper axial blanket	-	-	10 cm	30 cm
Lower axial blanket	-	-	10 cm	36 cm
Number of batches	3			
Refueling interval / time	1 year / 30 d			
Core HN inventory	8.9 t	10.2 t	13.2 t	12.1 t
Blanket HN inventory	-	-	9.6 t	20.1 t

* Depending on the feed

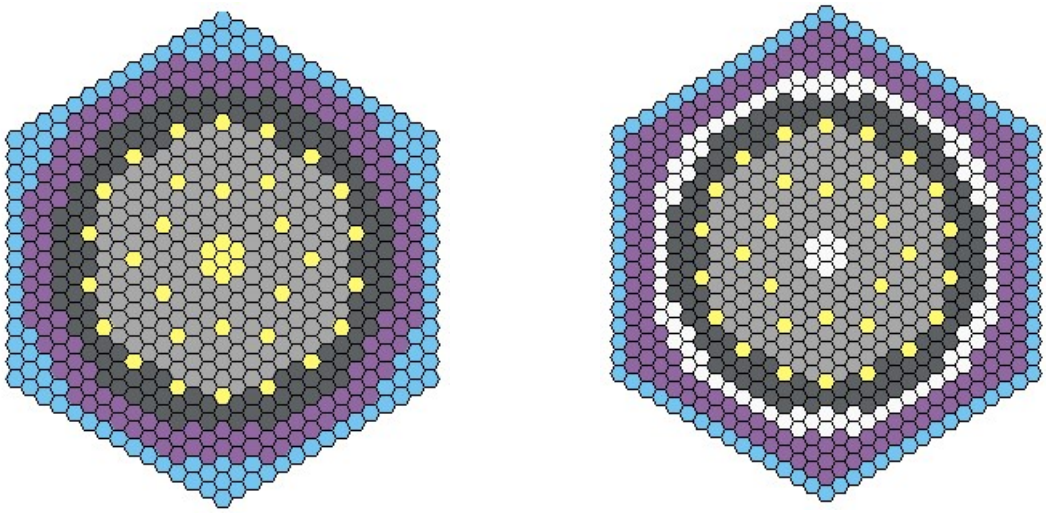

(a) (b)

FIG. 68. ARR core layout: (a) U- or Th-based burner; and (b) U- or Th-based iso-breeder. Light grey=inner core; dark grey=outer core; yellow=control rods; violet=steel shield; blue=B_4C shield; white=blanket (reproduced from Ref. [86] with permission).

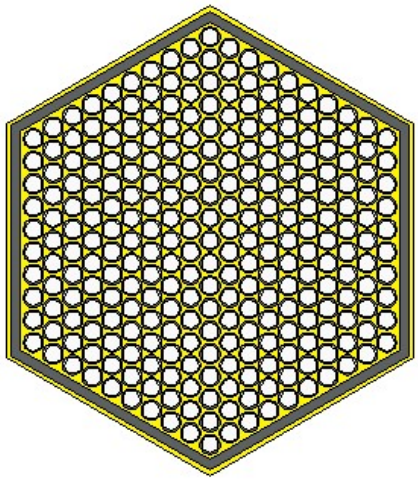

FIG. 69. ARR assembly layout (reproduced from Ref. [86] with permission).

The oxide fuel option has been retained for the burner configuration developed for this study, but the axial lower blanket has been removed to further decrease the CR. As concerns the iso-breeder cores, Zr-alloyed metallic fuel was chosen for the U iso-breeder configuration due to the superior breeding performance compared to U oxide fuel fostered by the higher heavy nuclide (HN) density. Metallic Th features lower HN density [78] than nitride Th fuel, further decreased if Zr-alloying is adopted. Therefore nitrides (95% enriched in ^{15}N) have been selected for the iso-breeder Th configuration. Unlike the burner ARR design, the iso-breeder U and Th designs employ blankets of respectively ZrU with depleted U and ThN. The radial blankets consist of a peripheral blanket and one blanket region at the center of the core. Axial blankets at the bottom and top of the active fuel are also employed. Compared to U, Th features same

radial blankets but a nearly 50 cm thicker axial blanket to compensate the deficit in breeding performance. Although not optimized, the two iso-breeder core designs adopted are suitable to compare the core physics performances of the two fuel options.

Smeared densities have been assumed equal to 85% TD except for the metal fuel case, where 75%TD smeared density has been employed. The linear expansion coefficients assumed are 11.2×10^{-6} K^{-1} and 12×10^{-6} K^{-1} for the U-based and Th-based oxide fuels, 14×10^{-6} K^{-1} and 8.2×10^{-6} K^{-1} for the U-based metallic fuel and the Th-based nitride fuel, respectively [76] [81].

While feasibility of the various options based on detailed power peak analysis has not been ascertained, the average fast fluence for the various cases in the single batch model adopted is within 15% of the 1.6×10^{23} n/cm^2 ARR design value. It is therefore reasonable to expect that optimized multi-batch refueling schemes can be found to convey similar peaking factors, and acceptable peak fast neutron fluences, for all cases investigated.

6.2.3. Molten salt fast reactor

The core of the MSFR is a cylinder with the diameter equal to the height, surrounded axially by steel reflectors, and radially by a fertile blanket, a boron carbide layer, and a reflector. The core is filled with the fuel salt and no core internals are envisioned to date. The fuel circulates out of the core through 16 external loops, each one including a pump and a heat exchanger. The primary circuit is connected to 2 other circuits for salt processing. The first one is a gas system envisioning He is bubbling into the fuel salt to extract gaseous and non-soluble fission products. A 30 second extraction time is assumed for both kinds of fission products. As a matter of fact, extraction of non-gaseous fission products will be slower, but time constants for the extraction extended to a few days would have a limited impact on the obtained results [85]. The second circuit connected to the primary circuit is the salt reprocessing system necessary to separate soluble fission products from the fuel salt. Extraction is assumed as continuous, or batch on a daily basis. A few liters or a few tens of liters of salts need to be extracted every day. The main core parameters are summarized in Table 29.

TABLE 29. MSFR CORE PARAMETERS [85, 86]

Thermal/electric power	3000 MW/1500 MW
Core inlet/outlet temperatures	923/1023 K
Fuel salt volume	18 m^3
Fraction of salt inside the core	50%
Number of loops for heat exchange	16
Flow rate	4.5 m^3/s
Salt velocity in pipes assuming 0.3 m diameter	~4 m/s
Blanket thickness	50 cm
Blanket salt volume	7.3 m^3
Boron carbide layer thickness	20 cm

The fuel salt is composed by LiF for 77.5 mole%, and by a mixture of $(HN)F_3$ and $(HN)F_4$ for 22.5% (HN indicates Heavy Nuclides). Table 30 summarizes the salt properties mainly of interest for this work. Solubility of trivalent elements shows important variations with temperature. At the lowest temperature in the MSFR (923 K) it reaches a ~5% value,

corresponding to ~20% the total amount of $(HN)F_3 + (HN)F_4$. The melting point is 85 K lower compared to the lowest operating temperature in the reactor. It is worth noticing that the melting point is expected to vary mildly with the fraction of $(HN)F_3$ and in case Th is partly substituted with U, which could be necessary to control the redox potential of the mixture. For simplicity and due to the lack of detailed data in this sense, these variations will be here neglected.

A first fundamental aspect that distinguishes the MSFR from solid-fuelled FRs is the neutron spectrum. In fact, the MSFR fuel salt contains a large amount of light elements like Li and F, causing a considerable neutron thermalization. Figure 70 compares the spectrum of the MSFR with that of the ELSY and of the ARR. In particular, a U-based version of the ELSY and a U-based burner version of the ARR are selected, but analogous results are obtained for thh-based options. The harder spectrum of the ARR compared to the ELSY is mainly related to the lower CR and higher fissile-to-fertile ratio.

TABLE 30. MSFR FUEL SALT PROPERTIES [85, 86]

Salt density [kg/m^3]	$4094-8.82\times10^{-1}\cdot(T[K]-1008)$
Salt kinematic viscosity [m^2/s]	$5.54\times10^{-8}\cdot\exp(3689/T[K])$
Solubility of trivalent elements at 823-923-1023 K [%]	2.70-4.86-7.51
Melting point [K]	838

The liquid fuel and the online reprocessing system allow the use of the MSFR as a flexible CR (Conversion Ratio) reactor since the CR can be adjusted by varying the reprocessing rate for soluble fission products. The reprocessing rate determines the quantity of fission products in the core, which in turn affects breeding through both increased captures and an increased fissile-to-fertile ratio necessary to achieve criticality. In the present work it is assumed that the total concentration of actinides and fission products is maintained during the fuel isotopic evolution, so that accumulation of fission products determines a lower actinide inventory in the core. Four options have been investigated, as summarized in Table 31 [87–91].

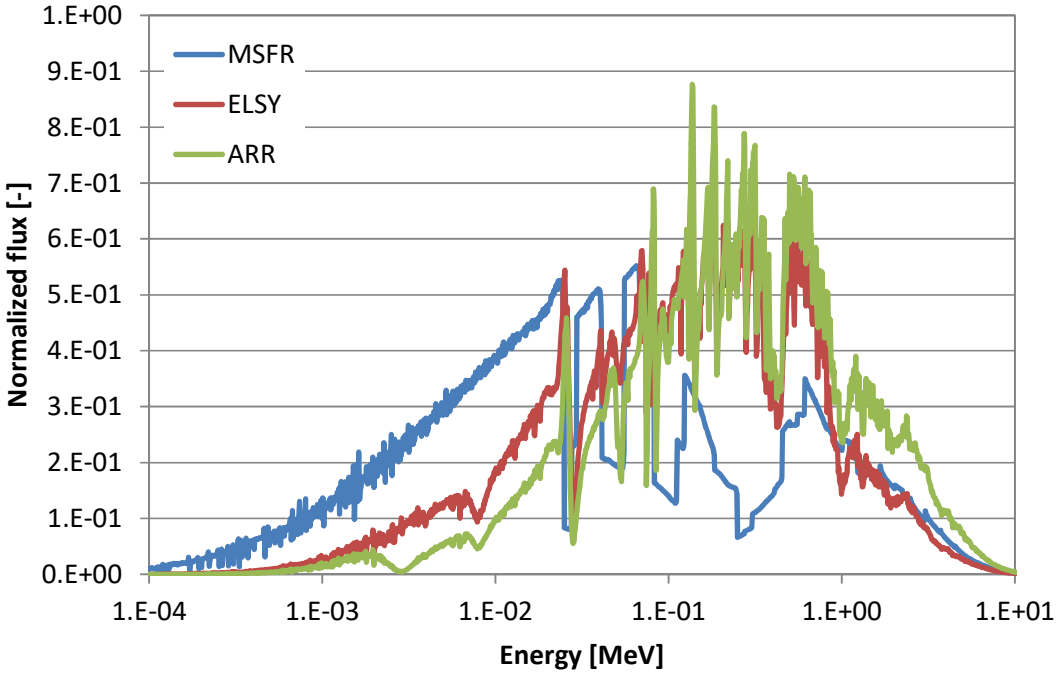

FIG. 70. MSFR spectrum and comparison with the ELSY (U-based) and the ARR (U-based burner version) (reproduced from Ref. [86] with permission).

TABLE 31. FEED OPTIONS FOR MSFR AND ENSUING FRACTIONOF TRIVALENT ISOTOPES AT EQUILIBRIUM [86]

Option name	General strategy	Feed composition	Reprocessing rate [l/d]	Fraction of trivalent isotopes in the salt at equilibrium [%]
Th-feed	Breeding: Th feed, ^{233}U from blanket to be used for other reactors	• 100 wt% Th.	86.5	0.35
ThU3-feed	Iso-breeding: Th feed, ^{233}U from blanket reinserted in the core	• 89.3 wt% Th; • 10.7 wt% ^{233}U (from blanket).	6.49	2.24
ThU3TRU-feed	TRU burning: Th-TRU feed, ^{233}U from blanket reinserted in the core	• 69.3 wt% Th; • 20.0 wt% TRU; • 10.7 wt% ^{233}U (from blanket)	3.29	5.57
ThU3MA-feed	MA burning: Th-MA feed, ^{233}U from blanket reinserted in the core MA composition from Yang (2008)	• 69.3 wt% Th; • 20.0 wt% MA; • 10.7 wt% ^{233}U (from blanket)	4.35	5.35

6.3. METHODOLOGY

In order to evaluate the performances of the MSFR and of the traditional FRs, the EQL3D ERANOS-based [92] procedure, developed at the Paul Scherrer Institute (PSI), Switzerland is employed [93, 94]. The ORIGEN-S code is also used to assess decay heat and radiotoxicity calculations [95].

6.3.1. ERANOS and EQL3D procedure for analysis of solid fueled fast reactors

ERANOS 2.2N is a deterministic code system purpose-made for FR analysis [92]. The ERANOS-based EQL3D procedure simulates the cycle-by-cycle behavior of a reactor. The main assumptions are constant imposed reactor power, constant mass of actinides in the fabricated fuel and constant fuel management. In th model, the core is represented in its full dimensionality, thus allowing a meaningful characterization in terms of core performance as well as safety-related parameters, both at equilibrium and during the transition toward it.

Full recycle of actinides has been assumed for all cases presented in the work, i.e. during reprocessing fission products are removed, all actinides are recycled and an actinide feed is added until the total inventory of the initial fresh fuel is restored. Due to the scoping nature of the calculations performed, a single-batch irradiation scheme has been assumed for convenience. Under the assumed scheme, the core is irradiated for a period corresponding to the batch irradiation time, unloaded (and ideally replaced with another one), cooled for an equally long period, reprocessed, and reloaded once again.

Full core flux and burnup calculations have been performed with ERANOS in a 33 energy-group structure optimized for FR calculations. The multi-group nodal transport theory code VARIANT has been used for flux calculations employing a P3 approximation with simplified spherical harmonics [96]. The 33-group cross-sections have been obtained from assembly-wise lattice calculations using the collision-probability code ECCO in 1968 energy groups based on the JEFF3.1 library available in ERANOS [97].

Each fuel assembly has been discretized in 6 to 8 axial nodes for fuel depletion calculations. Evolution of masses is computed for each node according to the specific power derived through the full core flux calculations. During each cycle (corresponding to the entire irradiation time in a single-batch approximation), fluxes are recalculated 9 times. Between two flux recalculations, macroscopic cross-sections are computed 3 times, and the specific power of each node is accordingly renormalized to maintain a constant core power. The microscopic cross-sections are calculated every few cycles, the exact number depending on the rate of variation of the fuel composition. A set of microscopic cross-sections is calculated for each radial core zone (e.g., inner, middle, and outer in the ELSY).

6.4. APPLICATION TO MSFR

Also, for the MSFR, the lattice data for the core calculations have been generated using the ECCO cell code with JEFF 3.1 based 1968-group neutronic library [94, 85, 90]. The core calculations have instead been performed using the transport BISTRO calculation scheme [94] with S-16 discretization and 33 group energy collapsed lattice data from ECCO. For symmetry reasons (see Section 1), a 2-D r-z geometry is analyzed and only the bottom half of the core is simulated [98]. The entire primary circuit is treated as a single fuel depletion node to take into account the continuous salt mixing. Online removal of fission products is simulated by adding "chemical decay constants" to the physical ones. The addition of the actinide feed is instead performed every year, which has been proved to bring negligible errors compared to a core reloading performed on a daily basis. In the time interval between two actinides reloads, fluxes and macroscopic cross-sections are recalculated 9 times. The microscopic cross-sections are generally calculated at each actinide reloading (i.e., every year) at the beginning of the simulation, and every few reloadings afterwards.

6.4.1. Fuel cycle performances in iso-breeders

A very limited build-up of TRUs is observed in the closed Th cycle, for both the traditional FRs and the MSFR as seen from Table 32 [83–84]. As shown in Fig. 71**,** radiotoxicity generation is noticeably reduced compared to traditional U-Pu FRs in the first few thousands of years. On the other hand, Th use causes a higher specific radiotoxicity in the long term due to the progenies of ^{233}U and ^{234}U. Similar pros and cons have been observed for the decay heat, but in this case the long-term peaking is of limited concern, showing that the Th cycle is a factual option to potentially reduce the number of required geological repositories. As a drawback, ^{233}U has a three times higher fission yield for ^{90}Sr compared to ^{239}Pu, causing a high decay heat level

in the first several tens of years, with possible incremental costs for interim fuel storage or initial forced cooling in a geological repository.

The MSFR features higher specific radiotoxicity and decay heat compared to the solid-fuelled counterparts. This is due to the softer spectrum and ensuing build-up of heavy actinides (especially ^{238}Pu). However, for given reprocessing efficiencies, waste generation also depends on the average fuel burnup. In fact, higher burnups limit the reprocessing requirements and ultimately the actinide reprocessing losses. For the iso-breeder MSFR, the high average burnup allowed by the liquid fuel offsets the higher TRU content and makes this reactor preferable to the traditional FRs in terms of waste generation (Fig. 71).

TABLE 32. HEAVY NUCLIDE CONTENT FOR THE BREAKEVEN MSFR, ELSY AND ISOBREEDER, ARR AFTER 9 GWTH YR/THM OF CUMULATIVE BURNUP [86]

		MSFR Th-feed	MSFR ThU3-feed	Th-U ELSY	Th-U ARR	U-Pu ELSY	U-Pu ARR
HN inventory in the active core [t]		42.3	33.8	72.2	12.1	51.1	13.2
Core composition* [wt%]	^{232}Th	81.8	79.2	85.5	77.7	~0	~0
	^{231}Pa	$1.91\cdot10^{-2}$	$1.68\cdot10^{-2}$	$2.31\cdot10^{-2}$	$5.69\cdot10^{-2}$	~0	~0
	^{232}U	$2.40\cdot10^{-2}$	$2.12\cdot10^{-2}$	$1.96\cdot10^{-2}$	$4.94\cdot10^{-2}$	~0	~0
	^{233}U	11.1	12.6	9.56	16.0	~0	~0
	^{234}U	3.84	4.29	3.13	4.39	$3.15\cdot10^{-1}$	$6.09\cdot10^{-2}$
	^{235}U	1.02	1.17	$6.82\cdot10^{-1}$	$8.28\cdot10^{-1}$	$1.75\cdot10^{-1}$	$4.05\cdot10^{-2}$
	^{236}U	1.14	1.32	$7.27\cdot10^{-1}$	$7.49\cdot10^{-1}$	$2.32\cdot10^{-1}$	$6.09\cdot10^{-2}$
	^{238}U	$2.32\cdot10^{-3}$	$3.19\cdot10^{-3}$	~0	~0	79.7	80.6
	^{237}Np	$2.86\cdot10^{-1}$	$3.38\cdot10^{-1}$	$1.60\cdot10^{-1}$	$1.45\cdot10^{-1}$	$1.30\cdot10^{-1}$	$1.14\cdot10^{-1}$
	^{238}Pu	$3.25\cdot10^{-1}$	$3.95\cdot10^{-1}$	$1.02\cdot10^{-1}$	$8.38\cdot10^{-2}$	$5.05\cdot10^{-1}$	$2.31\cdot10^{-1}$
	^{239}Pu	$9.92\cdot10^{-2}$	$1.24\cdot10^{-1}$	$2.44\cdot10^{-2}$	$1.64\cdot10^{-2}$	9.83	12.5
	^{240}Pu	$8.39\cdot10^{-2}$	$1.10\cdot10^{-1}$	$1.48\cdot10^{-2}$	$6.75\cdot10^{-3}$	6.72	5.02
	^{241}Pu	$1.63\cdot10^{-2}$	$2.25\cdot10^{-2}$	$9.64\cdot10^{-4}$	$6.09\cdot10^{-4}$	$5.11\cdot10^{-1}$	$4.31\cdot10^{-1}$
	^{242}Pu	$1.17\cdot10^{-2}$	$1.70\cdot10^{-2}$	$1.41\cdot10^{-3}$	$4.28\cdot10^{-4}$	$6.73\cdot10^{-1}$	$3.59\cdot10^{-1}$
	Am	$7.59\cdot10^{-3}$	$1.04\cdot10^{-2}$	$2.61\cdot10^{-3}$	$5.81\cdot10^{-4}$	1.07	$4.51\cdot10^{-1}$
	Cm	$5.75\cdot10^{-3}$	$9.48\cdot10^{-3}$	$2.25\cdot10^{-4}$	$7.36\cdot10^{-5}$	$1.58\cdot10^{-1}$	$7.19\cdot10^{-2}$
	Cf	$9.83\cdot10^{-6}$	$2.28\cdot10^{-5}$	$3.61\cdot10^{-7}$	$3.03\cdot10^{-8}$	$4.33\cdot10^{-4}$	$5.86\cdot10^{-5}$

*At discharge for the ELSY and the ARR

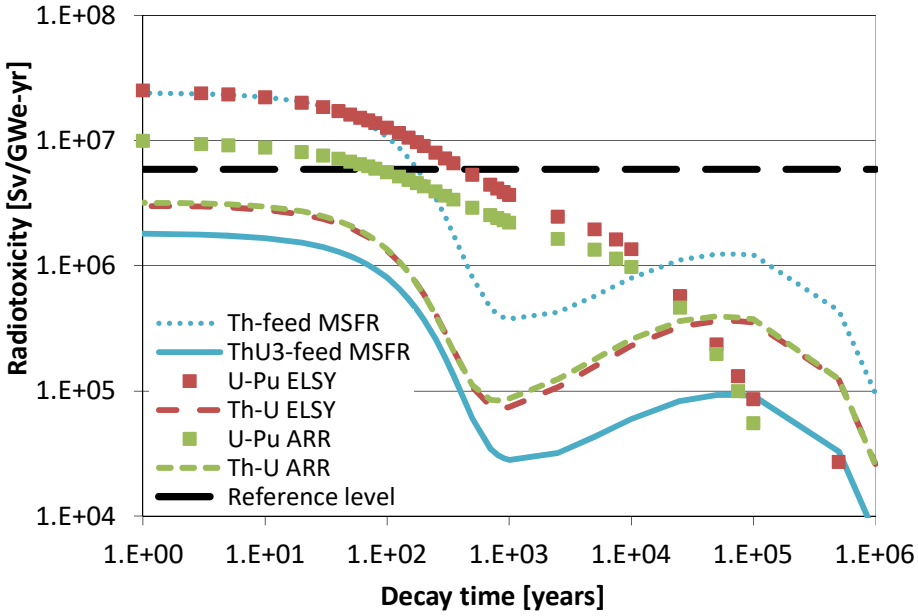

FIG. 71. Radiotoxicity generation at equilibrium from 0.1% actinide reprocessing losses for the different reactor concept, reference level computed as the radiotoxicity of the natural uranium necessary to fuel a traditional LWR (reproduced from Ref. [86] with permission).

Despite the possible advantages in terms of waste management, fuel transportation and fabrication represent formidable challenges for Th use in traditional FRs (while they would be of little concern for the liquid-fuelled MSR). The gamma dose rate at 0.5 meters (a typical working distance for glove-box operations) from a 5 kg sphere of ^{233}U containing 1500 ppm of ^{232}U is ~0.2 Sv/hr [99]. Exposed workers would reach the annual dose limit in few minutes, and a few hours of exposure would be life-threatening. As a matter of fact, the first and longest lived daughter of ^{232}U is the 1.9 years halflife of ^{228}Th. If Th is separated from the other actinides during reprocessing the fuel would be momentarily free from the gamma-emitting ^{232}U progeny. However, this will require a dedicated heavily shielded storage facility with a storing capacity of several hundreds of tonnes of highly radioactive Th. In addition, fuel fabrication and transportation would have to be performed soon after reprocessing to avoid the build-up of the ^{232}U progeny. Figure 72 plots the gamma sources from U based and Th-based ARR assemblies after reprocessing and compares them to that of a U based burner version of the ARR [100]. The gamma emission from a Th-based assembly would reach that of the burner ARR assembly in only one year. In addition, Fig. 73 shows that most of the gammas are emitted at high energies. A clear idea of the problem of ^{232}U gamma emission has been given by WENNER, M et al [68], who used the equilibrium actinide concentrations obtained in this work for the ARR to demonstrate that, for a given shielded facility for fuel fabrication, the dose to workers in case of Th based fuel assemblies would be tens of times higher compared to a U-based fuel assembly, even considering the reduced neutron emission fostered by the lower TRU build-up in the Th case.

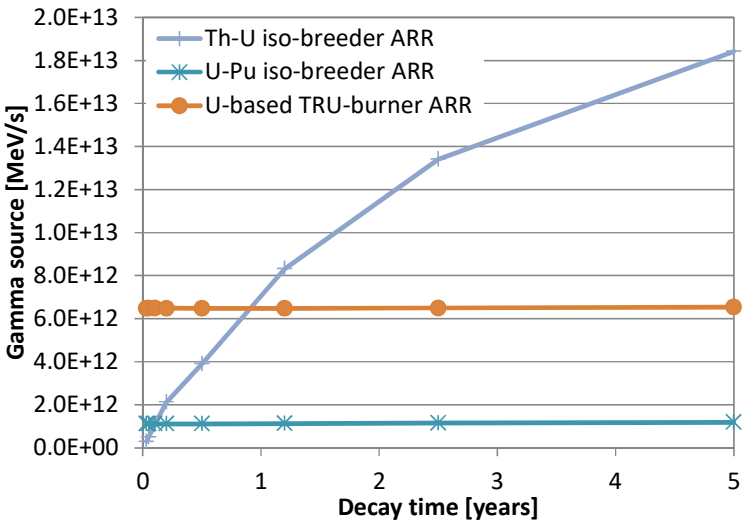

FIG. 72. Gamma source from an assembly in different ARR (reproduced from Ref. [86] with permission).

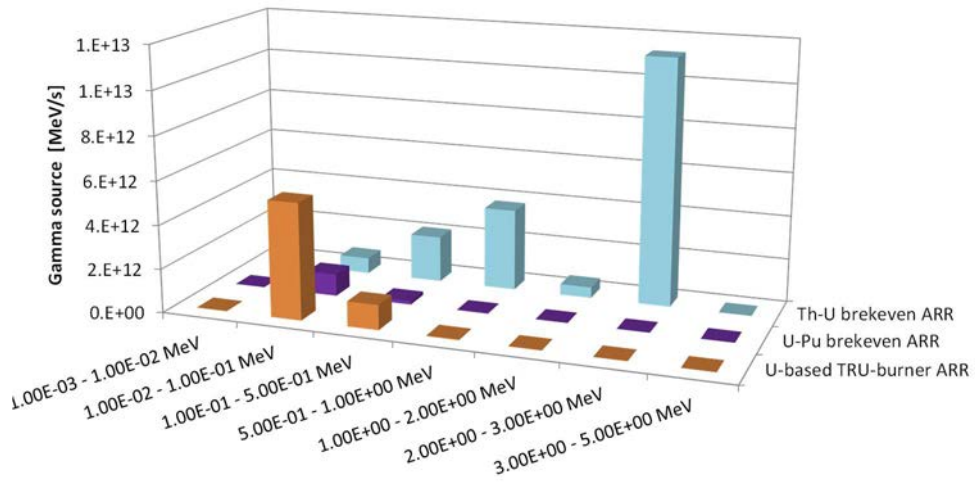

FIG. 73. Gamma source from an assembly after 5 years of cooling for different energies and ARR versions (reproduced from Ref. [86] with permission).

As regards proliferation issues, it is worth noting that the Th-U cycle is often claimed as proliferation resistant thanks to the ^{232}U gamma emission. This claim is however controversial. It is a fact that U handling is made difficult by the presence of ^{232}U progeny. As a matter of fact, 24 000 ppm of ^{232}U in U would be necessary to meet IAEA's standard for reduced physical protection requirements >1 Sv/hr at 1 meter. In addition, shielding high energy (2.6 MeV) gammas is difficult and the characteristic energetic peak would make the U easily detectable. Ten days after purification, a one-gram sample of ^{233}U containing 100 ppm ^{232}U will be detectable through a 2 inch of lead shielding by a standard type of doorway monitor equipped with NaI detectors. On the other hand, the intense gamma field could interfere with other types of instruments, like the passive gamma ray nondestructive assembly measurement techniques. In addition, even though separation of Th from U requires special techniques (e.g. the THOREX process), separation of the first ^{228}Th daughter, namely ^{224}Ra, is expected to be much easier thanks to the markedly different chemical behavior. ^{224}Ra has a half-life of 3.66 days, which

would allow a reasonable margin for fuel handling. It is also worth noting that ^{232}Pa and ^{233}Pa have half-lives of 1.3 days and 27 days, respectively. Approximately 10 days after discharge, the Pa in the fuel would be almost free from ^{232}Pa and would lead to the generation of nearly pure ^{233}U if separated from in-bred U. Since, Pa separation is relatively easy, this possible route for the generation of ^{233}U represents a major concern related to the deployment of Th-based reactors [101]. As regards the specific case of the MSFR, the low fissile inventories and the online reprocessing system limit the ^{233}U amount outside the power plant and minimize the potential risk of its diversion. Thanks to the liquid fuel, the possibility also exists of denaturing the ^{233}U with addition of ^{238}U. On the other hand, the relatively easy extraction of ^{233}U through fluorination and the very high quality of U produced in the blankets increase proliferation risks related to the use of the MSFR technology.

6.4.2. Fuel cycle performances in burner reactors

Two possibilities exist for TRU burning in FRs [83]. The first one consists in loading initially the reactor with TRUs and operating the reactor in a closed cycle till the initial loading has been transmuted into the equilibrium core compositions. The second, more effective, option is to use low-CR (Conversion Ratio) reactors and use a feed composed by Th or U (natural or depleted) and by a TRU fissile top-up.

As regards the possibility to transmute an initial TRU loading through a subsequent prolonged operation, a comparison between start-up and equilibrium radiotoxicities is reported in Fig. 74, with similar results obtained also for decay heat. This strategy is ineffective if U-based traditional FRs are used, since radiotoxicity and decay heat of the equilibrium core are comparable to those of the initial TRU loading. If Th is used as feed, radiotoxicity and decay heat profiles are instead significantly affected. The equilibrium core will have a lower radiotoxicity and decay heat for several thousands of years compared to the initial TRU loading. On the other hand, these fuel cycle metrics will be worse in the very long term. Benefits of transmutation are then questionable in terms of radiotoxicity, whose peak value is reduced at the cost of a higher integral value e.g., over 106 years. The lower decay heat in the short-middle term is instead a factual advantage of the equilibrium Th-U composition vs the initial TRU loading as it would reduce number and/or costs of the geological repositories for final waste disposal. In this scenario, the MSFR presents both pros and cons. A disadvantage comes from the softer spectrum, causing a higher buildup of ^{238}Pu, and ultimately a higher radiotoxicity and decay heat of the equilibrium core. A major advantage is instead given by the high specific power, which combines with the lack of out-of-core cooling time for the fuel to yield a short transmutation time (Fig. 75), thus making the MSFR a promising option for a quick transition from the current U-based fuel cycle to a closed Th-U cycle.

As regards waste transmutation via a TRU feed in low CR reactors, traditional FRs are limited by the deterioration of safety with increasing TRU content (see next section), and by fuel fabrication issues associated to the intense heat load and radiation field in a TRU-rich multi-recycled fuel. By assuming a traditional 5% limit on the content of MA (Np, Am, Cm and Cf), it turns out that only TRUs from once-through LWR can be used as feed in a low-CR reactor like the ARR (CR~0.4), while TRUs from multi-recycled LWR fuel would lead to an excessive MA content [84]. This constraint is independent of the adopted fertile material, since endogenous generation of TRUs is small and the MA inventory is mainly determined by the quantity of TRUs fed to the core. This determines a maximum achievable TRU burning rate equal to ~500 and ~600 kg/GWe-yr for the U and Th based cores, respectively, corresponding to a MA burning rate equal to 60–70 kg/GWe-yr. As expected, TRU burning rate is slightly increased by Th use thanks to the inherently lower neutron economy. On the other hand, Th use

exacerbates problems of fuel handling due to the intense and penetrating gamma rays emitted by the progeny of ^{232}U.

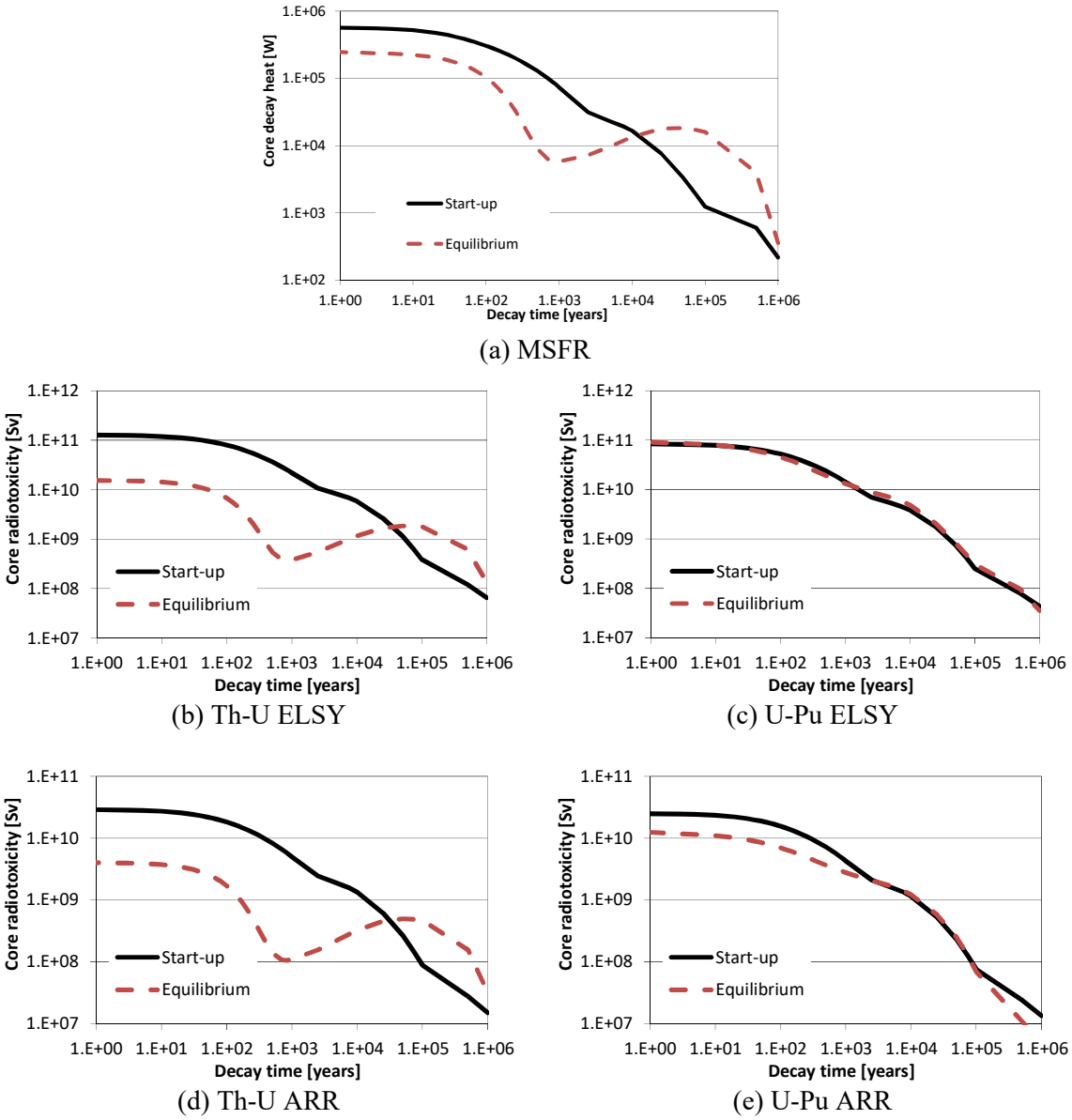

FIG. 74. Radiotoxicity profiles of TRU start-up core and equilibrium actinide inventory for: (a) the iso-breeder MSFR, b) the Th-U ELSY; (c) the U-Pu ELSY; (d) the Th-U ARR; and (e) the U-Pu ARR (reproduced from Ref. [86] with permission).

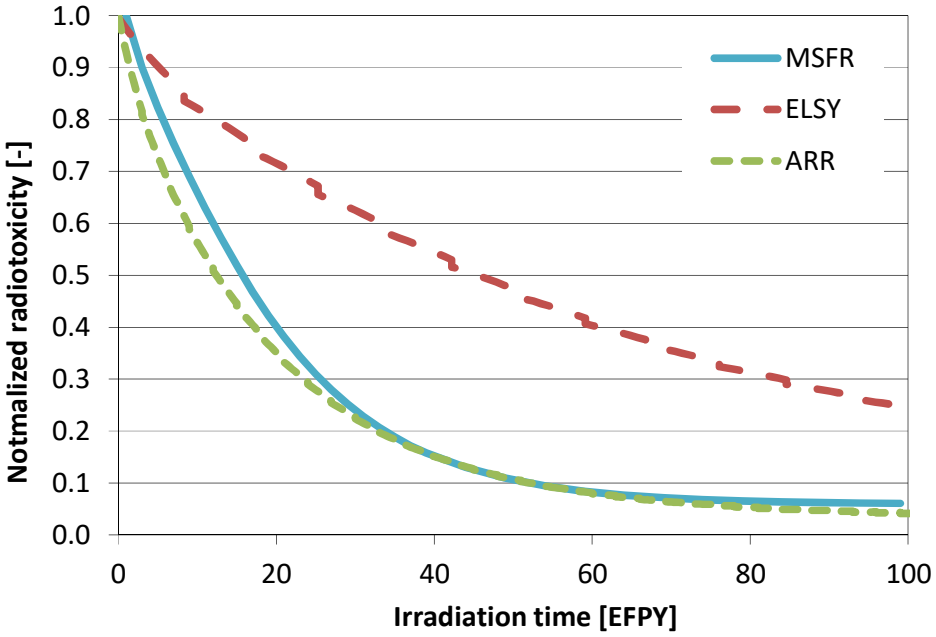

FIG. 75. Radiotoxicity associated to the evolving actinide inventory, after 300 years of cooling (reproduced from Ref. [86] with permission).

As previously explained, a low CR is achievable in the MSFR through a low reprocessing rate and ensuing high content of fission products in the core. The solubility of TRUs in the fed salt sets the upper limit for the TRU transmutation rate to ~150 kg/GWe-yr, which translates into a lower limit for the CR equal to ~0.8. An interesting aspect of the MSFR that differentiates it from traditional FRs is that the composition of the TRU feed is not strictly limited by issues of fuel fabrication and transportation. This allows for the use of the MSFR as a MA-burner reactor, with Pu recycled in other reactors [94]. The resulting MA burning rate of ~150 kg/GWe-yr would be 2 times higher compared to that achievable in the ARR. A main drawback of the MSFR is once again the softer spectrum, causing a substantial increment of radiotoxicity and decay heat of the equilibrium fuel.

6.4.3. Safety parameters

Th use in fast-spectrum systems determines a lower reactivity increment due to spectrum hardening thanks to the lower cross-section and higher threshold for fission of ^{232}Th vs ^{238}U, and to the steeper fission cross-section and flatter capture cross-section of ^{233}U vs ^{239}Pu (Fig. 76). As shown in Table 33, this determines notable improvements of the core void reactivity, which becomes negative in the Th based isobreeder ARR. Spectrum hardening plays a role also in the Doppler phenomenology, determining some advantages for the Th option in case a significant amount of ^{233}U is present in the core [102-103]. As a drawback, Th use lowers the negative feedback coefficients associated to core and fuel expansion, both effects being related to spectrum softening.

Use of Th has consequences also on the βeff. In particular, ^{233}U has a higher delayed neutron yield compared to ^{239} Pu while the possible beneficial effect of fissions in fertile isotopes is frustrated by the very low fission rate of ^{232}Th compared to ^{238}U. As a result, βeff for Th based isobreeder FRs is comparable to that of the U counterparts thanks to the sufficient amount of ^{233}U, while the Th option presents lower values in burner core configurations. This combines with the higher burnup reactivity swing (due to the lower internal breeding) to yield a considerably higher number of required control rods in Th vs U traditional FRs.

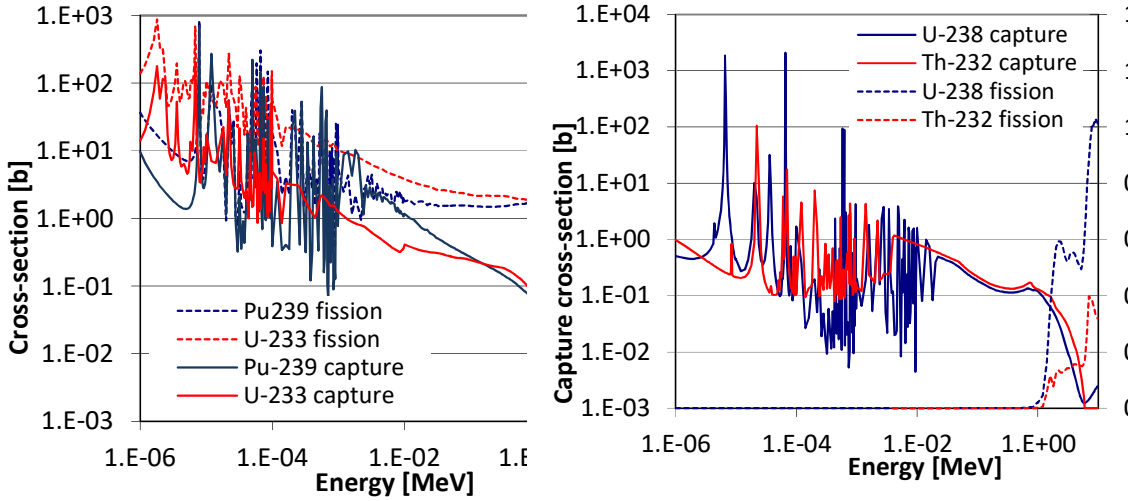

(a) Fissile isotopes (b) Fertile isotopes

FIG. 76. Cross-sections for the main fissile and fertile isotopes (reproduced from Ref. [86] with permission).

Investigation of the MSFR safety parameters has shown that only Doppler and fuel expansions induce significant reactivity feedbacks (Table 34) [84]. The Doppler coefficient is characterized by the same phenomenology as for traditional FRs, with an increment of captures in ^{232}Th and an ensuing spectrum hardening causing a reduced fission rate in the fissile isotopes. However, Th use and a softer spectrum combine to give a notably stronger coefficient, nearly one order of magnitude higher compared e.g., to the ARR. Dependency of the Doppler coefficient with temperature and composition is analogous to traditional FRs, with a logarithmic trend of reactivity vs temperature and a reduction of Doppler with lower CR and higher Am content. The fuel expansion coefficient presents instead a phenomenology that deeply differentiates it from traditional FRs It results from a change of the neutron diffusion length in the core and from the ensuing increase of leakages [104]. Spectrum softening due to an increased coolant-to-fuel ratio is instead mainly responsible for the fuel expansion feedback in traditional FRs. The resulting negative feedback is tens of times higher in the MSFR, increases with fuel temperature, and is only mildly affected by core compositions, thus assisting the fuel cycle flexibility of this kind of reactor. In addition to Doppler and fuel expansion, only blanket density and core expansion can affect the core reactivity. Blanket density variation causes negative feedback, but negligible. Core expansion is potentially positive feedback, but it has been proved to be 10 times lower compared to the fuel salt expansion. In addition, it would act in a delayed way, and it could be triggered mainly by salt heating, thus slightly reducing the fuel expansion coefficient without acting per se as positive feedback.

TABLE 33. EQUILIBRIUM SAFETY PARAMETERS AT THE END OF EQUILIBRIUM CYCLE FOR THE INVESTGATED ARR CORES AND FEED/FERTILE ISOTOPOE OPTIONS [86].

Core type	Burner		Iso-breeder	
Fertile	U	Th	U	Th
Fissile make-up feed	TRUs	TRUs	—	—
MA/Pu ratio in the feed	~0.1	~0.1		
CR [-]	0.47	0.36	1	1
Active core voiding [pcm]	1322	757	1772	-346
Coolant expansion coefficient - active core [pcm /K]	0.34	0.20	0.46	-0.09
Coolant expansion coefficient - whole core [pcm /K]	-0.55	-0.82	-0.18	-0.82
Doppler coefficient [pcm /K]	-0.28	-0.25	-0.37	-0.66
Fuel exp. coeff. [pcm /K]	-0.12	-0.09	-0.19	-0.06
Fuel coefficient (Doppler + expansion) [pcm /K]	-0.40	-0.34	-0.56	-0.72
Radial exp. coeff. [pcm /K]	-0.94	-0.92	-1.01	-0.77
β_{eff} [pcm]	315	285	361	342
Generation time [μs]	0.35	0.37	0.29	0.39
Burnup reactivity swing [pcm]	5138	5602	2905	4885
Required control rods to comply with a 0.8 $ limit [-]	21	25	11	18

TABLE 34. MSFR EQUILIBRIUM SAFETY PARAMETERS [86]

	MSFR Th-feed	MSFR ThU3-feed	MSFR ThU3TRU-feed	MSFR ThU3MA-feed
Doppler coeff. [pcm/K]	-3.25	-2.91	-1.89	-1.52
Fuel exp. coeff. [pcm/K]	-3.01	-3.23	-3.25	-3.01
Fuel coeff. (expansion + Doppler) [pcm/K]	-6.26	-6.14	-5.14	-4.53
Coolant exp. coeff. [pcm/K]	—	—	—	—
Core exp. coeff. [pcm/K]	~0	~0	~0	~0
Generation time [μs]	0.95	1.01	0.96	0.80
β_{eff} [pcm]*	334.8	332.1	321.7	291.0

* The reported values of β_{eff} do not take into account the fuel salt circulation and out-of-core decay of the delayed neutron precursors

7. EVALUATION OF ACTINIDE RECYCLE AND BURN IN A MULTI-TIER REACTOR SYSTEM

7.1. BACKGROUND AND MOTIVATION

The transmutation of long-lived actinides drastically reduces the amount of long-lived components of the waste and improve the repository performance by reducing the heat load of the waste packages during long term disposal. The present study discusses some of the challenges of actinide recycle and transmutation by analyzing a multi-stage transmutation scenario, starting with or without an interim Pu burn in current LWRs and implementing full actinide recycle in advanced reactors, specifically Reduced Moderation PWRs and BWRs and Sodium Fast Reactors. The performance with either U or Th-based fuel is analyzed to show potential pros and cons of each option, the areas deserving further investigation and the needed future developmental programmes.

7.2. OVERVIEW OF THE TRANSMUTATION SCHEME

The primary goal of the transmutation scheme is to evaluate the recycling and burning long-lived transuranic isotopes (TRU) employing the minimum number of transmutation reactors to reduce associated costs. The multi-stage reactor scheme is employed without interim Pu recycle in LWRs and with interim Pu recycle in LWRs [105]. The reactors in the first tier are the current LWRs operating with the current fuel cycle and infrastructure, attaining optimal economic performance. A second tier of reactors is then assumed to be gradually introduced for burning the actinides recovered from the used fuel of the first-tier reactors in either a U or Th fertile carrier. As the TRU loading supplied to these reactors will 9not be completely burned in a single irradiation cycle, and newly generated long-lived actinides will be produced, these reactors need to enable continuous recycle of actinides in their own discharged fuel, for, in principle, an indefinite number of irradiation cycles. By pursuing full actinide recycle, high level waste (HLW) generated by this nuclear system will in principle consist of fission products (FPs) plus some inevitable but low levels of actinide losses.

The reactors envisaged for the second tier are: Reduced Moderation Pressurized Water Reactors (RMPWRs), Reduced Moderation Boiling Water Reactors (RBWRs) and Sodium Fast Reactors (SFRs), with a summary of their design features [106–110]. The harder neutron spectrum of Reduced Moderation Light Water Reactors (RMLWRs) and especially SFRs, increases the likelihood of TRU destruction by fission instead of transmutation to higher mass number which is advantageous to implement a continuous recycle policy. While both RMLWRs and SFRs can in principle accomplish continuous actinide recycle, SFRs offer superior fuel cycle performance by virtue of the higher discharge burn-up (BU) thus enabling significantly lower fuel reprocessing and manufacturing requirements than the counterpart RMPWRs. RBWRs have the potential for discharge BU intermediate between the SFRs and RMPWRs. As evolution of current LWRs, RMLWRs have potentially shorter time to licensing and deployment than SFRs, plus some reactors in the current US reactor fleet, especially PWRs, could be converted to the reduced moderation mode of operation. This may reduce and delay the investment required for building SFRs. The technology and infrastructure to support either reactor types require a certain degree of development, lead time, financial risks and economic penalty compared to the current cycle.

7.3. RESULTS

A top-level quantitative analysis of the transmutation scheme devised has been performed adopting representative reactor designs for the reactor physics analysis [106–110].

7.3.1. Mass flows and inventories

The transmutation scheme analyzed describes fuel and reactor types at the various scenario stages. When the Pu recovered from UO_2 PWR (Stage 1) followed by the Pu burn in either as MOX or as TOX in a PWR (Stage 1a), and then full recycle in reduced moderation LWRs (RMLWRs) and sodium cooled fast reactor (SFR) (Stage 2), the residual Np, Am and Cm from spent UO_2 are recovered and recycled in RMLWRs and SFR (Stage 2) together with the TRU (and ^{233}U and Pa for ThOX) from MOX PWR and TOX MOX (Stage 1a) discharge. If Pu recycle in Stage 1a is not pursued, then all the TRU recovered from UO_2 PWR fuel will be directly recycled in RMLWRs or SFR (Stage 2). For the RMPWR recycle scheme, results only for the latter option are presented since preliminary analysis performed indicated that the interim Pu burn in UO_2 PWR (Stage 1) is undesirable when followed by Stage 2 RMPWR. For all schemes, the results have been calculated at the equilibrium cycles obtained by repeated recycle in Stage 2 reactors until the mass flows and isotopic inventory of each scenario have converged. The ensuing share of thermal energy for the various stages is derived from the reactors support ratio at these conditions, based on 40% energy conversion efficiency for the SFR, ~33% for the PWR and RMPWR stages and ~34% for the RBWR.

The results obtained indicate that direct recycle of actinides from Stage 1 to Stage 2 reactors entails ~30% of the total thermal energy produced by the transmutation reactors, with a ~10% decrease if interim Pu burn in Stage 1a is pursued. This shows that an intermediate MOX or ThOX stage will reduce the number of transmutation reactors, which would be particularly desirable for SFRs due to the anticipated high capital cost and operating expenses, and long time to deployment. Th-based transmutation in SFRs appears to have greater potential for minimization of the number of SFRs due to the inferior neutron economy compared to the U SFR cycle (lower fast-fission contribution from ^{232}Th compared to ^{238}U, lower average number of fission neutrons from ^{233}U compared to Pu and, as a result of the lower density compared to U-based oxide fuel, higher leakages with reduced internal breeding). Table 28 also shows the incineration rate for each stage, higher for SFRs and RMPWR and lower in the RMBWR. This results in the higher share of transmutation reactors for RBWR, ~40–50% of the fleet vs. ~20-30% for SFR and RMPWR. The highest incineration rate among the schemes and core design examined pertains to the multi-tier Th-SFR, with ~ 20% of the total fleet devoted to transmutation reactors. It is to be noted that the U-SFR could probably achieve similar transmutation rates by changing the core design to further increase core leakages and reduce conversion ratio, though this would require a safety analysis reassessment to ensure viability.

SFR-based schemes can achieve much higher discharge burnup (BU) than RMPWR and are more efficient from the incineration standpoint. The higher discharge BU, combined with the higher incineration rate, results in the larger values of kg burned/MT reprocessed pertaining to the Th-based SFR schemes. The slightly higher discharge BU of the Th vs. U SFR schemes is due to primarily to the lower density of Th-based fuels, while adopting the same fuel management scheme of U-based fuel. The RBWR has the potential, from a reactor physics viewpoint, to achieve relatively high discharge BU, ~80 GW. d/tHM, but has lower incineration rate, and thus perform similarly to RMPWRs in terms of incineration efficiency.

Fuel manufacturing and reprocessing requirements are key performance indicators. Fuel for Stage 1 reactors is standard LEU fuel made in hands-on facilities. Fuel incorporating Pu and/or fresh Th needs to be manufactured in a glove-box facility. Fuel containing minor actinides (Am, Cm) or U bred from Th needs to be performed remotely due to the high radiation field. Table 28 shows the breakdown of fuel manufacturing for each stage of the various schemes in terms of MT of fuel per GWe-yr produced. The dominant economic discriminators are the amount of fuel that needs to be fabricated remotely and the amount of fuel that needs to be reprocessed. SFRs fare significantly better than RMPWRs from these standpoints, while RBWR is similar to the SFRs for reprocessing requirements and intermediate between SFRs and RMPWR for remote fuel manufacturing requirements. It is to be noted that, for heterogeneous recycling, partition into various elemental streams (Th, ^{233}U, Pu, Am/Cm) would need to be realized by proper reprocessing technology; whether this can be achieved is unclear at this point and would likely require considerable development.

The SFR cores feature larger fissile proportions due to the combined effect of higher discharge BU, increased leakage and reduced fissile cross-sections. The higher discharge BU is beneficial to lower manufacturing and separation requirements, as discussed. As the fuel is irradiated through the various cycles, the isotopes reloaded from the previous stage(s) are only partially consumed in a given irradiation cycle, new fissile is bred from fertile elements, some isotopes are transmuted by neutron capture which leads to a buildup of isotopes with higher mass numbers, and some isotopes decay. Eventually an equilibrium state is reached where isotopic consumption and decay equates production and injection as external feed, which when achieved by all isotopes leads to a stable isotopic inventory. As the main neutronic properties are conferred by elements whose content is established relatively quickly, reactivity and mass flows take only a few cycles to converge. On the other hand, some isotopes which may be of low significance for reactor physics considerations but are important for their impact on front-end and back-end, e.g. for their high specific radiation field, or the long-term radiological threat they pose, may evolve for a much longer time. Multi-cycle simulations from start-up to the equilibrium cycle have thus been performed so that the buildup of the meaningful fuel cycle isotopes could be captured and compared across the various cases. More specifically, a total period of in-core irradiation of 110 Effective Full Power Years, (EFPY) plus cycle-to-cycle cooling time, reprocessing and reloading has been simulated. With a 5-year cooling time, this corresponds to over 200 years of recycling, at which point the isotopes at the upper end of the transmutation chain (e.g., ^{252}Cf) are also effectively converged.

In the Th single-stage reactors, the buildup of ^{232}U from start-up to equilibrium entails a decrease in the Pu inventory, contrasted to the Th multi-stage reactors where the presence of ^{233}U in the external feed from the prior ThOX stage and the poorer fissile quality of the Pu injected results in the opposite trend. In the U-SFR cases where Pu is also bred from U, in addition to the external feed, its content at equilibrium is slightly higher than at start-up. The content of Cm (and typically of Am) is increasing for all schemes, following the common prevailing consumption mechanism of Am, i.e. transmutation by neutron capture, which ultimately leads to the generation of Cm. Notably, despite the lower Pu inventory, the Th-SFR cases feature higher Am and Cm inventory compared to the U counterpart: this follows from their higher rate of external feed, which itself contains Am and Cm, which leads to the higher accumulation Am/Cm observed before equilibrium is reached. Note also that the higher fertile proportion, and lower incineration rate, of the RMPWR promotes comparatively lower proportions of Am and Cm, despite the higher chance of transmutation vs. fission in the softer spectrum relatively to the SFR. Table 34 shows a total Am+Cm content for the Th-SFR vs. RMPWR of ~5 % vs. 3% in the single stage scenario, and 9% for the Th-SFR vs. 2% in the

RBWR for the multi-stage scenario. The specific content of ^{232}U in the Th SFR is twice that of the RMPWR, primarily as a result of the larger fuel proportion of ^{233}U in the Th SFR.

7.3.2. Fuel cycle front end and backend metrics

As discussed, regardless of the spectrum and Th vs. U-supported actinide burning, isotopic multi-recycle inevitably leads to accumulation of higher actinides, Cm and eventually Cf, especially when some of these isotopes (Cm) and their precursors (Am) are also supplied as external feed. As a result, a considerable neutron source, predominantly from spontaneous fission reactions, arises. The neutron source at fabrication for the various schemes is an important discriminator for the various options, as remote fuel manufacturing requirements are expected to be among the dominant economic and technological factors.

A considerable neutron source, in the range of 10^4 to 10^6 n/s gHM, is seen in all cases of SFR, RMPWR and RBWR which translates into 10^8-10^{12} n/s/assembly. These sources require significant shielding, on the order of several feet of concrete, to maintain radiation exposure to the workers within acceptable limits. The RMPWR tends to have higher specific source due to larger generation of higher actinides in the softer spectrum; these impact particularly the generation of californium (Cf), since the content of Am and Cm is driven primarily by the external feed rate and so these isotopes are present at high content also in the SFRs. The higher content of Am/Cm in the external feed to the multi-stage transmutation scheme leads to higher neutron sources, especially during the first recycles. The higher proportion of fertile isotopes of the RMLWRs compared to the SFR counterbalances the higher generation rate of neutron emitters until the buildup of Cf becomes the predominant factor (after ~30 EFPY for the single-tier RMPWR scheme and ~50 EFPY for the RBWR multi-tier scheme). For the SFRs, the leading neutron source contributor remains Cm, even though the contribution of Cf increases as the irradiation progresses.

The U and Th FRs have very similar neutron sources, typically slightly higher for Th as a result of the higher feed rate of Am/Cm. There is however a significant difference in the gamma source between U and Th. The secondary gamma source from (n, gamma) reactions in the surrounding material is not considered here, but it represents an additional contributor in the determination of shielding requirements. The low gamma energy components, up to ~200 keV, of the primary gamma source are dominated by the decay of ^{241}Am and ^{243}Am, ^{244}Cm and ^{238}Pu, and so are the same or similar in U and Th-supported actinide burning. However, Th shows an additional significant gamma field at higher energy which is due to the decay of the daughter products of ^{232}U, primarily ^{212}Bi and ^{208}Tl. ^{208}Tl in particular is responsible for the emission of an intense and particularly penetrating 2.6 MeV gamma ray.^{232}U is an unavoidable byproduct of the Th cycle, especially in the driver fuel where it is generated by high energy neutron (n,2n) reactions with ^{232}Th and ^{233}U; it builds up relatively quickly, reaching equilibrium during the first few cycles of irradiation. The higher content of ^{232}U in the ThSFR fuel inventory leads to a larger gamma field, about twice in the 2.5–3 MeV bin, compared to the RMPWR. If Th is partitioned during the reprocessing and not immediately recycled, then the first and longest-lived daughter of ^{232}U, the 1.9-year half-life ^{228}Th, would be initially absent and the growth of ^{233}U daughters would be significantly delayed as now dependent on the 69-year half-life ^{232}U. The possibility of independently managing Th from the rest of the recycled actinides relies on devising a suitable reprocessing separation technique, plus the potential benefits of delaying the onset of the gamma field depend on the specific fuel manufacturing technique adopted and would certainly require collocation of separation and manufacturing facilities. Given the shielding requirements of fuel bearing Am and Cm, the benefits of Th partition materialize only if a heterogeneous recycling scheme with independent management of Pu and ^{233}U+Am+Cm is

a viable option so that Th-Pu can be manufactured in glovebox with only the remaining Th-^{233}U-Am-Cm fuel manufactured remotely. It is also be remarked in this context that the feasibility of fuel manufacturing with a relatively high content of Am and Cm, especially for the SFR multi-stage options examined, and even more so for heterogeneous schemes, needs to be determined.

Historically, the thick shielding required to cope with the high-energy gamma radiation associated to ^{232}U has been a cogent deterrent to the implementation of the Th cycle. In TRU-burning reactor schemes as the one investigated here, this challenge compounds difficulties related to the presence of a high neutron source, thus likely further penalizing economics. On the other hand, since substantial remote fuel manufacturing and handling would be required regardless of the choice of U and Th, when adopted in a TRU burning context the Th option appears less economically penalizing than in more traditional fast reactor breeding schemes, at least as far as fuel manufacturing is concerned.

Even assuming that a suitable remote fuel manufacturing technique can be found to produce the industrial amounts of highly radioactive fuel, and an advanced reactor fleet can be deployed for the transmutation, there remain significant technological gaps in the scheme described. A case in point is the extremely high actinide recovery ratio required, exceeding 99.9% for Pu and Am, and including partition of Cm from the FPs, to achieve a high level waste (HLW) with a ~300-year U ore radiotoxicity target. While partition with 99.9% recovery of Pu is conceivable in current state-of-the-art industrial reprocessing, partition with high recovery of Am and Cm require significant development before achieving industrial status. A potential reprocessing flowsheet for the Th-based transmutation fuel would use UREX process for Uranium removal, TRUEX process for fission products removal and TALSPEAK process for Th, Pa, transuranics and lanthanides separation. Further investigations and likely a pilot reprocessing program are required to understand what can be achieved in terms of elemental separation and recovery ratios. Reprocessing, together with fuel manufacturing, is certainly a key area requiring further work before being able to more sensibly discriminate among the various options. The waste radiotoxicity of all schemes is similar and, at decay times of >~300 years, is dominated by the actinides process losses. Transuranic isotopes are the primary contributors for decay times until ~10 000–50 000 years, with similar radiotoxicity for all schemes; U (and in particular the U in-bred from Th) is a long-term contributor.

7.4. SUMMARY

A multi-tier fuel cycle scheme for transmutation of long-lived actinides obtained from spent UO_2 fuel has been analyzed. The current LWRs are the first tier reactors and incinerate transuranics (TRUs) obtained from the first tier in the second tier reactors. For this purpose, the reactors investigated are RMLWRs with Th-based fuel and SFRs with either U-based or Th-based fuel.

The Th-based incineration route has greater potential for reducing the number of transmutation reactors, and a minimum is achieved when Th-SFRs transmutation preceded by an interim Pu burn in Th-PuO_2 PWRs is pursued. SFRs are in general more efficient incinerators than RMLWRs, especially RMPWRs, mainly because of the higher proportion of TRU that can be loaded and the significantly greater discharge BU that can be attained as a result. This, with the relatively high incineration rate promoted by their burner configuration, lowers reprocessing and fuel manufacturing requirements significantly, especially compared to RMPWRs

U-based schemes can build on far more developed knowledge basis and fuel infrastructure. However, part of this infrastructure is not directly applicable to transmutation, and substantial developments in fuel manufacturing and reprocessing will be required for all schemes, including U-based schemes.

U appears to be more likely short-term option if SFRs with heterogeneous transmutation cores are pursued, and for this scheme a minimum is achieved in the amount of fuel requiring remote manufacturing. Use of Th is required if RMPWRs are pursued. Th would be very beneficial but perhaps not strictly required for achieving a viable RBWR burning scheme. In SFRs, Th has the advantage of mitigating reactivity insertion following core voiding, but it is certainly not essential for viability.

With the current reactor portfolio and new builds dominated by LWRs, it is hard to conceive deployment of dedicated SFR burners to recycle actinides, especially in a market-driven environment. In this environment, the capability of retrofitting currently mature LWR technology to perform such mission appears as an asset, but even in this case a once-through fuel cycle emerges as the economically preferred solution for the foreseeable future. If actinide recycle is ever pursued, it will not be, in all credible circumstances, because of a distinct economic advantage over the once-through cycle but because of policymakers' decision weighting favorably other potential advantages of a closed fuel cycle (long-lived radiotoxic waste reduction, better use of resources etc.). In any case, substantial investments and development cost would need to be borne and a significant portion of the reactor fleet would need to be operated on a closed actinide recycle scheme.

Advances in reprocessing area is required for all schemes, mostly because of the high actinide recovery ratio required, including Am and Cm, to affect the claimed ~300-year HLW radiotoxicity target. Th is not favored in this aspect, at least in consideration of the absence of an existing supporting industrial process, and due to the increased difficulties in the dissolution stage and the larger span of isotopes to be recovered and recycled. Fuel manufacturing in the presence of a severe radiation field is another key challenge of every scheme, particularly of those related to Th where the difficulties of coping with the significant neutron source from Cm and, especially for the RMPWR, Cf, are compounded by the characteristic, and extremely penetrating, gamma rays from the decay products of ^{232}U.

Reactor licensing appears facilitated when pursuing RMLWRs due to already licensed LWR designs that could be converted to the reduced moderation scheme upon licensing of a new core; however other changes and licensing aspects would still be involved (e.g., reactivity control, fuel qualification, fuel transportation, safety analysis and associated codes etc.). In general, development of expensive and challenging technologies would be required for all schemes, inherently discouraging industrialization without an overriding, compelling driver.

In conclusion:

- All options investigated can in principle support full actinide recycle;
- No evident technical showstopper has emerged for any option considered but technical analysis is not conclusive;
- All options investigated face similar issues:
  - Lack of national policy supporting actinide recycle;
  - Lack of industrial infrastructure for actinide recycle;
  - Large initial capital investment and development costs;

    - Lack of licensing experience and interest from utilities.
— Retrofit RMPWR could be initial test bed but ultimately has limited efficiency due to poor fuel usage and high reprocessing/remote fuel manufacturing requirements;
— SFRs has the highest long-term potential for efficient fuel usage but the higher capital cost and lower capacity factor are major concerns;
— RBWR have the potential for good fuel usage and are attractive for their reliance on mature plant technology;
— Given the operating experience and predominance of LWR technology (including new builds) RMLWRs are attractive for actinide recycle at industrial scale.

8. TRANSURANIC RECYCLING WITH URANIUM AND THORIUM FUEL CYCLES OVER A LIMITED TIMEFRAME

8.1. INTRODUCTION

Spent nuclear fuel (SNF) consists of uranium, fission products and transuranic (TRU) elements. While the remaining uranium is of low radiotoxicity, and fission products decay to safe levels within ~1000 years, many TRU isotopes take ~100 000 years to decay, and hence represent the long-term storage liability in a nuclear waste repository. Nuclear waste decay time is often measured as the time taken for the waste to decay to a 'reference level', which is typically taken as the radiotoxicity of the natural uranium (including 'daughter' isotopes produced by decay) used to fuel the reactor. If losses during reprocessing and fuel fabrication are minimised, then the full recycling of transuranic isotopes can theoritically lead to a reduction in radiotoxicity levels to as little as ~500 years for repository. This strategy is utilized in many envisaged future 'sustainable' nuclear fuel cycle schemes [69, 111].

This section draws extensively on work published in the paper "The effectiveness of full actinide recycles as a nuclear waste management strategy when implemented over a limited timeframe — Part II: Thorium fuel cycle", by LINDLEY, B.A., FIORINA, C., GREGG, R., FRANCESCHINI, F. and PARKS, G.T, Progress in Nuclear Energy 87 (2016) 144–155 in order to have a better understanding of the waste management strategy through actinide recycling for the thorium fuel cycle

Although most nuclear reactors currently operating are light water reactors (LWRs), which have a thermal neutron spectrum, fast reactors are usually considered for full recycle of TRU isotopes, as a fast neutron spectrum is beneficial for increasing the fission probability of many TRU isotopes. However, it is also possible to fully recycle TRU isotopes in LWRs, provided the LWRs are fuelled with a mixture of conventional low-enriched-uranium (LEU) fuel and TRU-bearing fuel such as mixed-oxide fuel (MOX).

TRU recycling, however implemented, requires a long-term commitment to recycling [119]. Over a limited timeframe, the radiotoxicity of the 'final' core can dominate over reprocessing losses, leading to a much lower reduction in radiotoxicity compared to that achievable at equilibrium [112–113].

The repository size is determined by not only radio-toxicity due to heavy radionuclides but also by the decay heat due to fission products (e.g. isotopes of I, Cs and Tc) at least for first few hundre years at the time of placement [114–115].

For direct disposal of waste, the radiotoxicity of the Pu dominates. However, full Pu recycle without 'minor actinide' (MA — mostly Np, Am, Cm) recycling limits the reduction in waste storage time [116]. Comparison of different partitioning and transmutation schemes, e.g. Pu-only, Pu + Am, Pu + Np, Pu +Np + Am, Pu + Np + Am + Cm, is the subject of numerous studies [117–118]. The main considerations are:

- Pu-only recycle can only reduce the radiotoxicity by a factor of ~3 due to Am production;
- Np recycle, potentially performed by co-extraction with Pu does not reduce the radiotoxicity until the ~1-million-year mark (compared to recycle of Pu only), by which time the TRUs have decayed well below the reference level;
- Am recycle allows a reduction in radiotoxicity by a factor of ~10 over ~100–10,000 years, compared to recycle of Pu only, the effectiveness being limited by Cm production from the recycled Am;
- Am + Cm recycle allows a further reduction in radiotoxicity by 1–2 orders of magnitude over ~100–10 000 years, compared to recycle of Pu+Am, notionally allowing the radiotoxicity to decay to the reference level in <1000 years, depending on reprocessing losses.

While Np, Cm and Am all introduce fuel reprocessing, fabrication and handling challenges, this is particularly true of Cm. Hence Am-only transmutation, either homogeneously or in heterogeneous assemblies, is often considered as it is easier to implement [119]. This may be combined with homogeneous recycling of Np [120].

An attractive strategy is to burn Am in very-high-burn-up once-through moderated targets, such that the Cm is burned in situ without the need to fabricate Cm-bearing fuel. This is not considered in this study.

Theoretical and computational modeling of time-dependent scenarios for accelerator-driven-system-based transmutation of a fixed initial inventory were considered [121]. The reactor fleet was assumed to reduce over successive generations, to burn the waste left over from the preceding generation. The findings included:

- A large number of reactor generations are necessary before the final core inventory does not dominate the radiotoxicity, resulting in a timeframe of several hundred years for transmutation;
- The radiotoxicity reduction factor became sensitive to the reprocessing losses after ~5 generations;
- Cm recycling became beneficial after ~4 generations of reactors;
- Delaying Cm recycling for ~1 generation, allowing it to decay (by α emission into isotopes of Pu), did not greatly reduce transmutation performance.

In this study, the effectiveness of Pu and Pu + MA recycling schemes are considered, allowing conclusions to be reached on the number of generations required for a scheme to deliver the claimed benefits. Scenarios consider reprocessing of TRUs produced by 'new build' LWRs, thus making them of reasonably general validity. Legacy stockpiles vary greatly between countries and in many cases may not be reprocessed [122].

Comparison is made between break-even and burner reactors, and the performance of U and Th as the fertile component of the fuel is compared. Sodium-cooled fast reactors (SFRs) are considered as both break-even and burner fuel cycles. For the U cycle, 'CORAIL' scenarios are also considered, where LWRs operate with zero net Pu/TRU production by using a mix of LEU and MOX fuel [123–126]. For the Th cycle reduced moderation boiling water reactors

(RBWRs) have been shown to be effective for operating break-even and burner fuel cycles and are considered here.

The radiotoxicity of Th break-even and burner fuel cycles at equilibrium for SFRs and RBWRs is comparable [127] but since RBWRs have a relatively low power density compared to SFRs and which is therefore expected to slow their transition to equilibrium. These scenarios give representative cases for fast and epithermal reactors operating at typical power densities. The molten salt reactors may have a fast or epithermal neutron spectrum with a power density somewhat similar to SFRs; however, the cases considered may not be representative of highly moderated reactors operating a Th break-even fuel cycle due to the substantially different neutron spectrum [128]. Finally, hybrid scenarios which consider a mix of U and Th fuel are not considered, e.g. in RBWRs [129] or using a combination of SFRs and heavy-water moderated reactors [130].

Closed Th-based fuel cycles are well known to have lower equilibrium radiotoxicity than U-based fuel cycles due to much lower TRU production from ^{232}Th than from ^{238}U [131-132]. This is only the case for a period up to ~35 000 years, after which the radiotoxicity of ^{233}U and its daughters becomes most significant [133]. The equilibrium Th fuel cycles can be realised due to long time to equilibrium. Since route to ^{232}U production is through ^{231}Pa capture and reprocessing of Pa is challenging, ^{231}Pa remains with the fission products after THOREX fuel reprocessing. ^{232}U production can be reduced by ~70% by not recycling Pa, reducing the gamma source at fuel fabrication.

The radiotoxicity beyond the shutdown of the 'final' reactors is considered. For scenarios of a few hundred years, the repository radiotoxicity (or the radiotoxicity of long-term surface storage) is also considerable. It is to be noted that the radiotoxicity, normalized in per GWeyr terms, is a somewhat abstract concept, as it is generally acknowledged that a deep geological repository is necessary in any case [134–135].

8.2. SCENARIOS CONSIDERED

The simulation of transition fuel cycle scenario from an open cycle with LWRs to closed fuel cycle involving SFRs or LWRs has been done using ORION fuel cycle code. In this scenario a fleet of ten LWRs of 1.15GWe, totaling 11.5GWe are assumed online at year 1 and in year 41, the SFRs or LWRs with closed fuel cycle are switched on each having 60 years operating life without replacement of LWRs at the end of their life.Successively recycling reactors are started after preceeding generation reactors reach end of life.Though in practice reactors would have slightly different start and end dates, it is assumed that simultaneous replacement of all reactors in the fleet despite there would be scarcity of material to refuel the material and hence life of preceeding generation of reactors is instead extended.The fuel from 40 years of operation of LWRs is reprocessed for simplicity for use in closed fuel cycle reactors.The cooling period of 5 years is assumed before reprocessing and reprocessing and fuel fabrication take a single time step of six months in each case in ORION.

For burner scenarios, the ratio of LEU-fuelled reactors to SFRs/RBWRs and the ratio of reactors in successive generations of SFRs/RBWRs are constrained by the core inventories (i.e. TRU availability) required to start up and fuel the SFRs/RBWRs. In general, it is difficult or impractical to size the fleet of each successive generation of reactors such that it uses all the available TRU but does not run out of fuel. In any case, there will be out-of-core inventories at the end of scenario from recently discharged fuel which has not been reprocessed. In addition to the discharged core of the recycling reactors at the end of the scenario, this severely limits the proportion of heavy metal which can be recycled.

It is assumed that the net Pu/TRU production is zero once the LEU-fuelled LWRs go offline for a break even and CORAIL scenarios and it. Here, it is assumed the fleet of recycling reactors can be more readily scaled to use all the TRU, such that there is no unused TRU except for recently discharged fuel which has not yet been reprocessed and which is not counted in the spent fuel. In particular: LWRs can be only part-loaded with CORAIL fuel assemblies (with the remainder being LEU assemblies) if insufficient TRU is available at any step to fuel the reactors, hence it is relatively easy to ensure the TRU is efficiently used.

The reprocessing losses 0.1% are assumed in the ORION models which is a typical assumption for closed nuclear fuel cycles. In reality, reprocessing losses may be higher, with losses occurring in the head end (where the fuel is chopped up); in the aqueous or pyrochemical separation of elements; and in fabrication. Therefore, the effect of 1% reprocessing losses is also discussed. The scenarios considered are summarized in Table 35.

TABLE 35. SCENARIOS CONSIDERED

Scenario	Reactor	Fuel	Fuel Cycle
LEU-OT	PWR	LEU	Once-through
SFR-Bu-MA#	SFR	U-Pu-MA	Burner
SFR-Bu-Pu#	SFR	U-Pu	Burner
SFR-BE-MA#	SFR	U-Pu-MA	Break-even
SFR-BE-Pu#	SFR	U-Pu	Break-even
CORAIL-MA#	PWR	LEU/U-Pu-MA	Zero net TRU
CORAIL-Pu#	PWR	LEU/U-Pu	Zero net TRU
Th-SFR-Bu-MA#	SFR	Th-Pa-U3-TRU	Burner
Th-SFR-Bu-NoPa#	SFR	Th-U3-TRU	Burner
Th-SFR-Bu-Pu#	SFR	Th-U3-Pu	Burner
Th-SFR-BE-MA#	SFR	Th-Pa-U3-TRU	Break-even
Th-SFR-BE-NoPa#	SFR	Th-U3-TRU	Break-even
Th-SFR-BE-Pu#	SFR	Th-U3-Pu	Break-even
Th-RBWR-Bu-MA#	RBWR	Th-Pa-U3-TRU	Burner
Th-RBWR-Bu-NoPa#	RBWR	Th-U3-TRU	Burner
Th-RBWR-Bu-Pu#	RBWR	Th-U3-Pu	Burner
Th-RBWR-BE-MA#	RBWR	Th-Pa-U3-TRU	Break-even
Th-RBWR-BE-NoPa#	RBWR	Th-U3-TRU	Break-even
Th-RBWR-BE-Pu#	RBWR	Th-U3-Pu	Break-even

# Denotes that 1, 2, 3, 4 and 5 generations of reactors are considered respectively

8.3. SCENARIO MODELLING

The reactor parameters are given in Table 36. The cross-sections and spectra results from a reactor physics code are used in ORION to estimate the compositions of the discharged fuel as a function of loaded fuel compositions which changes throughout the scenario due to decay

processes and inventories changes from other reactors in the scenario. The infinite dilution cross sections from TRAIL [136] for isotopes not significant from reactor physics perspectives, are grouped together in one group using flux spectra from reactor physics code.

Based on the Advanced Recycling Reactor [81], a 1000 MWth SFR operating with a burner fuel cycle and oxide fuel is considered with three batches and a one-year cycle length. For the U-fuelled burner, the SFR TRU loading is 44.9% and 38.1% with and without MAs respectively. This leads to a TRU incineration rate of ~17.8% per pass in both cases, corresponding to ~249 kg/GW_{th}yr with MAs, ~212 kg/GW_{th}yr without MAs. The break-even U-fuelled SFR uses metallic fuel, with 18.7% and 16.9% TRU loading with and without MAs respectively. The ^{233}U+TRU loading for Th-fuelled SFR burner s 44.2% and 38.1% with and without MAs respectively leading to a TRU incineration rate of ~16% and ~20% per pass respectively and corresponding to ~273 kg/GW_{th}yr in both cases. In case of the Th-fuelled SFR with a break-even fuel cycle, the seed has 25.9% and 21.5% TRU+^{233}U loading with and without MAs respectively where nitride fuel has been used over the first generation of SFRs. Predominantly Th-^{233}U with 20.5% TRU+^{233}U loading are contained in the core in both cases. The core configurations are shown in Fig. 77.

Four-loop Westinghouse pressurized water reactors (PWRs) are considered in all cases. CORAIL-Pu and CORAIL-MA are based on designs considered in reference [135]. These are heterogeneous assemblies containing a mixture of ~1/3 U-TRU and ~2/3 LEU pins. The CORAIL-Pu design uses the same pin diameter as a normal PWR, while the CORAIL-MA design utilizes a high moderation lattice to limit the equilibrium MA fraction in the pins. The fuel assembly designs are shown in Fig. 78. In this study, the CORAIL-Pu design utilized a Pu loading of 9.05% in the U-Pu pins, and the CORAIL-MA design utilized a TRU loading of 13% in the U-TRU pins, to give zero net TRU production in both cases. These are greater than the values of 8.45% and 10.56% found appropriate in Ref. [123].

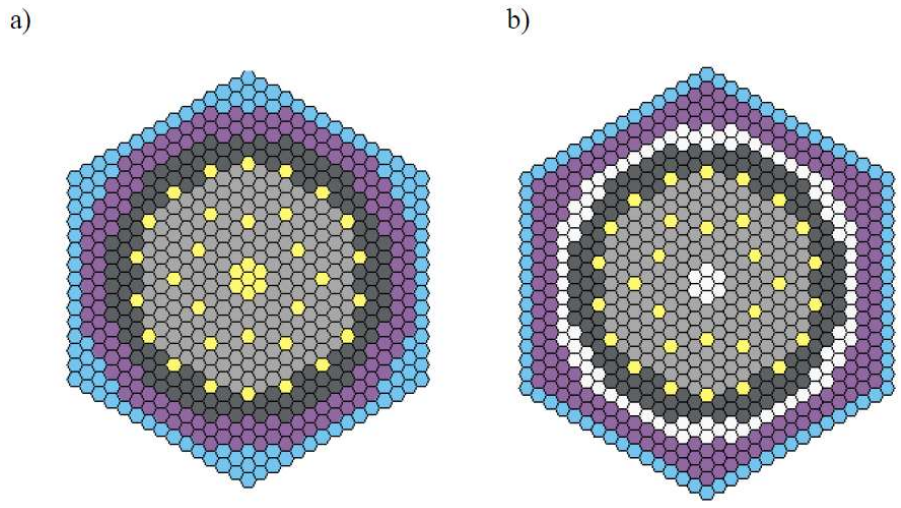

FIG. 77. SFR core layouts for burner (a) and break-even (b) designs. Light grey = inner core, dark grey = outer core; yellow = control rods; violet = steel shield; blue = B_4C shield; white = blanket (reproduced from Ref. [135] with permission).

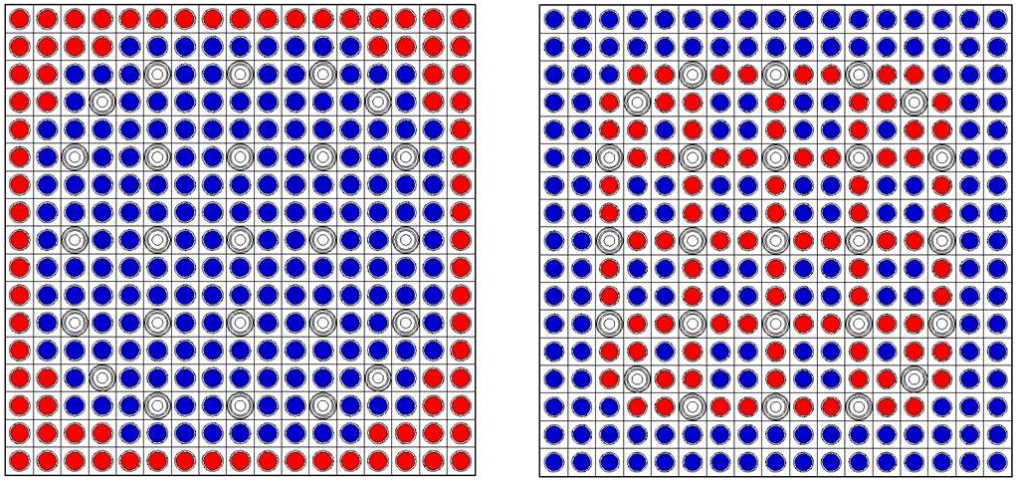

FIG. 78. CORAIL assemblies with LEU pins (blue) and U-Pu/U-Pu-MA pins (red). Left: CORAIL-Pu assembly; Right: CORAIL-TRU assembly (reproduced from Ref. [135] with permission).

The RBWRs operate a mixed 4/5-batch strategy with a cycle length of 2 years in the equilibrium study and the axial blanket in the SFR will reside in the core and the seed for same length of time, i.e. 3 years. The ORION simulations need to have simplified model with these approximations else having fuel elements operate with different batch strategies requires defining two reactors in the model.

The RBWR utilizes the same plant as an ABWR but with a tight pitch triangular lattice. The core contains 720 hexagonal assemblies (Fig. 79) and the core area is the same as the ABWR. The core rating is 3926 MWth. The average void fraction is ~53%. The neutronic performance of the RBWR operating with a burner fuel cycle is greatly improved by utilizing a heterogeneous assembly with Th-Pu-(MA) and Th-(Pa)-U3 pins in different areas of the fuel assembly (Fig. 80).

The ^{233}U+TRU loading is 23.9% and 20.5% with and without MAs respectively in a burner fuel cycle with the RBWR which leads to a TRU incineration rate of ~13% and 17% per pass respectively, corresponding to ~130 kg/GW$_{th}$yr with MAs and ~158 kg/GW$_{th}$yr without MAs. The incineration rate is lower than in the SFR as it is limited by the need to keep the void coefficient negative.The RBWRs with a break-even fuel cycle are loaded with 16.4% and 16% ^{233}U+TRU with and without MAs respectively.Since the higher TRU loading is likely to result in a positive void coefficient, the RBWR with both burner and break even fuel cycles may not be able to start up simultaneouslyto meet void coefficient and acceptable cycle length constraints.This issue can be solved by utilizing an intermediate pass of Th-Pu MOX fuel or utilizing wetter assemblies in the first pass as it would result in lower TRU loading to maintain criticality. Since an intermediate pass with a different reactor configuration result in different mass flows and inventories, this has not been modelled in the simulation to simplification of the analysis for comparision between the SFR and the RBWR.This will affect only the first generation of recycling reactors as the difference in radiotoxicity from utilizing this intermediate step is relatively small.

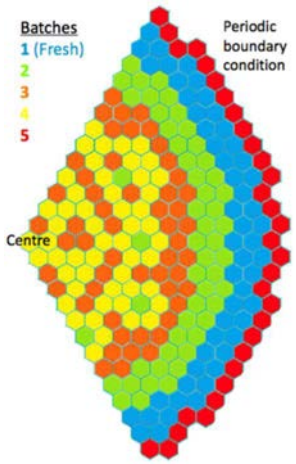

FIG. 79. RBWR core fuel loading pattern in one-third rotational symmetry (reproduced from Ref. [142] with permission).

TABLE 36. REACTOR PARAMETERS

Reactor	Fuel	Fuel residence time / Number of batches	Discharge burn-up (GW. d/t)	Specific power (MWth/t)	Isotope vector used for reactor physics calculations	Reactor physics method
PWR	LEU	4.5 / 3	52	38.1	4.4 wt% LEU	WIMS10 lattice calculation [137]
PWR (CORAIL)	U-Pu-(MA) oxide, LEU	3 / 3	45	38.6 (U-Pu) 42.7 (U-Pu-MA)	4.62 wt% LEU (U-Pu) / 5.11 wt% LEU (U-Pu-MA); Equilibrium TRU isotope vector from [123]	
SFR burner	U-Pu-(MA) oxide	3 / 3	113.6	114.6	Isotope vector from equilibrium study [137]	ERANOS core calculation [139]
Break-even SFR	U-Pu-(MA)-Zr	3 / 3 (seed) 6 / 3 (blanket)*	65.5 (seed) 14.0 (blanket)	70.3 (core) 7.5 (blanket)		
RBWR burner	Th-(Pa)-^{233}U-Pu-(MA) oxide	9 / 4 *	86.1	26.2	Isotope vector from equilibrium study [139]	WIMS10 lattice calculation [138]
Break-even RBWR		9 / 4 *	87.8 (seed) 3.9 (blanket)	26.7 (seed) 1.3 (blanket)		SERPENT 3D pincell calculation [140]
SFR burner		3 / 3	97.1	104.2		ERANOS core calculation [139]
Break-even SFR	Th-(Pa)-^{233}U-Pu-(MA) nitride	3 / 3 (seed) 6 / 3 (blanket)*	73.7 (seed) 5.0 (blanket)	79.2 (seed) 2.7 (blanket)		

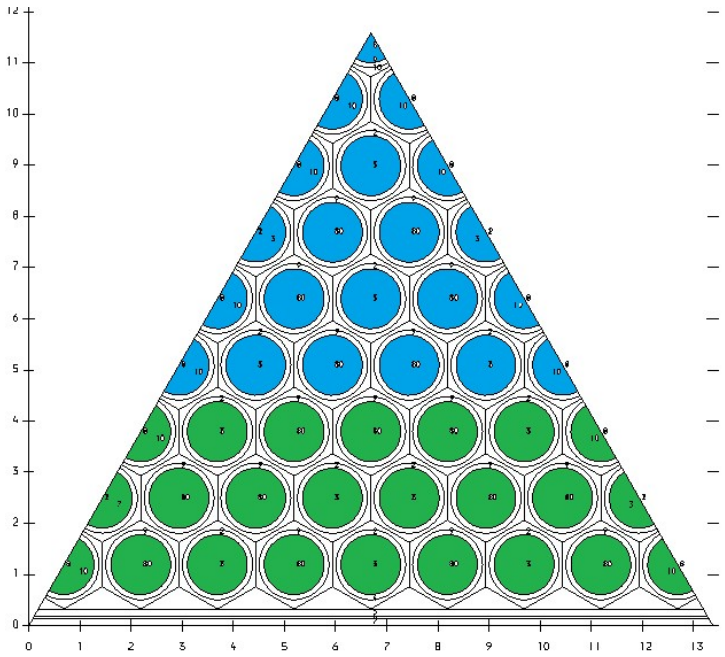

FIG. 80. RBWR fuel assembly design. Centre of assembly (blue) = Th-TRU. Periphery of assembly (green) = Th-^{233}U (reproduced from Ref. [142] with permission).

In this simulation model in ORION, the fuel fabrication facilities, reactors, fuel storage facilities and reprocessing and MA separation facilities have been considered. The radiotoxicity has been accurately calculated by tracking inventories of 2500 isotopes. A typical ORION model for the SFR burner used in this study is shown in Fig. 81.

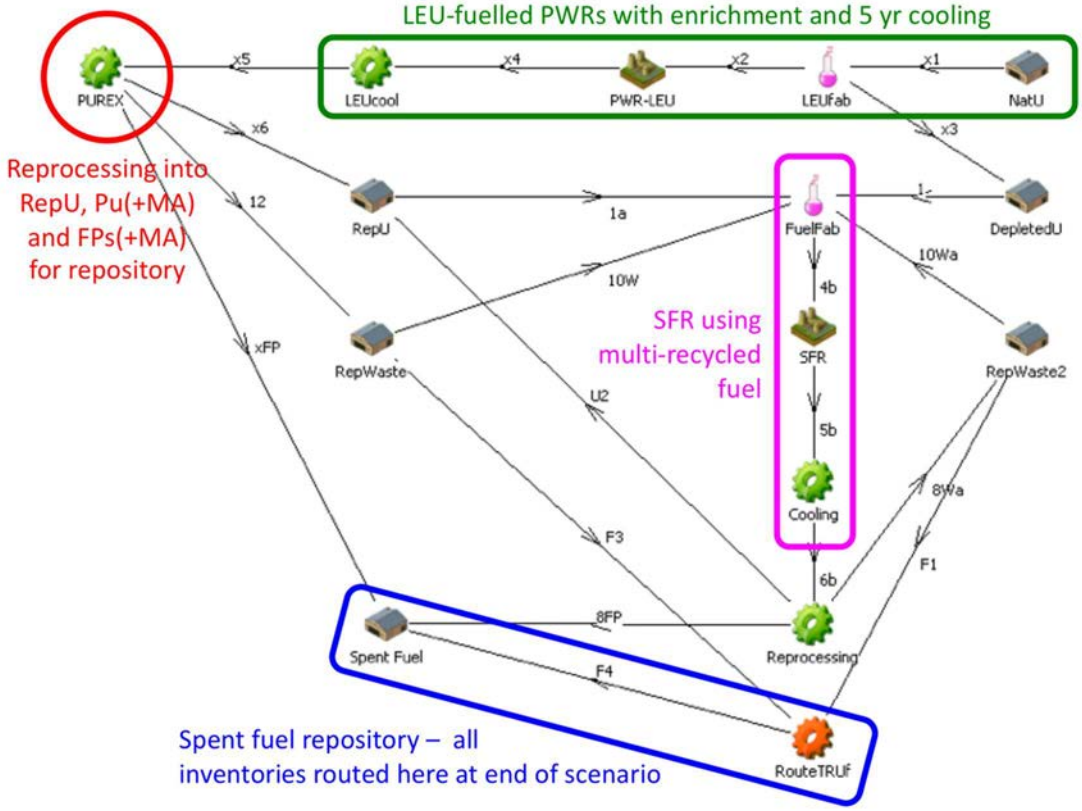

FIG. 81. ORION fuel cycle scenario model (reproduced from Ref. [135] with permission).

In order to allow ^{228}Th and its daughters (notably high-energy gamma sources ^{208}Tl and ^{212}Bi) to decay, Th recovered from reactors through reprocessing is cooled for a further 20 years before fuel fabrication. ^{228}Th (half life of 1.9 years) is produced by ^{232}U decay (half-lives of 69 years) present in the ^{233}U, replenishing the high-energy gamma source in the short term. After about 20 years, it is easier to fabricate fuel using recovered Th as the hard gamma energy emitters have decayed away and does not affect the results presented in this study.

In the break-even scenarios, the core and blanket were modeled separately, with different reactors and cross-sections. The blanket was fuelled exclusively with reprocessed U or Th. In the burner scenarios, the ratio of LEU-fuelled PWRs and burner reactors in each generation, an important parameter to scale a large reactor fleet, is limited by TRU availability. The generations of LWRs and their associated burners will result in increasing the burner capacity beyond that considered for the scenario. The number of reactors in each generation for scenarios utilizing SFR burners and full TRU recycle is shown in Table 37.

TABLE 37. REACTOR FLEET SIZES FOR SFR BURNER SCENARIOS *(*reproduced curtesy of Elsevier [135])

Reactor generation	Starting year	Capacity (GWe)	
		U	Th
LEU-PWR	1	11.50	11.50
SFR Generation 1	41	2.940	2.730
SFR Generation 2	101	1.470	1.470
SFR Generation 3	161	0.840	0.630
SFR Generation 4	221	0.420	0.315
SFR Generation 5	281	0.315	0.158

Figure 82 shows the TRU inventory profile for SFR-Bu-MA5 is shown. Since the accumulated TRU from the LEU-fuelled PWRs is used to start SFRs after 40 years, the TRU inventory increases after start-up due to continued operation of LEU-fuelled PWRs and from 60 years onwards, the inventory decreases as no further TRU is produced by the LEU-fuelled PWRs. At Years 101, 161, 221 and 281 unloading of one generation of SFRs provides inventory for the next generation. The capacity (GWe) of each generation is roughly half the size of the preceding one.

The effect of having subsequent generations of LWRs on the TRU inventory is illustrated in Fig. 83. Here, SFR-Bu-MA5 is added to SFR-Bu-MA4 (delayed by 60 years), SFR-Bu-MA3 (delayed by 120 years), SFR-Bu-MA2 (delayed by 180 years) and SFR-Bu-MA1 (delayed by 240 years). Unless stated, the results presented here, e.g. for SFR-Bu-MA5, do not consider the subsequent generations of LWRs.

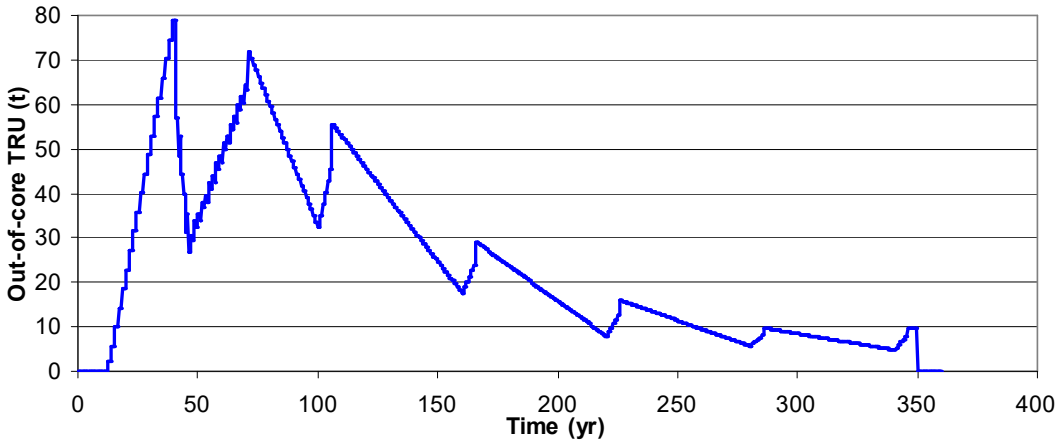

FIG. 82. TRU inventory for SFR-Bu-MA5 (reproduced from Ref. [135] with permission).

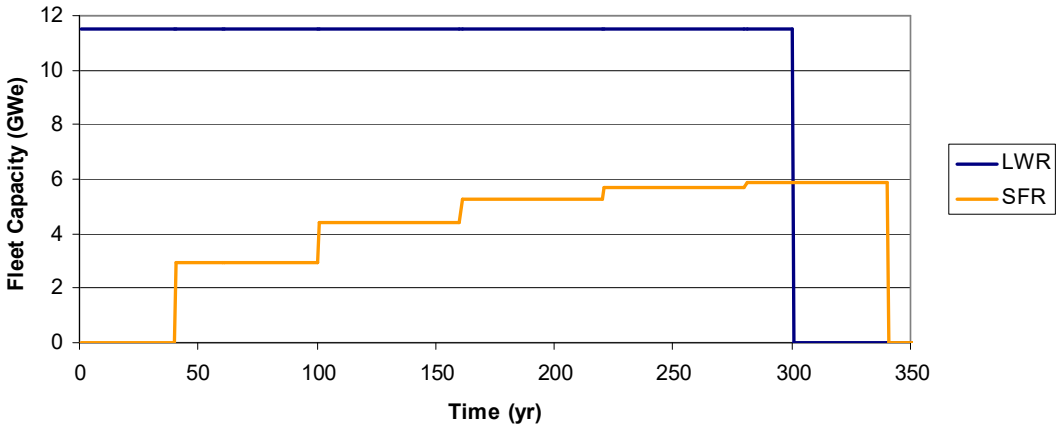

FIG. 83. Fleet capacity with 5 generations of LWRs (followed by TRU burning in SFRs), corresponding to the sum of SFR-Bu-MA1–5 prior to reactor switch-off (reproduced from Ref. [135] with permission).

8.4. RADIOTOXICITY

8.4.1. Radiotoxicity in U-fuelled SFRs with Pu + Am + Np + Cm recycle

Figure 84 gives the plot of the radiotoxicity of SFR burners over 5 generations and time is measured relative to the scenario end, which for multiple generations of SFRs is up to 300 years after the LWRs are switched off. With the generation number, there is a steady decrease of radiotoxicity in Year 1. However, on a timeframe of greater than 1000 years, decay prior to the end of the scenario becomes irrelevant and the radiotoxicity of the different cases becomes comparable.

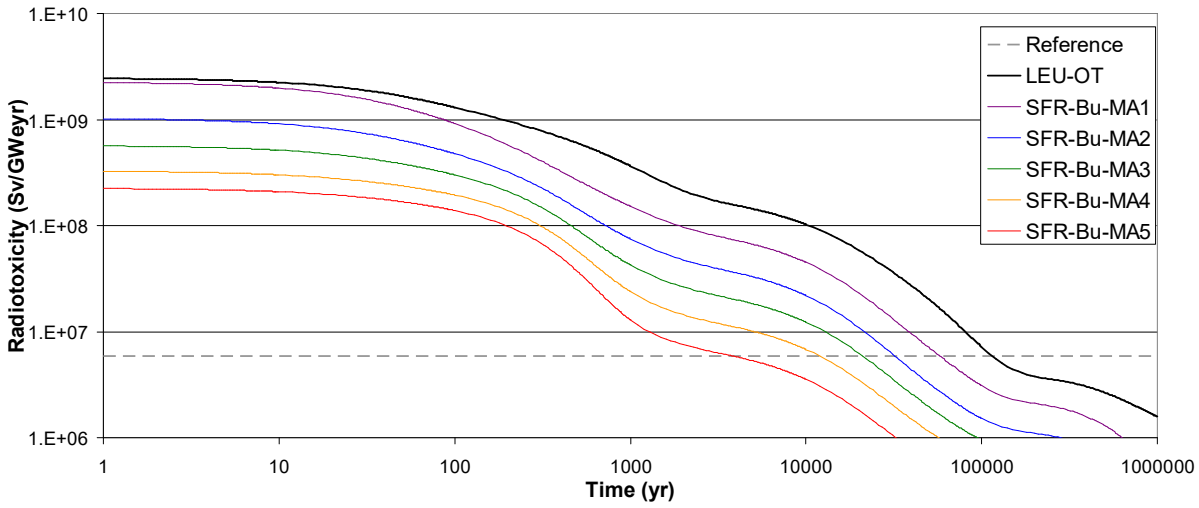

FIG. 84. Repository radiotoxicity for scenarios with MA recycling (reproduced from Ref. *[135]* with permission*).*

In each generation, the mass of TRU remaining roughly halves, and the time taken for the repository radiotoxicity to reduce to the reference level also roughly halves. After a few generations, the actinide isotope vector converges such that the radiotoxicity is essentially proportional to the TRU mass. The radiotoxicity curve is non-linear, such that the time taken

for the SNF to decay to the reference level is a non-linear function of TRU mass (Fig. 85). However, rough proportionality is still satisfied.

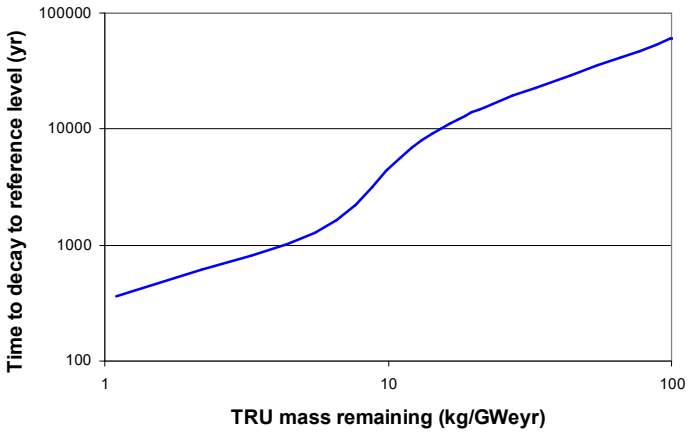

FIG. 85. Repository timeframe as a function of TRU mass (reproduced from Ref. [135] with permission).

The ORION scenarios give a fleet size that roughly halves each generation. Assuming the radiotoxicity is a constant function of TRU mass, (derived for 5 generations of SFRs in ORION), it is possible to derive the TRU mass and therefore radiotoxicity as a general function of: the number of SFR generations; reprocessing losses; cooling, reprocessing and fabrication times; and TRU utilization efficiency. To allow general conclusions to be drawn from the calculations performed and limit computational overhead, it was assumed that the number of SFRs for generations 6–10 is half the number in the immediately preceding generation, which is a slight approximation — this is further discussed below. The time to decay to the reference level under these assumptions is shown in Fig. 86. Reprocessing losses and final core inventory are loaded into the repository at different times, but this is not distinguished here.

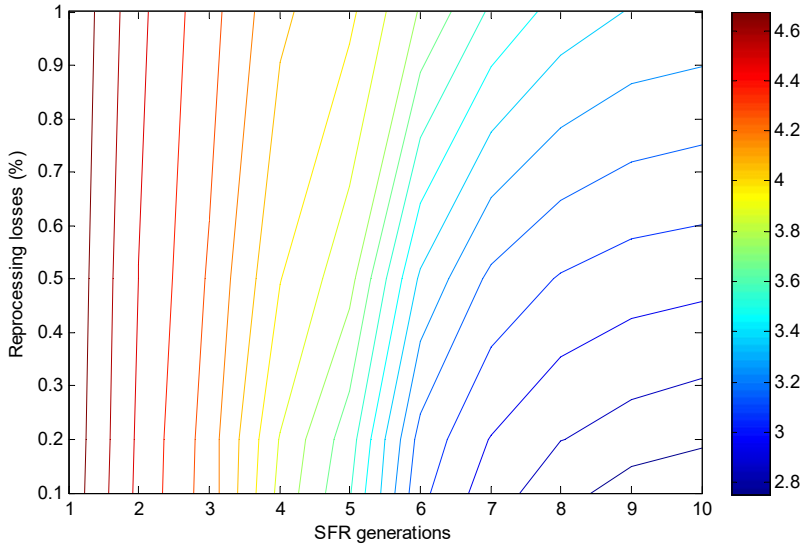

FIG. 86. Log_{10} (time to decay to reference level) as a function of reprocessing losses and number of SFR out-of- generations, with 5.75 years core time (reproduced from Ref. [135] with permission).

The fleet sizes in the ORION model are not optimized, i.e. the TRU is not utilized with 100% efficiency (~20–30% of the final TRU is not from the final core or the final out-of-core inventory). Note in particular that the TRU is utilized more efficiently in Generation 5 than Generation 4 which distorts as shown in Fig. 86. It is difficult to achieve 100% efficiency as the number of reactors of each generation much be exactly defined, such that all the TRU is either in the core or in cooling at end of life. In principle, if the TRU inventory is twice the minimum, then this corresponds to a loss of one reactor generation.

At least 7 generations of SFRs are required for the TRU to decay to the reference level within 1000 years. If out-of-core time is reduced to 1 year, then the out-of-core inventory is proportionally reduced. This allows the number of SFR generations to be reduced by ~1.

The above analysis assumes that only a single generation of LWRs is built. If the LWR fleet is held constant until the end of the fission program (, for 5 generations), then a much lower proportion of TRU can be incinerated before the end of the scenario. The scenario in Fig. 87 can be analyzed by summing the contributions to radiotoxicity levels and electricity from SFR-Bu-MA1–5. This results in SNF radiotoxicity somewhere between SFR-Bu-MA2 and SFR-Bu-MA3.

Over a larger number of generations (estimating the performance for SFR-Bu-MA6–10) then the reduction in performance becomes even worse — over 10 generations of SFRs, the time for decay to the reference level is of the order of 10 000 years. The radiotoxicity of lower generations (corresponding to the latest constructed LWRs) dominates over higher generations. A relatively low proportion of the TRU from the last LWRs can be incinerated and this TRU dominates over the small amount of TRU left over from preceding generations.

This analysis is obviously limited by the consideration of a large number of generations of LWRs. U resources will ultimately become scarce such that if nuclear power continues for several hundred years fast breeder reactors are expected to be deployed [141].

Hence reduction of radiotoxicity to the reference level within ~1000 years would in practice require the reactor fleet to be steadily reduced over a period of a few hundred years. In the absence of a 300-year phase-out plan for nuclear energy, reduction of radiotoxicity to the reference level with SFRs within ~1000 years appears impractical: a longer decay time may need to be specified.

8.4.2. Radiotoxicity in U-fuelled SFRs with Pu-only recycle

The repository radiotoxicity for SFR-Bu-Pu1–5 is given in Fig. 87. The radiotoxicity reduction is limited by ^{241}Am and ^{243}Am accumulation in the repository, such that at least ~24 000 years are required for the SNF to decay to the reference level. The MA loading saturates within ~4 generations of SFRs (Fig. 88), allowing the radiotoxicity for an infinite number of recycles to be reliably estimated. ~3 generations of SFRs are sufficient to approach the minimum achievable time for the radiotoxicity to decay to the reference level.

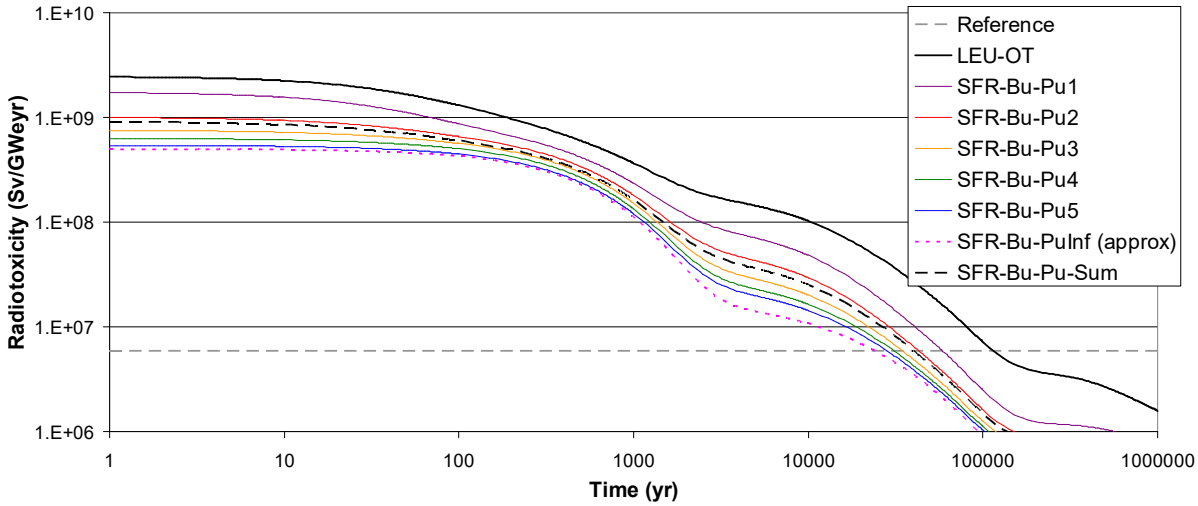

FIG. 87. Repository radiotoxicity for scenarios with Pu recycling (reproduced from Ref. [135] with permission).

The black dashed line in Fig. 87 shows the effect of continuing to build LWRs over 5 generations (with 5 generations of SFRs). As with SFR-Bu-MA, the radiotoxicity is between that of having 2 and 3 SFR generations with just 1 generation of LWRs, corresponding to ~40 000 years for the SNF to decay to the reference level. This is already reasonably close to the performance for an infinite number of generations, therefore achieving close to the 'equilibrium' radiotoxicity reduction does not require a gradual phase-out of nuclear power.

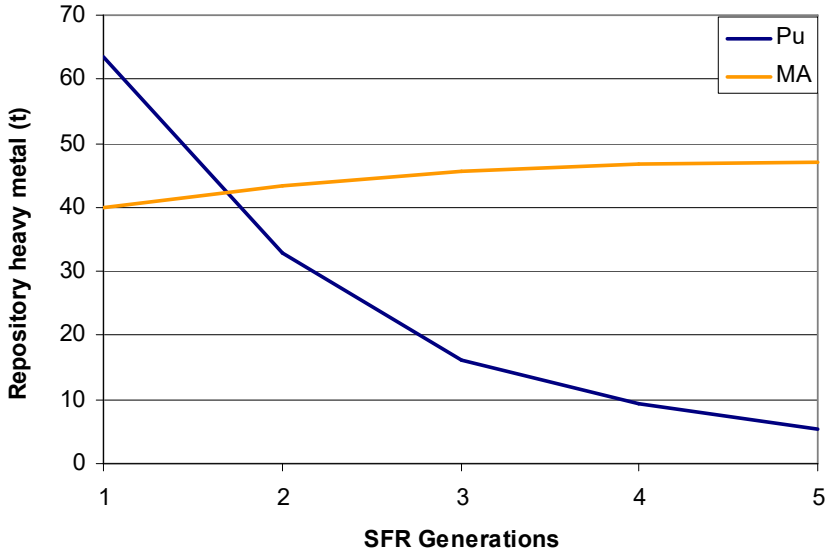

FIG. 88. Repository Pu and MA masses with Pu-only recycling (reproduced from Ref. [135] with permission).

8.4.3. Discussion and comparison with iso-breeder SFRs and CORAIL LWRs

The time taken for the radiotoxicity to reduce to the reference level is compared for all U-based recycle strategies in Fig. 89.

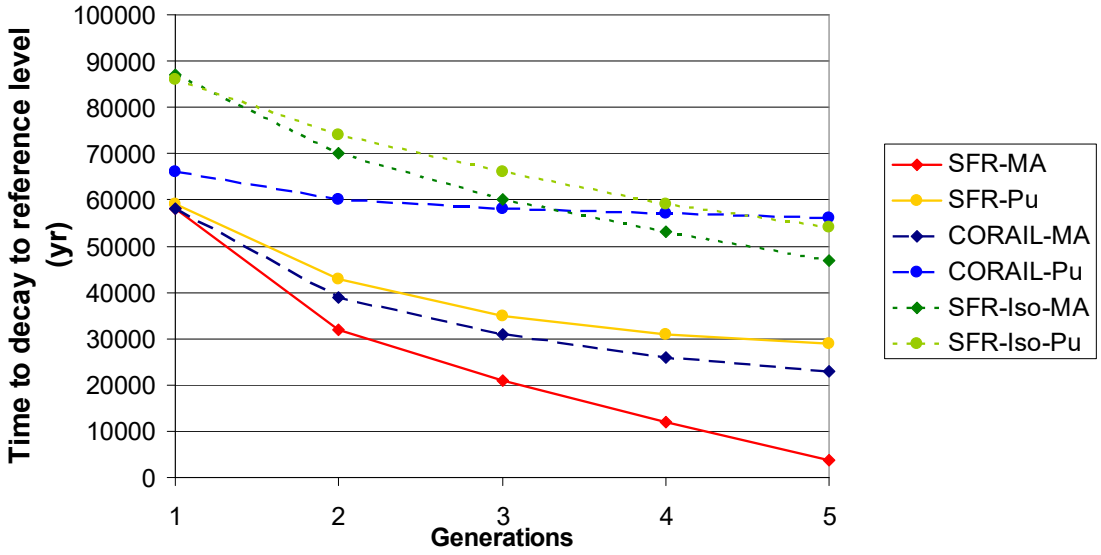

FIG. 89. Repository time to decay to reference level for different recycling strategies (reproduced from Ref. [135] with permission).

For burner and break-even SFRs, recycling Am only resulting in a reduction in decay time after more than 1 generation of SFRs. Beyond this, there is a significant advantage to Am recycle. Recycling Cm is only advantageous after >3 SFR generations, i.e. >220 years after the start of the scenario and, in this case, >160 years after the LWRs are switched off. As discussed, numerous studies have confirmed that the benefits of recycling Np are minor from a radiotoxicity standpoint — the difference between SFR-Bu-Am and SFR-Bu-MA is due to Cm recycle.

Break-even SFRs result in a much lower reduction in radiotoxicity as they do not reduce the TRU inventory, and this is not compensated for by the stabilization of the TRU inventory over a long electricity generation period. The radiotoxicity for the SFR-BE-MA5 scenario is ~26 times the reference level after 1000 years. Therefore, the scenario would have to be ~26 times longer for the energy generated by the reactors to be sufficient for the material to decay to the reference level within 1000 years (without accounting for reprocessing losses). This length of time can be shortened by reducing the out-of-core inventory of the reactor (i.e. by reducing the cooling time).

After 5 generations, CORAIL with MA recycling performs worse than a 'tapering' fleet of SFR burners but slightly better than a fleet of SFR burners operating in conjunction with a fleet of LEU-fuelled LWRs. In both cases around 2/3 of the fleet is LEU-fuelled LWRs. However, the total CORAIL in + out-of-core TRU inventory is slightly lower than the SFR burner case, due to the lower enrichment of TRU in the CORAIL core.

In contrast, the high MA generation rate in LWRs leads to the radiotoxicity reduction of CORAIL-Pu saturating within ~2 generations, with a much lower reduction in radiotoxicity than with SFR-Bu-Pu.

8.4.4. Brief discussion of alternative U-based scenarios

Scenarios utilizing SFRs with a breeding ratio greater than unity are now briefly considered. In this case, the SFR fleet size increases over the scenario. The final cores will continue to

dominate repository radiotoxicity. The final core inventory can be assumed to be similar that of a break-even SFR, and hence the final radiotoxicity will be similar to that of a scenario with break-even SFRs for a given fleet size. However, as the average fleet size over the course of the scenario is less than the final fleet size in this case, the repository radiotoxicity will be normalized over a lower amount of electricity production. Therefore, scenarios utilizing SFRs with a breeding ratio greater than unity will result in higher repository raditoxicity in per GWeyr terms than scenarios utilizing break-even SFRs only.

If SFRs with a breeding ratio greater than unity are first employed for a few generation(s) (implying an initial expansion of SFR capacity and Pu inventory), followed by stabilization of generating capacity with break-even SFRs, the repository radiotoxicity is again higher in per GWeyr terms than for the case with only break-even SFRs. However, the effect of the initial fleet expansion will become less significant over a greater number of generations, as the time-averaged fleet size tends towards the final fleet size.

For scenarios utilizing break-even SFRs, the repository radiotoxicity can be reduced by utilizing SFR burners towards the end of the scenario to reduce the final core inventory. As each generation of SFR burners roughly halves the TRU inventory, utilizing a single generation of SFR burners in this manner can roughly halve the number of generations of SFRs required to achieve a given reduction in repository radiotoxicity.

8.4.5. Th burner scenarios

The radiotoxicity over 5 generations of Th-fuelled SFRs scenarios with and without Pa recycling is plotted in Fig. 90 and time is again measured relative to the scenario end. The effect of recycling Pa becomes perceptible after around 3 generations of SFRs with a logarithmic representation of decay time, beyond which the radiotoxicity reduces but ^{231}Pa and its daughter ^{227}Ac become significant contributors after ~1000 years.

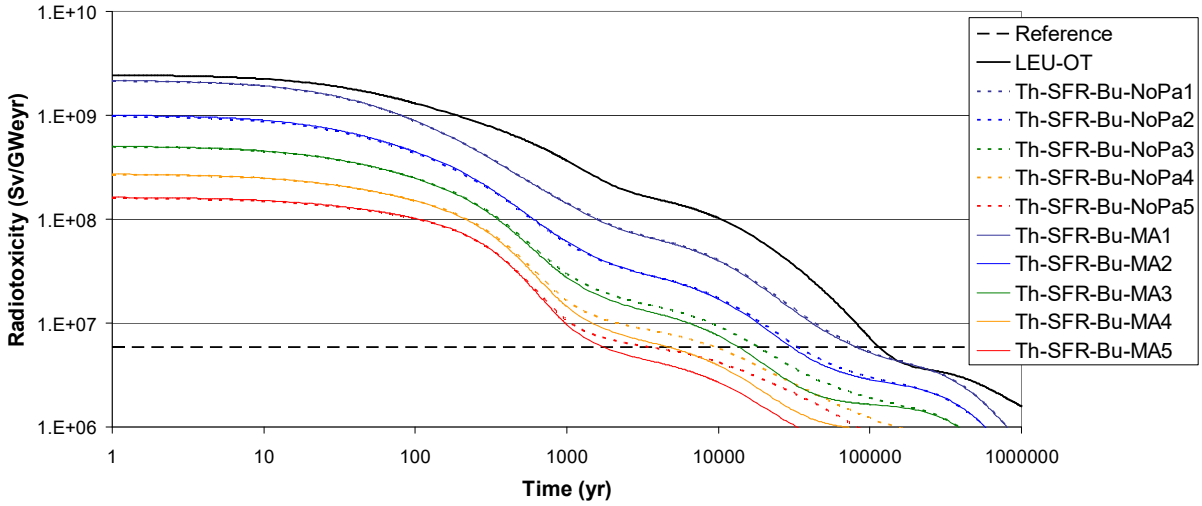

FIG. 90. Repository radiotoxicity for Th-fuelled SFR burner fuel cycle scenarios (reproduced from Ref. [142] with permission).

The mass of ^{233}U+TRU remaining roughly halves in each generation. The ^{233}U+TRU specific radiotoxicity also slightly reduces as the proportion of ^{233}U in the waste steadily rises over the

scenario with Pa recycling and is leads to a reduction of 30–40% in time taken for the waste to decay to the reference level for each additional generation.

The plot in Fig. 91 gives the radiotoxicity of RBWRs over 5 generations. Initially for first two generations the time take to decay to reference levels increases with reference to once through cycle because of the higher breeding of ^{233}U and its daughters since RBWR core is much larger than SFR core. But after 2 generation, the situation is reversed as ^{233}U inventory decreases at the end of scenario which is much more modest than SFRs which have smaller specific power. Hence 3-4 generations of RBWRs are necessary for Pa recycling fruitful.

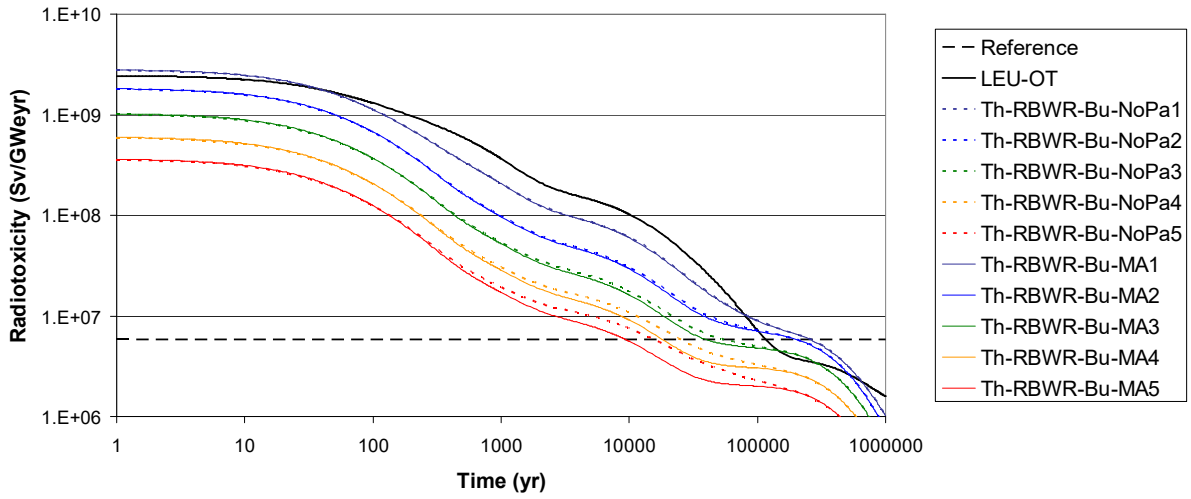

FIG. 91. Repository radiotoxicity for RBWR burner fuel cycle scenarios (reproduced from Ref. [142] with permission).

A comparision of burner fuel cycles in Fig. 92 shows the time to decay under different recycling strategies for multiple generations including SFRs with U cycle with full TRU recycle.

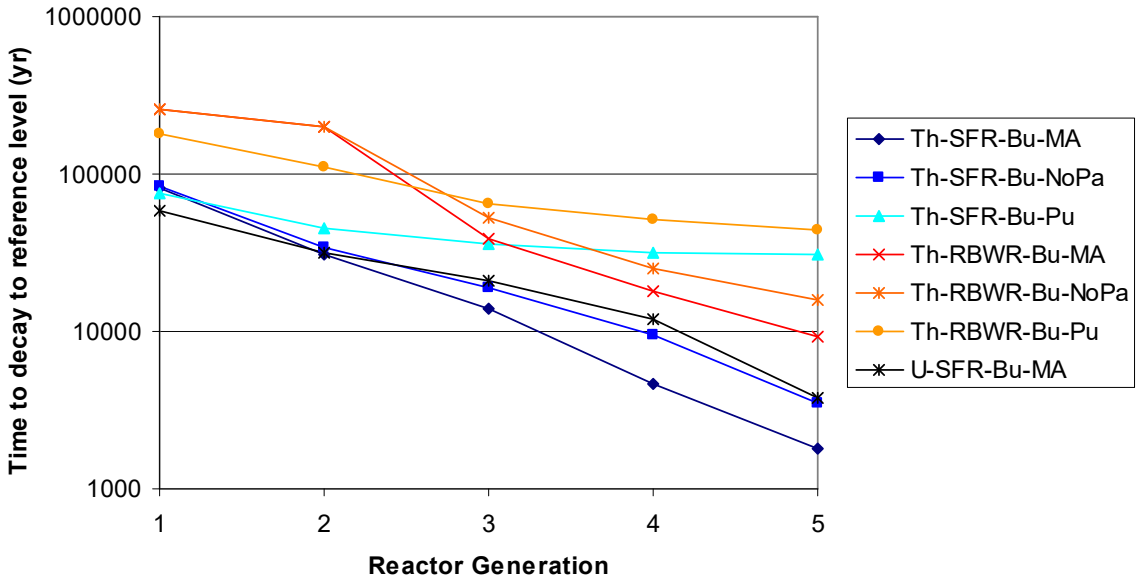

FIG. 92. Comparison of repository decay times for burner fuel cycle scenarios (reproduced from Ref. [142] with permission).

There is strong advantage with MA recycling in reduction of radiotoxicity else it saturates after 3–4 generations of SFRs. The RBWRs result in lowering decay time to reference level earlier in comparision to SFR at least by 1–2 generations. Similarly, Th-SFRs with all actinides recycling takes lower decay time to reference level tha U-SFRs for at least 3 generations of SFRs but with a condition of recycling of Pa without which they have similar radiotoxicity for first 5 generations of SFRs.

In case of higher reprocessing losses, say 1% in place of assumed 0.1%, since more of TRU feed will be lost in losses before it can be burned, will have more significant impact. The U-cycle results, where radiotoxicity after a few generations is proportional to non-fertile inventory will be closer to the Th-fuelled SFRs and RBWRs considered here since with Th fuel cycle the proportion of ^{233}U relative to TRU rises over time. Higher number of generations may be required for RBWRs at the end of scenario inventories before reprocessing losses become significant.

The reduction in repository radiotoxicity is much smaller in case further generations of LWRs are built beyond the assumed gradual phase-out of nuclear power over several generations of reactors in this study.

8.4.6. Break-even Th fuel cycle

The radiotoxicity of repository for a break-even Th fuel cycle with SFRs is shown in Fig. 93 which includes scenarios with (solid lines) and without Pa recycle (in dashed lines) are displayed. The time for the waste to decay to the reference level drops to ~1400 years within 3 generations for Pa recycle,

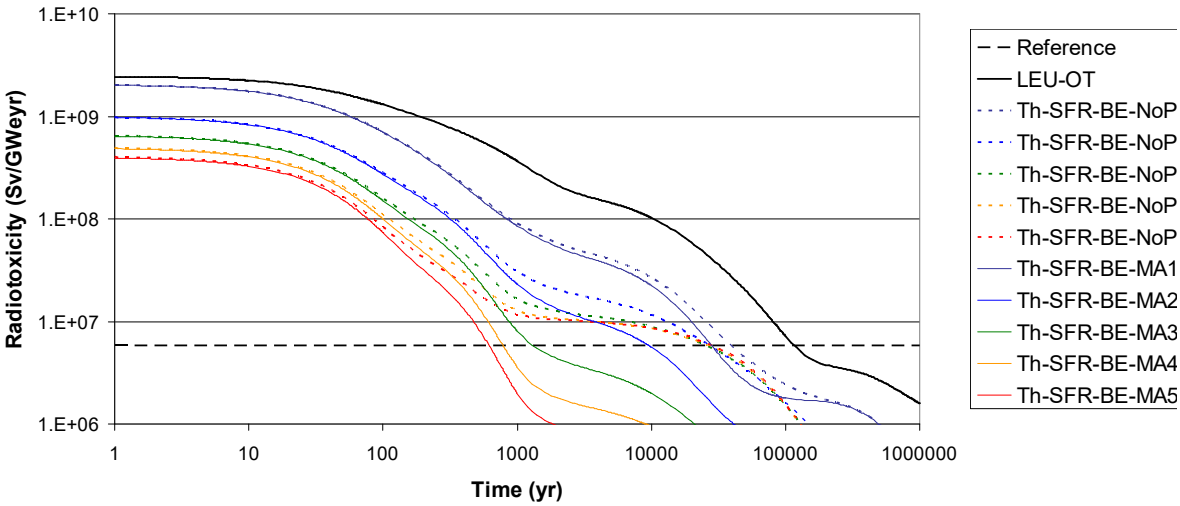

FIG. 93. Repository radiotoxicity for break-even Th fuel cycle scenarios with SFR (reproduced from Ref. [142] with permission).

There is no appreciable reduction in radiotoxicity for the repository without Pa recycle due to ^{231}Pa and actinides and further reduction leading to a long time of decay to reference level (~44 000 year) is achieved beyond 2 generations of SFRs. In Fig. 94, the radiotoxicity contributions for Th-SFR-BE-NoPa5 are shown where the radiotoxicity of ^{231}Pa + Actinide dominates for a timeframe of ~1000 to ~50 000 years which is around twice the reference level during this timeframe. But it is advantageous for fuel fabrication as no recycling Pa reduces ^{232}U in the fuel at fabrication by ~70%.

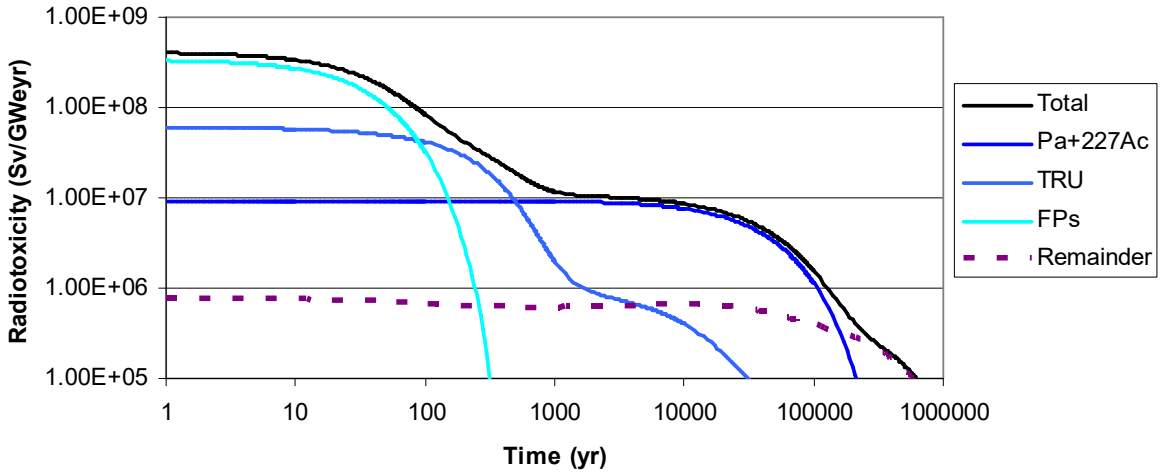

FIG. 94. Contributions to radiotoxicity of Th-SFR-BE-NoPa5 (reproduced from Ref. [142] with permission).

The break-even fuel cycle radiotoxicity with RBWRs and SFRs, follows a similar trend (Fig. 95). The RBWRs yield a lower reduction in radiotoxicity than the SFRs over ~1–3 generations with Pa recycle, but they slightly outperform SFRs over 4–5 generations (Fig. 96). But where as RBWRs yield a significantly higher reduction in time to decay to the reference level than SFRs for scenario without Pa recycle, in this case, the radiotoxicity of ^{231}Pa + ^{227}Ac is slightly below the reference level rather than slightly above it until ~50 000 years which is partly due to ~25% lower production of ^{231}Pa per GWe in the RBWR than the SFR. To generate sufficient Pu for start-up, the RBWR requires almost three times larger fleet of LWRs Thus for first few generations the radiotoxicity is increased due to higher TRU inventory but normalizes over higher energy production from LWRS initially over higher number of generations. The repository loading will be similar to SFR with hardly any improvement in radiotoxicity for the RBWR. The radiotoxicity in Sv/GWeyr is essentially a measure of repository loading per unit energy production.

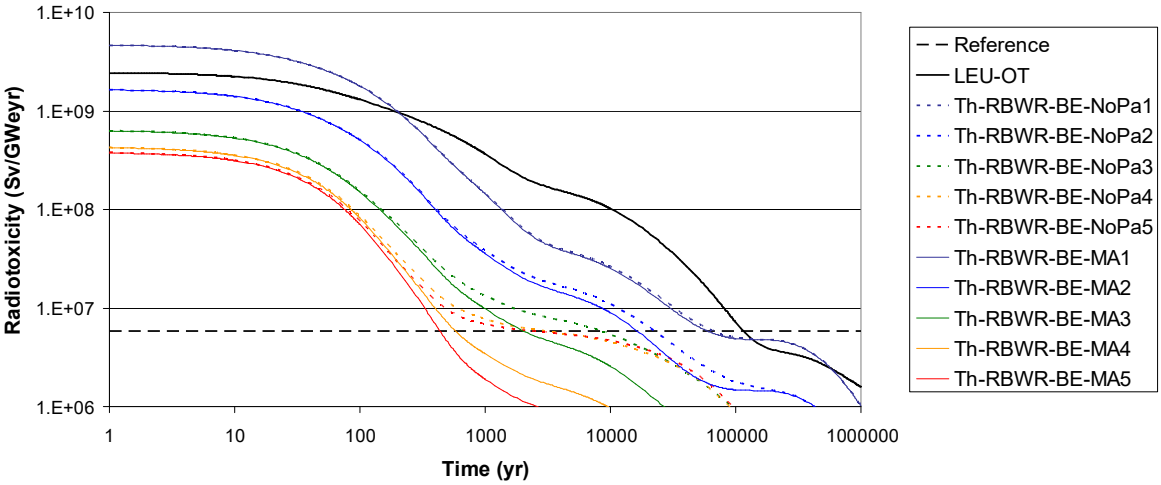

FIG. 95. Repository radiotoxicity for break-even Th fuel cycle scenarios with RBWRs (reproduced from Ref. [142] with permission).

Figure 96 also shows the effect of a break-even fuel cycle utilizing U-fuelled SFRs. Due to domination of final core inventory which contains a substantial amount of TRU, unlike the Th-fuelled core, the reduction in repository loading with the U fuel cycle is much lower. Indeed, the Th fuel cycle achieves comparable lower radiotoxicity than the U fuel cycle without MA recycle. However, there is greater challenges of recycling Th and ^{233}U than the recycling MAs.

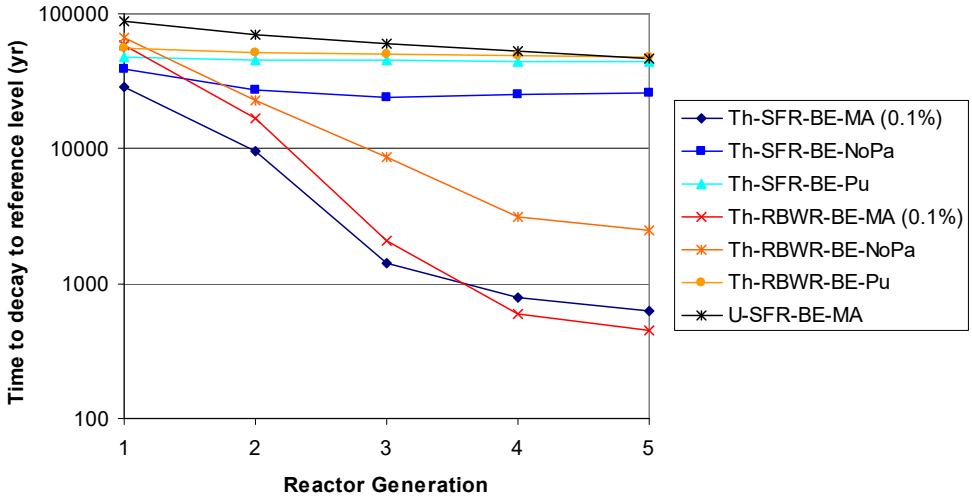

FIG. 96. Comparison of time to decay to the reference level for break-even fuel cycle scenarios (reproduced from Ref. [142] with permission).

Figure 97 shows the effect of 1% reprocessing losses which slightly reduces the available fissile inventory. The ORION model is not otherwise altered to make the comparison fair, the main effects are to reduce the amount of TRU that is recycled but to slightly increase the amount of ^{233}U that is burned (hence reducing the final ^{233}U inventory) for the same amount of energy is generated from each case.

The radiotoxicity of the repository becomes substantially higher for 1% losses than with 0.1% reprocessing losses over from 1st to 5th generations as the time taken for decay to the reference level increasing by a factor of ~3–6 for a given number of generations. Whereas in contrast, the U burner fuel cycle scenarios utilizing SFRs, about ~5 generations of SFRs are required before the reprocessing losses became significant. Since the reprocessing losses contain a relatively high proportion of TRU whereas the final core inventory contains very little TRU (mostly Th+^{233}U), the specific radiotoxicity of the final core inventory becomes much lower than the radiotoxicity of the reprocessing losses.

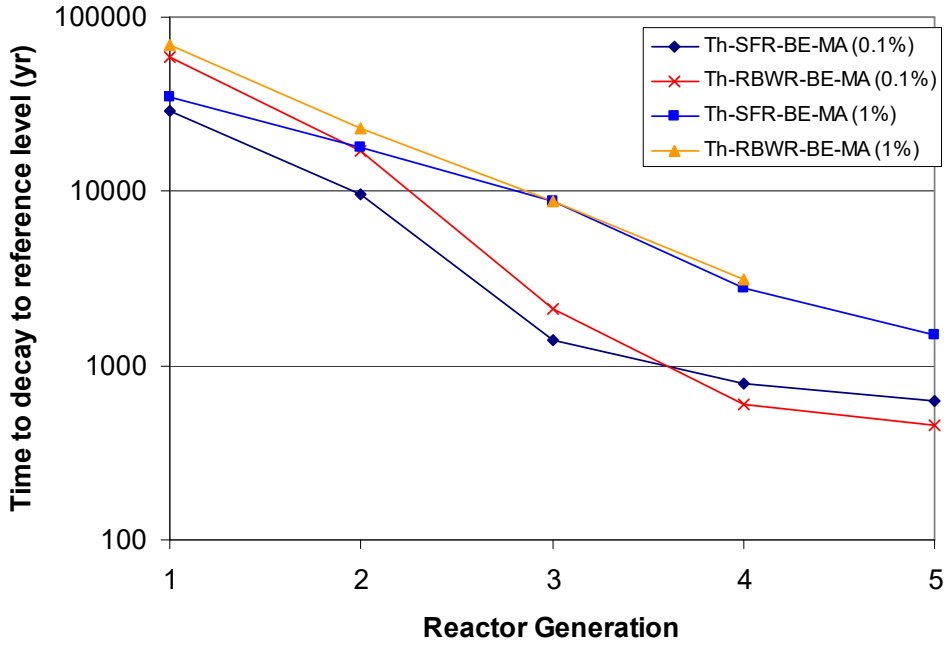

FIG. 97. Effect of 1% compared to 0.1% reprocessing losses on time to decay to the reference level for break-even fuel cycle scenarios (reproduced from Ref. [142] with permission).

8.5. DECAY HEAT

In this section, the decay heat for break-even fuel cycle scenarios is investigated, since recycling of Pu and MAs can also reduce the peak and integrated heat load in the repository. A general conclusion on the relative behaviour of Th and U fuel cycles and SFRs compared to RBWRs are described here. A detailed discussion of decay heat is presented in Ref. [142].

A scenario consisting of a fleet of 10 LEU-fuelled LWRs followed by 10 U-fuelled or Th-fuelled SFRs is considered. Since the decay heat of the Th cycle is not sensitive to whether Pa is recycled or as the ^{232}U contribution is relatively small. In case Th-SFRs (Fig. 98), the initial peak occurs when the LWRs are unloaded, after which there is a sizeable reduction in fleet size. But the repository decay heat is higher for Th-SFRs because of higher fission product namely ^{90}Sr, which is produced in greater quantities in the Th-SFR in comparison to U-SFRs (Fig. 98).

The high-level waste after the reprocessing is vitrified and stored for interom periods on the surface prior to loading in the repository. There is a limitation on maximum heat output from the glass (used for vitrification) due to material constraints else, it becomes leachable, and which puts a limit on maximum waste which can be loaded ito a glass canister. Though it is possible to store high-level liquid waste in undet ground waste storage tanks before allowing for the ^{90}Sr and ^{137}Cs to decay before vitrification, but not desirable due to hazardous nature of the waste.

An attractive option could be to vitrify the waste and store it with forced cooling for a period of ~100 years in an above-ground or near-ground repository. In theory, it is also possible to envisage mitigating this problem by separating ^{90}Sr and ^{137}Cs from the remaining waste, to be vitrified separately. This would reduce the amount of high-level waste as well the decay heat.

The peak repository decay heat at ~60 years is dominated by the LEU-fuelled LWRs and is virtually identical for the Th-SFRs and U-SFRs (Fig.98). However, the second peak at the time of final unloading of cores is higher for Th-SFRs for 1 or 2 generations of SFRs, after which it is lower. The relative magnitudes of the two peaks would depend on relative fleet sizes of the LWRs and SFRs in reality. In the present analysis, the LWR fleet has a larger electricity capacity than the SFR fleet and hence the first peak is larger. Recall that the SFR fleet size in this analysis is limited by TRU availability to start up the SFRs.

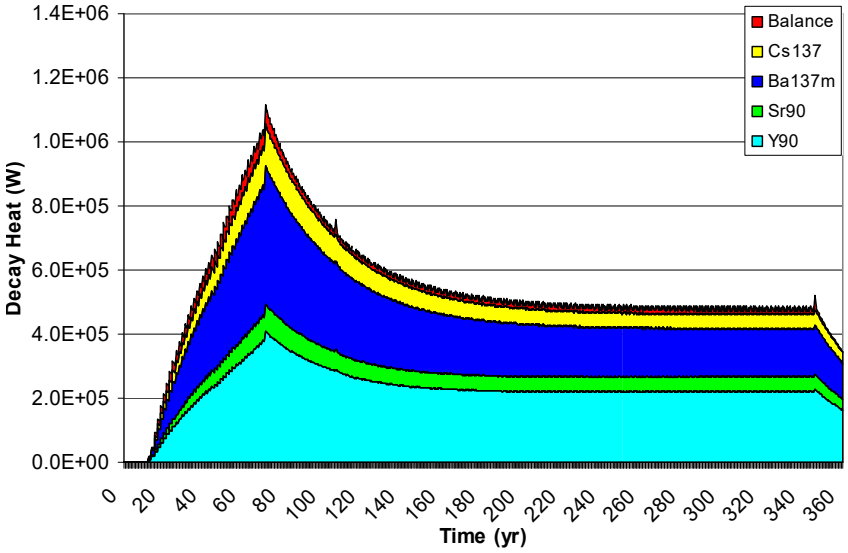

(a)

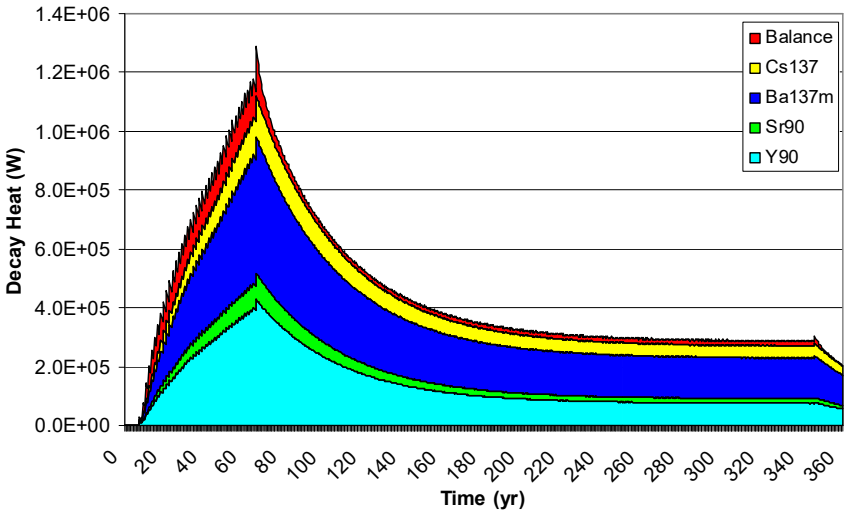

(b)

FIG. 98. Fission product decay heat for (a) Th-SFR-BE-MA5 and (b) U-SFR-BE-MA5. Th-SFR decay heat is generally substantially higher as a result of higher ^{90}Y production (reproduced from Ref. [142] with permission).

The final core decay heat of Th-SFRs becomes almost negligible, after a few generations in comparision to U-SFRs where the significant TRU loading increases repository decay heat. The integrated repository decay heat for Th-SFRs before final core discharge is almost twice as high for the Th-SFR scenarios, where as the decay heat at core discharge is comparable (Table 38). Initially, the recycled MAs can increase the peak heat load. The MA recycle is mainly effective at reducing the peak decay heat load compared to Pu recycle and also reduces the peak repository heat load over Pu+MA recycle for >1 generation of SFRs. The effect of breeding ^{238}Pu from ^{237}Np is significant. The radiotoxicity of the final core is essentially insignificant for any number of generations without MA recycle.

TABLE 38. DECAY HEAT (MW) BEFORE AND AFTER FINAL CORE DISCHARGE FOR THORIUM AND URANIUM SFR WITH BREAK-EVEN FUEL CYCLES (reproduced curtesy of Elsevier [142])

SFR generations	Before		After	
	Th-SFR-BE-MA#	U-SFR-BE-MA#	Th-SFR-BE-MA#	U-SFR-BE-MA#
1	6.7	5.7	10.3	8.2
2	4.9	3.3	6.6	5.4
3	4.6	2.7	5.4	4.9
4	4.5	2.6	5.0	4.8
5	4.5	2.6	4.8	4.8

8.5.1. Effect of varying reprocessing and fuel fabrication losses

The repository decay heat is not significantly increased if reprocessing losses are increased to 1%. But due to improvements in technology, it is possible that reprocessing and fuel fabrication losses would reduce over time. The lower reprocessing and fuel fabrication losses for scenarios utilizing break-even SFRs or CORAIL assemblies, would have a limited impact on repository radiotoxicity, as this is dominated by the final cores. However, the decay heat of the repository would somewhat reduce due to lower discharge of actinides from reprocessing and fuel fabrication over the scenario. The reprocessing losses become significant over a large number of generations in case of burner scenarios, however, these losses of the earlier generations dominate as the fleet size, and hence the mass flows, for these generations are larger. Thus, the impact of reduced reprocessing and fuel fabrication losses later in the scenario is again limited, and losses early on in the scenario will tend to dominate.

8.6. CONCLUSIONS

To achieve a repository radiotoxicity reduction approaching that achievable at equilibrium, ~6 generations of U-fuelled SFR burners or ~5 generations of Th-fuelled SFR burners are required to recycle the TRUs produced by LWRs. The fleet size exponentially decays over a timeframe of several hundred years in a gradual phase-out of nuclear power. Otherwise, repository radiotoxicity is dominated by the final core inventory. This appears challenging from an economic and energy security standpoint.

TRU recycle in PWRs with zero net actinide production provides similar performance to LEU-fuelled LWRs in equilibrium with a fleet of burner SFRs. However, it is not possible to reduce the TRU inventory over multiple generations of PWRs. Also, the high rate of MA production leads to a much larger repository decay heat than for the open cycle or SFR scenarios.

TRU recycle in break-even U-fuelled SFRs is much less effective from a point of view of reducing SNF radiotoxicity, although still effective from the point of view of reducing repository decay heat.

The integrated decay heat in repository over the scenario timeframe for SFRs operating a Th break-even fuel cycle is almost twice as high compared to a U break-even fuel cycle due to much higher ^{90}Sr production, which subsequently decays into 90Y. But at end-of-scenario, the final core decay heat from U-SFRs is comparable as decay heat in Th-SFRs the final core is much less significant. The interim storage periods of upto100 years at sub -surface answers the argument that the repository size depends on decay heat which is higher for Th cycle in initial generations.

While the challenges and disadvantages of the Th fuel cycle is not be downplayed and reducing repository radiotoxicity is arguably a lower priority compared to nuclear energy economics, security, proliferation resistance and safety, it can be argued based on results that the Th break-even fuel cycle is the only practical way of achieving a reduction in repository radiotoxicity to reference levels within 1000 years.

9. SUMMARY AND CONCLUSIONS

Thorium is three times more abundant in nature compared to uranium and occurs mainly as 'fertile' ^{232}Th. Thorium produces fissile ^{233}U during reactor irradiation. Among the fissile materials: ^{233}U, ^{235}U and ^{239}Pu, ^{233}U is the best in terms of ratio of neutron yield per fission to neutrons absorbed in thermal energy spectrum. Its fission products have less poisoning neutronic effects.

Apart from natural abundance of thorium resources, other incentives for use of thorium fuel cycle include better thermo-physical and neutronic properties of thorium including inherent proliferation resistance characteristics due to the presence of ^{232}U in ^{233}U (fertile ^{238} Th converts to fissile ^{233}U) because of its strong gamma emitting daughter products. There is also a significant drop in the generation of the amount of minor actinides in spent fuel. The thorium fuel cycle generates at least one order of magnitude less long lived minor actinides than uranium fuels. However, there are several technological challenges in the front and back end of the thorium fuel cycles. Irradiated thorium and thorium based spent fuels are difficult to dissolve in nitric acid and the high gamma radiation associated with the short lived daughter products of ^{232}U, which is always associated with ^{233}U, necessitates remote refabrication of fuel.

Oxide fuels of thorium, uranium and plutonium have similar physical characteristics enabling the manufacture of hybrid oxide fuels that may be promising for a wide range of applications.

Thorium fuel may be utilised either in a once-through manner (also called open fuel cycle), i.e. via breeding ^{233}U in a fuel element to be burnt once in a reactor or in a closed fuel cycle with spent fuel being reprocessed. Thorium offers several attractive features that can improve performance or enable new capabilities of nuclear energy systems.

There is a motivation for developing technologies to tap the large energy potential of thorium and the R&D activity now taking place worldwide aims to exploit several advanced capabilities of the thorium fuel cycle that include:

1) Trans-uranic actinide (plutonium and/or minor actinides) management;
2) Using the thermal fissile breeding capability of the Th–^{233}U system.

These studies were carried out for the development of reactor systems, thorium fuel cycle deployment scenarios, thorium fuel cycle enabling technologies and relevant properties.

For the use of thorium fuels, the reactor platforms that have been looked at include LWR, HWR, HTR, MSR and FR. Several new advanced variants of these reactor types to particularly take advantage of the neutronics characteristics of the Th-^{233} U fuels were also considered.

Based on the studies carried by the participating Institutes, following conclusions were made:

1) The studies confirmed that thorium can be used in conjunction with a range of actinides in a variety of nuclear reactor systems to achieve various fuel cycle objectives;
2) Technical, system specific, challenges were identified. However, no fundamental insurmountable barriers were found that would prevent the deployment of the studied systems;
3) The implementation path to adopting thorium fuel cycle would depend on the availability of suitable fissile material;
4) Substantial benefits can be derived from a closed thorium fuel cycle. Whereas the application of thorium through a once through fuel cycle offers only marginal benefits, except the niche application as a fuel matrix for plutonium disposition;
5) Closed thorium fuel cycles can, in principle, achieve net breeding of fissile ^{233} U in different reactor systems. Breeding or high conversion rate of thorium into fissile ^{233} U enable substantial natural resource savings;
6) A number of development paths are available to establish a closed thorium fuel cycle. Some could leverage existing technologies and operating experience, other, more advanced, systems which offer enhanced performances require further development;
7) There are potential long term waste management benefits by implementing a thorium closed fuel cycle versus a closed uranium fuel cycle. However, the transition time to a future in which all nuclear generation uses the closed thorium fuel cycle is long (on the order of decades). During this transition, waste management benefits are marginal as compared to the closed uranium fuel cycle;
8) The studies confirmed that thorium can be effectively used for a continuous recycling of transuranic actinides in a variety of reactor systems: reduced moderation LWRs, MSRs and fast reactors. The use of thorium fuel in this context is a key to achieving a defendable safety case due to more favourable reactivity feedback coefficients;
9) Since thorium irradiation generates a chain of nuclides with relatively small amounts of Pu and MAs, it is particularly a suitable fuel matrix for burning actinides produced in other reactor systems. This results in a need for fewer burner reactors to balance actinide generation in once through LWRs as compared with uranium fuel matrix based actinide burning systems.

Further studies would focus on enabling technologies for the thorium fuel cycle in order to reduce uncertainties associated with the development and performance assessment of reactor systems and fuel cycles. In particular:

1) Development of thorium fuel cycle enabling technologies including processes for chemical separations and remote fuel fabrication relevant to closed thorium based fuel cycles has to be a matter of high priority;
2) Nuclear data including neutron capture cross sections in epithermal energy range for ^{233}U, Pa and molten salt components;
3) Material properties for mixed actinide-thorium fuels envisaged in closed fuel cycle applications;
4) Closer investigation of thorium fuel cycle deployment scenarios in Member States;
5) Further investigation of potential benefits that can be derived from thoria being particularly stable fuel matrix which would allow achieving significantly higher burnup and / or irradiation time than conventional UO_2 based fuels. This feature, for example, can be of interest in the context of single batch Small Modular Reactor (SMR) design;
6) The studies suggest that pursuing closed thorium fuel cycle is particularly beneficial. This would imply a wide range of actinide recycling technologies. Therefore, future studies need to investigate approaches to effective safeguarding of fissile materials.

In the near term, thorium / uranium or thorium / plutonium based fuels may be implemented in existing water cooled reactors as once through fuel cycle. For the closed fuel cycle, there is a challenge for the development of technologies for reprocessing of spent fuel and recycled fuel fabrication which may be availbale only in the long term. However, it is to be noted that significant financial outlays will be necessary to reach the same large scale industrial status already reached with U/U-Pu fuel cycle.

REFERENCES

[1] INTERNATIONAL ATOMIC ENERGY AGENCY, Thorium Fuel Cycle: Potential Benefits and Challenges, IAEA-TECDOC-1450, IAEA, Vienna (2005).

[2] INTERNATIONAL ATOMIC ENERGY AGENCY, Potential of Thorium Based Fuel Cycles to Constrain Plutonium and Reduce Long Lived Waste Toxicity; IAEA-TECDOC-1349, IAEA, Vienna (2003).

[3] INTERNATIONAL ATOMIC ENERGY AGENCY, Thorium Fuel Utilization — Options and Trends, IAEA-TECDOC-1319, IAEA, Vienna (2002).

[4] INTERNATIONAL ATOMIC ENERGY AGENCY, Advanced Reactor Information System, ARIS.

[5] MISHRA, P., et al. Irradiation Behaviour of Thoria-Based Fuels. Thorium — Energy for the Future. Springer, Singapore (2019) 299–312.

[6] SCHMETZ, J.J., "Reprocessing of Spent Nuclear Fuels by Fluoride Volatility Processes", Atomic Energy Rev., 8 1(1970) 3.

[7] SHATALOV, V.V., SEREGIN, M.B., KHARIN, V.F., PONOMARYOV, L.A., "Gas-Fluoride Technology for Processing Spent Oxide Fuel", Atomic Energy, Vol. 90, No. 3 (2001) 224–234.

[8] JONKE, A., "Reprocessing of Nuclear Reactor Fuels by Processes Based on Volatilization, Fractional Distillation and Selective Adsorption", Atomic Energy Rev., Vol.3, No.1 (1965) 3–60.

[9] FERGUSON et al., "Chemical Technology Division Annual Progress Report for Period Ending May 31, 1965", ORNL-3830 (1965) 92–94.

[10] FRIEDRICH, H., KREUTZ, R, MASSONNE, J, "Volatilization of UF6 in a fixed bed and in a fluidized bed in the context of dry reprocessing of nuclear fuels containing thorium", Kerntechnik, 12 (1970) 105–109.

[11] SHIMADA, S., OKUMURA, I. HIGASHI, K., "Experimental Study on Fluoride Volatility Process for Thorium Fuels", J. Nuclear Science and Technology, 10 (1973) 689–695.

[12] NAIR, M.R., BASAK, U., RAMACHANDRAN, R., MAJUMDAR, S., Proceeding of the International Symposium and Annual Technical Meeting of Powder Metallurgy Association of India (PMAI), Hyderabad, India (1999) 53–56.

[13] SENGUPTA, A.K., GANGULY, C., MAJUMDAR, S., ROY, P. R., Proceedings of the 5th National symposium on Thermal Analysis, IIT Kharagpur, India, Dec 1985.

[14] CLARK, L. M and TAYLOR, R. E., "Radiation loss in the flash method for thermal diffusivity", Journal of Applied Physics, 46 (1975) 714.

[15] BAKKER, K., et al., Critical evaluation of the thermal propertie of ThO2, and Th 1-y UyO2 and a survey of the literature data on Th 1-y UyO2, J. Nucl. Mat., (1997) 250.

[16] FINK, J.K., Thermophysical properties of uranium dioxide, J. Nucl. Mater. (2000) 279.

[17] SCHULZ, B., "Thermal conductivity of porous and highly porous materials", High Temp.-High Press. 13 (1981) 649.

[18] MURABAYASHI, M., "Thermal conductivity of ceramic solid solutions", J. Nucl. Sci. Technol.,711 (1970) 559.

[19] TOULOUKIAN, Y.S., et al., "Thermal expansion, nonmetallic solids", IFI/Plenum, New York (1970).

[20] MARTIN, D. G., "The thermal expansion of solid UO2 and (U, Pu)O2 mixed oxides- A review and recommendations", J. Nucl. Mater, 152 (1988) 94.

[21] LATTA, R., DUDERSTADT, E., FRYXELL, R., Solidus and liquidus temperatures in the UO2-ThO2 system", J. Nucl. Mater., 35 (3) (1970) 347–9.

[22] INTERNATIONAL ATOMIC ENERGY AGENCY, IAEA-TECDOC-1496, “Thermophysical Properties Database of Materials for Light Water Reactors and Heavy Water Reactors”, IAEA-TECDOC-1496 (2006) 217–218.
[23] HANDBOOK, Thermo physical Properties, Nippon Netu Bussei Gakkai, Youkendou, Tokyo (1990).
[24] ANSTIS, G. R., et al., “A critical evaluation of Indentation techniques for measuring fracture toughness: I, Direct crack measurements”, J. Am. Ceram. Soc. 64 (1981) 533.
[25] SHINSUKE, Y., et al., “Mechanical properties of (U,Ce)O2 with and without Nd or Zr”, J. of Alloys and Compounds 327 (2001) 281.
[26] STAMMLER, R.J., HELIOS Methods. Studsvik Scandpower (2003).
[27] GALPERIN, A., GRIMM, P., RAIZES, V., 1995. Modelling and verification of the PWR burnable poison designs by ELCOS code system, Annals of Nuclear Energy 22 (1995) 317–325.
[28] FRIDMAN, E., KLIEM, S., Pu recycling in a full Th-MOX PWR core. Part I: Steady state analysis. Nuclear engineering and design 241.1 (2011) 193–202.
[29] DRISCOLL, M.J., DOWNAR, T.J., and PILAT, E.E., The Linear Reactivity Model for Nuclear Fuel Management, American Nuclear Society, La Grange Park, USA (1990).
[30] SENGLER, G., FORET, F., SCHLOSSER, G., LISDAT, R., STELLETTA, S., 1999. EPR core design, Nuclear Engineering and Design 187 (1999) 79.
[31] FETTERMAN, R. J., 2008. AP1000 core design with 50% MOX loading, Proc. PHYSOR 2008, Interlaken, Switzerland (2008).
[32] ELECTRIC POWER RESEARCH INSTITUTE, 1997. PWR Primary water Chemistry Guidelines: Revision 2, TR-107728-V2, Vol. 2, EPRI, Palo Alto, CA, USA (1997).
[33] ELECTRIC POWER RESEARCH INSTITUTE, An Evaluation of Enriched Boric Acid in European PWRs, TR-1003124, EPRI, Palo Alto, CA, USA (2001).
[34] PISOVANYI, V. D., VARLASHOVA, E. E., FRIDMAN, S. P., PONOMARENKO, V. B., and SHEHEGLOV, A. V., 2006. Comparative characteristics of absorber cluster assemblies of VVER-1000 and PWR reactors, Atomic Energy 84 (2006) 372.
[35] SANDERS, C. E., WAGNER, J. C., Parametric study of the effect of control rods for PWR burnup credit, ORNL/TM–2001/69, ORNL (2002).
[36] KASEMEYER, U., PARATTE, J. M., GRIMM, P., CHAWLA, R., 1998. Comparison of Pressurized Water Reactor Core Characteristics for 100% Plutonium-Containing Loadings, Nuclear Technology 122 (1998) 52–63.
[37] FRIDMAN, E., GALPERIN, A., SHWAGERAUS, E., 2006. Dissolution, Reactor, and Environmental Behavior of ZrO2-MgO Inert Fuel Matrix: Neutronic Evaluation of ZrO2-MgO Inert Fuels (Final Report), Reactor Analysis Group, Department of Nuclear Engineering, Ben-Gurion University of the Negev, Beer-Sheva, Israel (2006) http://aaa.nevada.edu/paper/trp19_09.pdf
[38] KLIEM, S., MITTAG, S., ROHDE, U., WEIB, F.P., 2009. ATWS analysis for PWR using the coupled code system DYN3D/ATHLET. Annals of Nuclear Energy 36 (2009) 1230–1234.
[39] NUCLEAR REGULATORY COMMISSION, Standard Technical Specifications — Westinghouse Plants, NUREG-1431, vol. 1, Rev. 3.0. US NRC, Washington, DC, USA (2004).
[40] ZAINUDDIN, N.Z., PARKS, G.T., SHWAGERAUS, E, The factors affecting MTC of thorium–plutonium-fuelled PWRs, Annals of Nuclear Energy 98 (2016) 132–143.
[41] ZAINUDDIN, N.Z., PARKS G.T., Shwageraus, E., Assembly-level analysis of heterogeneous Th–Pu PWR fuel, Annals of Nuclear Energy 100 (2017) 160–168.
[42] KOTLYAR, D., SHWAGERAUS, E., Neutronic Optimization in High Conversion Th-^{233}U Fuel Assembly with Simulated Annealing, Proc. PHYSOR-2012, Knoxville, TN USA (2012).

[43] PARATTE, J., FOSKOLOS, K., GRIMM, P., MAEDER, C., 1998. Das PSI Codesystem ELCOS zur stationaren Berechnung von Leichtwasserreaktoren, Proc. Jahrestagung Kerntechnik, Travemunde, Germany, 59 (1998).
[44] LEPPANEN, J., Development of a New Monte Carlo Reactor Physics Code, D.Sc. Thesis, Helsinki University of Technology, VTT Publications 640 (2007).
[45] KOTLYAR, D., SHAPOSHNIK, Y., FRIDMAN, E., SHWAGERAUS, E., Coupled neutronic thermo-hydraulic analysis of full PWR core with Monte-Carlo based BGCore system, Nuclear Engineering and Design 241, 9 (2011) 3777–3786.
[46] MARGULIS, M., SHWAGERAUS, E., High conversion pressurized water reactor with boiling channels, Nuclear Engineering and Design 292 (2015) 98–111.
[47] GUTMANN, H, HANSEN, U., LARSON, H and PRICE, M. S. T., "High-conversion HTRs and Their Fuel Cycle", Gas-cooled Reactors with Emphasis on Advanced Systems, Vol. 2, pp-461, 13–17 October 1975, Jülich, Germany.
[48] TEUCHERT, E. and RUTTEN, H. J., "Near-breeding Thorium Fuel Cycle in the Pebble-bed HTR", Gas-cooled Reactors with Emphasis on Advanced Systems, Vol. 2, pp-491, 13–17 October 1975, Jülich, Germany.
[49] XIA BING and LI FU, "Preliminary Study on the Feasibility of Utilizing the Thermal Fissile Breeding Capability of the Th-U Fuel Cycle in HTR-PM", Proceedings of the 21st International Conference on Nuclear Engineering, 29 July–2 August 2013, Chengdu, China.
[50] KRAMER, H., "The High-temperature Reactor in the Federal Republic of Germany: Present Situation, Development Programme and Future Aspects", Gas-cooled Reactors with Emphasis on Advanced Systems, Vol. 1, pp-25, 13–17 October 1975, Jülich, Germany.
[51] FORSBERG, C. W and MOSES, D. L, "Safeguards Challenges for Pebble-Bed Reactors Designed by People's Republic of China", ORNL/TM-2008/229, November 2009.
[52] ROSENTHAL, M. W., HAUBENREICH, P. N., MCCOY, F.E., MCNEESE, L. E. Atomic energy Review, 9 3 (1971) 601–650.
[53] UHLIR, J., "Prospects of Thorium-Fuel Reprocessing for Molten Salt Reactor Systems", Proc. of ICAPP '08, 8–12 June 2008, Anaheim, CA, USA.
[54] UHLÍŘ, J., Chemical processing of liquid fuel, Molten Salt Reactors and Thorium Energy, Woodhead Publishing, (2017) 209–230.
[55] ROBERTSON, R.C., BRIGGS, R.B., SMITH, O.L., BETTIS, E.L., "Two-Fluid Molten-Salt Breeder Reactor Design Study", ORNL, USA (1970).
[56] FRYBORT, J., VOCKA, R., "Neutronic Analysis of Two-Fluid Thorium Molten Salt Reactor, Proc. of ICAPP '09, 10–14 May 2009, Tokyo, Japan.
[57] KŘEPEL, J., et al. "Molten salt reactor with simplified fuel recycling and delayed carrier salt cleaning." International Conference on Nuclear Engineering. Vol. 45936. American Society of Mechanical Engineers (2014).
[58] CHUCHVALCOVABIMOVA, K., STRAKA, M., TULACKOVA, R., "Electroseparation Studies of Actinides and Lanthanides in Molten Fluoride Media", Proc. of OECD/NEA 10th IEMPT on Actinides and Fission Product Partitioning and Transmutation, 6–10 October 2008, Mito, Japan.
[59] STIKA, M., "Analysis of the fuel cycle of Molten Salt Reactor system with thorium fuel and single-fluid and double-fluid reactor core design", M.S. Thesis, Czech Technical University Prague, 2012.
[60] REVOL, J.P., BOURQUIN, M., KADI, Y., LILLESTOL, E., DE MESTRAL, J. C., SAMEC, K., "Thorium Energy for The World", Proceedings of the ThEC13 Conference, CERN, Globe of Science and Innovation, 27–31 October 2013, Geneva, Switzerland.

[61] MATHIEU, L. et al., “Possible Configurations for the Thorium Molten Salt Reactor and Advantages of the Fast Non-moderated Version”, Nuclear Science and Engineering 161 (2009) 78–89.
[62] KREPEL, J., et al, “Comparison of Several Recycling Strategies and Relevant Fuel cycles for Molten Salt reactor”, ICAPP 2015, 3–6 May 2015, Nice, France.
[63] ORNL Report No. 3936, 1966, Oak Ridge, Tennessee, USA.
[64] AUFIERO, M., et al., “An extended version of the SERPENT-2 code to investigate fuel burn-up and core material evolution of the Molten Salt Fast Reactor”, Journal of Nuclear Materials 441 (2013) 473–486.
[65] KREPEL, J, et al., Molten salt reactor with simplified fuel recycling and delayed carrier salt cleaning. ICONE 22. 7–11 July 2014, Prague, Czech Republic.
[66] HEUER, D., et al., “Towards the thorium fuel cycle with molten salt fast reactors, Annals of Nuclear Energy 64 (2011) 421–429.
[67] RAMANUJAM, A, “Purex and Thorex Processes (Aqueous Reprocessing)”, Encyclopedia of Materials: Science and Technology (2008), 7918–7924.
[68] WENNER, M., FRANCESCHINI, F., KULESZA, J., “Preliminary Comparative Shielding Analysis for Refabricating Different Fuel Vectors”, Proc. ANS Winter Meeting 2012, 11–15 November, San Diego, 2012, USA.
[69] GENERATION IV INTERNATIONAL FORUM, “A Technology Road Map for Generation IV Nuclear Energy Systems”, GIF-002–00, US DOE Nuclear Energy Research Advisory Committee and The Generation IV International Forum (2002).
[70] MATHIEU, L. et al., “The Thorium Molten Salt Reactor: Moving on from the MSBR”, Progress in Nuclear Energy 48 (2006) 664–679.
[71] MERLE-LUCOTTE, E., et al., “Launching the Thorium Fuel Cycle with the Molten Salt Fast Reactor”, Proc. ICAPP 2011, 2–5 May, Nice, France, 2011.
[72] EVOL Project 2012 — Evaluation and Viability of Liquid Fuel Fast Reactor Systems. Available at: http://www.li2c.upmc.fr/
[73] ALEMBERTI, A. et al, European lead fast reactor — ELSY. Nuclear Engineering and Design 241 (2011) 3470–3480.
[74] FIORINA, C., et al., “Comparative Analysis of Uranium and Thorium Fuel Cycles in a Lead –Cooled Fast Reactor from the Perspective of Safety and Waste Management”, GLOBAL 2011 International Conference, 11–16 December 2011, Chiba, Japan.
[75] FIORINA, C., et al., “Analysis of thorium and uranium fuel cycles in an iso-breeder Lead Fast Reactor using extended-EQL3D procedure”, Annals of Nuclear Energy, 53 (2013) 464–475.
[76] ARONSON, S., CISNEY, E., GINGERICH, K.A., Thermal expansion of some cubic refractory compounds of thorium. Journal of the American Ceramic Society 50 (1967) 248–252.
[77] BENEDICT, M., PIGFORD, T.H., LEVI, H. W, Nuclear Chemical Engineering (2nd Edition), McGraw Hill (1981).
[78] RODRIGUEZ, P., SUNDARAM, C. V., 1981. “Nuclear and materials aspects of the thorium fuel cycle”, Journal of Nuclear Materials 100 (1981) 227–249.
[79] SOBOLOV, V., et al, Design of a fuel element for a lead-cooled fast reactor, Journal of Nuclear Materials 385 (2009) 392–399.
[80] KOGUT, V.A., “Naturally safe lead-cooled fast reactor for large-scale nuclear power”, Final Report ISTC, Moscow, 2011.
[81] DOBSON, A. Deployment Studies Preliminary Conceptual Design Studies. Technical Report. Volume IV — Advanced Recycling Reactor, GNEP 2008.
[82] FIORINA, C., et al., “Thermal Fuel Cycle in Fast Reactors: Potential Benefits and Challenges”, NENE2012 International Conference, 5–7 September 2012, Ljubljana, Slovenia.

[83] FIORINA, C., et al., “Comparative Analysis of Thorium and Uranium Fuel for Transuranic Recycle in a Sodium Cooled Fast Reactor”. Annals of Nuclear Energy, 62 (2013) 26–39.
[84] STAUFF, N. E., et al., “Analysis of Fuel Options for the ARR Breakeven Core Configuration”., GLOBAL 2013 International Conference, 29 September–3 October 2013. Salt Lake City, USA.
[85] MERLE-LUCOTTE, E., et al., “Introduction to the Physics of Molten Salt Reactors, Materials Issues for Generation IV Systems”, NATO Science for Peace and Security Series B: Physics and Biophysics (2008) 501–521.
[86] FIORINA, C., The molten salt fast reactor as a fast spectrum candidate for thorium implementation, Ph.D Thesis, (https://www.politesi.polimi.it/handle/10589/74324), Italy (2013).
[87] HOMBOURGER, B., Parametric Lattice Study for Conception of a Molten Salt Reactor in Closed Thorium Fuel Cycle. Master’s Thesis, Joint EPFL-ETHZ Master of Science in Nuclear Engineering (2013).
[88] FIORINA, C. et al., “Analysis of the MSFR Core Neutronics Adopting Different Neutron-Transport Models”, Proc. ICONE 2012, 30 July–3 August, Anaheim, USA (2012).
[89] FIORINA, C., et al., “Preliminary Analysis of the MSFR Fuel Cycle Using Modified-EQL3D Procedure”, Proc. ICONE 2012, 30 July–3 August, Anaheim, USA (2012).
[90] FIORINA, C., et al. “MSFR TRU-burning potential and comparison with an SFR”, Pro. GLOBAL 2013 International Conference, 29 September–3 October 2013, Salt Lake City, USA.
[91] FIORINA, C., et. al., “The MSFR as a flexible CR reactor: the viewpoint of safety”, 29 September–3 October 2013, Salt Lake City, USA
[92] RIMPAULT, G., et al., The ERANOS code and data system for fast reactor neutronic analyses, PHYSOR 2002, 7–10 Oct. 2002, Seoul, Republic of Korea.
[93] KREPEL, J., et al., “EQL3D: ERANOS based equilibrium fuel cycle procedure for fast reactors”, Annals of Nuclear Energy 36 (2009) 550–561.
[94] FIORINA, C., et al., Investigation of the MSFR core physics and fuel cycle characteristics. Progress in Nuclear Energy 68 (2013) 153–168.
[95] SCALE: A Modular Code System for Performing Standardized Computer Analyses for Licensing Evaluations, ORNL/TM-2005/39, Version 5.1, Vols. I–III, November 2006. Available from Radiation Safety Information Computational Center at Oak Ridge National Laboratory as CCC-732.
[96] RUGGERI, J.M., “ERANOS: manuel des methodes: reconstruction fine d’un flux nodal”, Technical Report NT-SPRC-LEPH-99-217 (1999).
[97] SUBLET, J.C., et al., ECCOLIB-JEFF-3.1 libraries, Technical Report. CEA-R-6100 (2006).
[98] GHO, C.J., PALMIOTTI, G., “Bidimensionnel Sn transport optimise: un programme bidimensionnel de transport sn aux differences finies’, Technical Report, NT–SPRC–LEPh, 84–270, CEA, France (1984).
[99] KANG, J., HIPPEL, F.N., 2001. “^{232}U and the proliferation resistance of ^{233}U in spent fuel”, Science and Global Security 9 (2001)1–32.
[100] ASHLEY, S.F., et. al., “Thorium fuel has risks”, Nature 492 (2012) 31–33.
[101] FRANCESCHINI, F., LINDLEY L, B.A., FIORINA, C., LAHODA, E., WENNER, M., “Analysis of a fuel cycle strategy to achieve low-radiotoxicity waste”. Proc. Int. Conf. IEMPT2012, 24–27 September 2012, Prague, Czech Republic.
[102] FIORINA, C., et al., “Safety aspects of Th-use in FRs”. FR2013 Int. Conf., 4–7 March 2013. Paris, France (2013).

[103] FIORINA, C., et al., “Analysis of the safety-related parameters for thorium- and uranium-fuelled Lead Fast Reactors”. ICAPP 2013 International Conference, 14–18 April 2013, Jeju, Republic of Korea.
[104] FIORINA, C., et al., “Modelling and analysis of the MSFR transient behaviour”. Annals of Nuclear Energy 64 (2014) 485–498.
[105] FRANCESCHINI, F., LAHODA, E., FIORINA, C., PHILLIPS, C., WENNER, M., “Promises and Challenges of Thorium for Transuranic Waste Burning”, WM2013 Symposium, 24–28 February 2013, Phoenix, USA.
[106] FIORINA, C., STAUFF, N.E., FRANCESCHINI, F., WENNER, M.T., STANCULESCU, A., KIM, T.K., CAMMI, A., RICOTTI, M.E., HILL, R.N., TAIWO, T.A., SALVATORES, M., 2013. “Comparative Analysis of Thorium and Uranium Fuel for Transuranic Recycle in a Sodium Cooled Fast Reactor”, Annals of Nuclear Energy, 62 (2013) 26–39.
[107] LINDLEY, B.A., FIORINA, C., FRANCESCHIN, F., PARKS, G.T., “Thorium breeder and burner fuel cycles in reduced-moderation LWRs compared to fast reactors”, Progress in Nuclear Energy, 77 (2014).
[108] STAUFF, N.E., FIORINA, C., FRANCESCHINI, F., KIM, T.K., TAIWO, T.A., HILL, R.N., “Analysis of Fuel Options for the ARR Breakeven Core Configuration, Int. Cof. GLOBAL2013, 29 September–3 October 2013, Salt Lake City, USA.
[109] LINDLEY, B.A., ZAINUDDIN, N.Z., FERRONI, P., HALL, A., FRANCESCHINI, F., PARKS, G.T., “On the Use of Reduced Moderation LWRs for Transuranic Isotope Burning in Thorium Fuel-Part I: Assembly Analysis”, Nuclear Technology, 185 (2014) 127–146.
[110] LINDLEY, B.A., ZAINUDDIN, N.Z., FERRONI, P., HALL, A., FRANCESCHINI, F., PARKS, G.T., “On the Use of Reduced Moderation LWRs for Transuranic Isotope Burning in Thorium Fuel-Part I: Assembly Analysis”, Nuclear Technology, 185 (2014) 147–173.
[111] NUCLEAR ENERGY AGENCY (OECD), “Accelerator-Driven Systems (ADS) and Fast Reactors (FR) in Advanced Nuclear Fuel Cycles”, Technical Report NEA-3109 (2002).
[112] NATIONAL NUCLEAR LABORATORY, “Minor Actinide Transmutation – Positionpaper. http://www.nnl.co.uk/media/71280/minor_actinide_transmutation_-position_paper_-_final_for_web.1.pdf (2014).
[113] GREGG, R., HESKETH, K., “The benefits of a fast reactor closed fuel cycle in the UK”, Proc. Global 2013, Salt Lake City, Utah, USA (2013).
[114] LALIEUX, P., BOULANGER, D., VAN GEET, M., “Back-end requirements that need to be taken into account in the fuel design phase”, Proc. Top Fuel 2012, Manchester, UK (2012).
[115] NUCLEAR DECOMMISSIONING AUTHORITY, Geological Disposal: generic post-closure safety assessment, NDA/RWMD/030 (2010).
[116] DELPECH, M., TOMMASI, J., ZAETTA, A., MOUNEY, H., SALVATORES, M., VAMBENEPE, G., 1998. “Transmutation of americium and curium: review of solutions and impacts”, Proc. Fifth OECD/NEA Information Exchange Meeting on Actinide and Fission Product Partitioning and Transmutation (IEMPT), Mol, Belgium (1998).
[117] MAGILL, J., BERTHOU, V., HAAS, D., GALY, J., SCHENKEL, R., WIESE, H.-W., HEUSENER, G., TOMMASI, J., YOUINOU, G., “Impact limits of partitioning and transmutation scenarios on the radiotoxicity of actinides in radioactive waste”, Nucl. Energy 42 (2003) 265–277.
[118] INTERNATIONAL ATOMIC ENERGY AGENCY, 2008. “Spent Fuel Reprocessing Options”. IAEA-TECDOC-1587, Vienna, Austria (2008).
[119] VARAINE, F., BUIRON, L., BOUCHER, L., VERRIER, D., “Overview on homogeneous and heterogeneous transmutation in a French new SFR: Reactor and fuel

cycle impact", Proc. 11th International Exchange Meeting on Partition and Transmutation, 1–4 Nov. 2010, San Francisco, California, USA.
[120] BONNERT, J-M., et al., "Development program on minor actinide bearing blankets at CEA", Proc. 11th International Information Exchange Meeting on Partitioning and Transmutation, 1–4 Nov. 2010, San Francisco, California, USA (2010).
[121] NUCLEAR ENERGY AGENCY, OECD, "Physics and Safety of Transmutation Systems: a status report", Organisation for Economic Cooperation and Development, Paris, France (2006).
[122] INTERNATIONAL ATOMIC ENRGY AGENCY, 2005. Country Nuclear Fuel Cycle Profiles. Second edition. Technical Reports Series No. 425, IAEA, Vienna, Austria (2005).
[123] KIM, T.K., TAIWO, T.A., STILLMAN, J.A., HILL, R.N., FINCK, P.J., 2002. Assessment of the equilibrium state in reactor-based plutonium or transuranics multi-recycling, Proc. Seventh Information Exchange Meeting on Actinide and Fission Product Partitioning and Transmutation, 14–16 Oct. 2002, Jeju, Korea.
[124] GANDA, F., VUJICU, J., GREENSPAN, E., "Thorium self sustaining BWR cores", Proc. ICAPP 2011, 2–5 May 2011, Nice, France.
[125] LINDLEY, B.A., ZAINUDDIN, N.Z., FERRONI, P., HALL, A., FRANCESCHINI, F., PARKS, G.T., 2014. "On the use of reduced-moderation LWRs for transuranic isotope burning in thorium fuel — Part II: Core analysis", Nucl. Technol. 185 (2014) 147–173.
[126] LINDLEY, B.A., FIORINA, C., FRANCESCHINI, F., LAHODA, E.J., PARKS, G.T., Thorium breeder and burner fuel cycles in reduced-moderation LWRs compared to fast reactors, Prog. Nucl. Energy 77 (2014) 107–123.
[127] HESKETH, K., THOMAS, M., The potential role of the thorium fuel cycle in reducing the radiotoxicity level of long-lived waste — 13477, Proc. Waste Management Conference, 24–28 Feb. 2013, Phoenix, Arizona, USA.
[128] NUTTIN, A., GUILLEMIN, P., BIDAUD, A., CAPELLAN, N., CHAMBON, R., DAVID, S., MEPLAN, O., WILSON, J., "Comparative analysis of high conversion achievable in thorium-fuelled slightly modified CANDU and PWR reactors", Ann. Nucl. Energy 40 (2012) 171–189.
[129] GORMAN, P.M, ZHANG, G., SEIFRIED, J.E., VARELA, C.R., VUJIC, J.L., GREENSPAN, E., "The fuel-self-sustaining RBWR-Th core concept and parametric studies", Proc. ICAPP 2014, 6–9 Apr. 2014, Charlotte, North Carolina, USA.
[130] WORLD NUCLEAR ASSOCIATION, Nuclear Power in India. http://www.world-nuclear.org/info/Country-Profiles/Countries-G-N/India/ Accessed 30/10/14 (2014).
[131] FRANCESCHINI, F., FIORINA, C., HUANG, M., PETROVIC, B., WENNER, M., KREPEL, J., "Radiotoxicity characterization of multi-recycled thorium fuel" Proc. Waste Management Conference, 26 Feb.–1 March 2012, Phoenix, Arizona, USA.
[132] COATES, D.J., "The Implications of Actinide Generation and Destruction in Accelerator Driven Sub-Critical Reactors", University of Cambridge, PhD thesis (2011).
[133] FIORINA, C., KREPEL, J., CAMMI, A., FRANCESCHINI, F., MIKITYUK, K., RICOTTI, M.E., 2013. Analysis of thorium and uranium fuel cycles in an iso-breeder lead fast reactor using extended-EQL3D procedure. Ann. Nucl. Energy 53 (2013) 492–506.
[134] LINDLEY, B.A., PARKS, G.T., FIORINA, C., Gregg, R., FRANCESCHINI, F., "Impact of a single generation of uranium- and thorium-fuelled recycling reactors on repository loading", Proc. European Nuclear Conference, 11–14 May 2014, Marseilles, France, pp. 498–507.
[135] LINDLEY L, B.A., FIORINA, C., GREGG, R., FRANCESCHINI, F., PARKS, G.T., "The effectiveness of full actinide recycle as a nuclear waste management strategy when

implemented over a limited timeframe — Part I: Uranium fuel cycle", Prog. Nucl. Energy 85 (2015) 498–510.
[136] ANSWERS, "FISPIN-A Code for Nuclide Inventory Calculations", 2013. http://www.answerssoftwareservice.com/fispin/ Accessed 3/2/14
[137] LINDLEY, B.A., NEWTON, T., HOSKING, G., SMITH, P.N., POWNEY, D., TOLLIT, B., SMITH, P.J., "A versatile reactor physics code for thermal and fast systems", Proc. ICAPP 2015, 3–6 May 2015, Nice, France.
[138] FIORINA, C., STAUF, N.E., FRANCESCHINI, F., WENNER, M.T., STANCULESCU, A., KIM, T.K., CAMMI, A., RICOTTI, M.E., HILL, R.N., TAIWO, T.A., SALVATORES, M., "Comparative analysis of thorium and uranium for transuranic recycle in a sodium cooled fast reactor". Ann. Nucl. Energy 62 (2013) 26–39.
[139] RIMPAULT, G., PLISSONl, D., TOMASSI, J., JACQMIN, R., RIEUNIER, J., VERRIER, D., BIRON, D., "The ERANOS code and data system for fast reactor neutronic analyses", Proc. PHYSOR 2002, 7–10 Oct. 2002, Seoul, Korea.
[140] LEPPANEN, J., Development of a New Monte Carlo Reactor Physics Code. Helsinki University of Technology DSc thesis, VTT Publications 640 (2007).
[141] NUCLEAR ENERGY AGENCY, OECD, Uranium Resources, Production and Demand. Organisation for Economic Cooperation and Development, Paris, France (2011).
[142] LINDLEY L, B.A., FIORINA, C., GREGG, R., FRANCESCHINI, F., PARKS, G.T., "The effectiveness of full actinide recycle as a nuclear waste management strategy when implemented over a limited timeframe — Part II: Thorium fuel cycle", Prog. Nucl. Energy (2015).

ABBREVIATIONS

AHWR	Advanced heavy water reactor
AIC	Ag-In-Cd
ARR	Advanced recycle reactor
ASME	American society of mechanical engineers
BARC	Bhabha Atomic Research Centre
BOC	Beginning of cycle
BOL	Beginning of life
BP	Burnable poison
BWR	Boiling water reactor
CBC	Critical boron concentratio
CNL	Canadian nuclear laboratories
CRP	Coordinated research project
EFPD	Effective full power day
EFPY	Effective full power year
ELSY	European lead system
EOC	End of cycle
EOL	End of life
FIMA	Fission in Fuel Material
FIR	Fissile inventory ratio
FLIBE	Mixture of LiF-BeF_2
HEU	High enriched uranium
HFP	Hot full power
HLW	High level waste
HTGR	High temperature gas cooled reactor
HTR-PM	High temperature reactor-pebble module
HWR	Heavy water reactor
HZP	Hot zero power
IFBA	Integral fuel burnable absorber
LEU	Low enriched uranium
LRM	Linear reactivity model
LWR	Light water cooled reactor
MOX	Mixed oxide fuel (UO_2+PuO_2) or (UO_2+ThO_2)
MSBR	Molten salt breeder reactor
MSFR	Molten Salt Fast Reactor
MSR	Molten Salt Reactor
MTC	Moderator temperature coefficient
NRC	Nuclear regulatory commission
OTTO	Once through then out
PCM	Per cent mille
PHWR	Pressurized heavy water reactor
PIE	Post irradiation examination
PUREX	Plutonium uranium extraction
PWR	Pressurized water reactor
RBWR	Reduced moderation boiling water reactor
RCCA	Rod cluster control assembly
RFF	Radial form factor
RMLWR	Reduced moderation light water reactor

RMPWR	Reduced moderation pressurized water reactor
SDM	Shut down margin
SEM	Scanning electron microscope
SEP	Separate scheme
SFR	Sodium cooled fast reactor
SNF	Spent nuclear fuel
SOC	Start of cycle
TD	Theoretical density
THOREX	Thorium uranium extraction
THTR	Thorium high temperature gas reactor
TOX	Thorium plutonium mixed oxide
TRU	Trans uranic isotope
UREX	Uranium extraction
UOX	Uranium Oxide
VVER	Water-Water Energetic Reactor
WABA	Wet annular burnable absorber

CONTRIBUTORS TO DRAFTING AND REVIEW

Basak, U.	IAEA, Austria
Burgeron, A.	CNL, Canada
Fiorina, C.	Politecnico di Milano, Italy
Franceschini, F.	Wetinghouse Electric Company, USA
Fridman, E.	HZDR, Germany
Krepel, J.	PSI, Switzerland
Luzzi, L	Politecnico di Milanao, Italy
Mishra P.	BARC, India
Parks, G. T .	University of Cambridge, United Kingdom
Ricotti, M. E.	Politecnico di Milanao, Italy
Shwageraus, E.	University of Cambridge, United Kingdom
Uhlir, J.	NRI, Czech Republic
Vasudevan, S.	BARC, India
XIA Bing	INNET, Tsinghua University, China

Research Coordination Meetings

Vienna, Austria: 22–24 October 2012

Milan, Italy: 8–11 April 2014

Cambridge, United Kingdom: 1–4 September 2015

IAEA
International Atomic Energy Agency

No. 26

ORDERING LOCALLY

IAEA priced publications may be purchased from the sources listed below or from major local booksellers.

Orders for unpriced publications should be made directly to the IAEA. The contact details are given at the end of this list.

NORTH AMERICA

Bernan / Rowman & Littlefield

15250 NBN Way, Blue Ridge Summit, PA 17214, USA
Telephone: +1 800 462 6420 • Fax: +1 800 338 4550

Email: orders@rowman.com • Web site: www.rowman.com/bernan

REST OF WORLD

Please contact your preferred local supplier, or our lead distributor:

Eurospan Group

Gray's Inn House
127 Clerkenwell Road
London EC1R 5DB
United Kingdom

Trade orders and enquiries:

Telephone: +44 (0)176 760 4972 • Fax: +44 (0)176 760 1640
Email: eurospan@turpin-distribution.com

Individual orders:

www.eurospanbookstore.com/iaea

For further information:

Telephone: +44 (0)207 240 0856 • Fax: +44 (0)207 379 0609
Email: info@eurospangroup.com • Web site: www.eurospangroup.com

Orders for both priced and unpriced publications may be addressed directly to:

Marketing and Sales Unit
International Atomic Energy Agency
Vienna International Centre, PO Box 100, 1400 Vienna, Austria
Telephone: +43 1 2600 22529 or 22530 • Fax: +43 1 26007 22529
Email: sales.publications@iaea.org • Web site: www.iaea.org/publications

22-03879E

International Atomic Energy Agency
Vienna